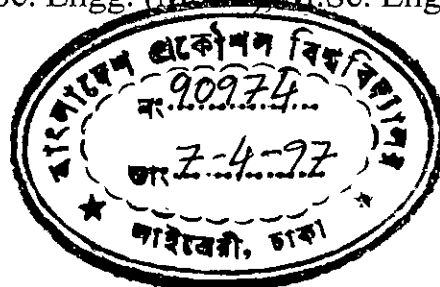


INSTABILITY OF COMPOSITE SHELLS OF REVOLUTION

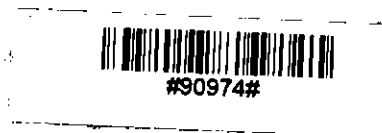
by

Md. Raisuddin Khan

B.Sc. Engg. (Mech.), M.Sc. Engg. (Mech.)



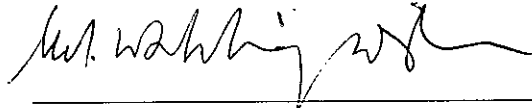
A THESIS SUBMITTED TO THE DEPARTMENT OF MECHANICAL ENGINEERING IN
PARTIAL FULFILLMENT OF THE REQUIREMENTS FOR THE DEGREE OF DOCTOR OF
PHILOSOPHY IN MECHANICAL ENGINEERING.



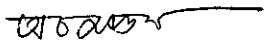
BANGLADESH UNIVERSITY OF ENGINEERING AND TECHNOLOGY, DHAKA
December, 1996

RECOMMENDATION OF THE BOARD OF EXAMINERS

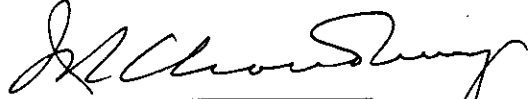
The board of examiners hereby recommends to the Department of Mechanical Engineering, BUET, Dhaka, acceptance of the thesis, "INSTABILITY OF COMPOSITE SHELLS OF REVOLUTION", submitted by Md. Raisuddin Khan, in partial fulfillment of the requirements for the degree of Doctor of Philosophy in Mechanical Engineering.



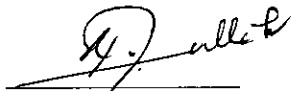
Dr. Md. Wahhaj Uddin (Supervisor), **Chairman**
Professor, Department of Mechanical Engineering,
BUET, Dhaka.



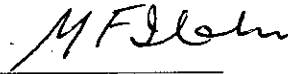
Dr. Amallesh Chandra Mandal (**Member**)
Professor and Head
Department of Mechanical Engineering
BUET, Dhaka.



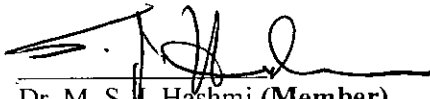
Dr. Jamilur Reza Chowdhury (**Member**)
Professor, Department of Civil Engineering
BUET, Dhaka.



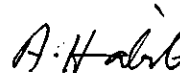
Dr. Md. Zakerullah (**Member**)
Professor, Department of Mathematics,
BUET, Dhaka.



Dr. Md. Fazle Elahi (**Member**)
Expert Faculty Member
Department of Mechanical &
Chemical Engineering
IIT, Board Bazar, Gazipur.



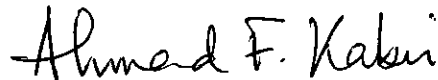
Dr. M. S. Hashmi (**Member**)
Professor and Head
School of Mechanical and
Manufacturing Engineering
Dublin City University
Dublin 9, Ireland.



Dr. Alamgir Habib (**Member - External**)
Professor, Department of Civil Engineering
BUET, Dhaka.



Dr. Sohrabuddin Ahmad (**Member - External**)
Professor, Department of Civil Engineering
BUET, Dhaka.



Dr. Ahmad Fazlul Kabir (**Member - External**)
Engineering Consultant
Advanced Engineering Consultancy Incorporated
180 Montogomery Street
Sanfrancisco, California, USA.

ABSTRACT

This thesis deals with the analytical and experimental studies of the instability of geometrically composite shells of revolution. Different axisymmetric composite shells under uniform external pressure are studied analytically for their use as end-closures of submarine hulls or of pressure vessels. The composite shells studied here are (a) cap-cone end-closures (b) cup-cylinder end-closures and (c) dome-cylinder end-closures. In the cap-cone end-closures a spherical cap is attached to the smaller end of a conical frustum in such a way that the tangent at their junction maintains continuity. In the cup-cylinder end-closure, a spherical cup is attached at an end of a cylinder and in the dome-cylinder end-closure, a spherical dome replaces the spherical cup of the cup-cylinder end-closure.

A computer program is developed and enclosed here in the appendix which can find both axisymmetric and asymmetric buckling load of shells of revolution under uniform external pressure. For the study of axisymmetric buckling, the program uses Reissner's theory of large deflection and interprets instability based on the two criteria of Thompson. The non-linear axisymmetric solutions of Reissner's theory are considered as prebuckling solution for asymmetric instability analysis based on eigen-value interpretation.

Axisymmetric analyses of the cap-cone end-closure for varying cone height, cone angle (ψ) and thickness ratio show that increasing the cone angle or thickness ratio leads to decreasing the buckling load. In the case of varying height, the buckling load remains almost the same over a wide range of height and starts decreasing at a certain small height reaching a minimum at zero height when it is a simple spherical cap.

The axisymmetric buckling load for cup-cylinder end-closures is found to be much higher than that of the dome-cylinder for the same thickness ratio, cylinder height and cup or dome angle. In the case of dome-cylinder end-closures, it is found that its buckling load is even lower than that of the cylinder. Circumferential stresses at the junction of a cup-cylinder end-closure at the axisymmetric critical load is so high that the failure of this end-closure would always be either due to yielding or asymmetric buckling.

A new experimental technique has also been developed for testing the instability of axisymmetric shells. Electrodeposited cap-cone model specimens are tested for instability using this experimental technique. Results of the experiment show that the cap-cone models of tip ratio, r_j/R , about 0.80 can sustain the highest load and is least imperfection sensitive. The conical portion of the cap-cone end-closures were found to buckle asymmetrically with a number of circumferential lobes.

Comparison of the analytical buckling load for both the axisymmetric as well as the asymmetric buckling with the experimental results show that the experimental results are in good agreement with asymmetric buckling load but the axisymmetric buckling loads are found to be about 10 to 15 times higher than the experimental results. At zero cone height, when it is a pure spherical cap with compatible angle $(180^\circ - \psi)$, axisymmetric analytical results are found to agree with the experimental results. It is also found that the spherical cap models are highly sensitive to imperfections.

ACKNOWLEDGEMENT

The author takes this opportunity to express his deep gratitude to his supervisor Dr. Md. Wahhaj Uddin, Professor, Department of Mechanical Engineering, Bangladesh University of Engineering & Technology (BUET), Dhaka, for his constant guidance and invaluable suggestions during this investigation and also for his patient reading and consequent correction of this manuscript.

The author also expresses his gratitude to the authorities of Bangladesh Industrial & Technical Assistance Centre (BITAC) for their interest and co-operation in fabricating the model shells for buckling experiments, Bakhrabad Gas Systems Limited (BGSL) for their assistance in procuring different valves for the experimental set-up, and the Civil Engineering Department of BUET for their permission and co-operation in using their laboratory for buckling tests of shells. Special thanks are extended to Mr. Md. Jalaluddin, Junior Engineer, BITAC, for his untiring effort in introducing the electrodepositing technique, in fabricating the model shells for this investigation.

The author expresses his indebtedness to the BUET authority for the financial assistance in pursuing this research program. Sincere co-operation of all the teachers of the Mechanical Engineering Department, BUET, specially of Mr. Sk. Reaz Ahmad, Assistant Professor, Mr. Khan Md. Saiful Islam, Assistant professor, Mr. M. Ashiqur Rahman, Lecturer and Mr. Prashanta Dutta, Lecturer, are cordially and thankfully acknowledged.

Very special tributes are paid to Mr. Belal Ahmad, Associate Professor, Mechanical Engineering Department, BUET, to Dr. Md. Quamrul Islam, Professor, Mechanical Engineering Department, BUET, and to the members of the doctoral committee of this thesis for their interest and constant encouragement during this work.

Thanks are also due to the authority, BIT Chittagong, for granting the author study leave to undertake this study.

The author feels thankful to Mr. M.A. Ali, SCI, Mr. M.S. Kaiser, AFI and Mr. M.S. Rogerio, BUET Shops for help in fabricating different components of the experimental set-up for the buckling test of shells, Mr. Abdus Salam, Mechanical Engineering Department, BUET for drafting different elements of the experimental set-up and to Mr. Fakhru Islam Hazra for his sincere effort in typing this thesis .

Finally, the author expresses his sincerest appreciation to his wife, Tahmina, for her constant inspiration and patient understanding and to his daughter, Taskia, for sacrifice of her due share of affection and for her sweet smile to cheer the author up whenever he was under duress.

DECLARATION

No portion of the work contained in this thesis has been submitted in support of an application for another degree or qualification of this or any other University or Institution of learning.

Md. Raisuddin Khan

December, 1996.

NOTATIONS

b_1, b_{M+1}	=	(m,1) matrices containing prescribed variables at the boundary
C	=	Eh: extensional rigidity
\bar{C}	=	$(1-\nu^2) \xi_e/R$
D	=	bending rigidity, $Eh^3/[12(1-\nu^2)]$
\bar{D}	=	$1/[12(1-\nu^2)\bar{P}\bar{T}^2\bar{R}]$
E	=	Young's modulus
H	=	radial stress resultant
\bar{H}	=	nondimensional radial stress resultant, H/PR
h	=	shell thickness
I	=	(m,m) unit matrix
k_θ, k_ξ	=	changes of curvature of the middle surface of shell
\bar{k}_θ	=	nondimensional value of $k_\theta, k_\theta \xi_e$
\bar{k}_ξ	=	nondimensional value of $k_\xi, k_\xi \xi_e$
\bar{L}	=	$\bar{R} / \bar{P}\bar{T}$
M	=	number of segments of shell
m	=	order of the system of differential equations
M_ξ	=	meridional couple resultant
M_θ	=	circumferential couple resultant
\bar{M}_ξ	=	nondimensional value of $M_\xi, M_\xi/PRh$
\bar{M}_θ	=	nondimensional value of $M_\theta, M_\theta/PRh$
$M_{\xi\theta}$	=	Inplane torsional moment
$\bar{M}_{\xi\theta}$	=	nondimensional value of $M_{\xi\theta}, M_{\xi\theta}/PRh$
N_ξ	=	meridional stress resultant
N_θ	=	circumferential stress resultant
\bar{N}_ξ	=	nondimensional value of $N_\xi, N_\xi/PR$

\overline{N}_θ	=	nondimensional value of N_θ , N_θ/PR
$N_{\xi\theta}$	=	Inplane shear stress resultant
$\overline{N}_{\xi\theta}$	=	nondimensional value of $N_{\xi\theta}$, $N_{\xi\theta}/PR$
P	=	outward normal pressure
\overline{P}	=	nondimensional value of P , P/E
P_{cr}	=	critical pressure
\overline{P}_{cr}	=	nondimensional value of P_{cr} , P/E
P_v	=	axial component of surface load
P_H	=	radial component of surface load
Q	=	transverse shear stress resultant
R	=	base radius of a shell
R_1	=	radius of the smaller end of a conical frustum
R_2	=	radius of the larger end of a conical frustum
\overline{R}	=	ξ_e/R
r_s	=	radius of curvature
R_ξ, R_θ	=	principal radii of curvature of middle surface of shell
r_0	=	radial distance of a point on undeformed middle surface from the axis of symmetry
r_j	=	radial distance r_0 at the junction of cap-cone shell
r	=	r_0+u : radial distance of a point on the deformed middle surface from axis of symmetry
\overline{r}_0	=	nondimensional value of r_0 , r_0/ξ_e
\overline{r}_j	=	tip ratio, r_j/R
S_i	=	i th segment of shell meridian
T_1, T_{M+1}	=	(m,m) matrices, given by boundary conditions
\overline{T}	=	thickness ratio, R/h
u	=	radial displacement of the middle surface of shell

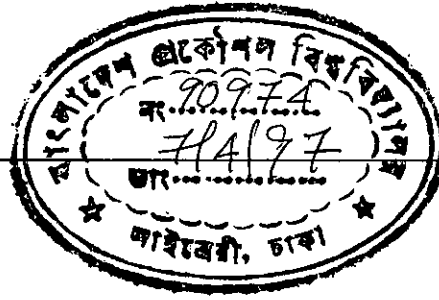
\bar{u}	=	nondimensional value of u , uEh/PR^2
u_ξ	=	displacement of points on the middle surface along the tangent of the meridian
\bar{u}_ξ	=	nondimensional value of u_ξ , $u_\xi Eh/PR^2$
u_θ	=	displacement of points on the middle surface along the tangent of the circumference
\bar{u}_θ	=	nondimensional value of u_θ , $u_\theta Eh/PR^2$
u_ζ	=	displacement of points on the middle surface along the normal of the shell surface
\bar{u}_ζ	=	nondimensional value of u_ζ , $u_\zeta Eh/PR^2$
V	=	axial stress resultant
\bar{V}	=	nondimensional value of V , V/PR
w	=	axial displacement
\bar{w}	=	nondimensional axial displacement, wEh/PR^2
x	=	independent variable
x_i	=	end point of segment i
$y(x)$	=	$(m,1)$ matrix, contains m dependent variables
z_0	=	axial distance of a point on undeformed middle surface of shell
z	=	axial distance of a point on deformed middle surface, z_0+w
\bar{z}	=	nondimensional value of z , z/R
α	=	parameter of meridian of deformed shell, defined in Eqn. (3.1c), or semi-apex angle of conical shell
α_0	=	value of α corresponding to undeformed shell
β	=	angle of rotation of normal after deformation
$\bar{\beta}$	=	β
$\varepsilon_\xi, \varepsilon_\theta$	=	middle surface strains
$\bar{\varepsilon}_\xi$	=	nondimensional value of ε_ξ , $\varepsilon_\xi Eh \xi_e/PR^2$
$\bar{\varepsilon}_\theta$	=	nondimensional value of ε_θ , $\varepsilon_\theta Eh \xi_e/PR^2$

ξ	=	parameter of shell meridian, or distance measured along the meridian
$\bar{\xi}$	=	nondimensional meridional distance between the center of the smaller end and the larger end junction, ξ/ξ_e
ξ_e	=	total meridional length of the composite shells
ξ_j	=	meridional length of the cap-cone shells from the tip to the junction of the spherical cap and the conical frustum
$\bar{\xi}_j$	=	nondimensional meridional distance, ξ_j/ξ_e
ϕ_0	=	angle between normal and the axis of symmetry before deformation
ϕ	=	angle between normal and axis of symmetry after deformation, $\phi_0 - \beta$
ν	=	Poisson's ratio
σ_{ai}	=	meridional stress at the inner surface, $N_\xi/h + 6M_\xi/h^2$
σ_{ao}	=	meridional stress at the outer surface, $N_\xi/h - 6M_\xi/h^2$
σ_{ci}	=	circumferential stress at the inner surface, $N_\theta/h + 6M_\theta/h^2$
σ_{co}	=	circumferential stress at the outer surface, $N_\theta/h - 6M_\theta/h^2$
$\bar{\sigma}_{ai}$	=	σ_{ai}/E
$\bar{\sigma}_{ao}$	=	σ_{ao}/E
$\bar{\sigma}_{ci}$	=	σ_{ci}/E
$\bar{\sigma}_{co}$	=	σ_{co}/E
$\bar{\sigma}_{nai}$	=	$\sigma_{ai}/(PR/h)$
$\bar{\sigma}_{nao}$	=	$\sigma_{ao}/(PR/h)$
$\bar{\sigma}_{nci}$	=	$\sigma_{ci}/(PR/h)$
$\bar{\sigma}_{nco}$	=	$\sigma_{co}/(PR/h)$
$(...)'$	=	derivative with respect to ξ or $\bar{\xi}$

CONTENTS

	Page No.
ABSTRACT	i
ACKNOWLEDGEMENT	iii
DECLARATION	v
NOTATIONS	vi
Chapter-1 Introduction	
1.1 Shell structures	1
1.2 Axisymmetric shells	1
1.3 Composite shells	1
1.4 Use of composite shells	2
1.5 Instability or buckling of shells	2
1.6 Analyses of shells	4
1.7 Present state of analyses	6
1.8 Objectives of the present investigation	10
Chapter-2 Literature Review	
2.1 Reviewing of shell theories	12
2.2 Review of shell analysis	14
2.3 Instability of cylindrical shells	17
2.4 Instability of sphere and spherical shells	19
2.5 Instability of conical caps and conical frusta	20
2.6 Instability of composite shells	20
Chapter-3 Theoretical Investigations	
3.1 Introduction	22
3.2 Governing equations for axisymmetric analysis	22
3.2.1 Reissner's theory	23
3.2.2 Field equation	24
3.2.3 Equations at the apex	26

5.2.1	CS100 Models	69
5.2.2	CS30 Models	70
5.2.3	CS60 Models	71
5.2.4	CS80 Models	71
5.3	Comparison of theoretical and experimental results	72
Chapter-6 Conclusions and Recommendations		
6.1	Conclusions	76
6.2	Recommendations for future work	77
References		79
Appendix A: Programming Features		
A.1	General features	93
A.2	Treatment of boundary conditions	94
A.3	On the use of the program	95
A.4	Output of the program	98
A.5	Table of input-output variables of the program	99
Appendix B: Program Listing		101
VITA AUCTORIS		148

**1.1 SHELL STRUCTURES**

The whole nature may be considered as a museum of shells. Every cell in a biological element is a shell. Thus structures like bamboos in the bush, eggs on the dining table and snails in the lawn are all shell structures. Shell elements, in general, can transmit the surface load primarily through the in-plane membrane forces by virtue of their curved surfaces, without the action of bending or twisting. This property makes them, as a rule, a much more rigid and more economical structure than a plate. Consequently, shell elements are indispensable parts in many engineering structures. Man-made shell structures are now widely used in many modern industries for these high load carrying capacity, especially the aerospace, nuclear, marine and petrochemical industries. Dramatic and sophisticated uses of shells are currently being made in missiles and space vehicles, submarines, nuclear reactor vessels, refinery equipment, and the like.

1.2 AXISYMMETRIC SHELLS

The load sustaining capacity of a shell-structure is strongly influenced by the shape of the shell. So scientists worked a lot on different shell geometry. The geometries so far considered are mainly standard geometric surfaces, developed by the generation of standard geometric curves around a straight line along a circular contour on a plane perpendicular to the axis of revolution and these are cylindrical, conical, spherical or ellipsoidal shells. Shells that are symmetric about their axis of revolution are known as axisymmetric shells and are in wide use as their fabrication techniques are very simple. Examples of axisymmetric shells are circular cylinder, cone, sphere, paraboloid, ellipsoid, etc. Shells that are combination of two or more axisymmetric shells having the same axis of revolution are also axisymmetric.

1.3 COMPOSITE SHELLS

Shells in most cases are found to be the combination of two or more simple axisymmetric shells like cylindrical, conical, spherical, ellipsoidal, etc. These combinations of shells of different geometry are termed as composite shells. Even when plates are used at the open ends of a

cylinder or a cone or a conical frustum to close the openings, the whole shell with its end-plates becomes a composite shell. Thus the cylindrical boiler drum with its spherical end-caps, the hull of a submarine, the fuselage of an aeroplane, etc. are all composite shells. A schematic diagram of a submarine hull, representative of composite shells is shown in Fig. 1.1.

1.4 USE OF COMPOSITE SHELLS

Starting from the small beverage can to the giant sea-going vessels, almost all the practical shells are composite shells. Fractionating towers in the petrochemical industries, jacketed boiling pans in the pharmaceutical industries, pipe lines for fluid flow, containers of liquid gaseous products, rockets, missiles, hulls of submarines are the examples of important practical composite shells.

Compositing of shells either becomes essential to cope with physical situation or is done intentionally to improve functional capability of shells. The unstiffened sphere is the most efficient containment structure for high external pressure and is indeed the basic pressure hull form for submersibles. It can lead to different interior arrangements and incurs large hydrodynamic drag which can be overcome by elongating the external form, for example, with fair streamlined outer casing structure.

Speed, noise and draft requirements dictate a cigar hull for naval submarines, incorporating a cylindrical pressure hull, perhaps with shallow conical transitions, and having torispherical or hemispherical ends. Ideally, a submersible that is to be used for dry transfer operations should have two adjoining pressure hulls -separated by a lock arrangement to avoid loss of the vehicle in the event of a mating seal failure. One of the pressure hulls is for control systems and pilots and the other for transfer operations. The transfer hull may in some cases be cylindrical to maximise the volume for personnel and materials. The US Navy's Deep Submergence Rescue Vehicle (DSRV) are trispheres. Recent trends show an increase in diver lockout and dry transfer operations.

1.5 INSTABILITY OR BUCKLING OF SHELLS

Shells are mainly designed on the basis of stress sustaining capacity of the shell materials. In this type of design approach stress analysis alone guides the dimension of the shell structure. With the

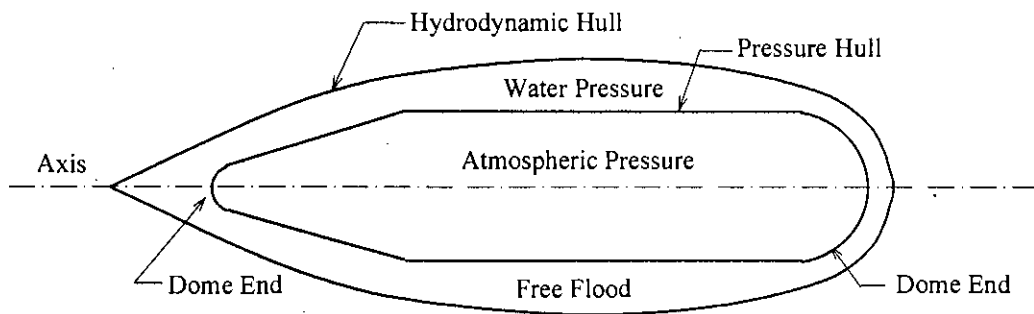


Fig. 1.1: Submarine pressure hull (conventional)

advent of time, newer materials are coming with high strengths. These materials, when used in shell structures, give thinner shells. But thin shells are found to fail due to instability or buckling. Buckling, to most laymen, evokes an image of failure of a structure which has been compressed in some way. In shell structure, membrane stiffness is in general several orders of magnitude greater than the bending stiffness. So shells can absorb much higher membrane strain energy without deforming much; and to absorb an equivalent amount of bending strain energy it needs to deform much more. In thin shells if the load is gradually increased in such a way that most of its strain energy is stored in the form of membrane compression then at a certain load level situation may arise when the stored membrane energy gets converted to bending energy, then large deflection of the shell must take place to accommodate the conversion process. This large deflection generally takes place suddenly without any notice and the shell fails in a process called buckling. The concept of stability of equilibrium is thus a strongly intuitive one, and it consequently arose quite early in the development of classical mechanics. The work of Euler [48] in this line appeared in 1744, and the contribution of Lagrange [88] in 1788. A century later a general bifurcation theory was sketched by Poincare [117] in 1885, and the definition of stability was given mathematical rigor in the treatise of Liapunov [91] in 1892.

If at any level of external cause (in the form of displacement, velocity, force etc.), a structure can sustain a small disturbance from its equilibrium state, then the structure is said to be in stable equilibrium at that level of external cause. It should be noted that sustaining the disturbance means the structure will oscillate with a small amplitude about its equilibrium position. On the other hand, if the structure does not go back to its original equilibrium position or vibrate with ever increasing amplitude due to the disturbance, then the structure is said to be in an unstable equilibrium state at that level of external cause. If the structure remains in the disturbed state without vibration, then the equilibrium is referred to as the neutral equilibrium state.

A close assessment of the critical load for simple mechanical stability models reveals that the system maintains its stable equilibrium states as long as the work done due to internal resisting forces is greater than that due to the external load for any disturbance from the equilibrium position. In other words, it is the balance between the potential energy due to the internal resisting forces, which will be called internal strain energy or simply strain energy from now on, and the potential energy due to the external force, which will be called external load potential or simply load potential from now on, which accounts for the stability of the system. At a certain level of

the external cause, the internal strain energy becomes equal to or less than the external load potential, and the system reaches its unstable equilibrium state. Any disturbance to this equilibrium state will upset equilibrium or bring the system to a new equilibrium state distinct from the previous one, depending on whether the internal strain energy is equal to or less than the load potential. In fact, these are the alternate statements of the energy method used to confirm the mechanical stability of a system.

1.6 ANALYSES OF SHELLS

In the earlier section of this chapter it has already been mentioned that buckling commences with a large deflection of a structural element. Large deflection of structural elements when considered in the governing equations introduces nonlinearity. As the use of shells gains momentum, more and more sophisticated mathematical analysis of shells are being sought. Shell structures can undergo a substantial amount of deformation before failure. This feature of shells submits them to the domain of non-linear mathematical analysis. The nonlinearity is introduced into the governing equations of elasticity in three ways:

- a. through the strain-displacement relations
- b. through the equations of equilibrium of a volume element of the body, and
- c. through the stress-strain relations.

In (a) and (b) the retention of non-linear terms is conditioned by geometric considerations, that is, the necessity of taking into account the angles of rotation in determining the changes of dimension of a line element and in the formulation of the conditions of equilibrium of a volume element. On the other hand, the non-linear terms appear in the third set of equations (c) if the material does not behave in a linearly elastic fashion.

Hence, there are two types of nonlinearity:

- i. geometric, and
- ii. material

In the problems of shell structures, the angles of rotation can be large, but the strains can be quite elastic. An example of this type of problem is the bending of a thin steel strip. It is well known that strips of high strength steel become straight without traces of residual deformation when released from a state of deformation with their ends brought together. This bears witness to the fact that in these strips, even for large displacement and angle of rotation, the stresses do not exceed the yield strength. Thus, many shell structures belong to a class of problems which are physically linear but geometrically non-linear.

The fact that linear shell analysis fails to give proper information about the shell stresses and deformations in many problems can be seen in papers on the non-linear shell analysis [49, 54, 64, 65, 72, 107, 123-125, 131, 152, 167, 168, 172-176, 187-189, 191]. For this reason, the use of non-linear theory has become rather widely accepted as a plausible basis for predictions of elastic strengths of shells of various geometries. Most of the papers currently found in the literature are concerned with the shells of revolution.

Numerous investigations have employed the basic concept of finite deflection analysis of Donnell [41] to establish collapse loads of cylindrical shells subjected to various loadings. Finite deflection analysis has also been successful in offering reasonable predictions of the elastic buckling loads of shallow spherical caps subjected to uniformly distributed external pressure. Kaplan and Fung [74] have presented a perturbation solution to the non-linear equations that agrees quite well with the results of their experiments for very shallow, clamped edged shells. Archer [11] extended the results of Kaplan and Fung to a greater range of shells. As can be seen from recent papers, very extensive work has been done in this field [64, 65, 72, 74, 125, 167, 168, 189]. Ball [14] has considered the problems of arbitrarily loaded shells of revolution and obtained solution for a clamped shallow spherical shell, uniformly loaded over one-half of its surface. A number of papers based on the non-linear analysis of stiffened shells, multilayered shells and sandwich shells can also be found in the current literature [6, 60, 77, 99, 101, 111, 118, 122, 134, 139, 183]. Based on Reissner's [126] large deflection analysis for general shells of revolution, Uddin [171] has presented large deflection analysis of composite shells of revolution and obtained extensive results for various pressure vessel problems [171-176]. Haque [61] analysed the stability of semi-ellipsoidal shells under external pressure. Rahman [119] extended this analysis to include imperfect shell geometry. Ali [7] analysed the stability and stresses of conical pipe reducers. Rahman extended these analysis to include stability of parabolic reducers [120]

while Dutta extended it to the case of toroidal reducers [44]. In all these cases the predictions of these theories are in better agreement with experimental evidence than those of the classical investigations based on infinitesimal deformations.

1.7 PRESENT STATE OF ANALYSES

Due to the very nature of the response of shell like structures under loading, their analyses, specifically their stability analyses, are based on the non-linear mathematical techniques. Unfortunately, the majority of such large deflection and stability problems of practical structural components cannot be solved in closed form. Therefore, one has to resort to approximate analytical and/or numerical discretization techniques for their solution. Prior to the advent of digital computers, various approximate analytical techniques were the standard tools for the non-linear analysis of structures.

The widespread availability of high speed computing machines, the fascination with numerical techniques due to their versatility in handling complex structures (e.g. shells with cutouts and stiffeners), and the simplicity of computer implementation have resulted in a relative stagnation in the development of effective analytical techniques. Analytical techniques have some advantages in providing physical insight into the nature of response. Moreover, analytical techniques can be used in conjunction with partitioning schemes for non-linear analysis of individual components of practical (geometrically composite) structures.

The most frequently used approximate analytical and numerical techniques in solving non-linear differential equations are :

1. asymptotic integration [103, 106, 126, 131]
2. perturbation techniques [108, 179]
3. Newton's method [64, 168]
4. method of power series expansion
5. hybrid analytical technique [3]
6. direct numerical integration [54, 92]
7. finite difference method [20, 192]
8. finite element method [16, 20, 155, 194]

9. method of multisegment integration [71,72]

In addition to the methods mentioned above, there are some others, namely, "Reversion Method" [39, 116], "Variation of Parameter" [39, 98, 106], "Averaging Methods Based on Residuals" - (a) Galerkin's Method [39] and (b) Ritz Method [39], and the principle of harmonic balance.

Asymptotic integration is not a general method and its scope of application is very limited as can be seen from Refs. [106, 126, 131]. Reissner discusses some of the solutions and limitations of this method in Ref. [126]. In the application of this method, the solution is expressed in the form of a series where the terms of the series are the inverse powers of the largest parameter in the differential equations [126]. Determination of the terms of the series becomes extremely difficult and the solutions generally contain only the first term approximation.

In the perturbation method, the fundamental unknowns are expanded in perturbation series in terms of unknown functions with preassigned coefficients. The unknown functions are obtained by solving a recursive set of differential equations which are generally simpler than the original governing equations of the problem [108, 179]. In contrast, in the Bubnov-Galerkin and Rayleigh-Ritz techniques, the fundamental unknowns are sought in the form of series of a priorly chosen co-ordinate functions (or modes) with known coefficients. Reviews of the many applications of these techniques are given in Ref. [156].

The perturbation method has two drawbacks. The first one stems from the fact that as the number of terms in the perturbation series increases, the mathematical complexity of the differential equations builds up rapidly. Therefore, for practical applications, the perturbation series has to be restricted to a few terms. The second drawback is the need to restrict the perturbation parameter to small values in order to obtain solutions of acceptable accuracy. The main difficulty of both the Bubnov-Galerkin and Rayleigh-Ritz techniques, from a practical view point, is the difficulty of selecting good co-ordinate functions (or modes) for structures with complicated geometry and/or complex response.

Newton's method for solving non-linear differential equations is the extension of Newton's method for calculating roots of algebraic equations. The approach is to express the solution as the sum of two parts; the first part is a known function and the second is a correction to the known

function. A governing equation for the correction is obtained by substituting the assumed function into the governing equations and neglecting terms which are non-linear [64]. This method does not require the perturbation parameter to be small as is necessary in the perturbation technique, but it involves the solution of a sequence of linear differential equations as in the latter. These linear equations have variable coefficients and generally cannot be solved in closed form. It is paradoxical that the greatest obstacle in solving non-linear problems is the inability to solve linear differential equations in closed form.

The hybrid analytical technique combines both the standard regular perturbation method and the classical Bubnov-Galerkin technique. The technique was shown to overcome the major drawbacks of the two parent techniques and to provide a more effective approximate analysis than either of the two techniques. Ref.[3] demonstrates the effectiveness of this technique by means of numerical examples.

The hybrid analytical technique is particularly useful for predicting non-linear response of structures with simple geometry but complex construction. Examples of such structures are ring and stringer-stiffened closed cylindrical shells and shell panels with discrete stiffener and rectangular or circular platform.

Though the direct integration approach has certain advantages, it has also a serious disadvantage, that is, when the length of the shell is large, a loss of accuracy invariably occurs. This phenomenon is clearly pointed out in Ref. [144]. The loss of accuracy does not occur from accumulative errors in integration, but it is caused by the subtraction of almost equal numbers in the process of determining the unknown boundary values. It follows that for every set of geometric and material parameters of the shell there is a critical length beyond which the solution loses all accuracy.

Finite difference methods are the most widely used techniques for solving non-linear differential equations. The advantage of the finite difference technique over direct integration is that it can avoid the above mentioned loss of accuracy. But it also has some drawbacks. Firstly, it ultimately leads to the solution of a large number of non-linear algebraic equations which have to be solved by iterative techniques and often the solution fails due to nonconvergence. Secondly, bound by the requirement of using regular mesh spacings or the condition that the grid lines must be

parallel to the co-ordinate axes, it is very much restricted to domains of regular geometry. However, curvilinear finite difference (CFD) technique, as proposed in Refs. [82-85], now relaxes these restrictions. Irregular meshes can now be employed in the analysis of shells with irregular boundary geometry.

In the literature, the structural analysis of general thin shells is one of the areas dominated by the finite element methods. One of the main advantages of using finite element methods is the flexibility in making discrete any unusual domain. However, in the course of extending the finite element methods to accommodate geometric nonlinearities, two different algorithms are generally adopted. They are namely: the linearized incremental approach and the Newton-Raphson iterative approach. The linearized incremental approach simplifies the programming works involved, but it has its own drawbacks. As linearized incremental equations are used, it is impossible to obtain the "exact" non-linear solution for a particular load level. On the other hand, the Newton-Raphson method always converges to "true numerical solutions". However, it requires numerical integration techniques [83], and the use of full Newton-Raphson procedures. As a result, various modified versions of Newton-Raphson methods appeared in the literature [16, 155].

The multisegment method of integration is the most recent method developed and used by Kalnins and Lestingi [72] to solve non-linear differential equations. This method involves:

- a. division of the total interval into a number of segments
- b. initial value integration of a system of first order differential equation over each segment
- c. solution of a system of matrix equations which ensures the continuity of the variables at the ends of the segments
- d. repetition of (b) and (c) till convergence is achieved
- e. integration of an initial value problem to obtain answers at any desired point within each segment

The main advantage of this method over the finite difference method is that the solution is obtained everywhere with uniform accuracy, and the iteration process with respect to mesh size, which is required with the finite difference approach, is eliminated. But the feature which makes this method most attractive is that any discontinuity, either in geometry or in loading, can be

easily handled by requiring that the end point of a segment coincides with the location of the discontinuity. As the integration is restricted at the beginning of each segment, the precise effect of the discontinuity is obtained by this method. Moreover, this method is the most accurate of all the numerical methods because the problem is solved in the form of a system of first order differential equations in which no derivatives of geometrical or elastic properties appear and no further numerical derivatives are essential to obtain any desired results in the calculation.

1.8 OBJECTIVES OF THE PRESENT INVESTIGATION

Though instability or buckling is a phenomenon very much related to compressive loading, in case of thin shell structures, this does not depend on only external pressure loading. There are thin shell structures which buckle even under internal pressure. A torispherical shell under internal hydrostatic pressure buckles at the knuckle of the torisphere [31-34], a thin closed spherical shell under tension at two points, diametrically opposite, also fails due to buckling. Thus thin composite shells in addition to stress analysis needs buckling analysis under all kinds of loading.

Design of thin shells on the basis of buckling is not new. Practical shells found in use are mostly composites of segments of two or more geometries. It is a common practice that, in case of shell structures which are combination of some standard shell elements like sphere, cone, cylinder, etc., the dimensions of the individual shell elements are determined on the basis of buckling of the individual segment. In doing so the effect of the junction is avoided which may have positive or negative influence on the overall buckling of the shell combination.

Uddin [171] pointed out that junctions of composite shells are usually the zones of compression. This happens even when the shells are under internal pressure. Thus the study of instability is of prime importance in case of composite shells.

Deep-sea exploration is getting importance with the advent of time. It is thought today that sea-bed is richer than land in resources. Increasing population is acting as a new dimension to sea-bed exploration. In exploring the sea-bed, composite shells would definitely act as the most ideal structures of deep-sea crafts. It is thus obvious that the study of instability of composite shell structures is getting every body's attention. Under these realities, this research program has been undertaken to study the instability of composite shells of revolution with the following objectives.

1. To develop a computer program for theoretical investigation of instability of composite shells, built-up of segment of different geometries, based on the non-linear shell theory of Reissner. (Example: Cylindrical and Spherical, Biconical, Conical and Cylindrical, etc.)
2. To study the variation of instability pressure against different parameters of shells. (Like Thickness ratio, apex angle of cone, etc.)
3. To develop a set-up for experimental investigation of buckling pressure of composite shells.
4. To compare theoretical and experimental values of critical pressures for determining the effect of manufacturing imperfections on the critical pressure.

In achieving these objectives the stability analyses of the following composite shells of revolution are carried out.

- a) Cap-cone composite shells
- b) Cup-cylinder composite shells
- c) Dome-cylinder composite shells

Geometry of these three types of composite shells are presented in Fig.1.2. The present theoretical analysis is based on the governing equations of Reissner's large deflection theory and the solutions are obtained by using the method of multisegment integration. Experimental investigation include the study of buckling of the cap-cone composite shells.

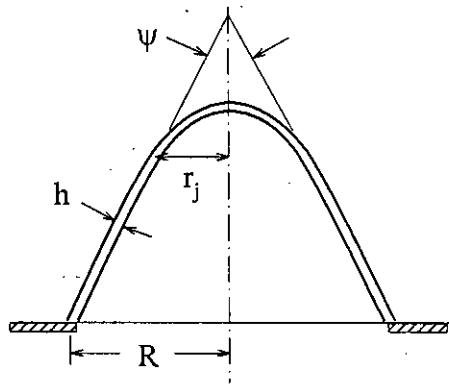


Fig. 1.2a: Schematic diagram of a cap-cone composite shell.

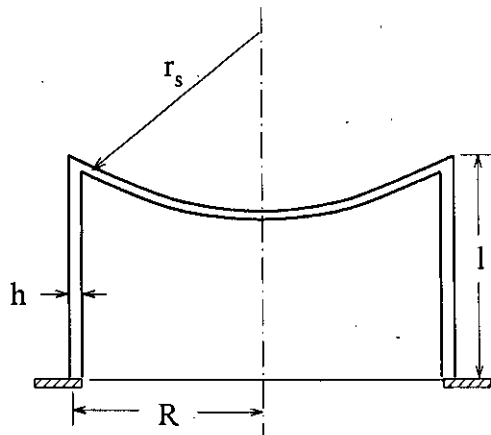


Fig. 1.2b: Schematic diagram of a cup-cylinder composite shell.

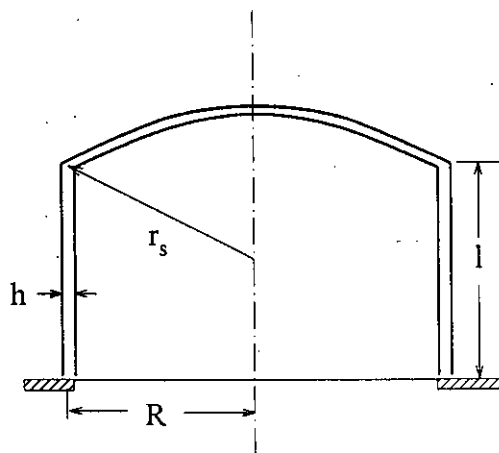


Fig. 1.2c: Schematic diagram of a dome-cylinder composite shell.

CHAPTER 2

LITERATURE REVIEW

2.1 REVIEWING OF SHELL THEORIES

The theory of shell structures has existed as a well-defined branch of structural mechanics for about a hundred years, and the literature is not only extensive but also rapidly growing. This growth has two main aspects- the first one is the development of shell theories based on various assumptions and approximations on different geometrical configurations of the shell meridian, and the second is the development of various exact and approximate analytical and numerical methods for solving these equations. The present review of literature is kept confined to only the non-linear theories of thin shells as the problems dealt with in this thesis, the stability of composite shells, lie entirely in the domain of the large deflection theories, as pointed out by Uddin [171].

Use of the non-linear strain-displacement equations in the development of shell theories is motivated by the need for an accurate prediction of load-deflection curves, analysis of stability and post-buckling behaviour, and natural vibration data for the design of shell structures.

Consideration of geometric nonlinearity in shells is originally due to Donnel [41], von Karman [180,181], Marguerre [100] and Mushtari [105], among others. Following these pioneering works several generalisations and modifications of the theories appeared in the literature. The geometric nonlinearity in shells is accounted in three different levels:

- i. The von Karman type nonlinearity that accounts only for the products and squares of the derivatives of the transverse deflection in the strain displacement equations;
- ii. The moderate rotation theories that account for moderate rotation terms;
- iii. The large rotation theories that account for large rotations.

Full non-linear theories are those which do not neglect any non-linear terms in the strain-displacement equations. However, full non-linear theories are not only complex but not warranted

in the analysis of most shell structures. As a result, several authors attempted to present non-linear shell theories at different stages of approximations.

The earliest work of some generality is Marguerre's non-linear theory of shallow shells [100]. Donnel [41] developed an approximate theory specially for cylinders and suggested its extension for a general middle surface. The result, a theory for what might be termed "quasi-shallow shells", has been worked out by a number of authors, notably Mushtari and Galimov [105].

The earliest work of a completely general nature appears to be the papers by Synge and Chien [157] followed by the two papers of Chien [37, 38]. The theory of shells developed by Synge and Chien avoids the use of displacements as unknowns in the equations. The theory is deduced from the three-dimensional theory of elasticity and then, by means of series expansion in powers of small thickness parameter, approximate theories of thin shells are derived.

Another general formulation of the problem is worked out by Ericksen and Truesdell [46]. They developed it as a two dimensional theory instead of attempting to deduce it from three-dimensional theory of elasticity. They were able to account for transverse shear and normal strains and the rotations associated with couple stresses. The two-dimensional approach to shell theory really evades the question of the approximations involved in the descent from three-dimensional, but this seems to be a virtue rather than a defect. Such questions are effectively isolated and shown to belong to the part of the theory in which constitutive relations are established.

Novozhilov [110] has presented an incomplete treatment of the general large deflection theory of thin shells based on the assumption of small middle surface strains. Peter [115] presented a quasi-linear approach to the rotationally symmetric deformations of thin elastic shells of revolution. In this approach, the shell strains and rotations are assumed to be small but, contrary to the approach of linear shell theory, the shell equilibrium conditions are fulfilled on the deformed shell.

Other developments which also employ linear constitutive relations are founded upon the Kirchhoff hypothesis and often contain other approximations. Among these are Reissner's [126, 127] formulation of axisymmetric deformation of shell of revolution and the more general works

of Sanders [136] and Leonard [89]. Beginning with the three-dimensional field equations Naghdi and Nordgren deduced an exact, complete, and fully general non-linear theory of elastic shells founded upon the Kirchhoff hypothesis.

Several non-linear theories for thin shells have been derived in increasing stages of approximations. In most cases, these are first approximative theories in the sense that transverse shears and normal strains are neglected. Such approximations and omissions are justified because the exact and general equations characterising the deformation of an elastic shell, even under the Kirchhoff hypothesis, are fairly complex and discouraging from the point of view of practical applications. However, as may be seen in the literature, with the advent of high speed computing machines and corresponding development and adaptation of efficient and versatile numerical techniques, some authors [17, 76, 122, 137, 171, 187] are tempted towards the analysis of more comprehensive and general non-linear shell theories and coming out with useful results.

2.2 REVIEW OF SHELL ANALYSIS

The majority of the large deflection and stability problems of practical structural components cannot be solved in closed form. Therefore, one has to resort to approximate numerical discretization techniques for their solution, leaving analytical techniques limited to comparatively simpler structural elements.

Ahmed [3] presented a two-step hybrid analytical technique for predicting the non-linear response of structural elements. They also discussed in length the potential of the proposed hybrid technique for non-linear analysis of structures.

The effectiveness of this technique was demonstrated by means of three numerical examples :

- i. non-linear axisymmetric response of clamped shallow spherical cap;
- ii. large deflection analysis of laminated anisotropic plate subjected to uniform transverse loading;
- iii. non-linear axisymmetric response of an isotropic circular plate subjected to combined uniform and concentrated load.

Based on extended Sander's shell theory, that accounts for the shear deformation and the von Karman strains, Reddy and Chandrashekara [123] presented numerical results for the laminated cylindrical and doubly curved shells. Simitses et al. [146] presented a comparison between analytical results of critical loads and experimental results of buckling loads for imperfect, laminated cylindrical thin shells. The loading consists of uniform axial compression and torsion, applied individually and in combination. The theoretical results are obtained from solution methodology based on non-linear kinematic relations, linearly elastic material behaviour, and the usual lamination theory.

In Ref. [159] an analytical formulation is made extending Reissner-Naghdi theory and numerical solutions are obtained for the elasto/visco-plastic deformation of multilayered cylindrical shells subjected to asymmetrical loading.

In Ref. [153] a modified mixed variational principle is established for a class of problems with one spatial as the independent variable. The specific applications are on three-dimensional deformations of elastic bodies and the nonsymmetric deformation of shells of revolution. The feature is the elimination in the variational formulation of the stress components which can not be prescribed on the boundaries.

Among the numerical techniques used in non-linear shell analysis, the finite element method is used rather extensively due to the flexibility in making discrete any unusual irregular domains. Teng and Rotter [163] developed a finite element formulation for elastic-plastic large deflection analysis of shells of revolution. Here, in place of widely used relations of Donnel, Novozhilov or Sanders, more comprehensive non-linear thin shell strain-displacement relations are used, which account for the nonlinearity caused by in-plane displacements. Unlike most other non-linear shell formulations, the in-plane shearing is included throughout this treatment. As asserted by the authors, this formulation contains most of the best features of non-linear finite element analysis currently available in the literature, together with some new numerical schemes to improve the capability, accuracy and speed of the computation.

In Ref. [113] the occurrence of dynamic buckling of thick rings responding to an impulse load is investigated using both analytical and finite element methods using the computer code ADINA. The results show that the non-linear solutions by the finite element method predict a significant reduction in the amplitude of buckling response and an increase in the predominant wavelength response with time in comparison to the linear analytical solution.

Kwok [82-85] presented a curvilinear finite difference energy approach to the geometrically non-linear analysis of general thin shells. This approach relaxes the requirement of usual finite difference method of using regular mesh spacings or the requirement that the grid lines must be parallel to the co-ordinate axes. Irregular meshes can now be employed in the analysis of shell with an irregular boundary geometry without any difficulty. The author developed a software named NAOSIS (Non-linear Analysis of Shallow Shells) based on this method. As asserted by the author, the main aspects of this finite difference formulation are firstly, its ability to implement the most general non-linear strain-displacement relationship directly in a tensor code; secondly, its ability to model any arbitrary shell geometry; and thirdly, its capability to use irregular computational meshes in a finite difference sense.

Recent efforts include the development of a number of general purpose computer programs [9, 29, 30, 104] for the linear and non-linear analysis of general shells of revolution. These programs are based either on finite element or on finite difference method of analyses. An overview of the current capabilities of some computer programs that can be used for the solution of non-linear structural and solid mechanics problems is available in Refs. [2, 16, 144]. A critical review of two such programs, namely, BOSOR4 [30] and BOSOR5 [29], is presented in Refs. [175, 176]. Here the authors have discussed precisely the causes of their disagreements with experimental evidences.

A few of the latest investigations on the instability of structures are reported in Refs. [7, 44, 78, 79, 113, 120, 130, 141, 145, 176].

Based on Reissner's [126] large deflection theory of shells of revolution, and using multisegment method of integration, Uddin [171] has developed a computer program for the analysis of

composite shells of revolution. He has found extensive numerical results on spherical, ellipsoidal, conical and composite head pressure vessels based on both the linear and non-linear theories and also obtained buckling pressure of general spherical shells and semi-ellipsoidal shells [171-176]. In all those investigations, he has exposed the conservativeness of linear theory and demonstrated the superiority of non-linear analysis over linear analysis. Later on, using the same program, Haque [61, 176] has made buckling analysis of ellipsoidal shells of revolution under external pressure and Rahman [119] has extended it to the case of imperfection in geometry.

Later on, Ali [7] carried out the stability and stress analysis of general truncated conical shells used as pipe reducers, modifying Uddin's original program. In his work, Ali [7] pointed out that the critical load for a conical reducer decreases almost linearly with increasing apex angle of the conical frusta.

So far, stability analysis which inherently involves complex non-linear mathematics has been mostly confined to shallow shells or circular plates. This is due to the fact that the non-linear equations of shells could be solved only when the simplifications pertaining to the shallowness of the shell were made, as pointed out by Uddin [171]. The simplified equations are then solved by different methods mentioned in the introduction. Also, some of the analyses have been made with the assumptions like the predetermined buckling modes of the structures [42,43] which may or may not exist at all.

Literature in the field of shell buckling prior to 1974 was mostly dealing with shells of simple geometry like sphere or spherical cap, cone and cylinder. These simple shells are widely used in many industries and still researchers are working with these shells. Recent trend is to improve the instability load of these shells using latest composite materials. Other than the composite users some are trying with different stiffeners. Some very important papers related to buckling of simple and geometrically composite shells are presented in the ensuing sections.

2.3 INSTABILITY OF CYLINDRICAL SHELLS

Among the different shell structures cylindrical shell has received the highest attention of the researchers because of its simple geometry. Further, its fabrication is very easy, it can

accommodate more space as pressure hulls of submarines and it is more manoeuvrable than any other types of shells.

Cylindrical shells in practice are used under different load conditions. Axial compressive, external lateral pressure, and torsional loading of cylindrical shells have undergone extensive investigation, both theoretical and experimental. Buckling of thin cylindrical shells under axial compression has received far more attention than most problems in structural mechanics because of the extraordinary discrepancy between test and theory which remained unexplained for so many years. Brush and Almroth [20] discussed this discrepancy with reference to Esslinger [47] and Hoff [62] and concluded that cylindrical shells under axial compression are highly sensitive to imperfections which were not accounted by the early investigators like Flugge [53], Lundquist [94] and Donnell [41]. A similar conclusion was also drawn by Dyme and Hoff [45] from a study of axially compressed cylindrical shells with small imperfection. Esslinger presented photographs from high speed movie in connection with a series of experiments with cylindrical shells under axial compression. His pictures show that the final shape of the buckles does not resemble the buckle mode at incipient buckling, the main objective of study in bifurcation buckling analysis.

In Ref. [20] theoretical and experimental buckling loads for four kinds of loading of cylindrical shells, namely, axial compression, torsion, uniform lateral pressure and hydrostatic pressure have been compared and conclusion has been made that load reductions for other methods of loading are somewhat less severe than those for axial compression.

Imperfection sensitivity of isotropic cylindrical shells forced the scientists to research with orthotropic, layered composite and stiffener stiffened cylindrical shells. Relevant literature [1, 6, 13, 80, 146, 148, 150, 151, 185] show that these cylinders are less sensitive to imperfections and theoretical results of these shells are in good agreement with experimental results. Experimental and theoretical results for buckling of axially compressed cylindrical shells with various wall construction presented by Bushnell [28] with reference to Almroth et al. [8] gives the picture of superiority of stiffened shells over monocoque shells at a glance.

Other than the above mentioned studies, cylinders with special features [19, 27, 51, 70, 86, 90, 96, 121, 132, 133, 135, 193] like cylinders under wind load, cylinders with different cut-outs or

holes, cylinder under dynamic or thermal load, etc., have also undergone buckling analysis and still receiving scientists' interest.

2.4 INSTABILITY OF SPHERE AND SPHERICAL SHELLS

From structural point of view, thin-walled spherical shell can withstand high uniform external pressure most efficiently, but in practice this is seldom used because of its vivid disadvantages associated with fabrication and use. Deep-diving bathyspheres or bathyscaphs are generally constructed with this shape. Kaplan [75] has given a thorough survey of buckling of spherical shells subjected to uniform external pressure.

Solution based on classical theory for the buckling of complete spherical shells under uniform external pressure available from different authors [68, 166, 170] are not in good agreement with the experimental results because of high imperfection sensitivity of the spherical shells. Other than the external loading of spheres, internal pressure loading also causes buckling. This generally happens in very large spherical tanks used for transporting liquid natural gas supported on short cylindrical shells near the equator. Pedersen and Jensen [112] have studied this problem in 1975. Buckling in this case occurs due to hoop compression that develops near the support.

Part of a spherical shell, known as a spherical cap, is also in wide use. Ends of cylindrical or truncated conical shells are generally closed with spherical caps in place of flat plates. The reason for using spherical caps in place of flat plates is that flat plates have no meridional curvature and that is why they resist the effect of pressure in flexure and in order to have equal strength to that of the attached cylindrical or conical shell their required thickness may be over ten times that of the spherical cap which is used as end-closure.

Spherical cap has been drawing much attention of the scientists for so many years with almost the same intensity and frequency as the axially compressed cylinders. In Ref. [20] critical pressure for a spherical cap under uniform external pressure has been presented, which is the same as that given for a complete spherical shell. Like complete spherical shells, spherical caps buckle under much lower pressure than the theoretical pressure. For practical applications, empirical formula as developed by Klopel and Jungbluth [81] from extensive experimental results are in common use.

As isotropic spheres and spherical caps are sensitive to imperfections, these shells have also undergone extensive research for evaluating the effects of imperfections, stiffeners, composite materials, etc. [15, 23, 24, 40, 58, 69, 73, 163, 169] with various types of loadings [11, 18, 25, 26, 36, 52, 59, 93, 114, 167, 178, 184, 192], relevant to practical uses.

2.5 INSTABILITY OF CONICAL CAPS AND CONICAL FRUSTA

Like the cylindrical and spherical shells, conical shells are also found in wide use. Specially, conical shell element is used as a transition piece between two cylindrical shells of different diameter or between a cylindrical shell and a spherical-cap.

Most of the theoretical and experimental works related to conical shells are with truncated conical shells, known as conical frusta, either under axial compressive load or uniform hydrostatic pressure [7, 66, 67, 87, 142, 147, 160, 164]. Conical shells have also undergone research related to buckling with other types of practical loading like torsion, thermal loading, combination of axial load and lateral pressure, dynamic loading, etc., along with different types of composite materials [4, 5, 42, 43, 95, 143, 161, 162].

2.6 INSTABILITY OF COMPOSITE SHELLS

Shells are mostly designed on the basis of individual shell elements, but in practice, shells are found to be combinations of two or more different geometries like cylinders with spherical caps, torispheres, cylinders with conical end-caps, etc.

Available works [22, 63, 154] on shell instability mostly presents buckling behaviour of shells of simple geometry like cylindrical, spherical, conical, etc., either with stiffeners or without any stiffener. Arbocz [10] and Brush [20] presented an extensive literature survey on shells up to 1975 but have not reported any study of buckling of combination of shells. Singer [149] presented a report of around one hundred pages on buckling experiments on shells in 1982. His report covers buckling experiments on shells from 1957 to 1981. Most of the experiments

presented in his report are on shells of simple geometry with or without stiffener. Only four of his references [24, 67-69] are related to experiments on buckling of composite shells.

In a recent paper Faulkner [50] showed a few uses of composite shells in different submersibles with some design guide-line. His design guide line is still based on segments of simple geometry of the combinations. The design guide-lines presented in BS 5500 [21] are in-line with that of the Faulkner's. BS 5500 designs torispherical shells only on the basis of the spherical cap of the combination, disregarding any effect of the knuckle radius of the toroidal section. Galletly [57] in 1987 showed that this sort of design is inefficient and can lead to vulnerable design in case of shallow torispheres.

During the last two decades, only a few scientists [12, 55-58, 129, 130, 138] have come forward with the problem of buckling of composite shells as a whole. Mainly two groups of research workers, the Liverpool group and the Lockheed group, are involved in this field with a Variational Finite Difference (VFD) based computer program called BOSOR. A critical review of two versions of BOSOR namely, BOSOR4 [30] and BOSOR5 [29] is presented by Uddin in Ref. [175]. Details of some BOSOR analyses along with experimental supports are presented below.

Galletly et. al. [55] studied cylinder cone combinations with BOSOR3 and BOSOR5 in 1974. The study included both analysis and experiment of six different cylinder-cone combinations with one thickness ratio and three different cone angles of 45° , 60° and 75° . Each of the cones was combined to two different cylinders of length to diameter ratio, (L/D), of 0.5 and 1.0. Diameters of all the cylinders are the same. Experimental results are found in good agreement with the analysis. Some of the experimental results, though very close to the BOSOR5 results, are found to be higher than the BOSOR5 results. Analytical results for L/D = 1.0 and cone angle of 45° and 60° are the same. Also for cone angle of 75° , they found that the results are the same for L/D ratio of 0.5 and 1.0.

THEORETICAL INVESTIGATIONS

3.1 INTRODUCTION

'Classical' or 'bifurcation' technique pertaining to a secondary mode of deformation needs solution of non-linear governing equations for a structure. In the present analysis geometrically composite shells of revolutions are studied for critical external pressure. Reissner's [126, 127] large deflection theory of shells of revolution is employed here for the determination of both stress and stability of a shell. The governing equations consist of three sets of equations, namely, the equilibrium equations, the constitutive equations and the kinematic equations. The equilibrium equations relate the external load with the internally induced stress and bending moment resultants. The constitutive equations are for linear stress-strain relations of the shell material. And the kinematic equations relate the internal strains with the physical deflections of the shell surface. These three sets of equations, together with the appropriate boundary conditions, constitute the mathematical embodiment of the problem.

3.2 GOVERNING EQUATIONS FOR AXISYMMETRIC ANALYSIS

The external load applied to a shell is resisted by the membrane stress as well as the internal resisting couples, that is, the shell wall is subjected to the combined action of stretching and bending. In general, the shell wall is a three dimensional body. But, the use of Kirchoff's hypothesis reduces the shell analysis to a two dimensional one. Further, in the case of axisymmetric deformations of shells of revolution, which comprise the majority of shells in practical use, the analysis becomes a one dimensional problem. Again, the analysis of the problem of shell structures is dominated by the geometry of the shell surface through the kinematic relations and the equilibrium equations. Therefore, as can be seen from the literature, different authors have attempted to present different shell analyses including the purely stretching 'membrane' theory, linear membrane and bending theory and the finite deflection 'non-linear' shell analyses for shells of varied configurations. But the large deflection theories can predict stressed states of a shell more realistically. Among the large deflection theories, Reissner's theory and relevant governing equations are much more involved and

comprehensive. As such Reissner's large deflection theory has been used in the present analysis and presented in following section.

3.2.1 Reissner's Theory

The basic equations of Reissner's theory of finite axisymmetric deformations of shells of revolution which form the basis of this analysis are presented here for ready reference.

The equation of the meridian of the shell is written in the parametric form as (Fig. 3.1),

$$r = r(\xi), \quad z = z(\xi) \quad (3.1a)$$

where ξ is the distance measured along the meridian of the axisymmetric shells.

The angle ϕ of the tangent to the meridian curve is given by

$$\cos\phi = r' / \alpha, \quad \sin\phi = z' / \alpha \quad (3.1b)$$

where primes denote differentiation with respect to ξ and α is given by

$$\alpha = [(r')^2 + (z')^2]^{1/2} \quad (3.1c)$$

The principal radii of curvature of the middle surface of the shell are given by

$$R_\xi = \alpha / \phi', \quad R_\theta = r / \sin\phi \quad (3.1d)$$

With reference to Fig. 3.2, the equation of the deformed middle surface is written in the form,

$$r = r_o + u, \quad z = z_o + w \quad (3.2a)$$

where the subscript "o" refers to undeformed middle surface and the quantities u and w are, respectively, the radial and axial components of displacements.

The angle enclosed by the tangents to the deformed and undeformed meridian, at the same material point, is given by

$$\beta = \phi_o - \phi \quad (3.2b)$$

With the above definition of displacements and rotation, the strain components and curvature changes of the deformed middle surface are given by the following equations

$$\varepsilon_\xi = (\alpha - \alpha_o) / \alpha_o = (\cos\phi_o / \cos\phi)(1 + u' / r'_o) - 1 \quad (3.2c)$$

$$\varepsilon_\theta = u / r_o \quad (3.2d)$$

$$k_{\xi} = -(\phi' - \phi'_0) / \alpha_0 = \beta' / \alpha_0 \quad (3.2e)$$

$$k_{\theta} = -(\sin \phi - \sin \phi_0) / r_0 \quad (3.2f)$$

The equation containing the axial displacement component w is introduced as

$$w' = \alpha \sin \phi - z'_0 \quad (3.2g)$$

With the definition of stress resultants and stress couples as shown in Fig. 3.2 and Fig. 3.3, the three equations of equilibrium are written as

$$(rV)' + r\alpha P_v = 0 \quad (3.3a)$$

$$(rH)' - \alpha N_{\theta} + r\alpha P_H = 0 \quad (3.3b)$$

$$(rM_{\xi})' - \alpha \cos \phi M_{\theta} + r\alpha(H \sin \phi - V \cos \phi) = 0 \quad (3.3c)$$

Equation (3.3a) is the condition of force equilibrium in the axial direction, Eqn. (3.3b) the condition of force equilibrium in the radial direction, while Eqn. (3.3c) is the condition of moment equilibrium about circumferential tangent.

With the assumption that the behaviour is elastic, the relations between strains and stress resultants are given by

$$C\varepsilon_{\xi} = N_{\xi} - \nu N_{\theta}, \quad C\varepsilon_{\theta} = N_{\theta} - \nu N_{\xi} \quad (3.4a)$$

$$M_{\xi} = D(k_{\xi} + \nu k_{\theta}), \quad M_{\theta} = D(k_{\theta} + \nu k_{\xi}) \quad (3.4b)$$

where $C = Eh$, $D = Eh^3/[12(1-\nu^2)]$, and h is the thickness of the shell. The radial stress resultant H and axial stress resultant V are related to N_{ξ} and transverse shear, Q , as follows:

$$N_{\xi} = H \cos \phi + V \sin \phi, \quad Q = -H \sin \phi + V \cos \phi \quad (3.4c)$$

3.2.2 Field Equations

The order of the system of equations (3.2-3.4) is six with respect to ξ , and consequently it is possible to reduce Eqns. (3.2-3.4) to six first-order differential equations which involve six unknowns. In the following derivation the six fundamental variables are taken as u , β , w , V , H , M_{ξ} and the differential equations are expressed in terms of these variables. The independent variable ξ is taken as the distance measured from the apex along the meridian of shell so that the differential equation can be used for all possible geometries of the meridian. With this definition of ξ , from equation (3.1c), it is found that

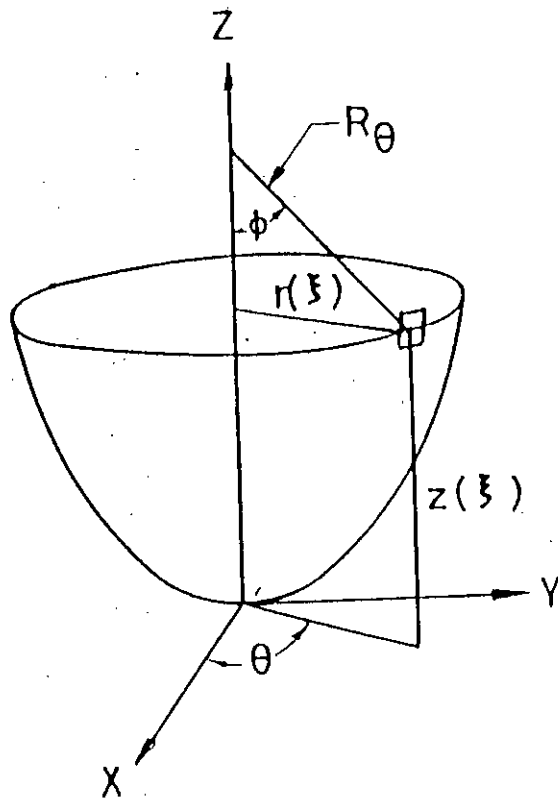


Fig. 3.1: Middle surface of shell.

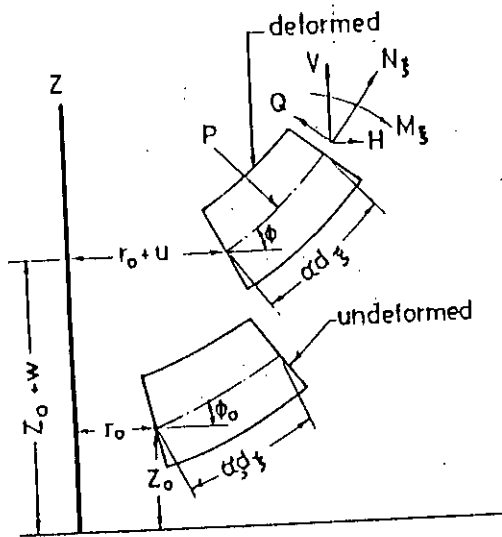


Fig. 3.2: Side view of elements of shell in deformed and undeformed states.

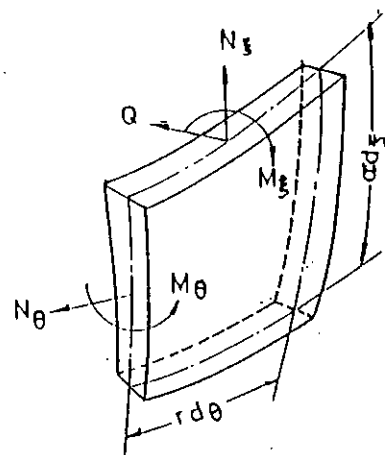


Fig. 3.3: Elements of shell showing stress resultants and couples.

$$\alpha_o = \left[(r'_o)^2 + (z'_o)^2 \right]^{1/2} = 1$$

The geometry of the meridian is given by

$$r_o = r_o(\xi) \quad (3.5a)$$

$$\phi_o = \phi_o(\xi) \quad (3.5b)$$

which is not yet specified.

The following equations are written from the previous section in such an order that, when evaluated serially, they are in terms of the fundamental variables. This is done in order to keep the fundamental set of differential equations as simple as possible.

Rewriting Eqns. (3.2d), (3.2a), (3.2b), (3.2f), (3.4c), (3.4b) in that order,

$$\varepsilon_\theta = u/r_o \quad (3.5c)$$

$$r = r_o + u \quad (3.5d)$$

$$\phi = \phi_o - \beta \quad (3.5e)$$

$$k_\theta = (\sin\phi_o - \sin\phi)/r_o \quad (3.5f)$$

$$N_\xi = H \cos\phi + V \sin\phi \quad (3.5g)$$

$$k_\xi = M_\xi/D - \nu k_\theta \quad (3.5h)$$

$$M_\theta = D(k_\theta + \nu k_\xi) \quad (3.5i)$$

Eliminating N_θ from Eqns. (3.4a) it follows that

$$\varepsilon_\xi = (1-\nu^2)/C \cdot N_\xi - \nu \varepsilon_\theta \quad (3.5j)$$

Similarly, eliminating N_ξ from Eqns. (3.4a) and rearranging,

$$N_\theta = \left\{ \frac{C}{(1-\nu^2)} \right\} \{ \varepsilon_\theta + \nu \varepsilon_\xi \} \quad (3.5k)$$

Rearrangement of Eqn. (3.2c) and substitution of $\alpha_o = 1$ leads to

$$\alpha = 1 + \varepsilon_\xi \quad (3.5l)$$

Elimination of z'_o from Eqn. (3.2g) by means of Eqn. (3.1b) gives

$$\frac{dw}{d\xi} = \alpha \sin\phi - \sin\phi_o \quad (3.5m)$$

Substitution of the values of ϵ_ξ from Eqn. (3.5l) and r'_0 from Eqn. (3.1b) in the Eqn. (3.2c), gives

$$\frac{du}{d\xi} = \alpha \cos \phi - \cos \phi_0 \quad (3.5n)$$

From Eqn. (3.2e) an expression for β' is obtained in the following form.

$$\frac{d\beta}{d\xi} = k_\xi \quad (3.5o)$$

Expansion of the three equations of equilibrium and elimination of P_V , P_H and r' from these equations result in the following expressions for V' , H' and M'_ξ .

$$\frac{dV}{d\xi} = -\alpha [(V \cos \phi) / r - P \cos \phi] \quad (3.5p)$$

$$\frac{dH}{d\xi} = -\alpha [(H \cos \phi - N_\theta) / r + P \sin \phi] \quad (3.5q)$$

$$\frac{dM_\xi}{d\xi} = \alpha \cos \phi (M_\theta - M_\xi) / r - \alpha (H \sin \phi - V \cos \phi) \quad (3.5r)$$

where P is the outward normal pressure.

Eqns. (3.5) are the non-linear governing equations of the axisymmetric deformations of shells of revolution expressed in terms of the fundamental variables. It should be noted that this fundamental set of differential and algebraic equations are expressed in such a manner that all the quantities of physical importance are evaluated during the process of solution of these equations.

3.2.3 Equations at the Apex

The fundamental set of equations derived in the previous section is singular at the apex of axisymmetric shells, (Fig. 3.1). In order to remove this singularity, the condition that all the physical quantities must be regular at the apex should be imposed. From the symmetry at the pole, it is found that

$$u = \beta = 0,$$

and as there is no concentrated load at the pole, it follows that

$$V = 0.$$

In the following derivation, it is assumed that ξ is measured from the pole of the axisymmetric shell.

Since ε_θ and ε'_θ must be regular at $\xi = 0$, Eqn. (3.5c) gives

$$\lim_{\xi \rightarrow 0} \varepsilon_\theta = \frac{u'}{r'_0} \text{ (By L' Hospital's principle)}$$

$$\text{and } \lim_{\xi \rightarrow 0} \varepsilon'_\theta = \frac{u'' r'_0 - u' r''_0}{2(r'_0)^2}$$

From Eqn. (3.1b), it is found that

$$r'_0 = \cos\phi_0$$

and therefore,

$$r''_0 = -\sin\phi_0 \cdot \phi'_0.$$

Substitution of the values of r'_0 and r''_0 into the expression of ε_θ and ε'_θ give

$$\lim_{\xi \rightarrow 0} \varepsilon_\theta = \frac{u'}{\cos\phi_0}$$

$$\lim_{\xi \rightarrow 0} \varepsilon'_\theta = \frac{u'' \cos\phi_0 + u' \phi'_0 \sin\phi_0}{2 \cos^2\phi_0}$$

Similarly, the following equations can be deduced from Eqns. (3.1a - 3.5r) by taking the limit as $\xi \rightarrow 0$:

$$\lim_{\xi \rightarrow 0} \phi = \phi_0 \tag{3.6a}$$

$$\lim_{\xi \rightarrow 0} \phi' = \phi'_0 - \beta' \tag{3.6b}$$

$$\lim_{\xi \rightarrow 0} k_\theta = \beta' \tag{3.6c}$$

$$\lim_{\xi \rightarrow 0} k'_\theta = \frac{1}{2}(\beta'' - \phi' \beta' \tan\phi_0) \tag{3.6d}$$

$$\lim_{\xi \rightarrow 0} N_{\xi} = H \cos \phi_0 \quad (3.6e)$$

$$\lim_{\xi \rightarrow 0} N'_{\xi} = H' \cos \phi_0 - H \phi' \sin \phi_0 + V' \sin \phi_0 \quad (3.6f)$$

$$\lim_{\xi \rightarrow 0} M'_{\theta} = \lim_{\xi \rightarrow 0} (D(1 - \nu^2) k'_{\theta} + \nu M'_{\xi}) \quad (3.6g)$$

$$\lim_{\xi \rightarrow 0} N'_{\theta} = \lim_{\xi \rightarrow 0} (C \varepsilon'_{\theta} + \nu N_{\xi}) \quad (3.6h)$$

$$\lim_{\xi \rightarrow 0} \alpha = \left(1 + \frac{1 - \nu^2}{C}\right) H \cos \phi_0 - \frac{u' \nu}{\cos \phi_0} \quad (3.6i)$$

$$\lim_{\xi \rightarrow 0} \alpha' = \lim_{\xi \rightarrow 0} \left[\left(\frac{1 - \nu^2}{C}\right) N'_{\xi} - \nu \varepsilon'_{\theta} \right] \quad (3.6j)$$

$$\lim_{\xi \rightarrow 0} u' = \left(\frac{1 - \nu}{C}\right) H \cos^2 \phi_0 \quad (3.6k)$$

$$\lim_{\xi \rightarrow 0} \beta' = \frac{M_{\xi}}{D(1 + \nu)} \quad (3.6l)$$

$$\lim_{\xi \rightarrow 0} w' = \left(\frac{1 - \nu}{C}\right) H \sin \phi_0 \cos \phi_0 \quad (3.6m)$$

Substitution of Eqn. (3.6k) in Eqn. (3.6i) gives

$$\lim_{\xi \rightarrow 0} \alpha = 1 + \frac{1 - \nu}{C} H \cos \phi_0 \quad (3.6n)$$

Now $\lim_{\xi \rightarrow 0} \frac{V'}{r} = \frac{V'}{\alpha \cos \phi_0} \quad (3.6o)$

Substituting Eqn. (3.6o) in Eqn. (3.5p) and solving for V' at the apex, it is found that

$$\lim_{\xi \rightarrow 0} V' = \frac{1}{2} \alpha P \cos \phi_0 \quad (3.6p)$$

By differentiating Eqn. (3.5n) and taking the limit as $\xi \rightarrow 0$, the expression for u'' at the pole can be derived as

$$\lim_{\xi \rightarrow 0} u'' = \left(\frac{2}{2+\nu}\right) \left(\frac{1-\nu^2}{C} N'_{\xi} \cos \phi_0 + \alpha \beta' \sin \phi_0\right) - u' \phi'_0 \tan \phi_0$$

hence from Eqn. (3.6h)

$$\lim_{\xi \rightarrow 0} N'_{\theta} = \frac{1}{2+\nu} [(1+2\nu) N'_{\xi} + C \alpha \beta' \tan \phi_0]$$

Taking the limit of Eqn. (3.5q) and eliminating N'_{θ} , it is found that

$$\lim_{\xi \rightarrow 0} H' = \frac{1}{3} \left[(1-\nu) \phi' H + \frac{\alpha C \beta'}{\cos \phi_0} \right] \tan \phi_0 - \frac{\alpha P}{2} \sin \phi_0 \quad (3.6q)$$

In order to evaluate M_{ξ}' at the pole, the expression of M_{θ}' in terms of M_{ξ}' has to be derived first.

Differentiating the Eqn. (3.5q) and taking the limit as $\xi \rightarrow 0$ result in

$$\lim_{\xi \rightarrow 0} \beta'' = \frac{2}{2+\nu} \left(\frac{M'_{\xi}}{D} + \frac{\nu \beta' \phi'}{2} \tan \phi_0 \right)$$

which, when substituted in Eqn. (3.5g), gives

$$\lim_{\xi \rightarrow 0} M'_{\theta} = \left(\frac{1+2\nu}{2+\nu}\right) M'_{\xi} - \left(\frac{1-\nu^2}{2+\nu}\right) \phi' \beta' \tan \phi_0$$

Taking the limit of Eqn. (3.5r) and eliminating M_{θ}' , the expression for M_{ξ}' is found to be

$$\lim_{\xi \rightarrow 0} M'_{\xi} = -\frac{1}{3} [\alpha(2+\nu)H \sin \phi_0 + D(1-\nu^2)\beta' \phi' \tan \phi_0] \quad (3.6r)$$

Thus Eqns. (3.6k), (3.6l), (3.6m), (3.6p), (3.6r) form the fundamental set of differential equations applicable only at the pole, where α and ϕ' appearing in these equations are given by Eqns. (3.6n) and (3.6b) respectively. These equations can further be simplified if it is assumed that the curvature of the undeformed shell is continuous at the pole. In this case, $\phi = 0$ and, thus, the fundamental set becomes

$$u' = (1 - \nu)H / C \quad (3.6.1a)$$

$$\beta' = M_{\xi}' / [D(1 + \nu)] \quad (3.6.1b)$$

$$w' = 0 \quad (3.6.1c)$$

$$\alpha = 1 + (1 - \nu) H / C \quad (3.6.1d)$$

$$V' = \alpha P / 2 \quad (3.6.1e)$$

$$H' = 0 \quad (3.6.1f)$$

$$M'_{\xi} = 0 \quad (3.6.1g)$$

3.2.4 Linearized Equations

The field equations, which were derived earlier in sections 3.2.2 and 3.2.3, are non-linear. These non-linear equations are always solved by the method of iteration in which arbitrary initial values have to be assigned to the fundamental dependent variables of these equations. Unless the initial values assigned to the dependent variables are a good approximation to their actual values, the iteration process fails to converge. For achieving convergence in the iteration process of solving non-linear equations, it is usually necessary to solve first the linearized version of the corresponding non-linear equations. The results of the linear solution are then assigned as the initial values to the dependent variables of the non-linear equations. The linear governing equations of axisymmetric deformation of shells of revolution are thus derived in this section.

The equations of small-deflection theory follow from the foregoing Eqns. (3.5) by referring the differential equations of equilibrium (3.5p) to (3.5r) together with (3.5g) to the undeformed shell and by omitting all non-linear terms in the remaining equations of the fundamental set (3.5).

The resulting equations are recorded below for ready reference.

$$\varepsilon_{\theta} = u / r_0 \quad (3.7a)$$

$$k_{\theta} = \beta \cos \phi_0 / r_0 \quad (3.7b)$$

$$N_{\xi} = H \cos \phi_0 + V \sin \phi_0 \quad (3.7c)$$

$$\varepsilon_{\xi} = \frac{1 - \nu^2}{C} N_{\xi} - \nu \varepsilon_{\theta} \quad (3.7d)$$

$$k_{\xi} = \frac{M_{\xi}}{D} - \nu k_{\theta} \quad (3.7e)$$

$$N_{\theta} = \left(\frac{C}{1 - \nu^2} \right) (\varepsilon_{\theta} + \nu \varepsilon_{\xi}) \quad (3.7f)$$

$$M_\theta = D(k_\theta + \nu k_\xi) \quad (3.7g)$$

$$w' = \varepsilon_\xi \sin \phi_0 - \beta \cos \phi_0 \quad (3.7h)$$

$$u' = \varepsilon_\xi \cos \phi_0 - \beta \sin \phi_0 \quad (3.7i)$$

$$\beta' = k_\xi \quad (3.7j)$$

$$V' = - \left(\frac{V \cos \phi_0}{r_0} - P \cos \phi_0 \right) \quad (3.7k)$$

$$H' = - \left[\frac{H \cos \phi_0 - N_\theta}{r_0} + P \sin \phi_0 \right] \quad (3.7l)$$

$$M'_\xi = - \cos \phi_0 \frac{(M'_\xi - M_\theta)}{r_0} - (H \sin \phi_0 - V \cos \phi_0) \quad (3.7m)$$

The corresponding linearized equations at the pole are obtained in the same manner as Eqns. (3.7). Expressions for u' , β' and w' remain the same, whereas, the three equations for equilibrium reduce to

$$V' = \frac{P \cos \phi_0}{2} \quad (3.7.1a)$$

$$H' = \frac{1}{3} \left[(1 - \nu) \phi'_0 H + \frac{C \beta'}{\cos \phi_0} \right] \tan \phi_0 - \frac{P \sin \phi_0}{2} \quad (3.7.1b)$$

$$M'_\xi = - \frac{1}{3} \left[(2 + \nu) H \sin \phi_0 + D(1 - \nu) \beta' \phi'_0 \tan \phi_0 \right] \quad (3.7.1c)$$

In case of continuous curvature of the meridian at the apex, linearized equations applicable at the apex remain the same as the Eqns. (3.6.1) except that the value of α is to be replaced by unity in Eqn. (3.6.1e).

3.2.5 Nondimensionalized Equations

It is always desirable to solve any engineering problem in terms of non-dimensional quantities in order to decrease the number of input physical parameters as well as to increase the applicability of the solution. With this in mind and also to make the variables more or less of the same order of magnitude the displacement components and stress resultants are expressed as

ratios of their actual values to those of the circumferential displacement and stress resultant of an unrestrained thin cylindrical shell. The independent variable ξ is nondimensionalized in such a manner that ξ_e , the total length of the shell meridian, corresponds to unity (Fig. 1.2). The nondimensionalized quantities are defined mathematically by the following equations:

$$\begin{aligned}\bar{w} &= \frac{wEh}{PR^2}, \quad \bar{u} = \frac{uEh}{PR^2}, \quad \bar{H} = \frac{H}{PR}, \quad \bar{V} = \frac{V}{PR}, \quad \bar{\beta} = \beta \\ \bar{M}_\xi &= \frac{M_\xi}{PRh}, \quad \bar{M}_\theta = \frac{M_\theta}{PRh}, \quad \bar{N}_\xi = \frac{N_\xi}{PR}, \quad \bar{N}_\theta = \frac{N_\theta}{PR} \\ \bar{\varepsilon}_\theta &= \varepsilon_\theta Eh \xi_e / (PR^2), \quad \bar{\varepsilon}_\xi = \varepsilon_\xi Eh \xi_e / (PR^2), \quad \bar{k}_\theta = k_\theta \cdot \xi_e \\ \bar{k}_\xi &= k_\xi \cdot \xi_e, \quad \bar{\xi} = \xi / \xi_e, \quad \bar{C} = (1 - \nu^2) \xi_e / R, \quad \bar{P} = \frac{P}{E}, \quad \bar{T} = \frac{R}{h} \\ \bar{R} &= \xi_e / R, \quad \bar{D} = 1 / [12(1 - \nu^2) \bar{P} \bar{T}^2 \bar{R}], \quad \bar{L} = \bar{R} / (\bar{P} \cdot \bar{T}), \quad \bar{r}_0 = r_0 / \xi_e.\end{aligned}\tag{3.8}$$

where R is the base radius of the shell. With the help of the nondimensionalized quantities, defined in Eqns. (3.8), the fundamental set of differential Eqns. (3.7) (linear theory) becomes

$$\bar{\varepsilon}_\theta = \bar{u}' / \bar{r}_0 \tag{3.9a}$$

$$\bar{k}_\theta = \bar{\beta} \cos \phi_0 / \bar{r}_0 \tag{3.9b}$$

$$\bar{N}_\xi = \bar{H} \cos \phi_0 + \bar{V} \sin \phi_0 \tag{3.9c}$$

$$\bar{\varepsilon}_\xi = \bar{C} \bar{N}_\xi - \nu \bar{\varepsilon}_\theta \tag{3.9d}$$

$$\bar{k}_\xi = \bar{M}_\xi / \bar{D} - \nu \bar{k}_\theta \tag{3.9e}$$

$$\bar{N}_\theta = (\bar{\varepsilon}_\theta + \nu \bar{\varepsilon}_\xi) / \bar{C} \tag{3.9f}$$

$$\bar{M}_\theta = \bar{D} (\bar{k}_\theta + \nu \bar{k}_\xi) \tag{3.9g}$$

$$\bar{w}' = \bar{\varepsilon}_\xi \sin \phi_0 - \bar{\beta} \cos \phi_0 \cdot \bar{L} \tag{3.9h}$$

$$\bar{u}' = \bar{\varepsilon}_\xi \cos \phi_0 + \bar{\beta} \sin \phi_0 \cdot \bar{L} \tag{3.9i}$$

$$\bar{\beta}' = \bar{k}_\xi \tag{3.9j}$$

$$\bar{V}' = - (\bar{V} \cos \phi_0 / \bar{r}_0 - \bar{R} \cos \phi_0) \tag{3.9k}$$

$$\bar{H}' = \{ (\bar{H} \cos \phi_0 - \bar{N}_\theta) / \bar{r}_0 + \bar{R} \sin \phi_0 \} \tag{3.9l}$$

$$\overline{M}'_{\xi} = -\cos\phi_0(\overline{M}_{\xi} - \overline{M}_{\theta})/\overline{r}_0 - \overline{R}\overline{T}(\overline{H}\sin\phi_0 - \overline{V}\cos\phi_0) \quad (3.9m)$$

$$\text{where } (\dots)' = \frac{d}{d\xi} (\dots)$$

The corresponding non-linear Equations of the fundamental set in non-dimensional form are as follows:

$$\overline{\varepsilon}_{\theta} = \overline{u}/\overline{r}_0 \quad (3.10a)$$

$$\phi = \phi_0 - \overline{\beta} \quad (3.10b)$$

$$\overline{k}_{\theta} = (\sin\phi_0 - \sin\phi)/\overline{r}_0 \quad (3.10c)$$

$$\overline{N}_{\xi} = \overline{H}\cos\phi + \overline{V}\sin\phi \quad (3.10d)$$

$$\overline{\varepsilon}_{\xi} = \overline{C}\overline{N}_{\xi} - \nu\overline{\varepsilon}_{\theta} \quad (3.10e)$$

$$\overline{k}_{\xi} = \overline{M}_{\xi}/\overline{D} - \nu\overline{k}_{\theta} \quad (3.10f)$$

$$\overline{N}_{\theta} = (\overline{\varepsilon}_{\theta} + \nu\overline{\varepsilon}_{\xi})/\overline{C} \quad (3.10g)$$

$$\overline{M}_{\theta} = \overline{D}(\overline{k}_{\theta} + \nu\overline{k}_{\xi}) \quad (3.10h)$$

$$\overline{\alpha} = \overline{L} + \overline{\varepsilon}_{\xi} \quad (3.10i)$$

$$\overline{r} = \overline{L}\overline{r}_0 + \overline{u} \quad (3.10j)$$

$$\overline{w}' = \overline{\alpha}\sin\phi - \overline{L}\sin\phi_0 \quad (3.10k)$$

$$\overline{u}' = \overline{\alpha}\cos\phi - \overline{L}\cos\phi_0 \quad (3.10l)$$

$$\overline{\beta}' = \overline{k}_{\xi} \quad (3.10m)$$

$$\overline{V}' = -\overline{\alpha}\cos\phi(\overline{V}/\overline{r} - \overline{P}\overline{T}) \quad (3.10n)$$

$$\overline{H}' = -\overline{\alpha}(\overline{H}\cos\phi - \overline{N}_{\theta})/\overline{r} + \overline{P}\overline{T}\sin\phi \quad (3.10o)$$

$$\begin{aligned} \overline{M}'_{\xi} &= \overline{\alpha}\cos\phi(\overline{M}_{\theta} - \overline{M}_{\xi})/\overline{r} \\ &\quad - \overline{\alpha}\overline{P}\overline{T}^2(\overline{H}\sin\phi - \overline{V}\cos\phi) \end{aligned} \quad (3.10p)$$

The equations at the pole corresponding to the non-linear set take the following form after nondimensionalization and simplification :

$$\overline{u}' = \overline{C}\overline{H}/(1 + \nu) \quad (3.10.1a)$$

$$\overline{W}' = 0 \quad (3.10.1b)$$

$$\overline{\beta}' = \overline{M}_\xi / \{\overline{D}(1 + \nu)\} \quad (3.10.1c)$$

$$\overline{V}' = \overline{\alpha P} / 2 \quad (3.10.1d)$$

$$\overline{H}' = 0 \quad (3.10.1e)$$

$$\overline{M}'_\xi = 0 \quad (3.10.1f)$$

It should be noted that some of the nondimensional shell parameters in Eqns. (3.8) are defined in terms of ξ_c which will depend on the geometry of the meridian and thus should be derived for each individual case. In some cases there is no closed form expression for ξ_c and, therefore, ξ_c has to be evaluated either from a series expression or by numerical integration. In the present analysis, geometrically composite shells of revolution consisting of spherical cap, conical frustum, cylindrical shells, etc., are studied. The expressions of r_o and ϕ_o in terms of ξ_c in these cases are very simple. The meridional length ξ for a spherical cap is simply the product of the radius of curvature of the cap and the subtended angle ϕ at the centre of curvature of the cap, and for a cylindrical segment it is equal to the height of the cylindrical segment. In case of a conical frustum, the slant height is taken as ξ_{cone} and is calculated from the following expression:

$$\xi_{\text{cone}} = (R_2 - R_1) / \cos \phi_o$$

where,

R_1 = radius of smaller end of the cone,

R_2 = radius of the larger end of the cone, and

ϕ_o = angle between the normal to the shell surface and the axis of revolution of the shell

3.3 GOVERNING EQUATIONS FOR ASYMMETRIC ANALYSIS

Asymmetric buckling analysis is generally done from the eigen value solution of linearized governing equations, derived from general equations with perturbation of variables, generally known as the stability equations. General equations of shells of revolution contain some more variables in excess of axisymmetric governing equations like u_θ , $\epsilon_{\xi\theta}$, $K_{\xi\theta}$, $N_{\xi\theta}$, $M_{\xi\theta}$. Description of the variables used in the general governing equations are defined in Figs. 3.4, 3.5 and 3.6. The same method of nondimensionalization of variables as that of axisymmetric analysis has

been adopted in the derivation of nondimensionalized stability equations for asymmetric analysis and are presented below.

$$\begin{aligned}
& (\bar{r}_0 \bar{N}_{\xi 1})' + \dot{\bar{N}}_{\xi \theta 1} - \bar{r}_0' \bar{N}_{\theta 1} + \frac{1}{\overline{\text{TRR}}_1} \left\{ (\bar{r}_0 \bar{M}_{\xi 1})' + \dot{\bar{M}}_{\xi \theta 1} - \bar{r}_0' \bar{M}_{\theta 1} \right\} \\
& - \frac{\bar{r}_0}{\bar{R}_1} \left\{ \bar{\beta}_{\xi 0} \bar{N}_{\xi 1} + \bar{N}_{\xi 0} \bar{\beta}_{\xi 1} + \bar{\beta}_{\theta 0} \bar{N}_{\xi \theta 1} + \bar{N}_{\xi \theta 0} \bar{\beta}_{\theta 1} \right\} = 0
\end{aligned} \tag{3.11(a)}$$

$$\begin{aligned}
& \dot{\bar{N}}_{\theta 1} + (\bar{r}_0 \bar{N}_{\xi \theta 1})' + \bar{r}_0' \bar{N}_{\xi \theta 1} + \frac{1}{\overline{\text{TRR}}_2} \left\{ \dot{\bar{M}}_{\theta 1} + (\bar{r}_0 \bar{M}_{\xi \theta 1})' + \bar{r}_0' \bar{M}_{\xi \theta 1} \right\} \\
& - \frac{\bar{r}_0}{\bar{R}_2} \left\{ \bar{\beta}_{\theta 0} \bar{N}_{\theta 1} + \bar{N}_{\theta 0} \bar{\beta}_{\theta 1} + \bar{\beta}_{\xi 0} \bar{N}_{\xi \theta 1} + \bar{N}_{\xi \theta 0} \bar{\beta}_{\xi 1} \right\} = 0
\end{aligned} \tag{3.11(b)}$$

$$\begin{aligned}
& \frac{1}{\overline{\text{TR}}} \left\{ (\bar{r}_0 \bar{M}_{\xi 1})'' - (\bar{r}_0' \bar{M}_{\theta 1})' + \dot{\bar{M}}_{\xi \theta 1} + \frac{2}{\bar{r}_0} \bar{r}_0' \dot{\bar{M}}_{\xi \theta 1} \right\} \\
& - \bar{r}_0 \left(\frac{\bar{N}_{\xi 1}}{\bar{R}_1} + \frac{\bar{N}_{\theta 1}}{\bar{R}_2} \right) - \left[(\bar{r}_0 \bar{N}_{\xi 0} \bar{\beta}_{\xi 1} + \bar{r}_0 \bar{N}_{\xi \theta 0} \bar{\beta}_{\theta 1})' \right. \\
& \left. + (\bar{r}_0 \bar{\beta}_{\xi 1} \bar{N}_{\xi 1} + \bar{r}_0 \bar{\beta}_{\theta 0} \bar{N}_{\xi \theta 1})' + (\bar{N}_{\theta 0} \bar{\beta}_{\theta 1} + \bar{N}_{\xi \theta 0} \bar{\beta}_{\xi 1})^0 \right] = 0
\end{aligned} \tag{3.11(c)}$$

Perturbation of variables considered in the derivation of the above governing equations were

$$\bar{u}_\xi = \bar{u}_{\xi 0}(\xi) + \bar{u}_{\xi 1}(\xi, \theta)$$

$$\bar{u}_\theta = \bar{u}_{\theta 1}(\xi, \theta)$$

$$\bar{u}_\zeta = \bar{u}_{\zeta 0}(\xi) + \bar{u}_{\zeta 1}(\xi, \theta)$$

$$\bar{N}_\xi = \bar{N}_{\xi 0} + \bar{N}_{\xi 1}$$

$$\bar{N}_\theta = \bar{N}_{\theta 0} + \bar{N}_{\theta 1}$$

$$\bar{M}_\xi = \bar{M}_{\xi 0} + \bar{M}_{\xi 1}$$

$$\bar{M}_\theta = \bar{M}_{\theta 0} + \bar{M}_{\theta 1}$$

$$\bar{N}_{\xi \theta} = \bar{N}_{\xi \theta 0} + \bar{N}_{\xi \theta 1}$$

$$\bar{M}_{\xi \theta} = \bar{M}_{\xi \theta 0} + \bar{M}_{\xi \theta 1}$$

where,

$$\bar{N}_{\xi_1} = \frac{1}{C} (\bar{\varepsilon}_{\xi_1} + \nu \bar{\varepsilon}_{\theta_1})$$

$$\bar{N}_{\theta_1} = \frac{1}{C} (\bar{\varepsilon}_{\theta_1} + \nu \bar{\varepsilon}_{\xi_1})$$

$$\bar{M}_{\xi_1} = \bar{D} (\bar{k}_{\xi_1} + \nu \bar{k}_{\theta_1})$$

$$\bar{M}_{\theta_1} = \bar{D} (\bar{k}_{\theta_1} + \nu \bar{k}_{\xi_1})$$

$$\bar{N}_{\xi\theta_1} = \frac{1}{C} \left(\frac{1-\nu}{2} \right) \bar{\varepsilon}_{\xi\theta_1}$$

$$\bar{M}_{\xi\theta_1} = \bar{D} \left(\frac{1-\nu}{2} \right) \bar{k}_{\xi\theta_1}$$

$$\bar{k}_{\xi_1} = \bar{\beta}'_{\xi_1}$$

$$\bar{k}_{\theta_1} = \frac{1}{\bar{r}_0} \dot{\bar{\beta}}_{\theta_1} + \frac{1}{\bar{r}_0} \bar{r}'_0 \bar{\beta}'_{\xi_1}$$

$$\bar{k}_{\xi\theta_1} = \frac{1}{2} \left[\bar{\beta}'_{\theta_1} + \frac{1}{\bar{r}_0} \dot{\bar{\beta}}_{\xi_1} - \frac{1}{\bar{r}_0} \bar{r}'_0 \bar{\beta}_{\xi_1} \right]$$

$$\bar{\beta}_{\xi_1} = \left(-\bar{u}'_{\xi_1} + \frac{1}{R_1} \bar{u}_{\xi_1} \right) \frac{\bar{P}\bar{T}}{\bar{R}}$$

$$\bar{\beta}_{\theta_1} = \left(-\frac{1}{\bar{r}_0} \dot{\bar{u}}_{\xi_1} + \frac{\bar{u}_{\theta_1}}{\bar{R}_2} \right) \frac{\bar{P}\bar{T}}{\bar{R}}$$

$$\bar{\varepsilon}_{\xi_1} = \bar{u}'_{\xi_1} + \frac{\bar{u}_{\xi_1}}{\bar{R}_1} + \frac{\bar{R}}{\bar{P}\bar{T}} \bar{\beta}_{\xi_0} \bar{\beta}_{\xi_1}$$

$$\bar{\varepsilon}_{\theta_1} = \frac{1}{\bar{r}_0} \dot{\bar{u}}_{\theta_1} + \frac{1}{\bar{r}_0} \bar{r}'_0 \bar{u}_{\xi_1} + \frac{\bar{u}_{\xi_1}}{\bar{R}_2} + \frac{\bar{R}}{\bar{P}\bar{T}} \bar{\beta}_{\theta_0} \bar{\beta}_{\theta_1}$$

$$\bar{\varepsilon}_{\xi\theta_1} = \frac{1}{2} \left[\bar{u}'_{\theta_1} + \frac{1}{\bar{r}_0} \dot{\bar{u}}_{\xi_1} - \frac{1}{\bar{r}_0} \bar{r}'_0 \bar{u}_{\theta_1} + \frac{\bar{R}}{\bar{P}\bar{T}} \bar{\beta}_{\xi_0} \bar{\beta}_{\theta_1} + \frac{\bar{R}}{\bar{P}\bar{T}} \bar{\beta}_{\theta_0} \bar{\beta}_{\xi_1} \right]$$

$$\bar{u}_{\xi_1} = \bar{u}_{\xi_1}(\xi) \cos(n\theta)$$

$$\bar{u}_{\theta_1} = \bar{u}_{\theta_1}(\xi) \sin(n\theta)$$

$$\bar{u}_{\xi_1} = \bar{u}_{\xi_1}(\xi) \cos(n\theta)$$

The symbols with suffix 'o' are variables obtained from the solution of prebuckling non-linear governing equations of axisymmetric shells of revolution. Dot and prime superscripted variables represent derivatives with respect to θ and $\bar{\xi}$, respectively, and n stands for number of circumferential waves that form during asymmetric buckling.

3.4 BOUNDARY CONDITIONS

The general boundary conditions of a shell on an edge $\xi_1 = \text{constant}$ are to prescribe, in Sander's [136] notations, are

N_{11} or U_1 ,

$$N_{12} + \frac{1}{2}(3R_2^{-1} - R_1^{-1})M_{12} + \frac{1}{2}(M_{11} + N_{22})\phi \text{ or } U_2 ,$$

$$Q_1 + \alpha_2^{-1} \frac{\partial M_{12}}{\partial \xi_2} - \phi_1 N_{11} - \phi_2 N_{12} \text{ or } w , \quad (3.12a)$$

and M_{11} or ϕ_1 ,

where ξ_1 and ξ_2 are the shell co-ordinates along the principal lines of curvature; N and M are the stress and couple resultants; ϕ 's are the rotations about respective axes; u and w are tangential and normal displacement components.

When the quantities in (3.12a) are specialised for axisymmetric deformations of shells of revolution they reduce to prescribing

N_{11} or u_1 ,

$$Q_1 - \phi_1 N_{11} \text{ or } w, \quad (3.12b)$$

and M_{11} or ϕ_1 ,

on an edge $\xi_1 = \text{constant}$.

From (3.12b) it is seen that the boundary conditions consists of the specification of rotational, tangential and normal restraints at an edge. But in most of the practical cases of shell problems the conditions of the horizontal and vertical restraints are known rather than those of the normal and tangential restraints. So it is concluded that it will be preferable to specify the boundary

conditions in terms of the horizontal and vertical restraints from the point of view of practical application. When this is done, the boundary conditions in terms of the notations used in the body of this thesis will be to prescribe

$$\begin{aligned} & H \quad \text{or} \quad u \quad , \\ & M_{\xi} \quad \text{or} \quad \beta \quad , \\ \text{and} \quad & V \quad \text{or} \quad w \quad . \end{aligned} \tag{3.12c}$$

on an edge, $\xi = \text{constant}$.

3.5 METHOD OF SOLUTION

3.5.1 Axisymmetric Solution

The fundamental set of linear Eqns. (3.9) and non-linear Eqns. (3.10) together with the boundary conditions (3.12c) on two edges have to be integrated over a finite range of the independent variable $\bar{\xi}$. But numerical integration of these equations is not possible beyond a very limited range of $\bar{\xi}$ due to the loss of accuracy in solving for the unknown boundary values, as pointed out by Kalnins [71], and thus the multisegment method of integration developed by Kalnins and Lestingi [72] is used for the present analysis.

3.5.1.1 Multisegment method of integration

The multisegment method of integration of a system of m first order ordinary differential equations of the following form

$$\frac{dy(x)}{dx} = F[x, y^1(x), y^2(x), \dots, y^m(x)] \tag{3.13a}$$

in the interval $(x_1 \leq x \leq x_{M+1})$ consists of

- (a) the division of the given interval into M segments (Fig. 3.7),
- (b) $(m+1)$ initial-value integrations over each segment,

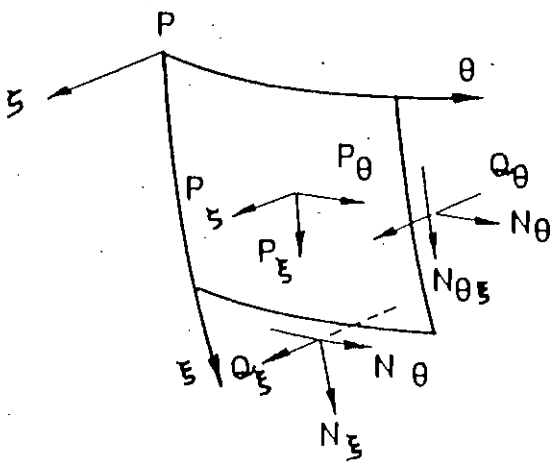


Fig. 3.4: Element of general shell showing stress resultants and forces.

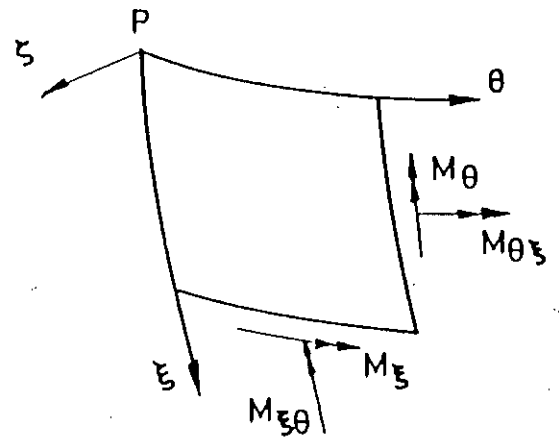


Fig. 3.5: Elements of general shell showing couples.

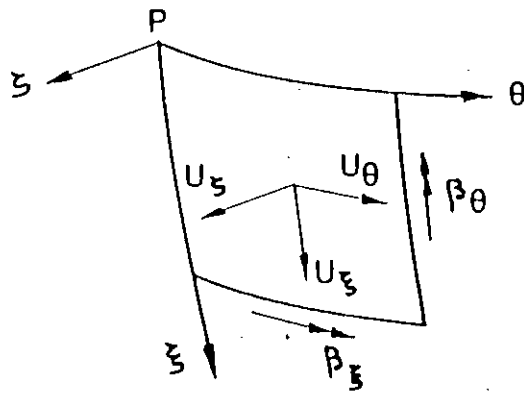


Fig. 3.6: Elements of general shell showing displacements.

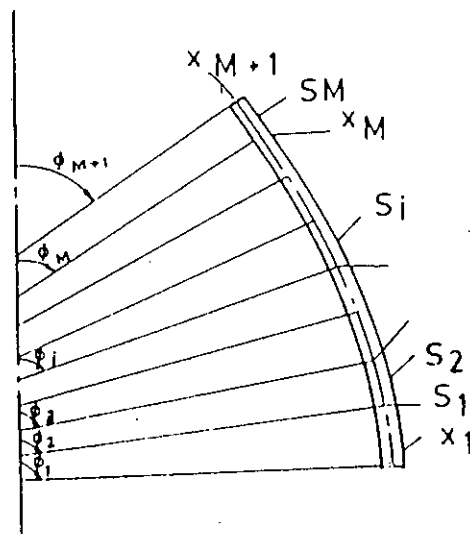


Fig. 3.7: Division of a shell for Multisegment Integration.

- (c) solution of a system of matrix equations which ensures continuity of the dependent variables at the nodal points of the segments, and
- (d) repetition of (b) and (c) until continuity of the dependent variables at the nodal points is achieved.

In Eqns. (3.13a), the symbol $y(x)$ represents a column matrix whose elements are m dependent variables, denoted by $y^j(x)$ ($j = 1, 2, \dots, m$); F represents m functions arranged in a column matrix form; and x is the independent variable. It is assumed here for convenience that the first $m/2$ elements of $y(x_1)$ and the last $m/2$ elements of $y(x_{M+1})$ are prescribed by the boundary conditions.

If at the initial point x_i of the segment S_i (Fig. 3.7) a set of values $y(x_i)$ is prescribed for the variables of Eqns. (3.13a) then the variables at any x within S_i can be expressed as

$$y(x) = f[y^1(x_i), y^2(x_i), \dots, y^m(x_i)] \tag{3.13b}$$

where the function f is uniquely dependent on x and the system of equations (3.13a). From Eqns. (3.13b), the small changes $\delta y(x)$ can be expressed to a first order approximation by the following linear equations:

$$\delta y(x) = Y_i(x) \delta y(x_i) \tag{3.13c}$$

where,

$$Y_i(x) = \begin{bmatrix} \frac{\partial y^1(x)}{\partial y^1(x_i)} & \frac{\partial y^1(x)}{\partial y^2(x_i)} & \dots & \frac{\partial y^1(x)}{\partial y^m(x_i)} \\ \frac{\partial y^2(x)}{\partial y^1(x_i)} & \dots & \dots & \frac{\partial y^2(x)}{\partial y^m(x_i)} \\ \vdots & & & \\ \frac{\partial y^m(x)}{\partial y^1(x_i)} & \dots & \dots & \frac{\partial y^m(x)}{\partial y^m(x_i)} \end{bmatrix} \tag{3.13d}$$

Expressing Eqns. (3.13c) in finite difference form and evaluating them at $x = x_{i+1}$,

$$y^t(x_{i+1}) - y(x_{i+1}) = Y_i(x_{i+1})[y^t(x_i) - y(x_i)] \quad (3.13e)$$

where y^t denotes a trial solution state and y denotes an iterated solution state based on the condition of continuity of the variables at the nodal points. Eqns. (3.13e) is rearranged as

$$Y_i(x_{i+1})y(x_i) - y(x_{i+1}) = -Z_i(x_{i+1}) \quad (3.13f)$$

where $Z_i(x_{i+1}) = y^t(x_{i+1}) - Y_i(x_{i+1})y^t(x_i)$

In order to determine the coefficients $Y_i(x)$ in Eqns. (3.13f), the j th column of $Y_i(x)$ can be regarded as a set of new variables, which is a solution of an initial value problem governed within each segment by a linear system of first order differential equations, obtained from Eqns. (3.13a) by differentiation with respect to $y^j(x_i)$ in the form

$$\frac{d}{dx} \left[\frac{\partial y(x)}{\partial y^j(x_i)} \right] = \frac{\partial}{\partial y^j(x_i)} \left\{ F[x, y^1(x), y^2(x), \dots, y^m(x)] \right\} \quad (3.13g)$$

Thus the columns of the matrix $Y_i(x)$ are defined as the solutions of m initial value problems governed in S_i by eqn. (3.13g) ($j = 1, 2, \dots, m$) with the initial values, in view of Eqns. (3.13c), specified by

$$Y_i(x_i) = I \quad (3.13h)$$

where I denotes the (m,m) unit matrix. To obtain the iterated solution $y(x_i)$, Eqns. (3.13f) are rewritten as a partitioned matrix product of the form

$$\begin{bmatrix} y_1(x_{i+1}) \\ \dots \\ y_2(x_{i+1}) \end{bmatrix} = \begin{bmatrix} Y_i^1(x_{i+1}) & \dots & Y_i^2(x_{i+1}) \\ \dots & \dots & \dots \\ Y_i^3(x_{i+1}) & \dots & Y_i^4(x_{i+1}) \end{bmatrix} \begin{bmatrix} y_1(x_i) \\ \dots \\ y_2(x_i) \end{bmatrix} + \begin{bmatrix} Z_i^1(x_{i+1}) \\ \dots \\ Z_i^2(x_{i+1}) \end{bmatrix}$$

so that the known boundary conditions are separated from the unknowns and, therefore, it turns into a pair of matrix equations given by

$$\begin{aligned} Y_i^1(x_{i+1})y_1(x_i) + Y_i^2(x_{i+1})y_2(x_i) - y_1(x_{i+1}) &= -Z_i^1(x_{i+1}) \\ Y_i^3(x_{i+1})y_1(x_i) + Y_i^4(x_{i+1})y_2(x_i) - y_1(x_{i+1}) &= -Z_i^2(x_{i+1}) \end{aligned} \quad (3.13i)$$

The result is a simultaneous system of $2M$ linear matrix equations, in which the known coefficients $Y_i^j(x_{i+1})$ and $Z_i^j(x_{i+1})$ are $(m/2, m/2)$ and $(m/2, 1)$ matrices, respectively, and the unknown, $y_j(x_i)$ are $(m/2, 1)$ matrices. Since $y_1(x_1)$ and $y_2(x_{M+1})$ are known, there are exactly $2M$ unknowns: $y_1(x_i)$, $i = 2, 3, \dots, M + 1$, and $y_2(x_i)$, $i = 1, 2, \dots, M$.

By means of Gaussian elimination, the system of equations (3.13i) is first brought to the form

$$\begin{aligned} E_i y_2(x_i) - y_1(x_{i+1}) &= A_i \\ C_i y_1(x_{i+1}) - y_2(x_{i+1}) &= B_i \end{aligned} \quad (3.13j)$$

for $i = 1, 2, \dots, M$. Using the notations Z_i^j and Y_i^j in place of the symbols $Z_i^j(x_{i+1})$ and $Y_i^j(x_{i+1})$, the $(m/2, m/2)$ matrices E_i and C_i in the Eqns. (3.13j) are defined by

$$E_1 = Y_1^2, \quad C_1 = Y_1^4 (Y_1^2)^{-1}$$

$$\text{and} \quad E_i = Y_i^2 + Y_i^1 C_{i-1}^{-1}$$

$$C_i = (Y_i^4 + Y_i^3 C_{i-1}^{-1}) E_i^{-1}$$

for $i = 2, 3, \dots, M$.

The $(m/2, 1)$ matrices A_i and B_i are given by

$$A_1 = -Z_1^1 - Y_1^1 y_1(x_1)$$

$$B_1 = -Z_1^2 - Y_1^2 y_1(x_1) - Y_1^4 E_1^{-1} A_1$$

$$\text{and} \quad A_i = -Z_i^1 - Y_i^1 C_{i-1}^{-1} B_{i-1}$$

$$B_i = -Z_i^2 - Y_i^3 C_{i-1}^{-1} B_{i-1} - (Y_i^4 + Y_i^3 C_{i-1}^{-1}) E_i^{-1} A_i$$

for $i = 2, 3, \dots, M$.

Then the unknowns of Eqns.(3.13i) are obtained from

$$y_1(x_{M+1}) = C_M^{-1} [B_M - y_2(x_{M+1})]$$

$$y_2(x_M) = E_M^{-1} [y_1(x_{M+1}) + A_M]$$

$$\text{and} \quad y_1(x_{M-i+1}) = C_{M-i}^{-1} [y_2(x_{M-i+1}) + B_{M-i}]$$

$$y_2(x_{M-i}) = E_{M-i}^{-1} [y_1(x_{M-i+1}) + A_{M-i}]$$

for $i = 1, 2, \dots, M-1$.

Assuming $y(x_i)$ as the next trial solution $y^l(x_i)$, the process is repeated until the integration results of Eqns. (3.13a) at x_{i+1} , as obtained from the integrations in segment S_i with the initial values $y(x_i)$, match with the elements of $y(x_{i+1})$ as obtained from Eqns.(3.13f) and also with the boundary conditions at x_{M+1} .

3.5.1.2 Derivation of additional equations of multisegment integration

In the multisegment integration technique for a set of ordinary differential equations, it has already been noted that in addition to the integration of the given set of equations, another m sets of equations represented by Eqns.(3.13g) has to be integrated. Thus, in order to apply the method of multisegment integration, differential equations corresponding to Eqns. (3.13g) for the m^2 additional variables as represented in Eqns. (3.13d) have to be derived. These differential equations are obtained by differentiating Eqns. (3.9) for the linear case and Eqns. (3.10) for the non-linear case with respect to each of the fundamental variables. As the variables in any column of Eqns.(3.13d) have the same form, the system of Eqns. (3.13g) is derived here for the variables of any one column of Eqns.(3.13d) where the new variables are identified from the fundamental variables by the subscript 'a'.

From the non-linear Eqns. (3.10), by differentiation in succession, the equations governing the new variables are derived as

$$\bar{\varepsilon}_{\theta a} = \bar{u}_a / \bar{r}_0 \quad (3.14a)$$

$$\bar{\phi}_a = -\bar{\beta}_a \quad (3.14b)$$

$$\bar{k}_{\theta a} = \bar{\beta}_a \cos \phi / \bar{r}_0 \quad (3.14c)$$

$$\bar{N}_{\xi a} = (\bar{H}_a - \bar{V} \bar{\beta}_a) \cos \phi + (\bar{H} \bar{\beta}_a + \bar{V}_a) \sin \phi \quad (3.14d)$$

$$\bar{\varepsilon}_{\xi a} = \bar{C} \bar{N}_{\xi a} - \nu \bar{\varepsilon}_{\theta a} \quad (3.14e)$$

$$\bar{k}_{\xi a} = \bar{M}_{\xi a} / \bar{D} - \nu \bar{k}_{\theta a} \quad (3.14f)$$

$$\bar{N}_{\theta a} = \left(\bar{\varepsilon}_{\theta a} + \nu \bar{\varepsilon}_{\xi a} \right) / \bar{C} \quad (3.14g)$$

$$\bar{M}_{\theta a} = \bar{D}(\bar{k}_{\theta a} + \nu \bar{k}_{\xi a}) \quad (3.14h)$$

$$\bar{\alpha}_a = \bar{\varepsilon}_{\xi a} \quad (3.14i)$$

$$\bar{r}_a = \bar{u}_a \quad (3.14j)$$

$$\bar{u}'_a = \bar{\alpha}_a \cos \phi + \bar{\beta}_a \bar{\alpha} \sin \phi \quad (3.14k)$$

$$\bar{w}'_a = \bar{\alpha}_a \sin \phi - \bar{\alpha}_a \bar{\beta} \cos \phi \quad (3.14l)$$

$$\bar{\beta}'_a = \bar{k}_{\xi a} \quad (3.14m)$$

$$\begin{aligned} \bar{V}'_a = & - (\bar{\alpha}_a \cos \phi + \bar{\alpha} \bar{\beta}_a \sin \phi)(\bar{V} / \bar{r} - \bar{P} \bar{T}) \\ & - \bar{\alpha} \cos \phi (\bar{V}_a / \bar{r} - \bar{V} \bar{r}_a / \bar{r}^2) \end{aligned} \quad (3.14n)$$

$$\begin{aligned} \bar{H}'_a = & - \bar{\alpha}_a \{ (\bar{H} \cos \phi - \bar{N}_{\theta}) / \bar{r} + \bar{P} \bar{T} \sin \phi \} - \bar{\alpha} \{ [\bar{H}_a \cos \phi \\ & + \bar{\beta}_a \bar{H} \sin \phi - \bar{N}_{\theta a} - \bar{u}_a (\bar{H} \cos \phi - \bar{N}_{\theta}) / \bar{r}] / \bar{r} - \bar{P} \bar{T} \bar{\beta}_a \cos \phi \} \end{aligned} \quad (3.14o)$$

$$\begin{aligned} \bar{M}'_{\xi a} = & (\bar{\alpha}_a \cos \phi + \bar{\beta}_a \bar{\alpha} \sin \phi) \{ (\bar{M}_{\theta} - \bar{M}_{\xi}) / \bar{r} + \bar{P} \bar{T}^2 \bar{V} \} \\ & + \bar{\alpha} (\cos \phi [\bar{P} \bar{T}^2 \bar{V}_a + (\bar{M}_{\theta a} - \bar{M}_{\xi a} - \bar{u}_a (\bar{M}_{\theta} - \bar{M}_{\xi}) / \bar{r}) \\ & - \bar{P} \bar{T}^2 \bar{H}_a \sin \phi] - \bar{P} \bar{T}^2 \bar{H} (\bar{\alpha}_a \sin \phi - \bar{\alpha} \bar{\beta}_a \cos \phi) \end{aligned} \quad (3.14p)$$

Eqns. (3.14a - 3.14p) have to be integrated as initial value problems, m times in each segment, with the initial values given by Eqns. (3.13h). It should be noted here that Eqns. (3.14) contain not only the variables of Eqns. (3.13d) but also the variables of the fundamental set. Thus, Eqns. (3.14) can not be integrated unless the fundamental set of equations is integrated first and the values of the fundamental variables are stored for use in Eqns. (3.14). It should be further pointed out that one point integration formula can not be used for the integration of Eqns. (3.14) since this formula needs evaluation of the derivatives at intermediate points where the variables are never evaluated.

The corresponding equations for the linear theory are given by the homogeneous form of Eqns. (3.9) and thus readily obtainable by dropping the load terms in Eqns. (3.9).

3.5.1.3 Treatment of boundary conditions

In the introduction of the multisegment method of integration it was assumed that the first $m/2$ elements of $y(x)$ at x_1 and the last $m/2$ elements of $y(x)$ at x_{M+1} were prescribed as boundary conditions. But, in general, the boundary conditions are given as

$$\begin{aligned} T_1 y(x_1) &= b_1 \quad \text{at } x_1 \\ \text{and} \quad T_{M+1} y(x_{M+1}) &= b_{M+1} \quad \text{at } x_{M+1} \end{aligned} \quad (3.15a)$$

in which any $m/2$ elements of b_1 and any $m/2$ elements of b_{M+1} may be specified as boundary conditions. The symbols T_1 and T_{M+1} represent non-singular (m,m) matrices which are known from the specification of the boundary conditions at the ends of the interval.

By rearranging the rows of T_1 and T_{M+1} in a special order, Eqns. (3.15a) can always be stated in a manner such that the prescribed elements of b_1 and b_{M+1} become respectively the first and the last $m/2$ elements of b_1 and b_{M+1} . When this is achieved, evaluation of Eqns. (3.13f) at $i = 1$ and $i = M$, and then elimination of $y(x_1)$ and $y(x_{M+1})$ by means of Eqns. (3.15a) yield

$$Y_1(x_2) T_1^{-1} b_1 - y(x_2) = - Z_1(x_2) \quad (3.15b)$$

$$T_{M+1} Y_M(x_{M+1}) y(x_M) - b_{M+1} = - T_{M+1} Z_M(x_{M+1}) \quad (3.15c)$$

The form and notation of Eqns. (3.13f) can now be retained if the coefficient matrices $Y_1(x_2)$, $Y_M(x_{M+1})$, $Z_M(x_{M+1})$, occurring in Eqns. (3.13f), represent $Y_1(x_2) T_1^{-1}$, $T_{M+1} Y_M(x_{M+1})$, and $T_{M+1} Z_M(x_{M+1})$, respectively. In doing so, the solution of Eqns. (3.13f) will not yield $y(x_1)$ and $y(x_{M+1})$ but rather the transformed variables b_1 and b_{M+1} . When $y(x_1)$ and $y(x_{M+1})$ are desired, they can be obtained by the inversion of the matrix equations (3.15a).

It should be noted here that with reference to the boundary conditions (3.12c), stated in terms of the fundamental variables, the matrices T_1 and T_{M+1} are both unit matrices of order 6. The construction of T_1 and T_{M+1} , in accordance with any possible statement of (3.12c) so that equations (3.15a) are in order, is treated in Appendix A.

3.6 AXISYMMETRIC BUCKLING

A shell structure under a given level of external loading is in an equilibrium state when its total potential energy is stationary at that state and that equilibrium state is stable when this potential energy has got a relatively larger value in the neighbouring states. The governing differential equations which are solved here always seek for the state of deformation of the shell at which, for given external pressure, the potential energy in the deformed shape of the shell is stationary. The critical pressure for a particular shell is interpreted from the fact that any further increase in pressure above its critical value, no matter how small, will cause the shell to undergo enormous deformation (linear and rotational) indicating that the state of deformation of the shell which corresponds to the lowest potential energy is far off from that at the critical pressure. Uddin [171] has also pointed out that the method of solution of the non-linear governing equations for any value of the loading parameter will fail when the load exceeds its critical value in the sense that the shell must deform enormously to assume the configuration which corresponds to this load or that the shell passes on to a secondary mode of deformation. In both these cases, the shell is in a state of instability which leads to its buckling.

The steps followed in finding the critical pressure are as follows:

- i. First, the linear governing equations of the shell are solved by the multisegment method of integration as described earlier. With the linear solution providing initial values to the dependent variables, the non-linear equations are solved by the process of iteration at the initially assigned load.
- ii. The non-linear equations are then repeatedly solved for increasing values of the load parameter while the initial values for iteration process at any step of load parameter are provided by the solution for immediate previous step of loading.
- iii. If at any step of the scheme of increasing loading steps, the iteration process fails to converge, it first subtracts previous loading increment from the nondimensionalized loading, then halves the load increment and adds it to previous loading to arrive at the

new nondimensionalized loading. In this way the equilibrium configuration path is traced against increased loading.

- iv. The critical pressure is anticipated from the load-displacement curves, where the equilibrium configuration path is traced against increasing loading and the appearance of a secondary mode of deformation is searched. This appearance of a second solution always corresponds to the bifurcation point as pointed out by Thompson [166] and consequently, it is always the bifurcation point where the numerical solutions fail to converge as the shell structures become unstable as pointed out by Uddin [171].

It should be mentioned here that the term 'bifurcation point' is used here to refer to the point of initiation of a secondary mode of deformation, be it a limit point or a branching point.

3.7 ASYMMETRIC BUCKLING

Axisymmetric composite shells, made-up of axisymmetric segments joined to each other circumferentially, are observed to buckle either meridionally or circumferentially. These two modes of buckling of composite shells are usually referred to as axisymmetric buckling and asymmetric buckling. In axisymmetric buckling the fundamental axisymmetric configuration of the shell is maintained during the buckling process, only the meridional configuration of the shell changes suddenly. But, in asymmetric buckling, the instantaneous meridional configuration of the shell is maintained while the circumferential configuration suddenly passes on to new mode with the formation of a number of lobes around the circumference, all extending identically along the meridian.

Analysis of axisymmetric buckling is carried out by solving the governing non-linear equations of axisymmetric deformation for increasing level of loading up to the bifurcation point on the fundamental path, as stated earlier in this chapter. Asymmetric analysis may also be done from the solution of general non-linear governing equations containing terms like $N_{\xi\theta}$, $M_{\xi\theta}$, etc., but the method has not gained much popularity due to its complexity in solution. Asymmetric buckling analysis is generally done from eigen-value solution of linearized general governing

equations, derived from general governing equations in terms of perturbation of variables, known as the stability equations. The stability equations for asymmetric buckling of shells are presented in section 3.3.

The linearized stability equations, derived in section 3.3, are homogeneous. A finite difference scheme has been employed in the present investigation for the solution of these equations. The finite difference scheme reduces the governing equations along with the boundary conditions into a set of finite difference equations by confining the independent variables to a network of mesh points. The dependent variables have been selected in such a manner that the equations contain at best second order differential terms only. Thus a three point finite difference scheme is sufficient to convert the differential governing equations to finite difference equations.

The independent variable is the distance along the meridional length of a shell and its range is divided into N segments having lengths S1, S2 ,..... ,SN, starting at node point 2 at one boundary and ending at node point N+2 at the other. Two fictitious node points, 1 and N+3, are added outside the two boundary points. The difference equations in vector form are,

$$A_j Y_{j+1} + B_j Y_j + C_j Y_{j-1} = 0 \quad j = 2,3, \dots, N+2 \quad (3.16a)$$

where,

$$Y_j = \begin{bmatrix} u_\xi \\ u_\theta \\ u_\zeta \\ m_\xi \end{bmatrix}_j$$

$m_\xi = M_\xi / D$ and A_j, B_j, C_j are square matrices.

The boundary condition are expressed as

$$A_1 Y_3 + B_1 Y_2 + C_1 Y_1 = 0 \quad (3.16b)$$

$$A_{N+3} Y_{N+3} + B_{N+3} Y_{N+2} + C_{N+3} Y_{N+1} = 0 \quad (3.16c)$$

$$\text{Letting } Y_j = -P_j Y_{j+1} \quad , \quad j = 2,3 \dots, N+1 \quad (3.16d)$$

$$Y_{j-1} = -P_{j-1} Y_j \quad , \quad (3.16e)$$

Eqns. (3.16a) becomes

$$-A_j P_j^{-1} Y_j + B_j Y_j - C_j P_j^{-1} Y_j = 0 \quad (3.16f)$$

$$\text{or } P_j = (B_j - C_j P_{j-1})^{-1} A_j \quad (3.16g)$$

Elimination of Y_1 from the equations (3.16a) for $j=2$ and Eqns. (3.16b) yields

$$Y_2 + (B_1 - C_1 C_2^{-1} B_2)^{-1} (A_1 - C_1 C_2^{-1} A_2) Y_3 = 0 \quad (3.16h)$$

Comparing Eqns. (3.16h) with Eqns. (3.16e) gives

$$P_2 = (B_1 - C_1 C_2^{-1} B_2)^{-1} (A_1 - C_1 C_2^{-1} A_2) \quad (3.16i)$$

Now using the recurrence relation (3.16g) and the relation (3.16i) all the P_j 's can be calculated for $j = 2$ to $N+2$.

Since $Y_{N+2} = P_{N+2} Y_{N+3}$

$$Y_{N+1} = -P_{N+1} Y_{N+2} = P_{N+1} P_{N+2} Y_{N+3}$$

Equation (3.16c) can be written as

$$R Y_{N+3} = 0 \quad (3.16j)$$

$$\text{where } R = A_{N+2} + (C_{N+3} P_{N+1} - B_{N+3}) P_{N+2} \quad (3.16k)$$

For nontrivial solution, $Y_{N+3} \neq 0$

$$\text{and } |R| = 0. \quad (3.16l)$$

In general, for a given value of n , the determinant $|R|$ does not vanish if the external load P/E does not correspond to the buckling load.

To determine the asymmetric buckling load, at every load step the determinant $|R|$ is calculated for different values of circumferential lobe number n starting from 2, and the load corresponding to the vanishing determinant is selected as the buckling load, neglecting $n = 1$, as it corresponds to the translation of the shell.

3.8 ACCURACY AND RELIABILITY OF THE ANALYSES

In this work, both axisymmetric and asymmetric buckling behaviour of composite shells of revolution are studied both analytically and experimentally. To ensure the accuracy and reliability of solution, it is desirable that solutions obtained by any numerical technique be compared with the corresponding results in the literature, if available. This type of comparison

also helps to ascertain that no error in logic is committed in formulating the problem and no mistake has been made in the computer programming.

Multisegment method of integration has been employed here for obtaining the solution of non-linear governing equations of axisymmetric deformations of shells of revolution. The accuracy of the multisegment method of integration is actually self-ascertaining. Once the values of the fundamental variables at the nodal points are known from the multisegment method of integration, the fundamental set of differential equations is integrated over each segment of the meridian as an initial-value integration problem. If the values of the fundamental variables at the end of the segment S_i , as obtained from the initial-value integration, match up to a certain number of digits with their respective initial values for the segment S_{i+1} for $i = 1, 2, 3 \dots M$ and also with the given boundary conditions, only then the solution scheme accepts the results. In other words, the multisegment integration technique not only finds the solutions of a set of equations but also check that the solutions obtained satisfy the equations along with the boundary conditions.

Regarding the reliability of formulation of the problem and programming of computational technique, Ref. [171] can be referred to. In Ref. [171] solutions were found for uniformly loaded circular plate with clamped edge using the present formulation and methodology and it was found that the results are correct up to eight digits when compared with the results of the corresponding analytical solution. In Ref. [171], results were also obtained on the variation of meridional stress and circumferential stress along the meridian of ellipsoidal head pressure vessel based on both linear and non-linear theories by the present method of solution and were compared with previously established results. It was found that there was hardly any difference between these results. The results obtained for truncated conical shell by Ali [7] shows a fair agreement with those available in the literature for the identical boundary conditions. The observed deviations in the results were very much expected as the formulations of the problem and the criteria for predicting critical pressures are different for the two cases. That the used computer program can accurately calculate the critical pressure for axisymmetric shells of revolution of any geometry have been demonstrated by Uddin [171, 175, 176], Haque [61], Rahman [119], Ali [7], and Khan and Uddin [79].

For the determination of asymmetric buckling load, eigenvalue solution of the stability equations of general shells are required. The linearized stability equations of general shells contain prebuckling terms like $\bar{N}_{\xi 0}$, $\bar{N}'_{\xi 0}$, $\bar{N}_{\theta 0}$, which have been calculated here with the help of multisegment integration of the non-linear governing equations of axisymmetric shells of revolution. Tridiagonal matrix algorithm, a widely used solution technique, has been employed for the determination of the elements of the stability determinant. Some analytical and experimental problems of cylindrical and conical shells for which solutions are available in the literature, were tested to verify the code developed for asymmetric analysis here and the results from the current analysis were found to be around 10%-25% higher. This difference may be attributed to the reason that the results in the literature were found from the eigenvalue solution of stability equations with linear prebuckling data, whereas the present analysis uses non-linear prebuckling values obtained from the solution of governing equations derived considering large deflection of shells. As the prebuckling solution used in the buckling analysis is highly accurate the asymmetric results are also accurate and reliable.

EXPERIMENTAL INVESTIGATION

4.1 LITERATURE REVIEW ON EXPERIMENTAL PROCEDURE ON SHELL

BUCKLING

Experiments on buckling of shells has not yet been standardised. Researchers are continually developing newer experimental techniques in different ways to bring about a better correlation between analysis and test. Even when large powerful programs, like STAGS are employed for analysis, test results still differ considerably from prediction. These differences are partly due to the inaccuracies of inputs like shell geometry, boundary condition, imperfect shape, and amplitude, etc., and partly due to variations in buckling behaviour of the mathematical model and the shells tested. Experimental results are also found to depend on shell materials and manufacturing techniques.

Experiments on buckling of shells are generally done on their models because conduction of experiments on prototypes require large set-up, which is costly, as well as measurement of shell geometry becomes a tedious job. Experimental investigation of shells may be divided into two major steps , the first step is the fabrication of model shells and the second step is the experimental technique. Isotropic materials are common in fabricating shell models. Shells made of isotropic materials are found to be much imperfection sensitive than those of composite materials. So to achieve better results from isotropic shells, it needs precision manufacturing technology. Among the different shell fabrication techniques, spin forming, press forming, electrodepositing, explosive forming and copy milling are in wide use.

Literature on experimental techniques on buckling of shells are limited to only few different methodologies [10, 12, 13, 31, 32, 35, 55, 56, 97, 101, 109, 114, 130, 138, 140, 147, 165, 184, 185]. In most cases of shell buckling experiments very thin shell models are fabricated and, depending upon the opening of the shells, that is, either one end open or both ends open, the openings are closed with plates with proper sealing arrangements. Through one of the end-plates air is sucked out from interior of the shell with a vacuum pump so that atmospheric pressure outside the shell acts as external pressuring medium. The difference between the

pressure inside the shell and the atmospheric pressure outside the shell is considered as the net external pressure. Evacuation process continues until the buckling of the shell starts. Net external pressure at the point of buckling is considered as the buckling load. To study load-displacement behaviour of a shell, strain-gauges or displacement probes are placed at the salient points of the shell.

In Ref.[130], Ross and Palmer tested swedged-stiffened cylinders for buckling under uniform external pressure. The test cylinders were closed at both ends with end-closure plates keeping atmospheric air inside, and were put in a cylindrical pressure chamber. External pressure was applied to the shells by pumping in water inside the pressure chamber until the shells buckled with a fall in external pressure. In Ref.[55], instead of using end-closure plate at the open end of a cylindrical shell with one toriconical end, another such toriconical shell of same dimension was glued at the open end in such a manner that the assembly became a cylindrical pressure vessel with two toriconical ends. The remaining steps of this experiment was similar to that of Ref.[130].

New and Spring [109] developed a non-destructive experimental technique for determining incipient buckling pressures of thin shells subjected to external pressure. The salient feature of the technique is the filling of the internal volume of the shell with fluid, such as water, to control the magnitude and rate of shell deformation. The incipient buckling pressure was detected by noting the point at which the difference in internal and external pressure becomes constant. In Ref.[138] an attempt was made to find out a new non-destructive buckling test technique. This technique is based on the concept that natural frequency in the buckle mode shape goes to zero when the critical buckling load is reached. By measuring the modal parameters at various load levels below the critical buckling load one should, in principle, be able to predict the buckling load by extrapolating the load frequency interaction curve to zero frequency intercept. But till to date neither of the non-destructive tests received interest for some sort of inconveniences associated with the testing procedure as well as for unconservativeness in results.

In test set-ups, where external atmospheric pressure acts as loading medium, buckling load must always be less than the atmospheric pressure, which is the major limitation of this technique. Deflection measurement at predetermined locations is another limitation of this method, since

fabrication technique may dictate to such sort of imperfection that the shell may not buckle at the locations where deflections are measured. Keeping these disadvantages in mind, in the present work a new experimental technique is developed. The new method is very simple and capable of finding buckling loads for shells both above or below the atmospheric pressure. Electrodepositing technique has been employed for the fabrication of shell models for test. Model fabrication and experimental technique used for comparison of theory and test are described in the following sections.

4.2 PRESENT METHOD OF EXPERIMENTAL INVESTIGATION

4.2.1 Composite Experimental Shells

In the present work three different composite shells are studied namely cap-cone, cup-cylinder and dome-cylinder composite shells. From the analytical solutions presented in chapter-5 it is found that the cap-cone composite shells show some favourable buckling results. That is why experiment is done here only with the cap-cone shells. Geometries of cap-cone shells are shown in Figs. 4.1. For determining the buckling pressure of cap-cone composite shells, copper shell models with same apical angle and different tip ratio \bar{r}_j ($\bar{r}_j = r_j/R$) were fabricated by electrodepositing process. To keep the cone angle of the conical frustum portion of all the cap-cone composite shells the same, stainless steel die with the lowest tip ratio was first fabricated in a copying-lathe and then its corresponding shells were electrodeposited. In the succeeding steps the die was machined from the tip to conform to the next higher tip ratio, and the relevant shell models were electrodeposited. The procedure was repeated up to 4 values of tip ratio. The conical segment of the cap-cone shells, fabricated for experiment, had a semi apex angle of 30° . The die making steps are shown in Fig. 4.2.

A set-up, described below, was used for the evaluation of imperfections in the fabricated shells, the main purpose of which was to measure the physical dimensions of the shells. The tip ratio \bar{r}_j for each of the four sets of shells were calculated from the geometric data obtained from this set-up and were found to correspond to four values of 1.00, 0.80, 0.60 and 0.30 corresponding to the four sets of the shells respectively. The four sets of models are then designated as CS100, CS80, CS60 and CS30, corresponding to tip ratio of 1.00, 0.80, 0.60, and 0.30, respectively. There were no conical segments at the base of the CS100 shells. From the analysis of geometric

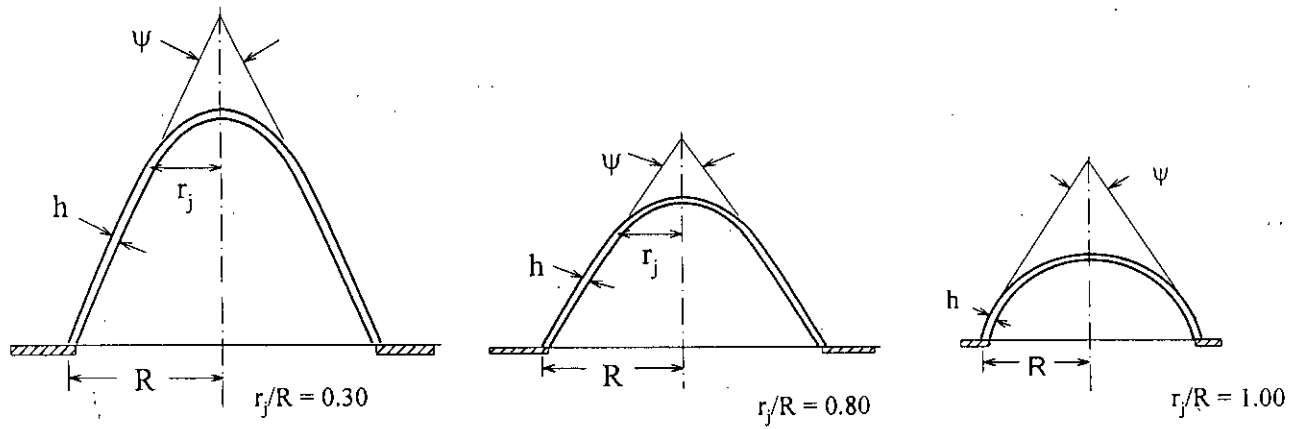


Fig. 4.1: Geometry of cap-cone shells with different tip ratio, r_j/R .

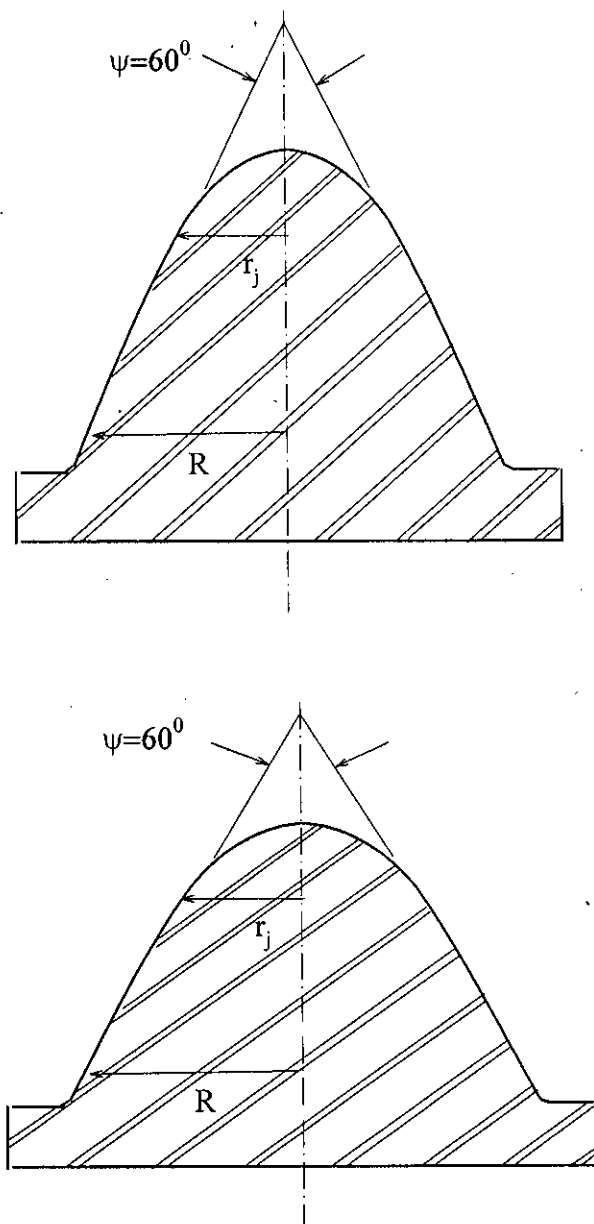


Fig. 4.2: Schematic diagram of die for electrodeposited test model.

data it was found that the meridian of the CS100 shells were composites of two circular arcs of different radii of curvature with the centres of curvature on the axis of the shells. The radius of curvature of the arc at the tip of the CS100 shells were larger than that of the other arc which extends from the junction of the arc at the tip to the base of the shell..

4.2.2 Experimental Set-Up for Imperfection Evaluation

After the fabrication of the four sets of experimental shells described earlier, the remaining die corresponded to the shell with the highest tip ratio. The spherical tip of this die was then removed by machining to fabricate a base for mounting the experimental shells in the test chamber. A piece of thick copper contour ring, as shown in Fig. 4.3(a), was then electrodeposited from the base for fixing the base of the experimental shells with the base-plate firmly. Finally the base of the die was machined to a base-attachment to suit the experiment. The final base is shown in Fig. 4.3(b). One mild steel ring shown in Fig. 4.3(c) was also fabricated for attaching the experimental shell models with the base-plate along with the copper contour ring so that the gripping pressure at the base of the shells become uniform.

The experimental shells and the fabricated base attachments were assembled together and the assembly was placed on a turn-table with the axis of the shell passing through the centre of the turn-table. The model-base assembly along with the turn-table was then placed on a level platform of a x-y-z co-ordinate measuring instrument (made by Mitutoyo, Japan). The accuracy of the co-ordinate measuring instrument was ± 0.01 mm. A fine-wire stylus was attached to the co-ordinate probe with an electric bulb and a battery in series with the shell to ascertain the contact of the probe with the shell. Schematic diagram of the geometry measuring set-up is shown in Fig. 4.4. Radial distances of points on the shells from the axis of the shells were then measured against axial distances of the shells along eight meridians at 45° intervals.

Geometric data of each shell was then processed with a graphical package to find the geometry of the shells. Different segmented curves were fitted to each of the meridian of a shell and the curve set for one of the meridian corresponding to minimum deviation was selected to represent the geometry of the shell. In the case of the cap-cone composite shells, two geometric curves

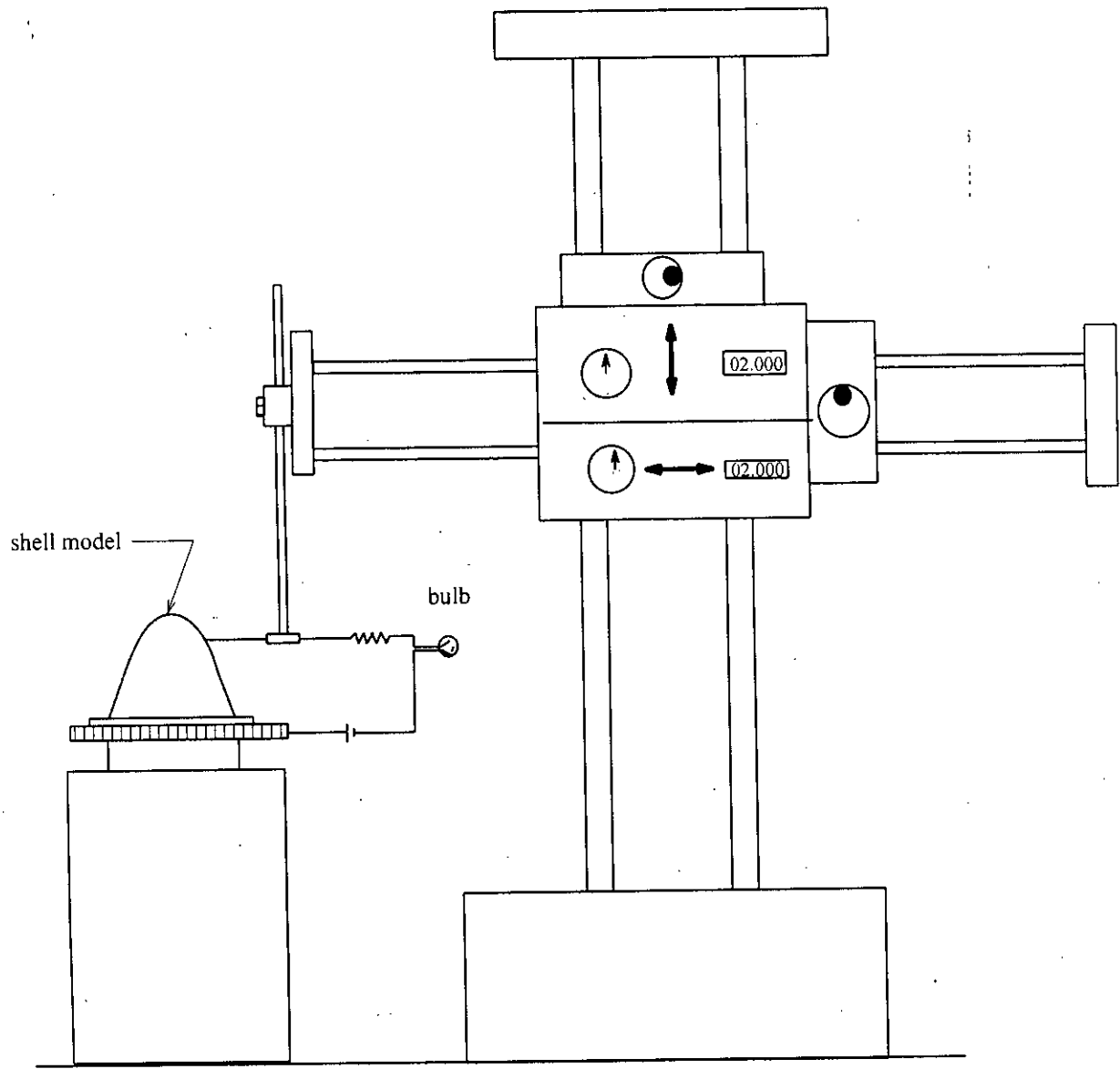


Fig.4.4: Schematic diagram of geometry measuring set-up.

were fitted to the meridians -a straight line to the conical portion of the shell and a circular arc to the spherical cap of the shell, meeting tangentially with the straight line. For the spherical caps ($\bar{r}_j = 1.0$) two circular arcs were fitted to the meridians. To determine the thickness of the shells, these were cut along three meridians after the experiment, and the thickness along these three meridians were measured with a precision micrometer. The accuracy of the micrometer was ± 0.001 inch. Description of the geometric parameters obtained from processed data are shown in Fig. 4.5. Geometric data and average thickness data of the shells are given in Tables 4.1 and 4.2

4.2.3 Experimental Set-Up for Buckling

A 10 inch high and 8 inch diameter triaxial test machine (made by ELE, U.K.) was used as the pressure chamber for the buckling test of the model shells. The wall of the pressure chamber was of transparent perspex cylinder of 0.5 inch thickness. The limiting pressure of the chamber was 250 psi. The top cover and the bottom platform of the pressure chamber were of metallic plates. The bottom platform could be isolated from the pressure chamber by removing the fastening bolts so that the experimental models could be firmly secured to it. There were a good number of ports on the base plate fitted with globe valves through which pumps, manometers, pressure gauges, volume meters, etc., could be connected. The schematic diagram of the set-up is shown in Fig. 4.6 .

4.2.4 Experimental Procedure

Schematic diagram of the experimental set-up with a shell-base assembly placed inside the pressure chamber is shown in Fig. 4.7. The experimental shell was filled with water and then was attached to the base-attachment along with a rubber ring, a rubber gasket and six 1/4 inch fastening bolts. Photograph of the elements of the base attachment are shown in Fig.4.8. The sectional view of the shell-base assembly inside the pressure chamber is shown in Fig. 4.6, and the relevant photograph of the shell-base assembly keeping the tip side up is shown in Fig. 4.9. A tripod was placed inside the pressure chamber to support the shell-base assembly keeping the tip of the model downwards and the base attachment upwards so that water inside the model could not come out through the hole at the base without the application of pressure external to

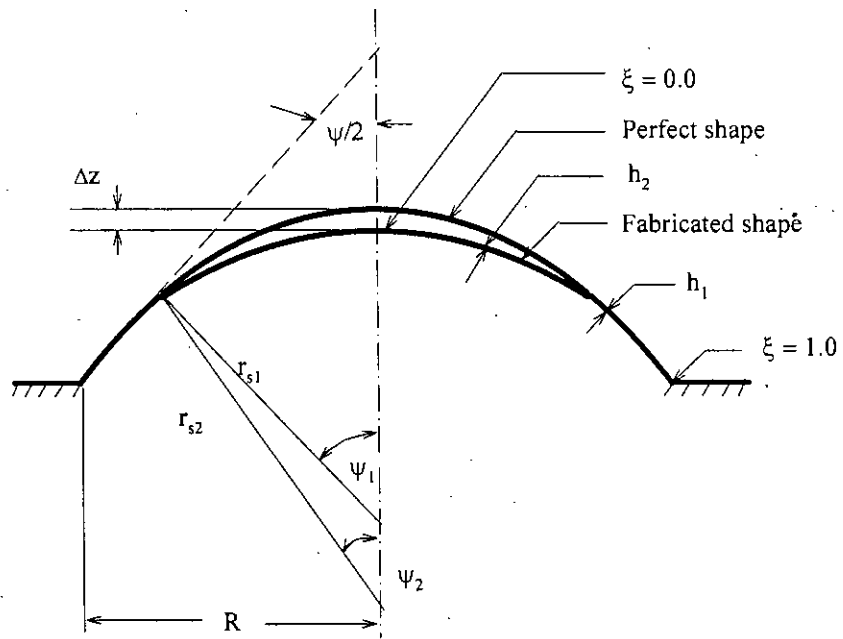


Fig. 4.5a: Geometry of spherical cap shell.

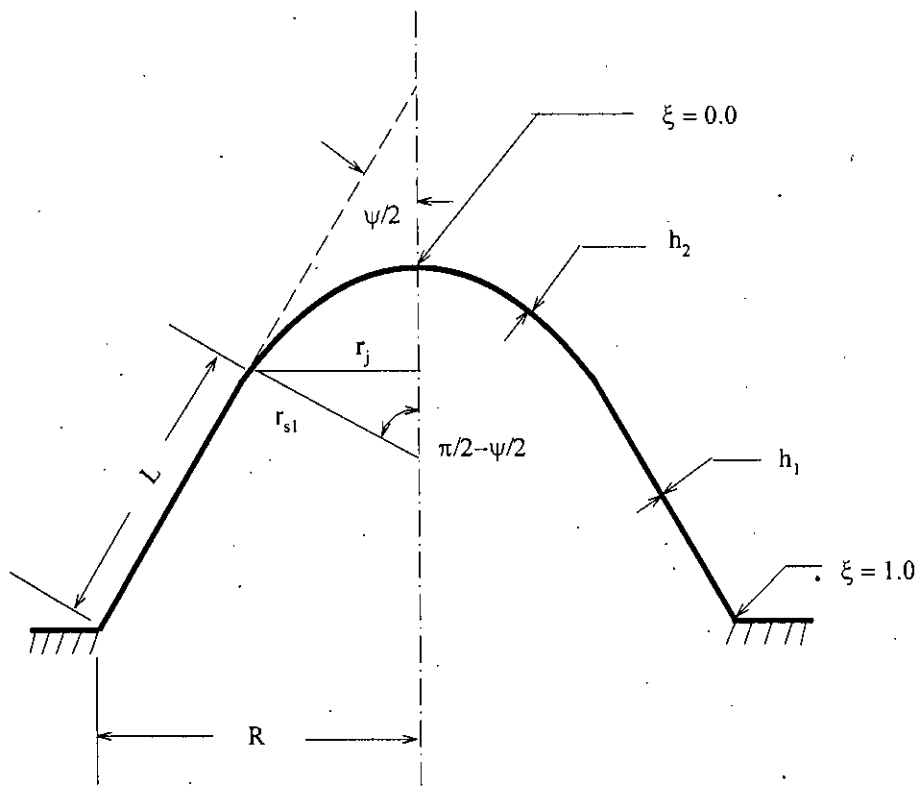


Fig. 4.5b: Geometry of cap-cone composite shell.

Table 4.1: Geometric data of fabricated spherical cap models CS100

Shell No.	$\Psi/2^\circ$	Ψ_1°	Ψ_2°	R mm	r_{s1} mm	r_{s2} mm	h_1 mm	h_2 mm	Δz mm
1	31.887	12.315	8.498	58.175	68.39	98.71	.102	.089	.49
2	31.365	13.127	9.678	58.14	68.09	91.98	.102	.076	.47
3	31.125	12.699	9.651	58.014	67.77	88.82	.108	.094	.40
4	31.92	11.565	9.087	58.256	68.63	87.12	.132	.109	.30
5	31.67	12.409	8.493	58.18	68.36	100.10	.109	.102	.421

Table 4.2: Geometric data of fabricated cap-cone models.

End-closure type	Model No.	$\Psi/2^\circ$	L mm	R mm	r_{s1} mm	r_j mm	h_1 mm	h_2 mm
CS30	1	29.886	81.413	58.046	20.16	17.479	0.089	0.127
	2	30.174	82.391	57.900	19.08	16.494	0.089	0.101
	3	30.029	81.486	57.800	19.66	17.185	0.089	0.114
CS60	1	30.174	46.436	58.139	40.06	34.639	0.109	0.0889
	2	30.029	45.700	58.381	40.44	35.014	0.132	0.088
	3	29.887	45.884	58.045	40.41	35.036	0.140	0.102
	4	30.029	46.395	57.803	40.10	34.713	0.135	0.102
CS80	1	30.174	15.987	57.965	57.78	49.890	0.102	0.097
	2	30.03	16.170	58.380	57.67	49.930	0.084	0.084
	3	30.174	16.090	57.965	57.59	49.530	0.094	0.076

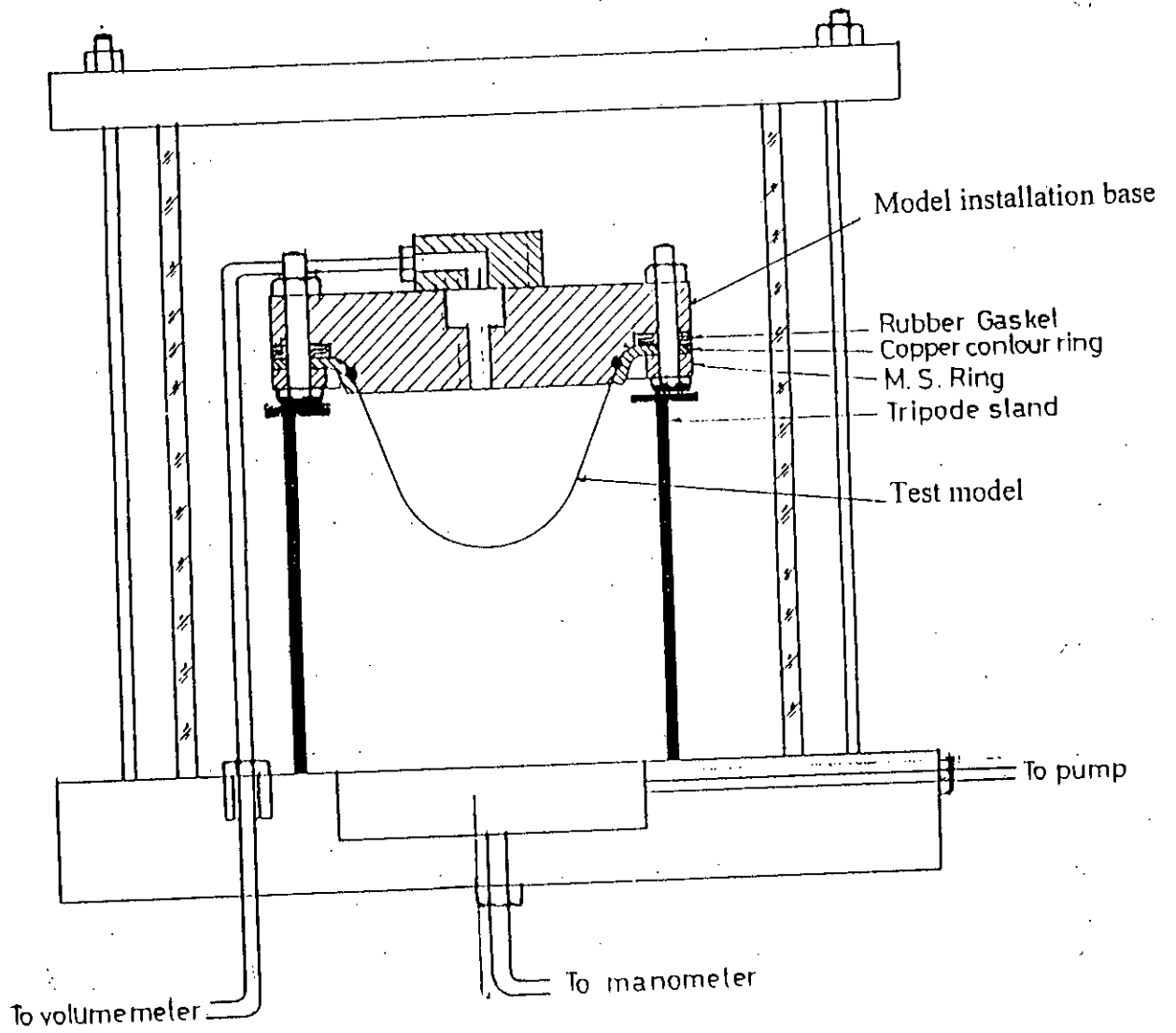


Fig. 4.6: Schematic diagram of pressure chamber with installed test model.

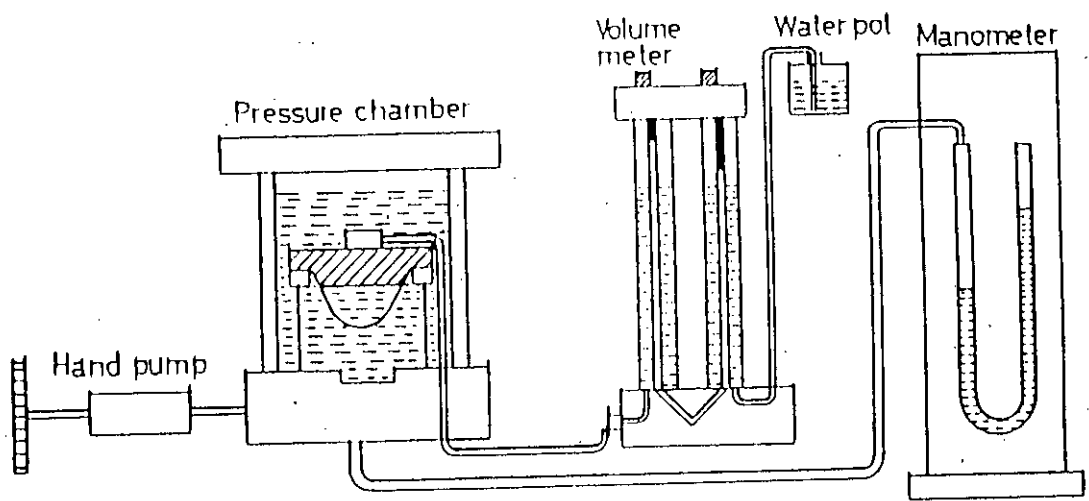


Fig. 4.7: Schematic diagram of buckling test set-up.

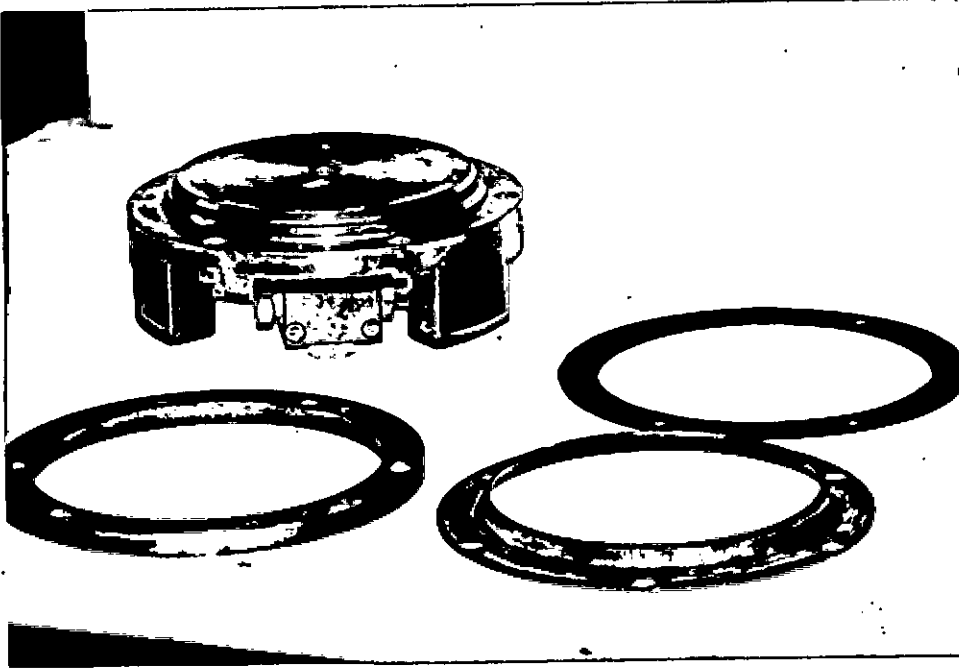


Fig.4.8: Test model installation elements.

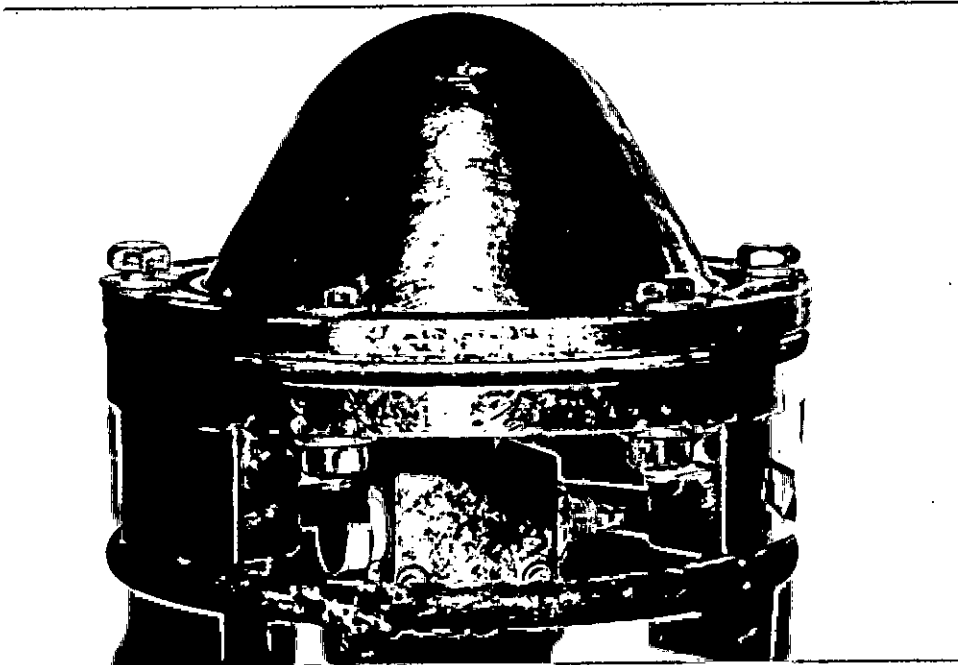


Fig.4.9: Test model installed on base.

the model. One end of a flexible tube that could sustain high external pressure without appreciable deformation was then connected with an adapter to the hole of the stainless-steel base. The other end of the flexible tube was connected to a double tube volume-meter through the base of the pressure chamber. The volume-meter was capable of measuring a change in volume of 0.1 ml. A mercury manometer was connected to the pressure chamber through the base of the pressure chamber. The pressure chamber was then filled with water through a hole at its top cover. Photograph of the experimental set-up is shown in Fig. 4.10.

Necessary leak test was done at every stage of the experiment. External pressure was applied to the shell by pumping in water by a screw type hand pump attached to the pressure chamber. The external pressure applied was gradually increased by steps and, at every step, the pressure was recorded. At every step of external pressure, the internal volume change of the model was recorded by the volume meter by measuring the amount of water coming out from inside of the model. The pressure was increased up to a limit when either the manometer reading remained constant or dropped suddenly with a large change in volume. The limiting pressure was observed to correspond either to a large deformation of the cap of the shells or of the conical base of the end-closure. This limiting pressure was considered to be the buckling load for the corresponding end-closure.



Fig.4.10: Photograph of experimental set-up.

RESULTS AND DISCUSSIONS

5.1 RESULTS OF THEORETICAL INVESTIGATION

5.1.1 Axisymmetric Analysis

Pressure vessels used in different pharmaceutical or petrochemical industries, or as hulls of submarines are generally constructed from combination of different geometries such as cylinders, cones, hemispheres, spherical caps, ellipsoids or some other exotic form. In majority of shell structures the main portion of the structure is cylindrical. The instability load under external pressure for a cylindrical shell becomes lower as the length of the cylinder increases. To improve the instability behaviour of long cylinders, number of ring stiffeners or bulk heads (in case of submarines) are provided in between the ends of the cylinder, where the segments of the cylinder between two consecutive rings or bulk heads act as short cylinders whose instability load is higher. But the pressure vessels of cylindrical shape need some other geometry like cone, spherical cap, hemisphere, etc., to close the ends. Among the end-closing shells, hemispherical, ellipsoidal or spherical caps are in wide use and the design of the whole pressure vessel which is a combination of different geometries is done on the basis of the buckling load sustaining capacity of the individual shell elements.

End-closures of the type mentioned above are very much sensitive to imperfections and thus the results of buckling load from analytical study are in wide disagreement with experiments. Experimental results of these shells are found to be about $\frac{1}{4}$ th to $\frac{1}{8}$ th of the analytical results. In contrast to the spherical or ellipsoidal end-closures, a conical end-closure may provide a better solution because its external pressure sustaining capacity is about 20% higher than the relevant cylindrical body. The sharp tip of a conical end-closure makes the space inside it useless as well as vulnerable to eccentric loading that may lead to failure either by yielding or by buckling in a translation mode and thus such conical shell has received less attention as end-closures of pressure vessels.

To find out a suitable end-closure of pressure vessels, different combination of shells of simple

geometry have been studied in this work , namely,

- 1) Cap-Cone composite shell [Fig.1.2(a)],
- 2) Cup-Cylinder composite shell [Fig.1.2(b)], and
- 3) Dome-Cylinder composite shell [Fig.1.2(c)].

Axisymmetric buckling of these end-closures with varying geometric parameters are discussed in the ensuing sections.

The non-linear differential equations of axisymmetric shells, which embody the principle of minimum potential energy, are solved for increasing values of load parameter till the first unstable state of equilibrium is reached. The onset of the first bifurcation point is hinted by a substantial increase in the displacements and stresses of the shell for very small increase in the load parameter. Right at the bifurcation point any increase of load parameter, however small, produces enormous deformations and, thus the numerical technique used here fails to converge to any solution.

That the present analysis based on axisymmetric deformations can predict the critical condition is justified by the following two theorems presented by Thompson [166].

Theorem-I: An initially stable (primary) equilibrium path rising monotonically with the loading parameter can not become unstable without intersecting a further distinct (secondary) equilibrium path.

Theorem-II: An initially-stable equilibrium path rising with the loading parameter cannot approach an unstable equilibrium state from which the system would exhibit a finite dynamic snap without the approach of an equilibrium path (which may or may not be an extension of the original path) at values of the loading parameter less than that of the unstable state.

Therefore, it is the initiation of the secondary path which the scheme of solution predicts, and up to this point, it is quite fair to assume that the deformations are axisymmetric.

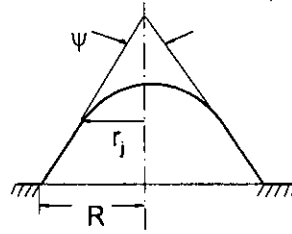
5.1.1.1 Cap-cone composite shell

Earlier, it has been mentioned that though conical shells can sustain high external pressure, they are not used as end-closures to pressure vessels because of their problems associated with the sharp tip. The problems relating to the tip of the conical shell may be eliminated by using a spherical cap assumed to be attached to the conical frustum in such a way that continuity of the slope at the cone-sphere junction is maintained [Fig.1.2(a)]. In this cap-cone composite shell, the radius of curvature of the spherical tip becomes smaller with the increase of slant height of the attached cone and is able to sustain higher buckling load if considered as an individual spherical cap shell. The geometric parameters of this cap-cone composite shell are the tip ratio, \bar{r}_j , ($\bar{r}_j = r_j/R$) the apex angle Ψ of the conical frustum, and the thickness ratio R/h , where r_j and R are respectively the radii of the cone at the sphere-cone and vessel-cone junctions and h is the thickness of the shell. Geometry of such combinations have already been defined in Fig. 4.5.

Critical pressures for cap-cone composite shells of three different apical angles of the conical frustum with different values of \bar{r}_j and R/h ratios were determined for axisymmetric buckling and are discussed here. It should be mentioned here that stability analysis is justified for thinner shells and thus the results presented are for higher R/h values like 100, 500, 1000 and 1500. For each value of the apical angle and the thickness ratio R/h , about 10 values of \bar{r}_j were studied and the results are presented in Table 5.1. Results of instability for values of parameters beyond this range can readily be obtained by using the computer program presented in Appendix-B of this thesis, if those are of any importance to the practising engineers. Critical pressure for all the shells of same apical angle and same thickness ratio, as presented in Table 5.1, are almost the same upto a certain range of \bar{r}_j , then decreases gradually to a minimum value at $\bar{r}_j = 1.00$

Summary of the results of the theoretical analysis for three sets of cap-cone end-closures of apical angle, $\Psi = 60^\circ, 120^\circ, 150^\circ$, for different R/h are presented in Figs.5.1-5.9. The results in these figures show that, for each apical angle, instability load is almost constant for a wide range of \bar{r}_j . From about $\bar{r}_j = 0.75$, for all the cases, buckling load decreases and is minimum at $\bar{r}_j = 1.0$ which corresponds to a pure spherical cap fitted to a cylinder of radius R . With the increase of either the cone angle or the thickness ratio, the buckling load is found to decrease. The constant

Table 5.1: Theoretical axisymmetric buckling pressure of cap-cone composite shells



Apex angle ψ°	Shell No	r_j/R	P_{cr}/E			
			$R/h=100$	$R/h=500$	$R/h=1000$	$R/h=1500$
60	1	0.25	1.29×10^{-4}	4.51×10^{-6}		
	2	0.35	1.29×10^{-4}	4.51×10^{-6}		
	3	0.50	1.29×10^{-4}	4.51×10^{-6}		
	4	0.60	1.29×10^{-4}	4.51×10^{-6}		
	5	0.75	1.29×10^{-4}	4.51×10^{-6}		
	6	0.80	1.30×10^{-4}	4.51×10^{-6}		
	7	0.85	1.10×10^{-4}	4.49×10^{-6}		
	8	0.90	9.75×10^{-5}	4.38×10^{-6}		
	9	0.95	9.31×10^{-5}	3.86×10^{-6}		
	10	1.00	9.03×10^{-5}	3.63×10^{-6}		
120	11	0.25	4.35×10^{-5}	1.70×10^{-6}	4.07×10^{-7}	1.74×10^{-7}
	12	0.35	4.35×10^{-5}	1.70×10^{-6}	4.07×10^{-7}	1.75×10^{-7}
	13	0.50	4.36×10^{-5}	1.70×10^{-6}	4.03×10^{-7}	1.75×10^{-7}
	14	0.60	4.34×10^{-5}	1.70×10^{-6}	4.07×10^{-7}	1.75×10^{-7}
	15	0.75	4.26×10^{-5}	1.71×10^{-6}	4.07×10^{-7}	1.74×10^{-7}
	16	0.80	3.97×10^{-5}	1.72×10^{-6}	4.03×10^{-7}	1.74×10^{-7}
	17	0.85	3.77×10^{-5}	1.59×10^{-6}	4.07×10^{-7}	1.73×10^{-7}
	18	0.90	-	1.44×10^{-6}	3.64×10^{-7}	1.59×10^{-7}
	19	0.95	3.28×10^{-5}	1.32×10^{-6}	3.00×10^{-7}	1.44×10^{-7}
	20	1.00	2.94×10^{-5}	1.15×10^{-6}	2.94×10^{-7}	1.34×10^{-7}
150	21	0.25	1.18×10^{-5}	4.62×10^{-7}	1.15×10^{-7}	4.35×10^{-8}
	22	0.35	1.16×10^{-5}	4.62×10^{-7}	1.15×10^{-7}	4.59×10^{-8}
	23	0.50	1.16×10^{-5}	4.62×10^{-7}	1.15×10^{-7}	5.02×10^{-8}
	24	0.60	1.16×10^{-5}	4.62×10^{-7}	1.13×10^{-7}	4.82×10^{-8}
	25	0.75	1.00×10^{-5}	4.58×10^{-7}	1.15×10^{-7}	4.87×10^{-8}
	26	0.80	9.27×10^{-6}	4.33×10^{-7}	1.14×10^{-7}	5.07×10^{-8}
	27	0.85	8.63×10^{-6}	3.91×10^{-7}	1.06×10^{-7}	3.91×10^{-8}
	28	0.90	8.04×10^{-6}	3.60×10^{-7}	7.75×10^{-8}	4.32×10^{-8}
	29	0.95	7.49×10^{-6}	3.41×10^{-7}	8.07×10^{-8}	3.91×10^{-8}
	30	1.00	6.99×10^{-6}	3.22×10^{-7}	7.68×10^{-8}	3.46×10^{-8}

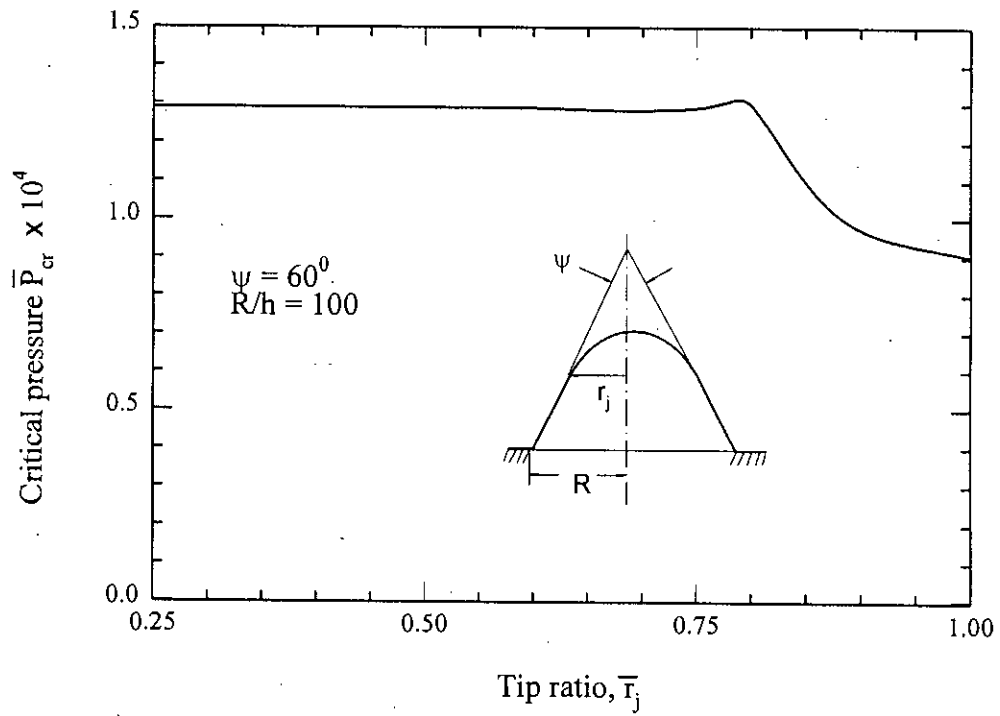


Fig. 5.1: Variation of critical pressure with tip ratio, \bar{T}_j of cap-cone composite shell.

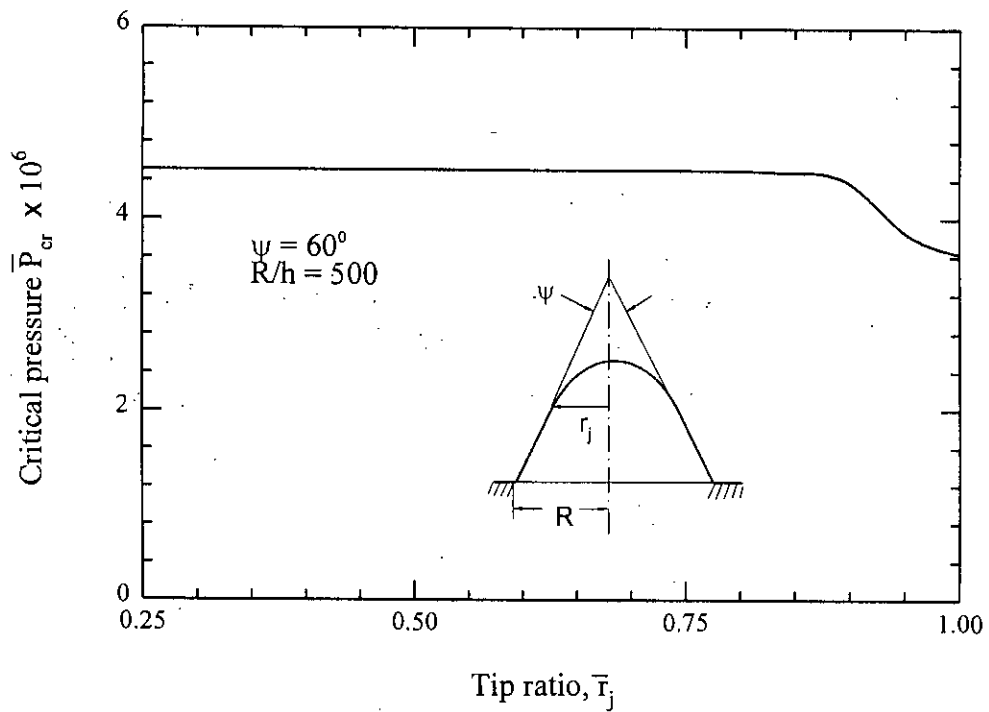


Fig. 5.2: Variation of critical pressure with tip ratio, \bar{T}_j of cap-cone composite shell.

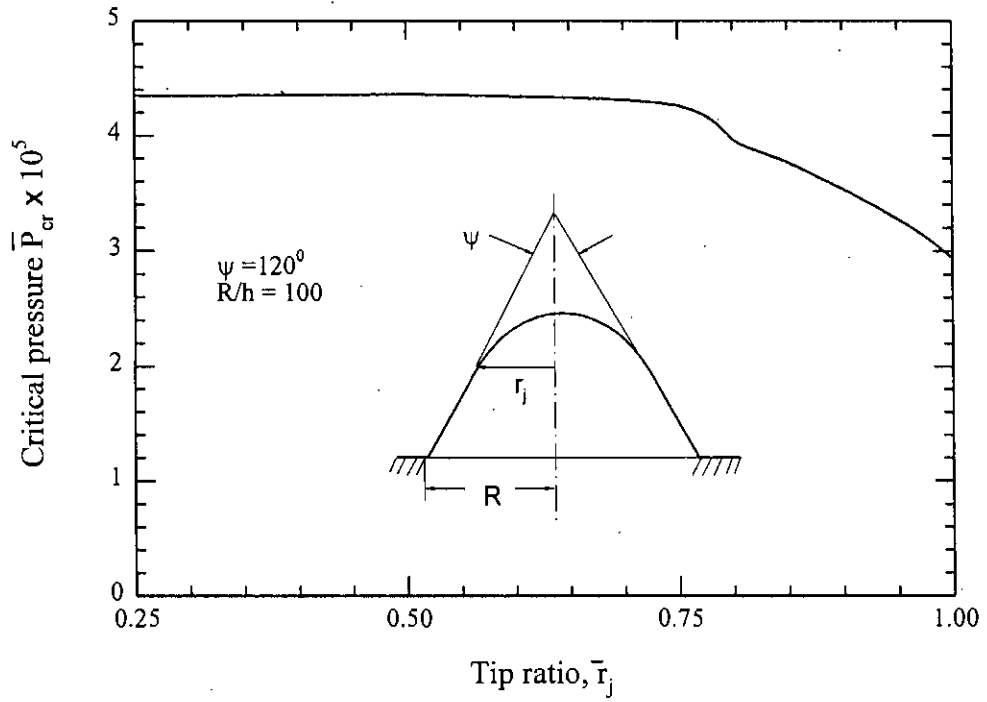


Fig. 5.3: Variation of critical pressure with tip ratio, \bar{r}_j of cap-cone composite shell.

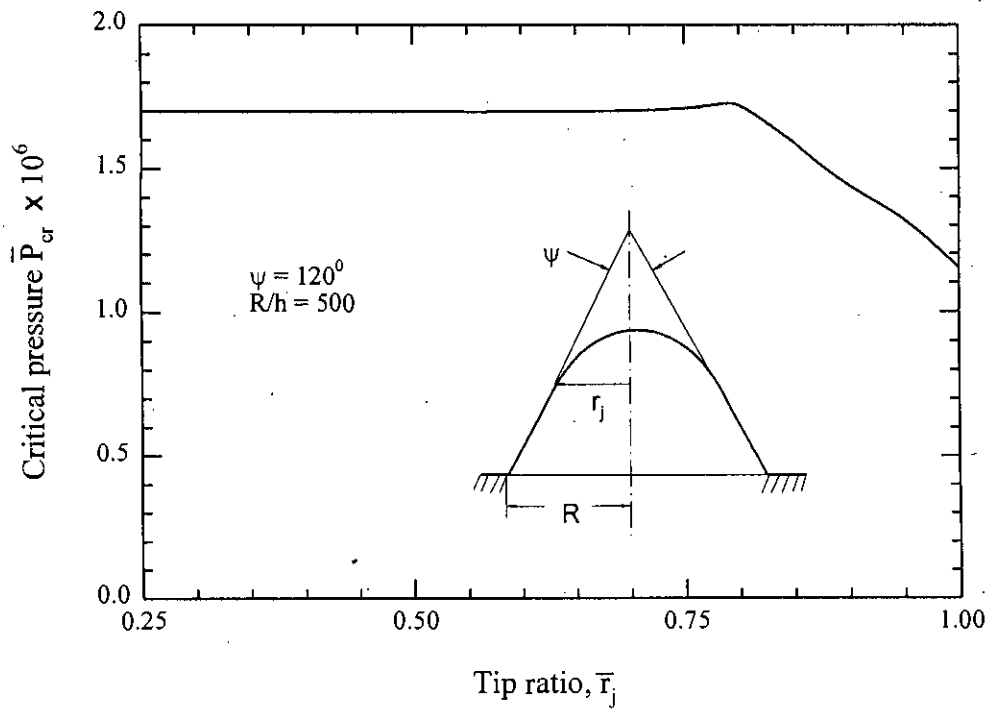


Fig. 5.4: Variation of critical pressure with tip ratio, \bar{r}_j of cap-cone composite shell.

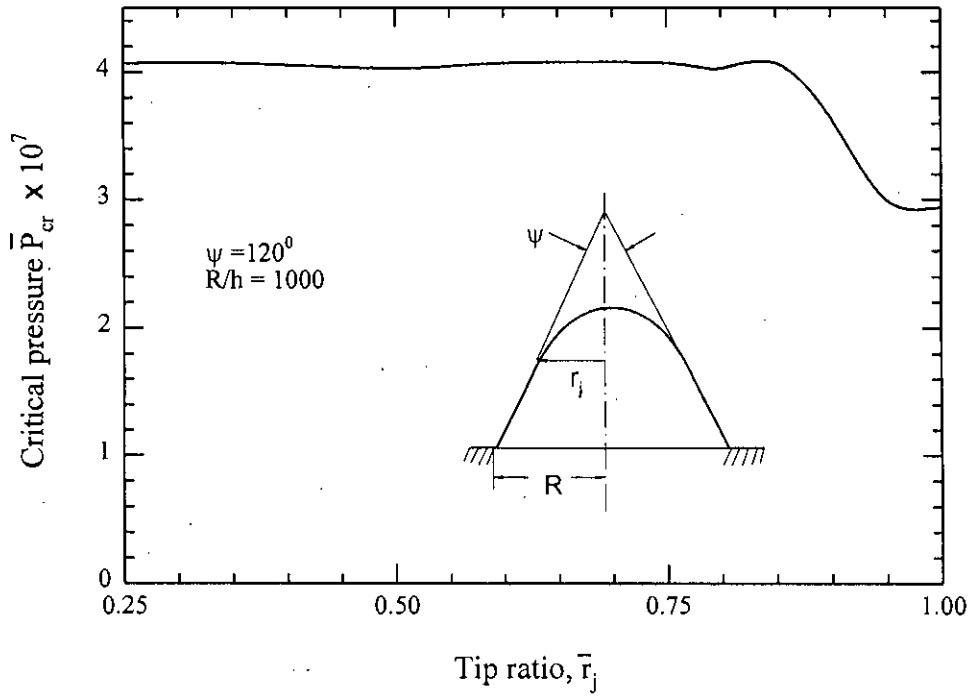


Fig. 5.5: Variation of critical pressure with tip ratio, \bar{r}_j of cap-cone composite shell.

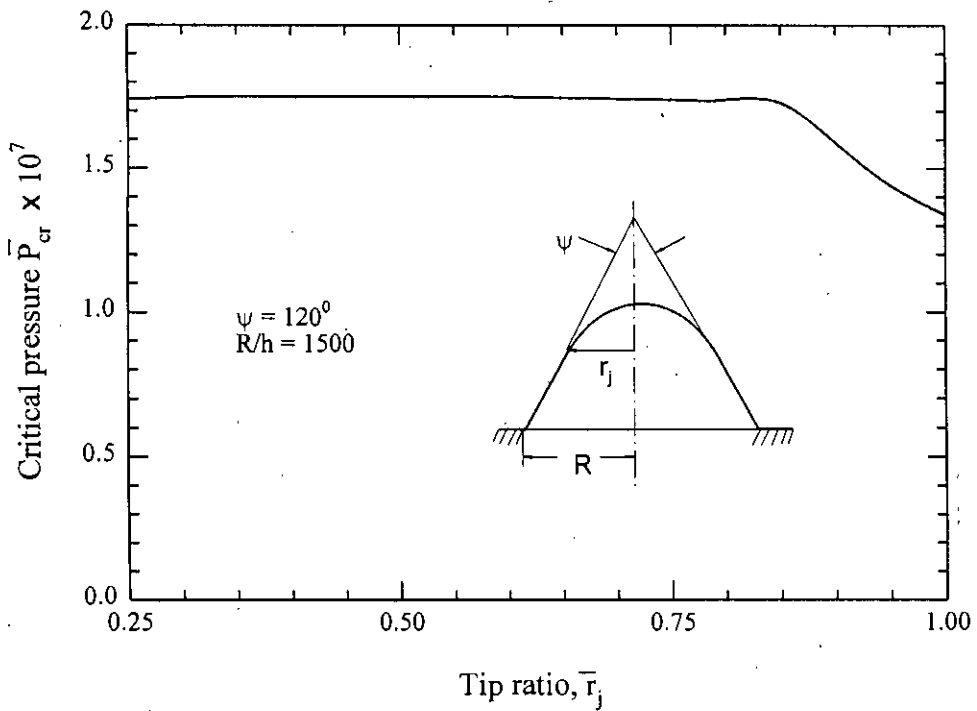


Fig. 5.6: Variation of critical pressure with tip ratio, \bar{r}_j of cap-cone composite shell.

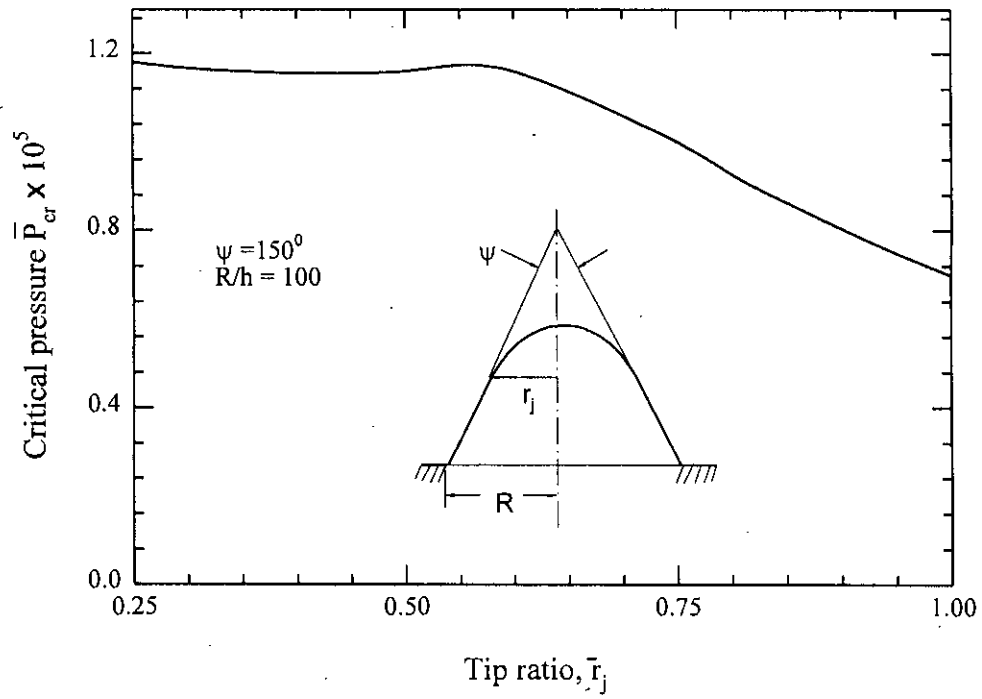


Fig. 5.7: Variation of critical pressure with tip ratio, \bar{r}_j of cap-cone composite shell.

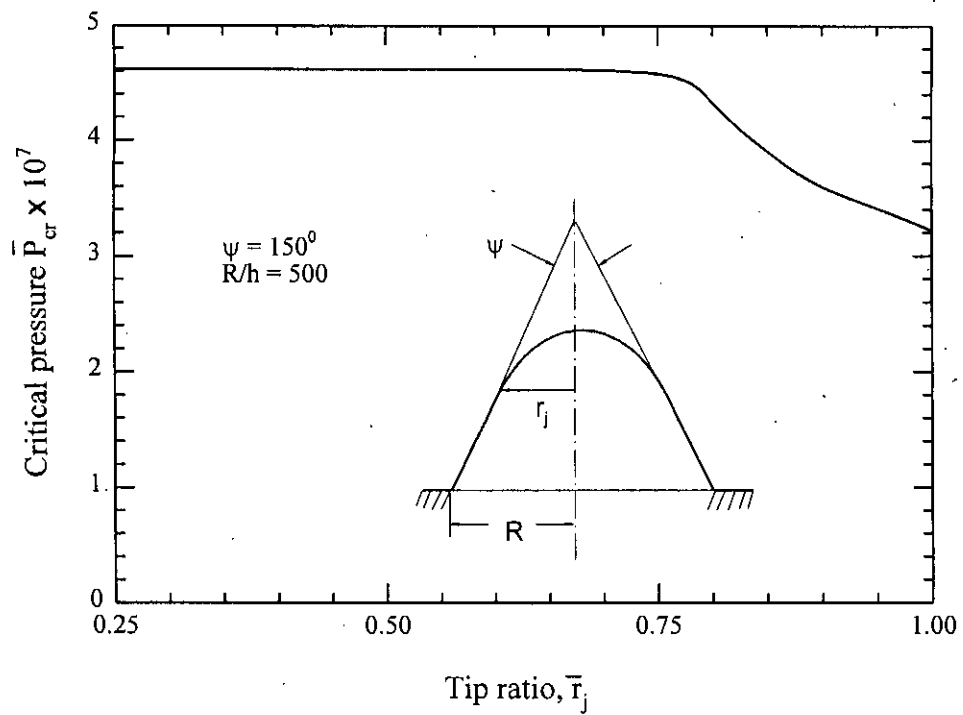


Fig. 5.8: Variation of critical pressure with tip ratio, \bar{r}_j of cap-cone composite shell.

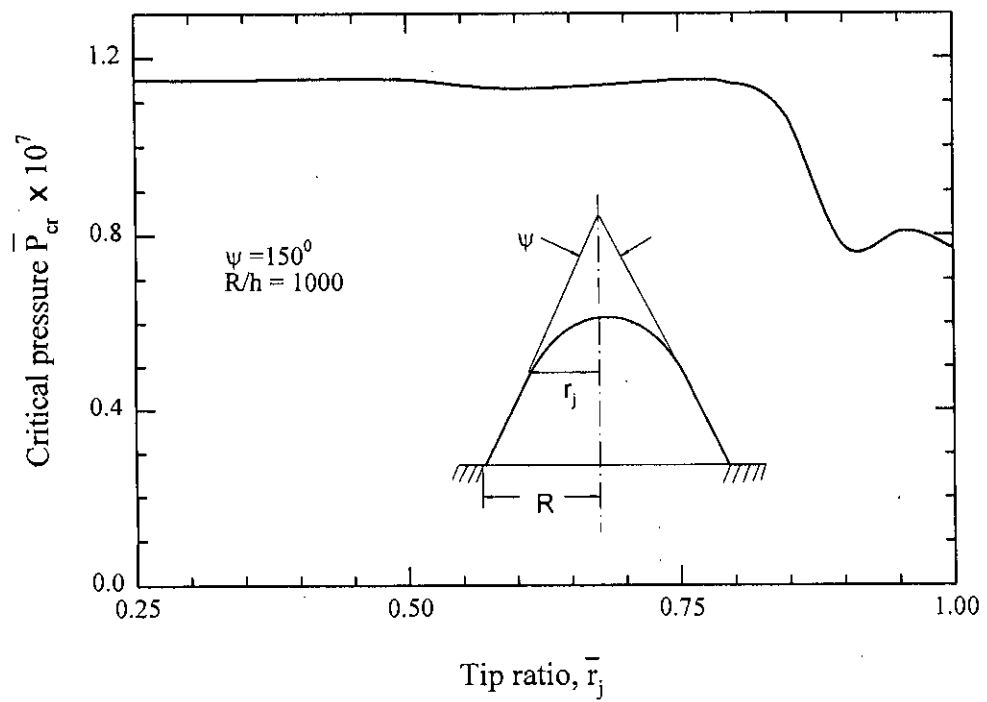


Fig. 5.9: Variation of critical pressure with tip ratio, \bar{r}_j of cap-cone composite shell.

value of buckling pressure is around 40%, 50% and 70% greater than their lowest value that occurs at $\bar{r}_j = 1.0$ and $R/h = 100$ for apex angle 60° , 120° and 150° , respectively. For the other higher R/h ratio, the trend is similar. Thus it seems that the addition of a conical extension to a spherical-cap end-closure may improve the external pressure sustaining capacity of the end-closure.

In Figs.5.10-5.13, the deformed configurations of four shells of $\bar{r}_j = 0.25, 0.50, 0.75$ and 1.00 , having $R/h = 100$ and apex angle $\psi = 120^\circ$, are shown schematically when loaded critically. The shells in Figs.5.10, 5.11 and 5.12, having conical base, deform severely near the base but the spherical tip remains almost unaffected. The deformation pattern of these three shells have close similarity. Such similarity is also observed in the case of the other cap-cone combinations of different apical angles and thickness ratios. The similarity in buckling load for these cap-cone combinations may be attributed to their similar deflection pattern. Fig.5.13 shows that the simple spherical cap with no conical base deforms severely throughout the shell meridian. All other spherical caps with different cap angles and thickness ratios also undergo severe deformation throughout their shell meridians.

The behaviour of the nondimensional axial and radial displacements against load for $\Psi=120^\circ$, $R/h=100$, and $\bar{r}_j = 0.25, 0.50, 0.75$ and 1.00 are shown in Figs.5.14-5.17 and in Figs.5.18-5.21, respectively. In Figs.5.14-5.16, irrespective of the values of \bar{r}_j , almost all the points on these shells maintain a common trend of inward deflection. In Fig.5.17, for $\bar{r}_j=1.00$, meaning a pure spherical cap without any conical extension at the base, it is found that most of the points along the meridian of the cap move inward with the increase of load except that near the middle of the meridian, which move inward initially with the increase of load and then outward at a very high rate near the critical load. Irrespective of the values of \bar{r}_j the load versus radial displacement behaviour of these shells shown in Figs.5.18-5.21, is similar to that of a pure spherical-cap ($\bar{r}_j=1.00$).

The meridional distribution of the nondimensional stress resultants \bar{N}_ξ and \bar{N}_θ , and the moment resultants \bar{M}_ξ and \bar{M}_θ are shown in Figs.5.22, 5.23, 5.24 and 5.25, respectively. Each one of

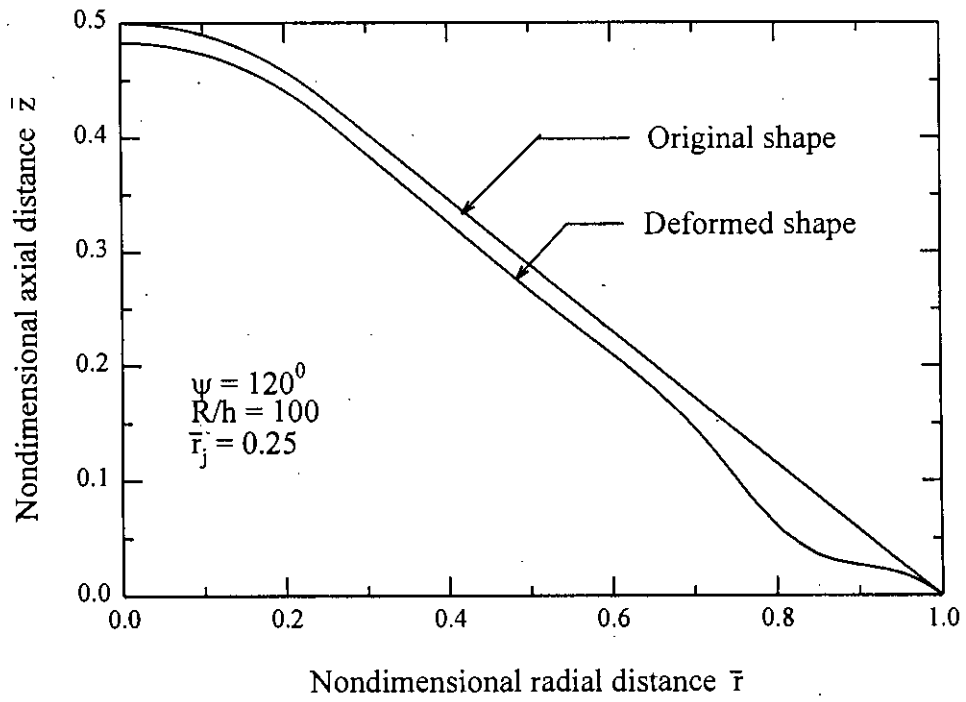


Fig. 5.10: Shape before and after buckling of cap-cone composite shell.

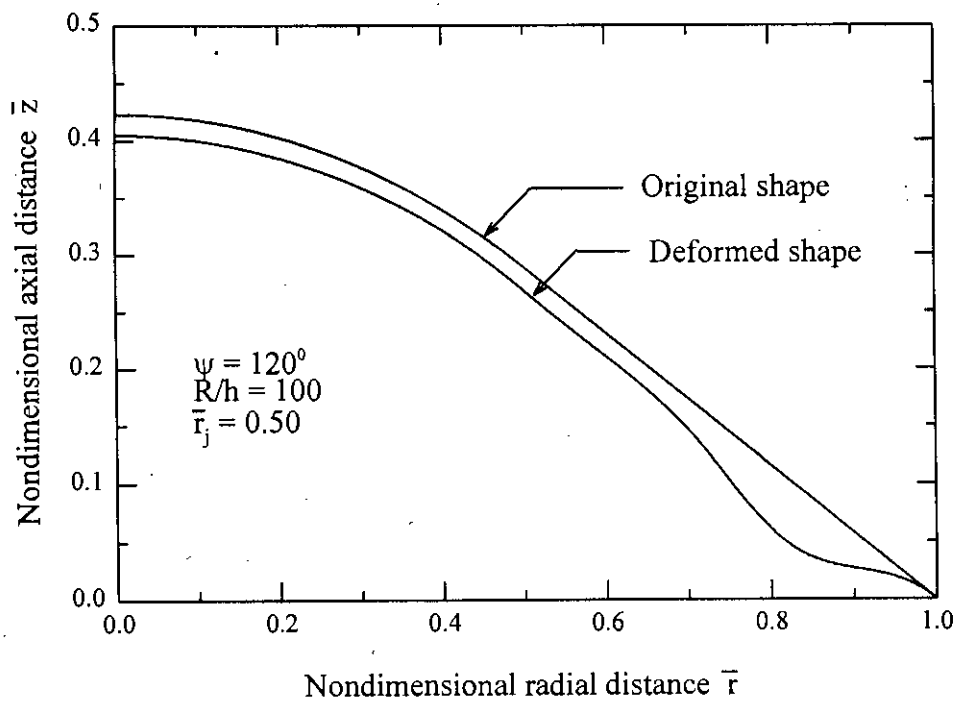


Fig. 5.11: Shape before and after buckling of cap-cone composite shell.

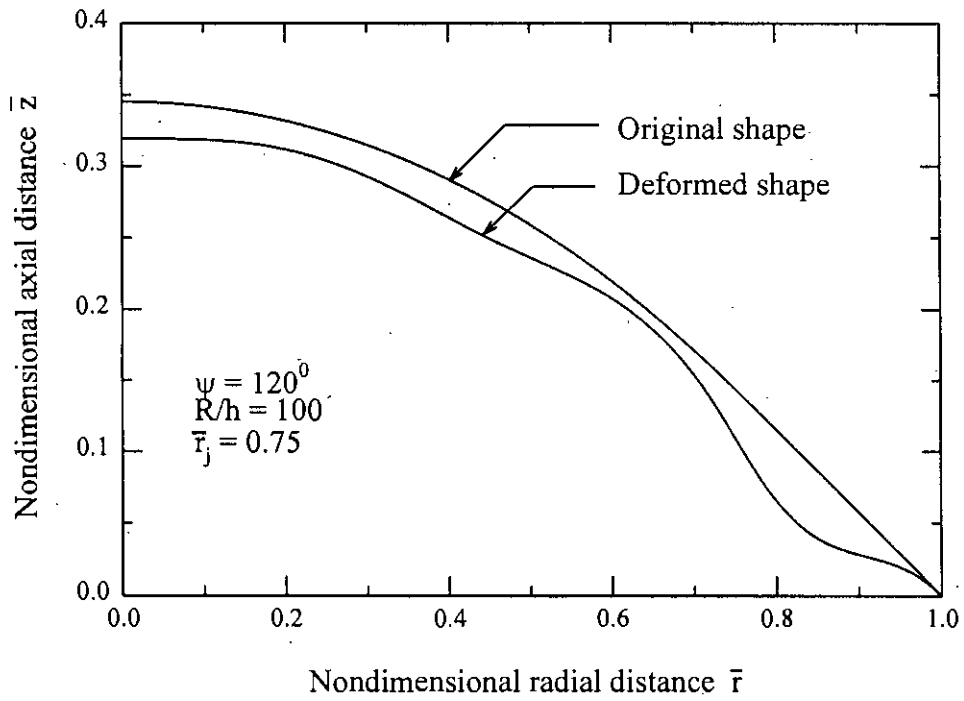


Fig. 5.12: Shape before and after buckling of cap-cone composite shell.

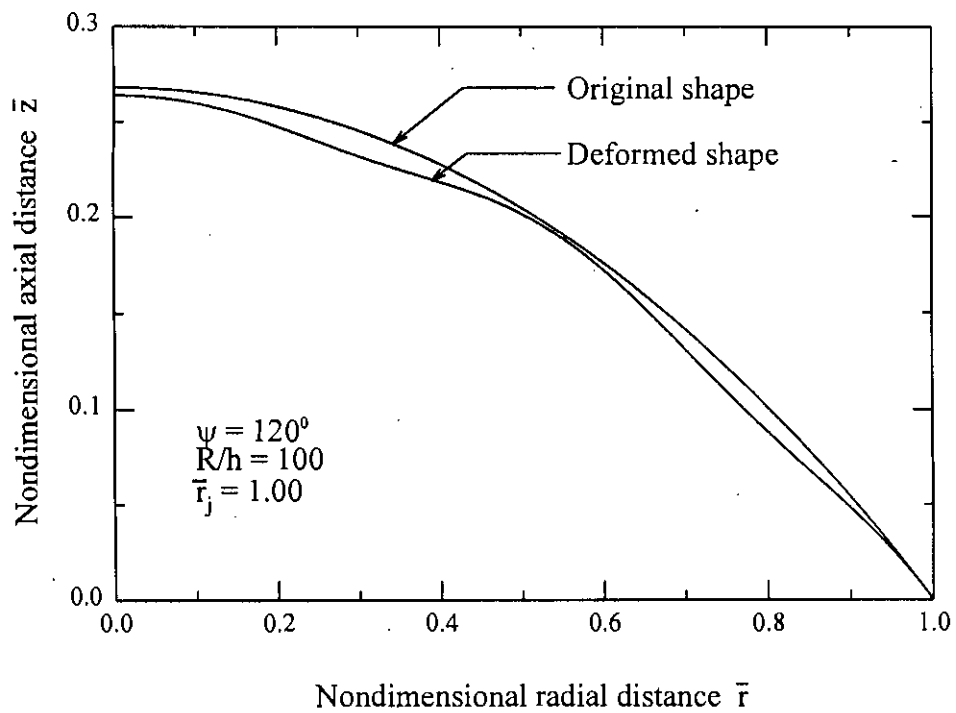


Fig. 5.13: Shape before and after buckling of cap-cone composite shell.

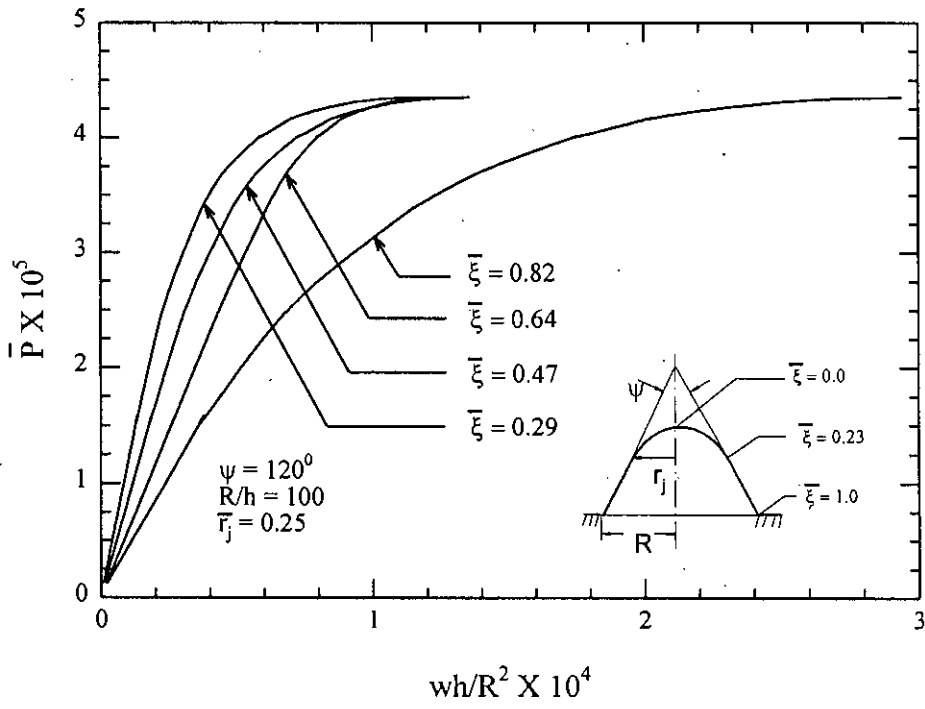


Fig. 5.14: Fundamental path of points on the surface of cap-cone composite end-closure.

90974

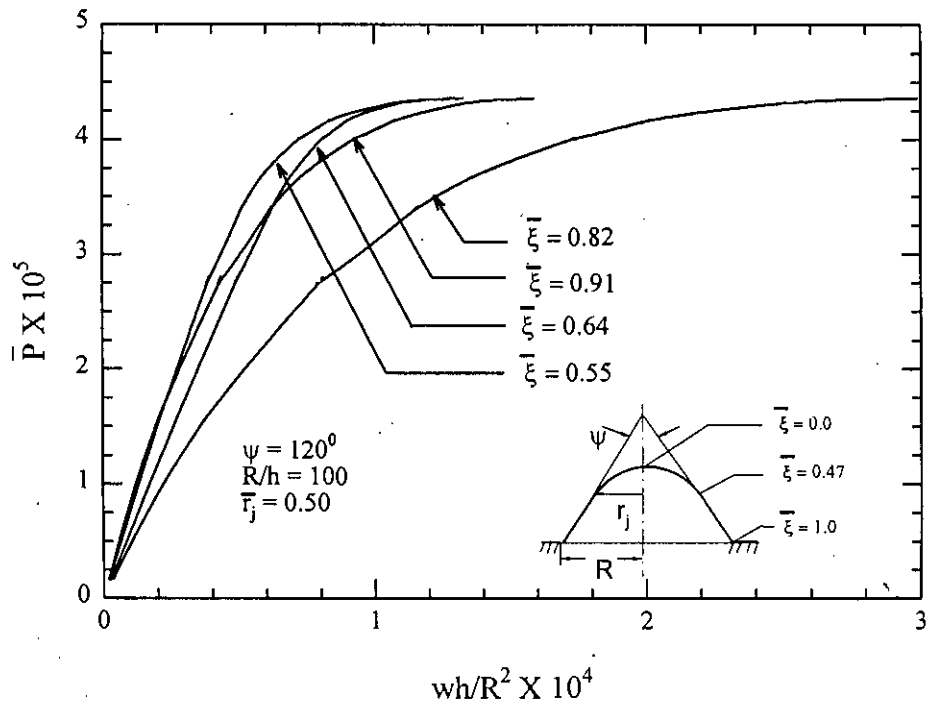


Fig. 5.15: Fundamental path of points on the surface of cap-cone composite end-closure.

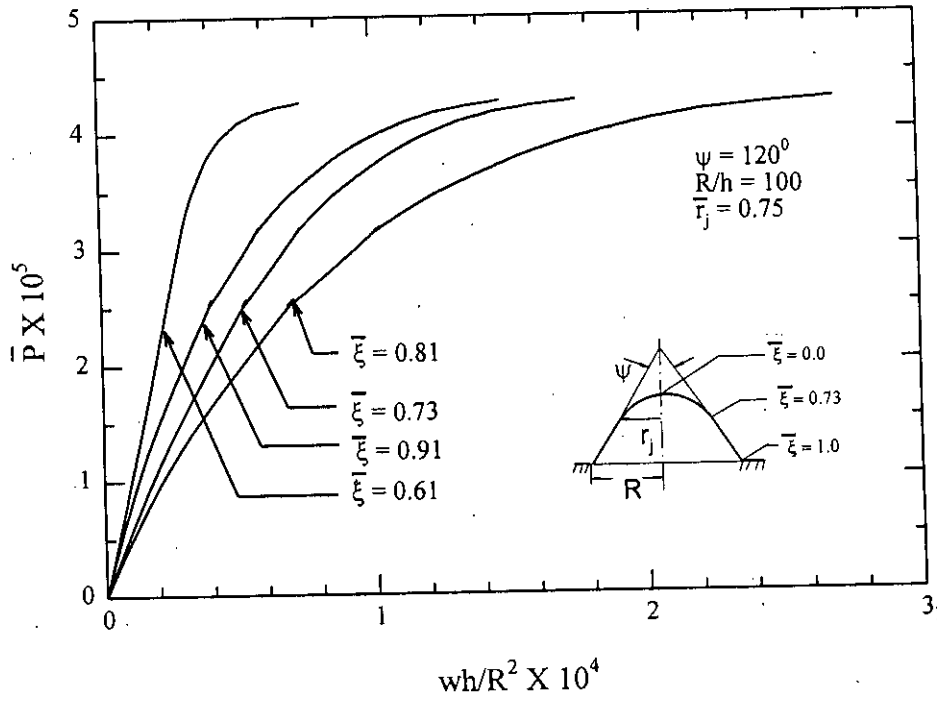


Fig. 5.16: Fundamental path of points on the surface of cap-cone composite end-closure.

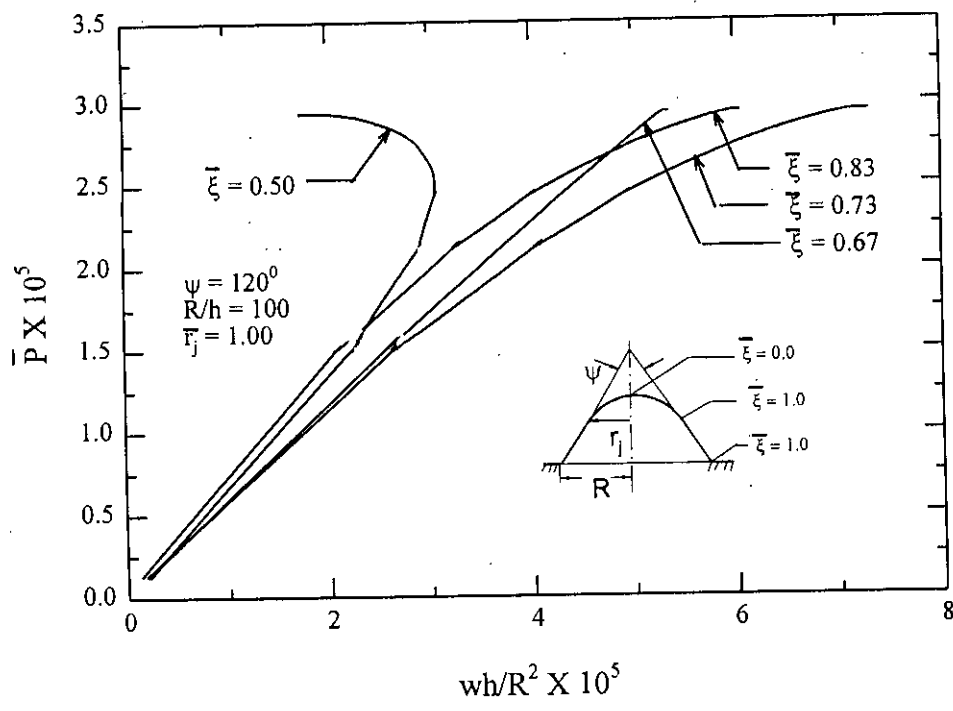


Fig. 5.17: Fundamental path of points on the surface of cap-cone composite end-closure.

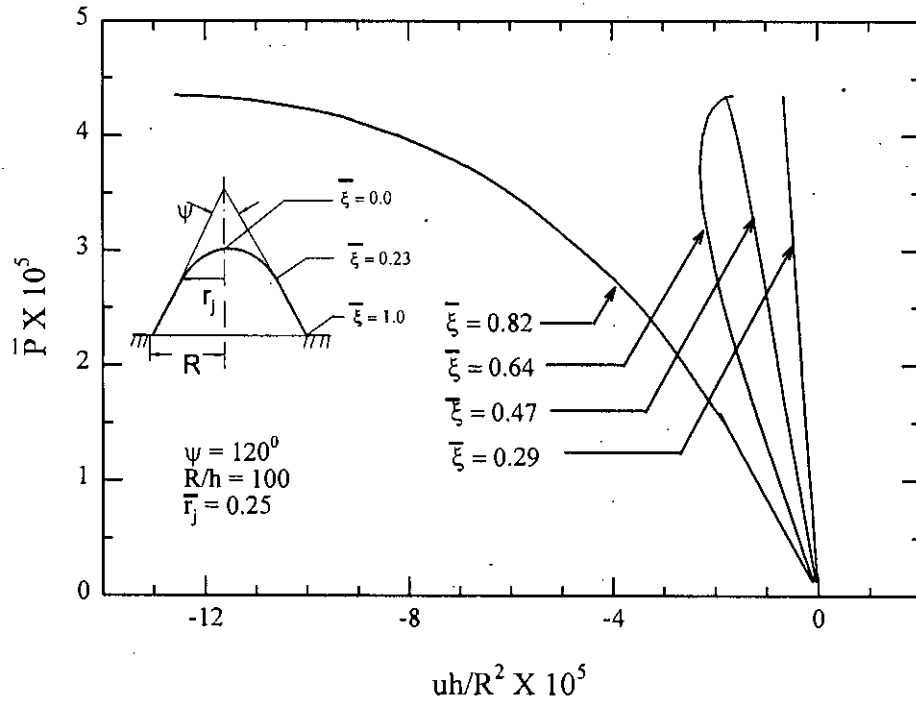


Fig. 5.18: Load versus radial displacement behaviour of cap-cone composite end-closure.

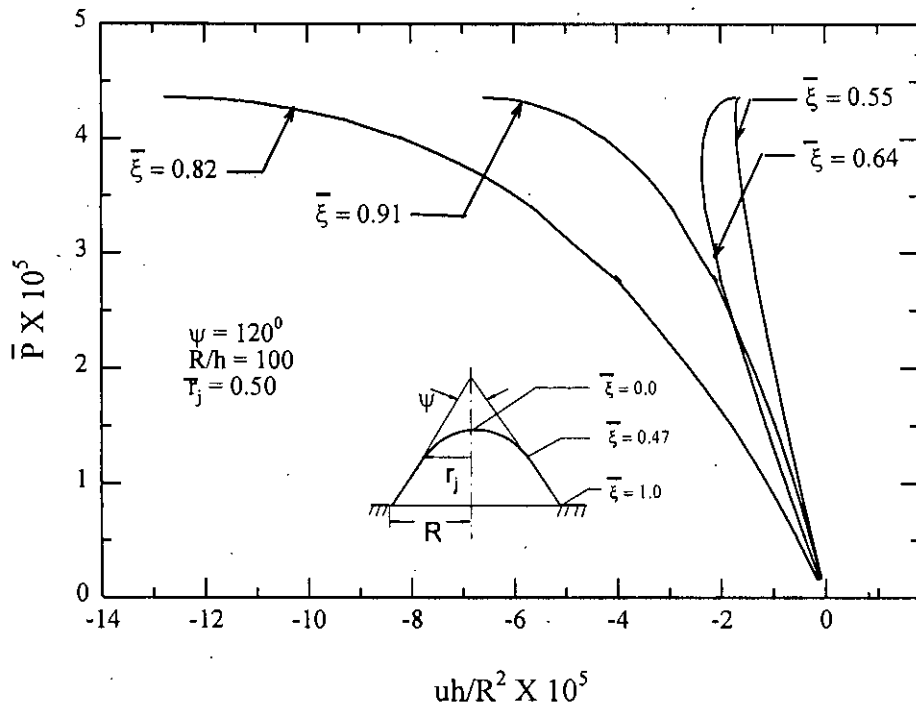


Fig. 5.19: Load versus radial displacement behaviour of cap-cone composite end-closure.

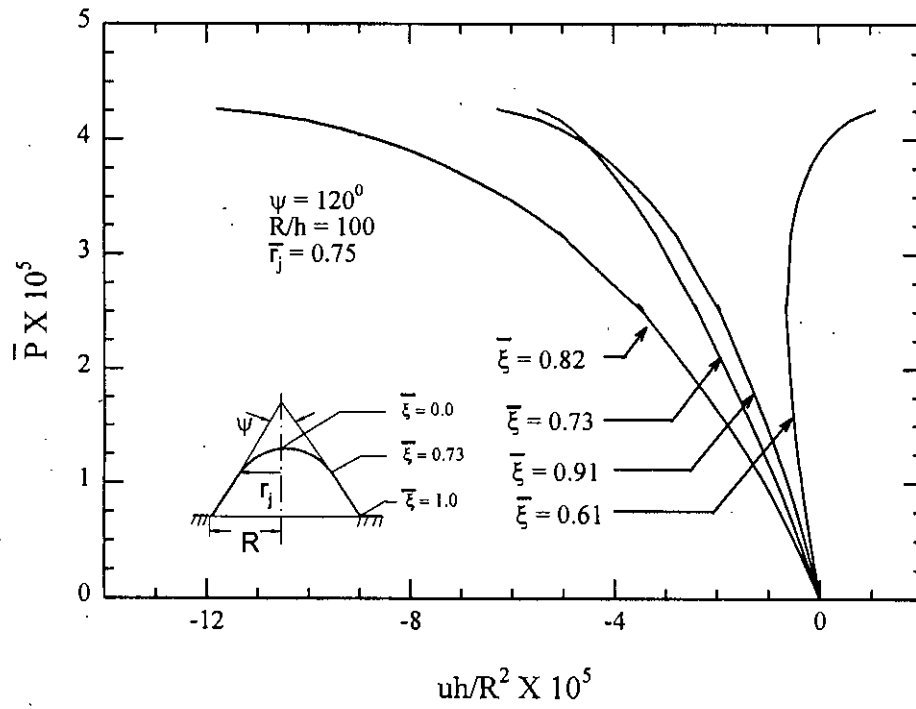


Fig. 5.20: Load versus radial displacement behaviour of cap-cone composite end-closure.

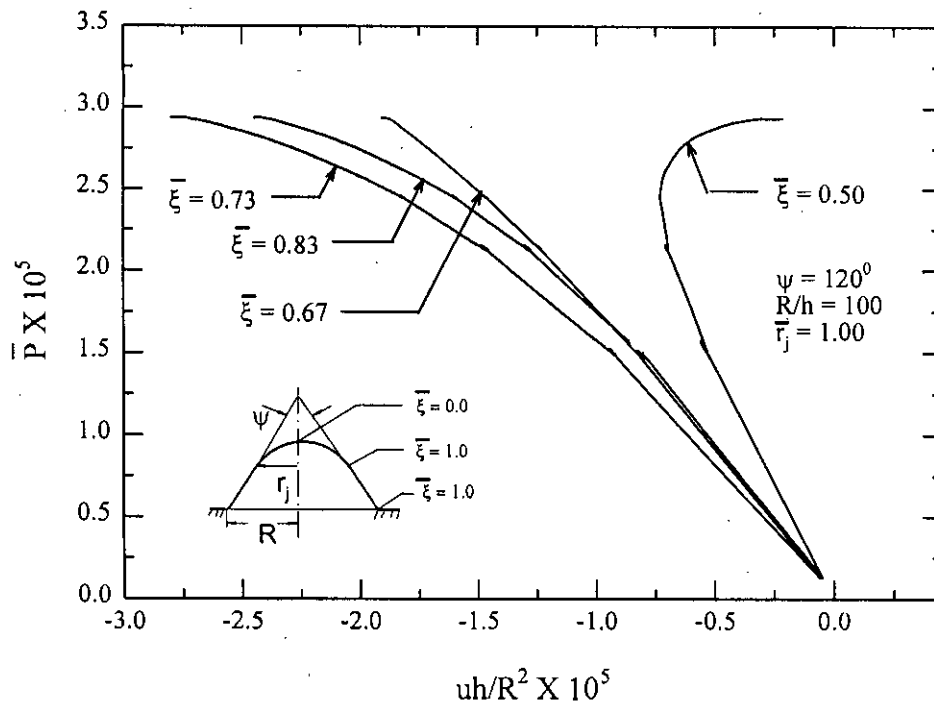


Fig. 5.21: Load versus radial displacement behaviour of cap-cone composite end-closure.

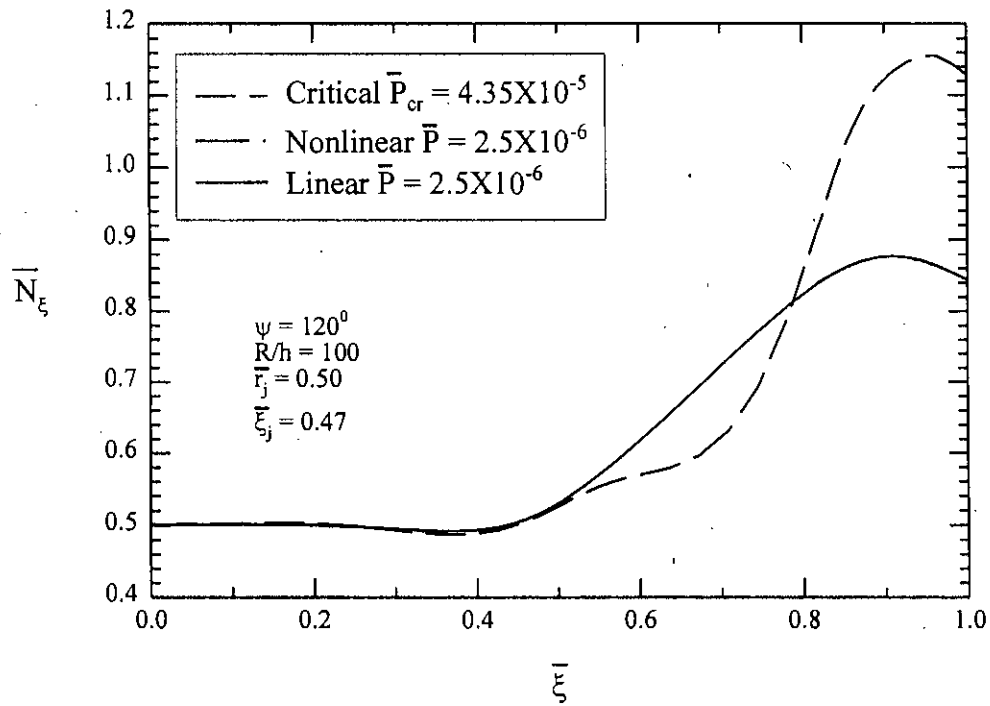


Fig. 5.22a: Variation of meridional stress resultant along the meridian in cap-cone composite end-closure.

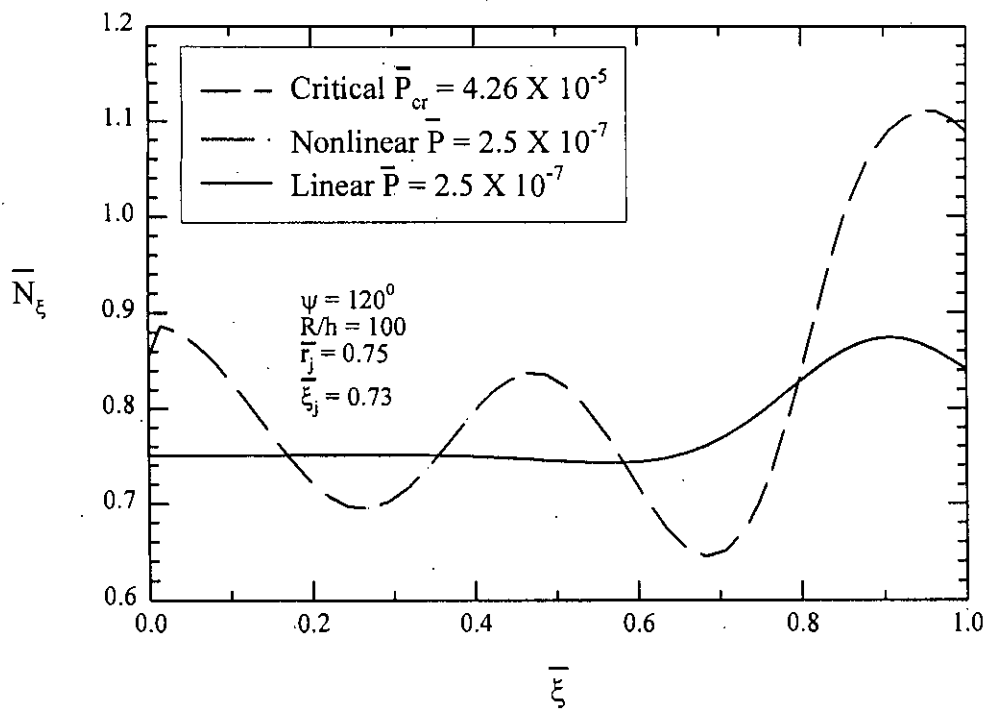


Fig. 5.22b: Variation of meridional stress resultant along the meridian in cap-cone composite end-closure.

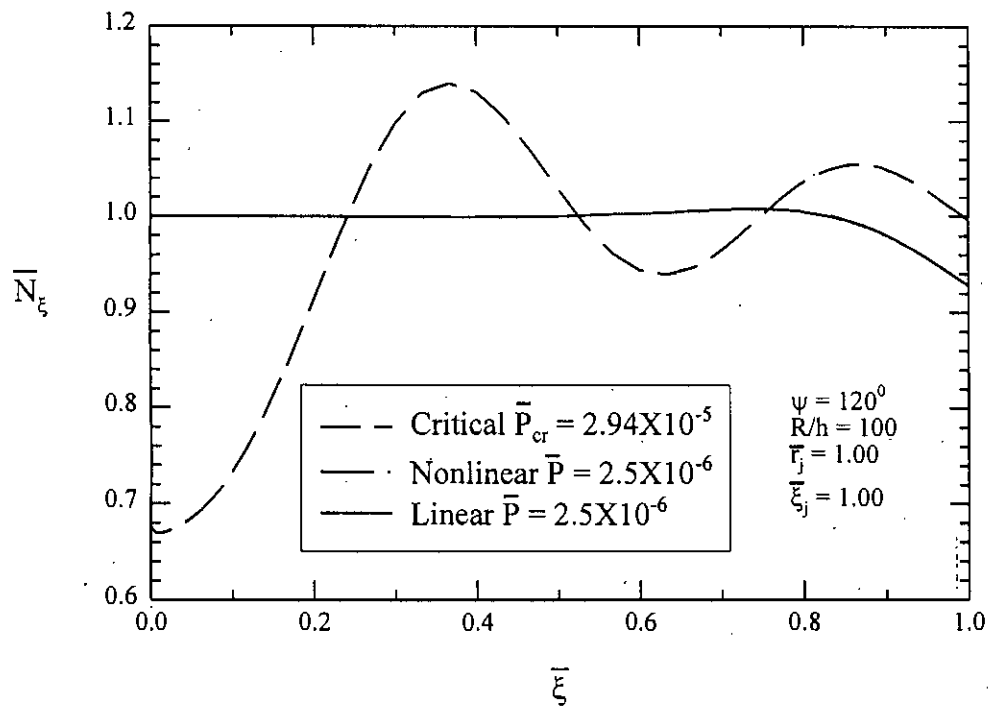


Fig. 5.22c: Variation of meridional stress resultant along the meridian in cap-cone composite end-closure.

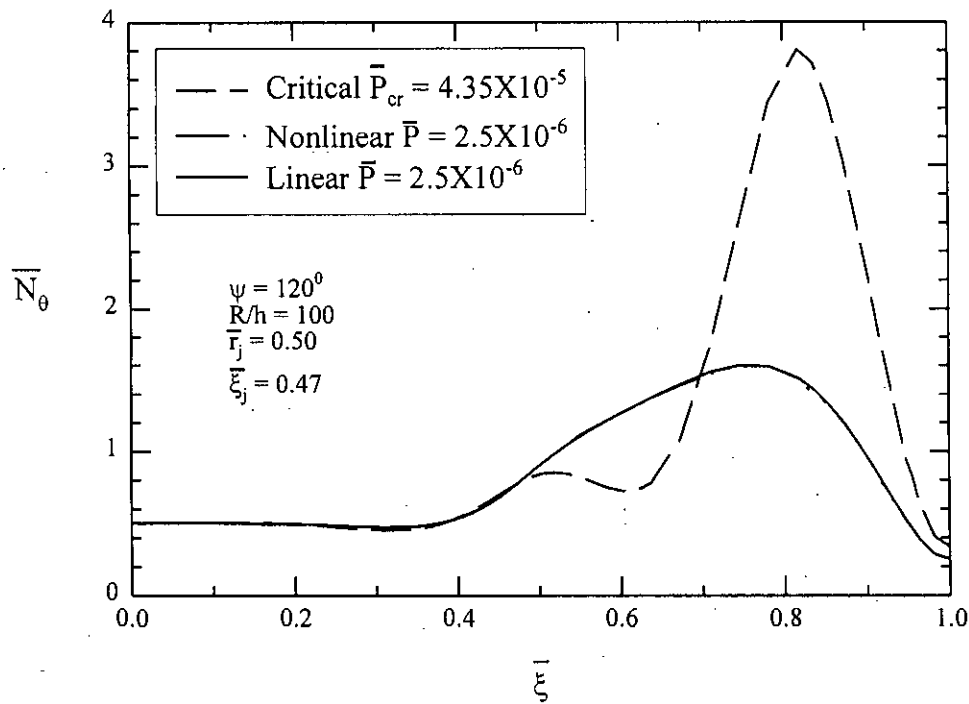


Fig. 5.23a: Variation of circumferential stress resultant along the meridian in cap-cone composite end-closure.

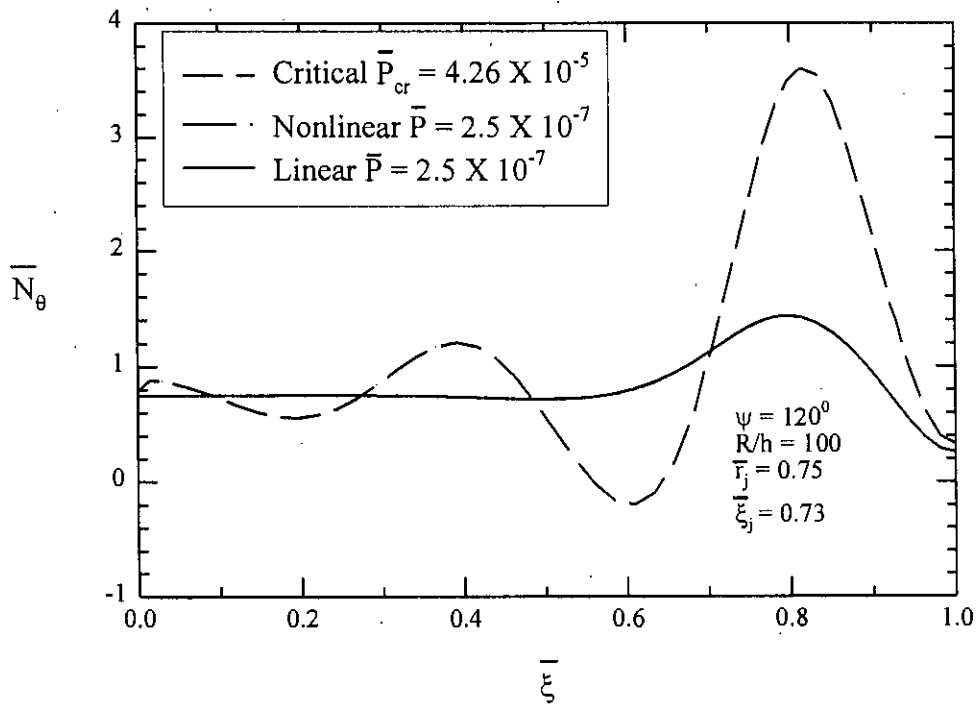


Fig. 5.23b: Variation of circumferential stress resultant along the meridian in cap-cone composite end-closure.

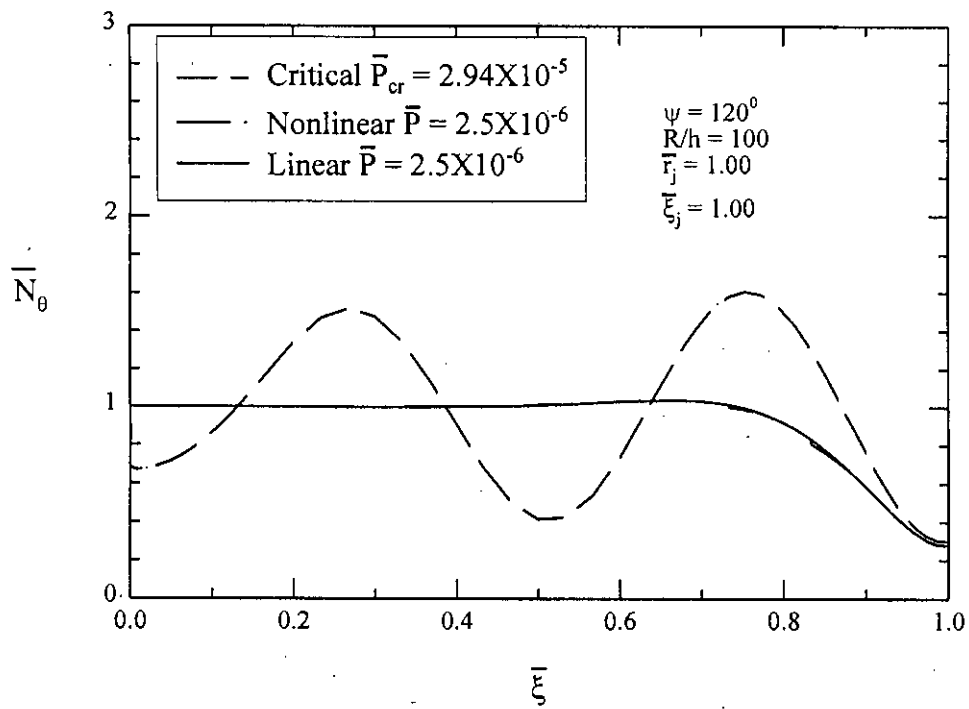


Fig. 5.23c: Variation of circumferential stress resultant along the meridian in cap-cone composite end-closure.

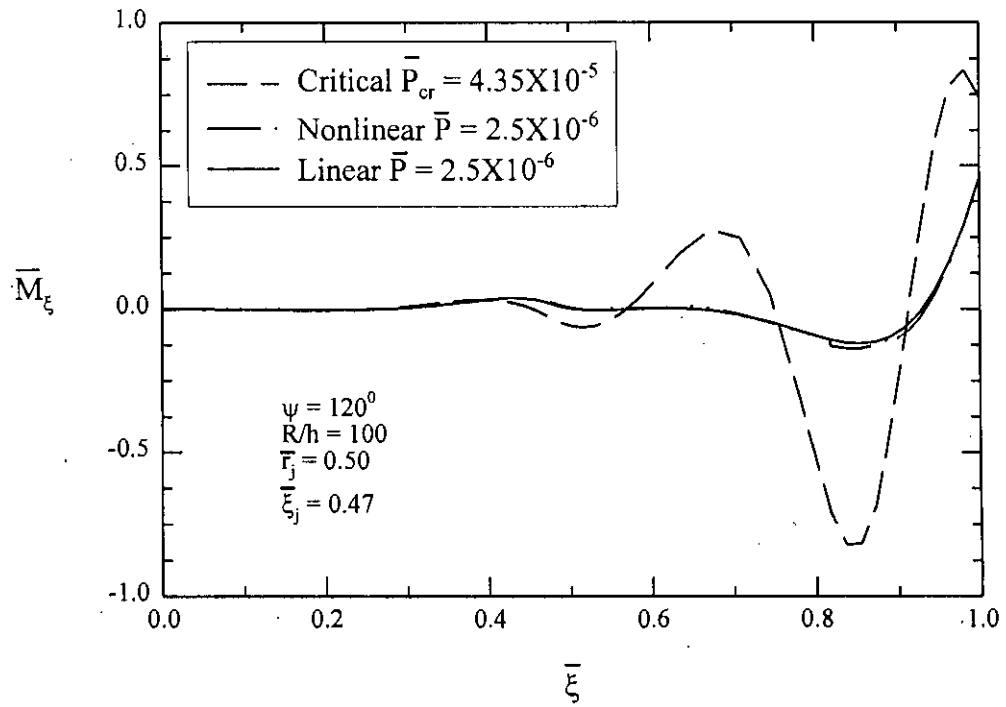


Fig. 5.24a: Variation of axial moments in cap-cone composite end-closure.

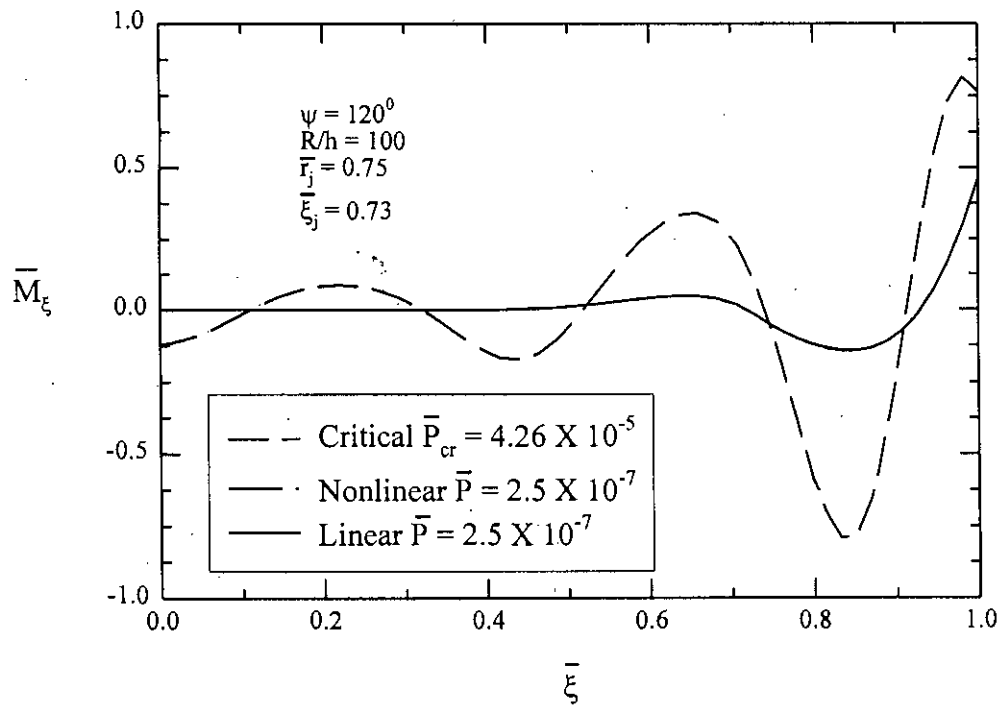


Fig. 5.24b: Variation of axial moments in cap-cone composite end-closure.

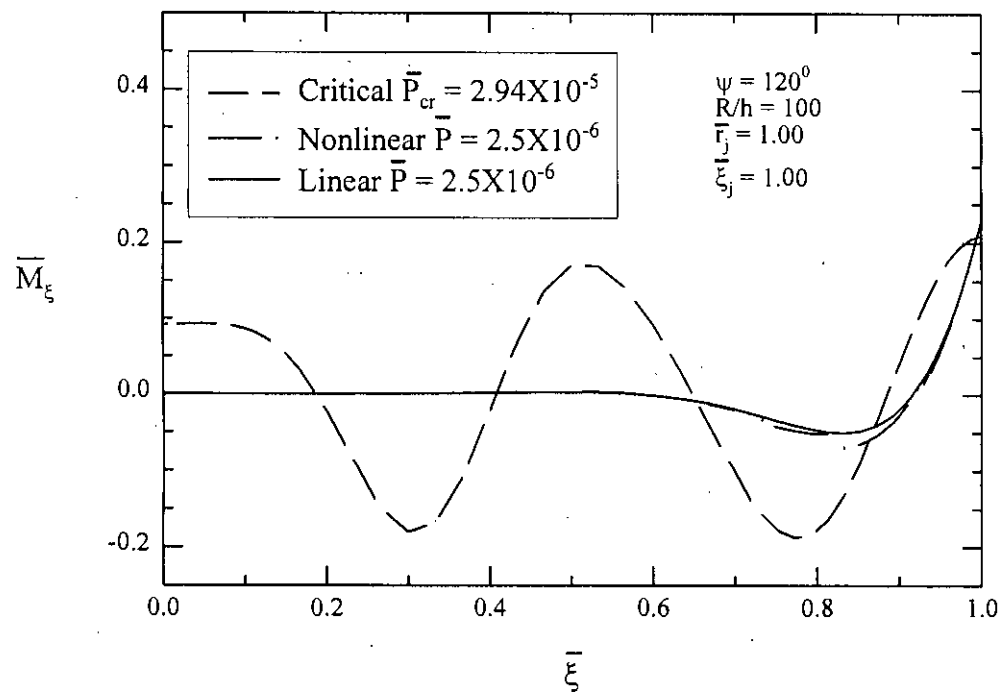


Fig. 5.24c: Variation of axial moments in cap-cone composite end-closure.

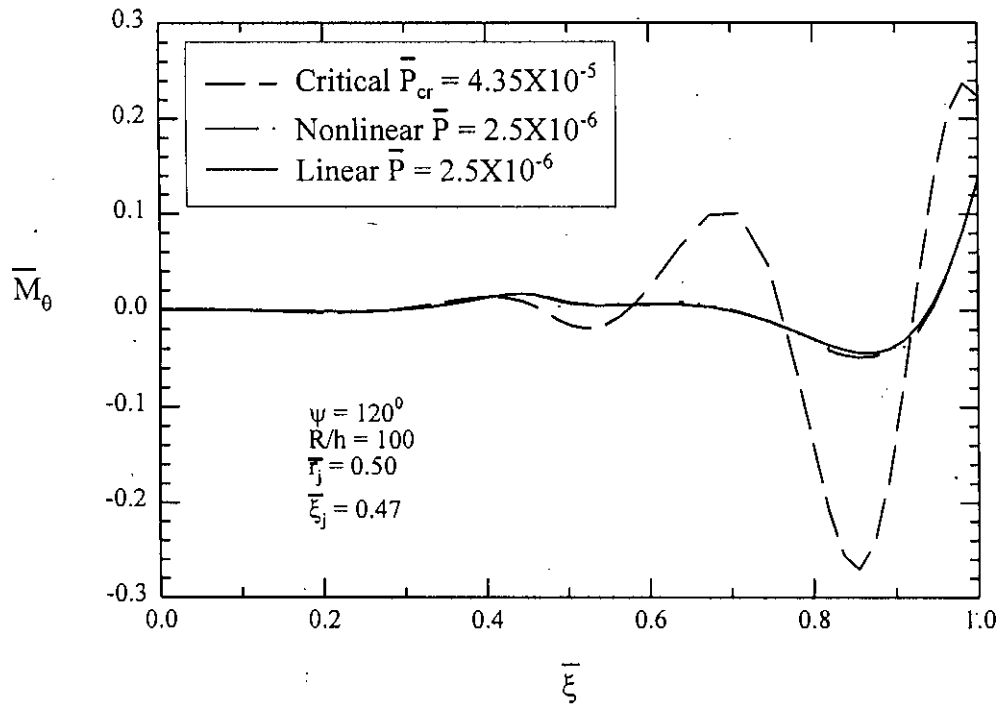


Fig. 5.25a: Variation of circumferential moment in cap-cone composite end-closure.

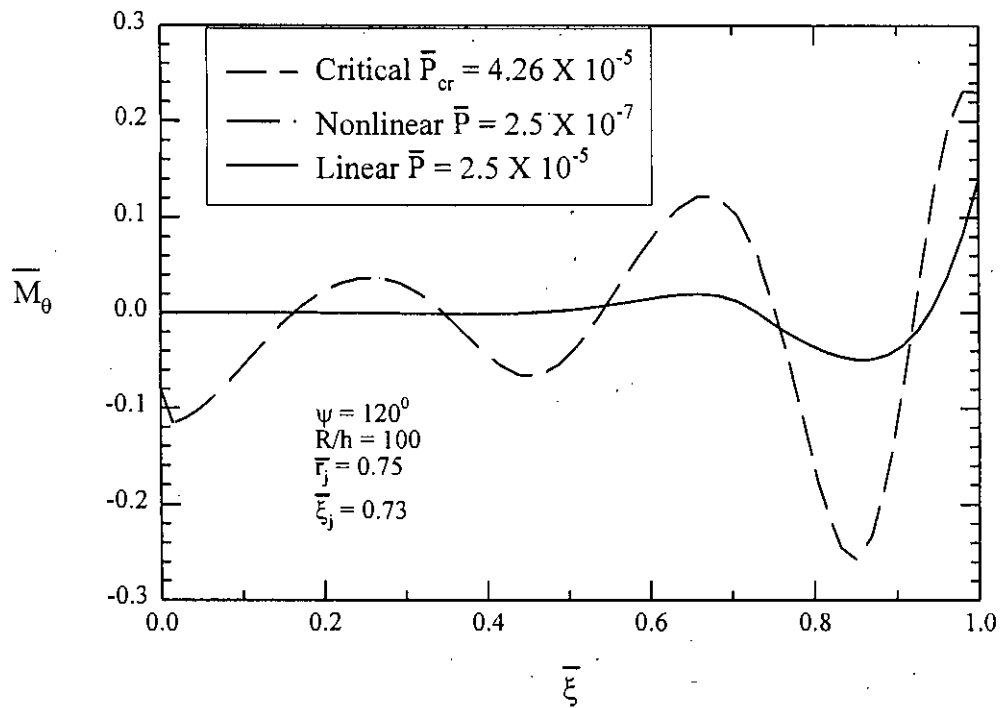


Fig. 5.25b: Variation of circumferential moment in cap-cone composite end-closure.

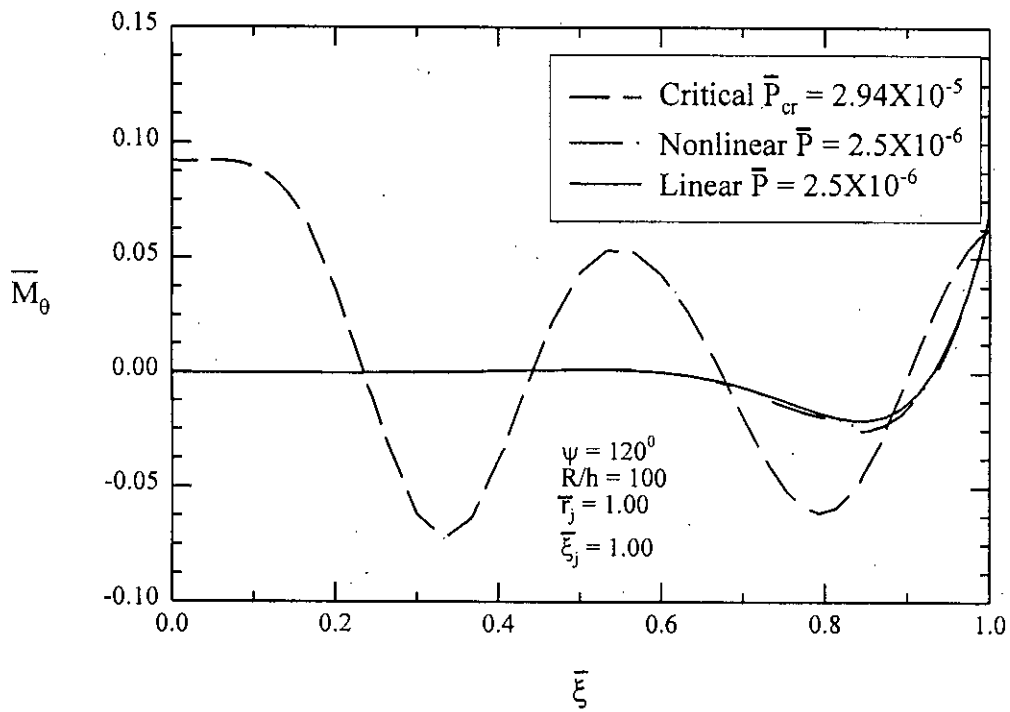


Fig. 5.25c: Variation of circumferential moment in cap-cone composite end-closure.

these four figures has components (a), (b), and (c) referring respectively to the values of 0.50, 0.75 and 1.00 of the tip ratio, \bar{r}_j , of the cap-cone end-closure.

It should be mentioned here that the magnitude of stress, strain, and displacement parameters at any point in an elastic body is a linear function of the load parameter in the case of linear theory. As the nondimensional values of stress and moment resultants are the ratios of their actual values to the values of the load parameters, the results of these stress and moment resultants of the linear theory remain constant irrespective of the values of the load. But the results of these stress and moment resultants are non-linear functions of the load parameter in the case of non-linear theory and hence their nondimensional values are variable with respect to loading. Further, when the value of the load parameter is very small, the results of the linear and non-linear theories are the same because the geometrical parameters which cause them to differ from each other, that is, the change in the shape of the body and the displacements (both rotational and linear) are negligibly small at the lower value of the load. Thus, the solid curves in Figs.5.22-5.25 represent the distribution of the linear result of concerned variable for all the values of the load and also that of the non-linear results at a very low value of the load. The non-linear results for a very high value of the load, near the critical values, are also given in these figures in broken lines for full comprehension of change taking place in the distribution of these stress and moment resultants up to and just prior to buckling.

Figure 5.22 shows the meridional distribution of \bar{N}_ξ . $\bar{N}_\xi = 0.5$ in cylindrical and spherical shells. As seen in Fig.5.22, at low value of load, although \bar{N}_ξ varies along the meridian, it does not exceed 1.0. However, at the tip of the cap-cone end-closure, \bar{N}_ξ increase with increasing values of \bar{r}_j , but remains more or less the same at the base end of the end-closure. Near the critical load, the distribution of \bar{N}_ξ becomes wavy with respect to meridional distance. It is also noted in Fig.5.22 that the maximum value of \bar{N}_ξ in the cap-cone composite end-closure increases with increasing load, specially near the critical load, and remembering that increasing \bar{N}_ξ indicates increasing sensitivity of stress in the structure to loading, it can be concluded that the sensitivity of stress to loading increases as the structure loses its stability. The term "sensitivity of stress" is used here to signify higher rate of increase of stress with respect to loading.

Figure 5.23 shows the distribution of the nondimensional circumferential stress resultant \bar{N}_θ in the cap-cone composite end-closure. \bar{N}_θ is 1.0 in a cylindrical shell and here its maximum value is observed to be about 3.8. It is also observed that \bar{N}_θ becomes wavy with respect to $\bar{\xi}$ and the stress becomes more sensitive to loading with increasing loss of stability of the composite end-closure.

The distribution of the meridional moment resultant \bar{M}_ξ in the cap-cone end-closure with respect to the meridional distance is shown in Fig.5.24. Remembering that moments are zero in the membrane state of shells, it is seen here that the membrane state of the end-closure is disturbed towards its base junction. It is also noted that there is no moment in the end-closure at the cap-cone junction. This is because of the fact that the cap-cone junction has no discontinuity of slope. Like the stresses, the distribution of moment resultants also become wavy with respect to the meridional distance and the stress resulting from the moment becomes more sensitive as the state of instability of the end-closure is increased. The distribution of the circumferential moment resultant \bar{M}_θ is shown in Fig.5.25. The behaviour of \bar{M}_θ is observed to be similar to that of \bar{M}_ξ .

Figures 5.26 and 5.27 show, respectively, the meridional variation of the nondimensional meridional and circumferential stresses in the cap-cone composite shell. Like the stress and moment resultants, the solid curves in these figures represent the results of linear theory which remain constant for all values of loading because of the method of nondimensionalization of these stresses. The solid curves also represent the non-linear results at very low values of load parameter for the same reason mentioned above in connection with stress resultants. The components (a), (b), and (c) of figures 5.26 and 5.27 correspond to the values of 0.50, 0.75, and 1.00 of tip ratio, \bar{r}_j , of the composite shell.

It should be recalled here that the nondimensional meridional stress in figures 5.26 and circumferential stress of figures 5.27 have values of 0.5 and 1.0 respectively in a cylindrical shell at places far away from the edges and junctions. Further, the difference between the inner and outer surface stresses is entirely due to the presence of bending moments in the shell. So, the

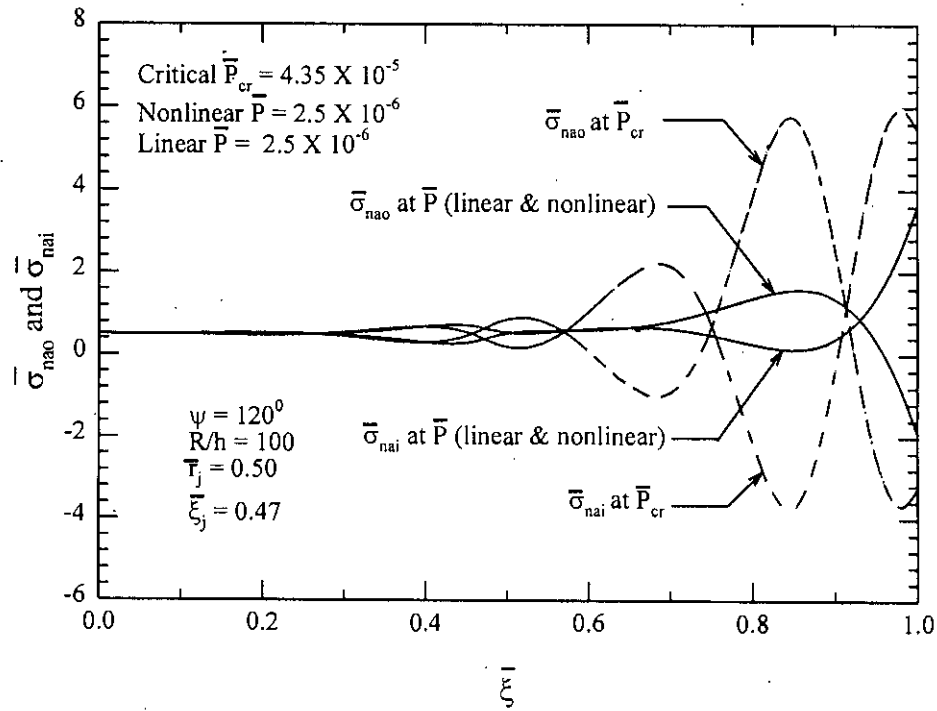


Fig. 5.26a: Meridional stresses at the inner and outer fiber of cap-cone composite end-closure.

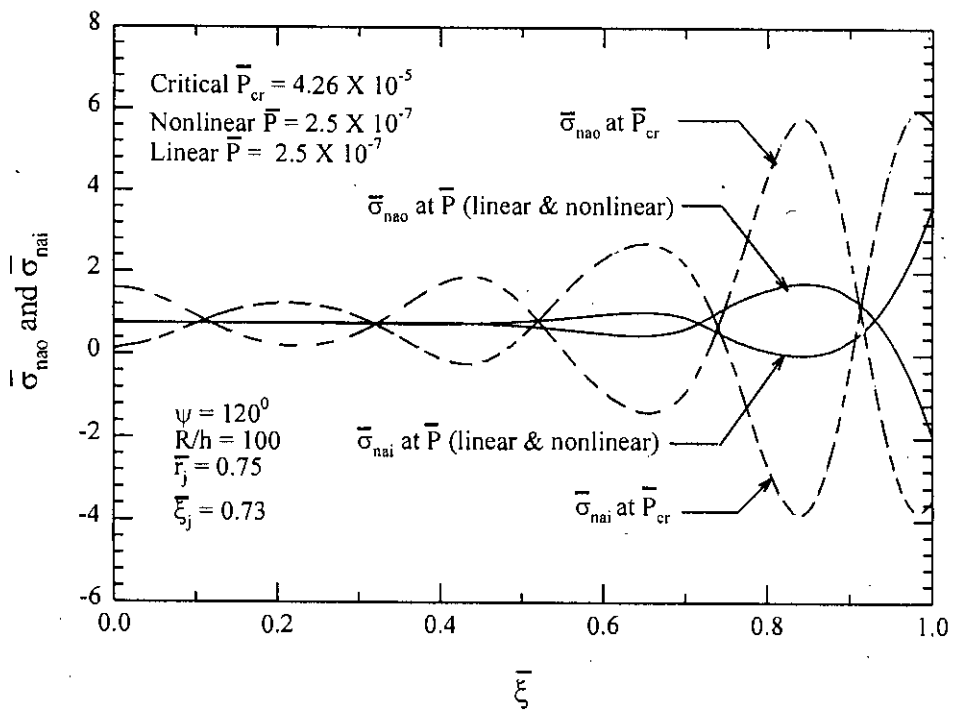


Fig. 5.26b: Meridional stresses at the inner and outer fiber of cap-cone composite end-closure.

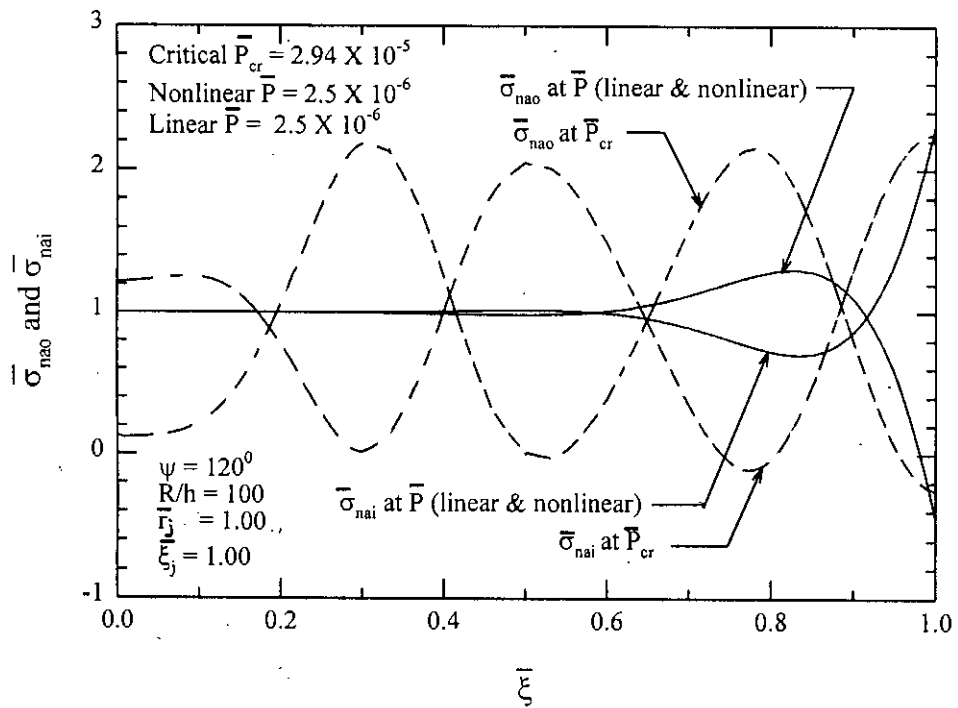


Fig. 5.26c: Meridional stresses at the inner and outer fiber of cap-cone composite end-closure.

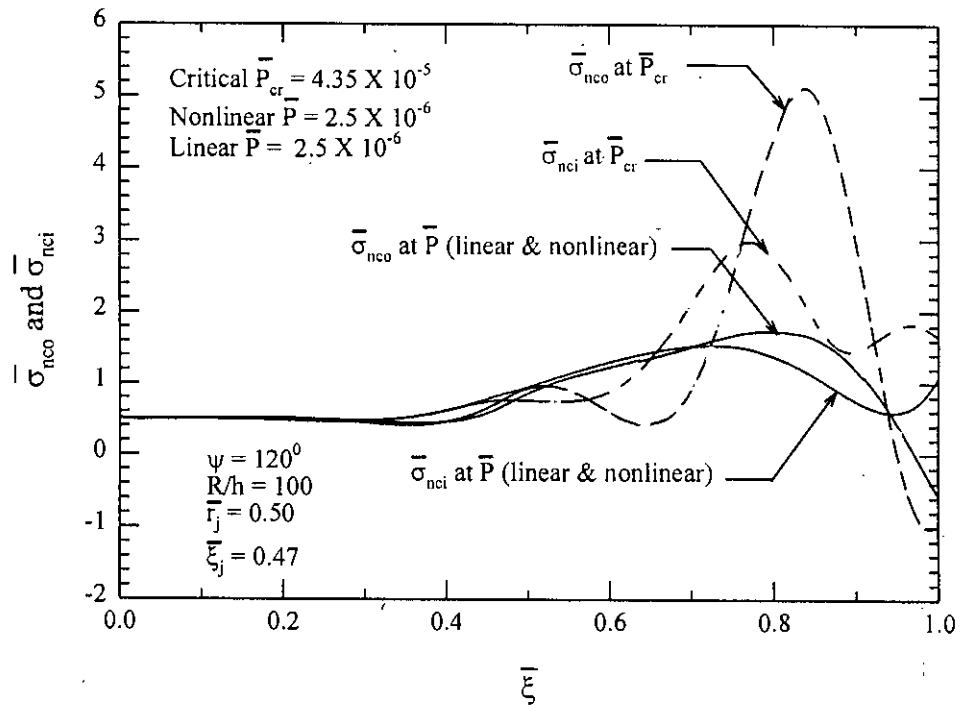


Fig. 5.27a: Circumferential stresses at the inner and outer fiber of cap-cone composite end-closure.

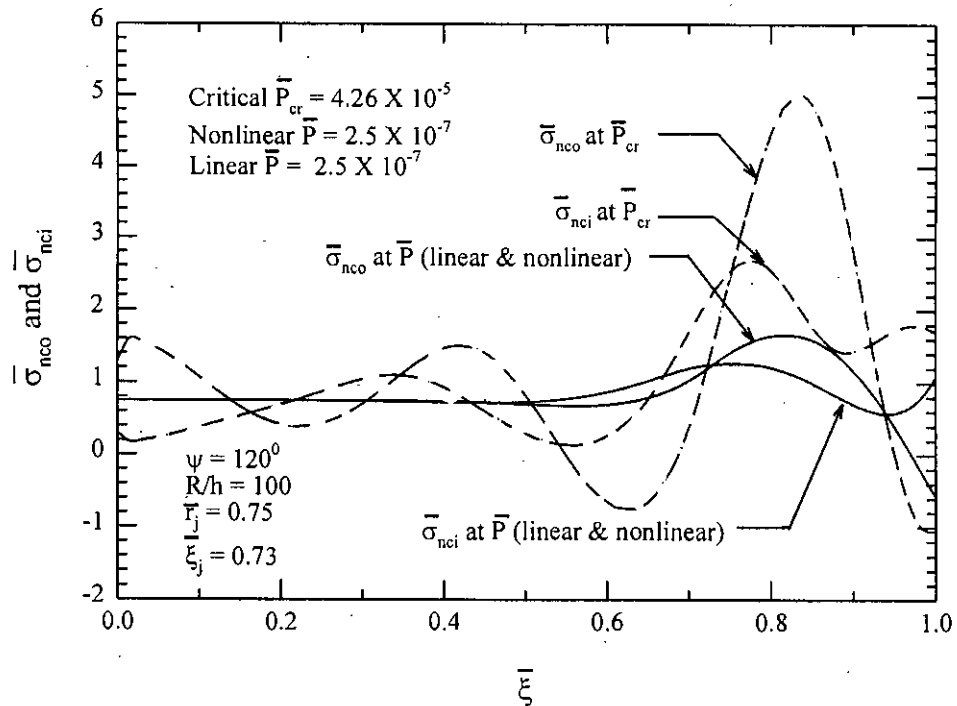


Fig. 5.27b: Circumferential stresses at the inner and outer fiber of cap-cone composite end-closure.

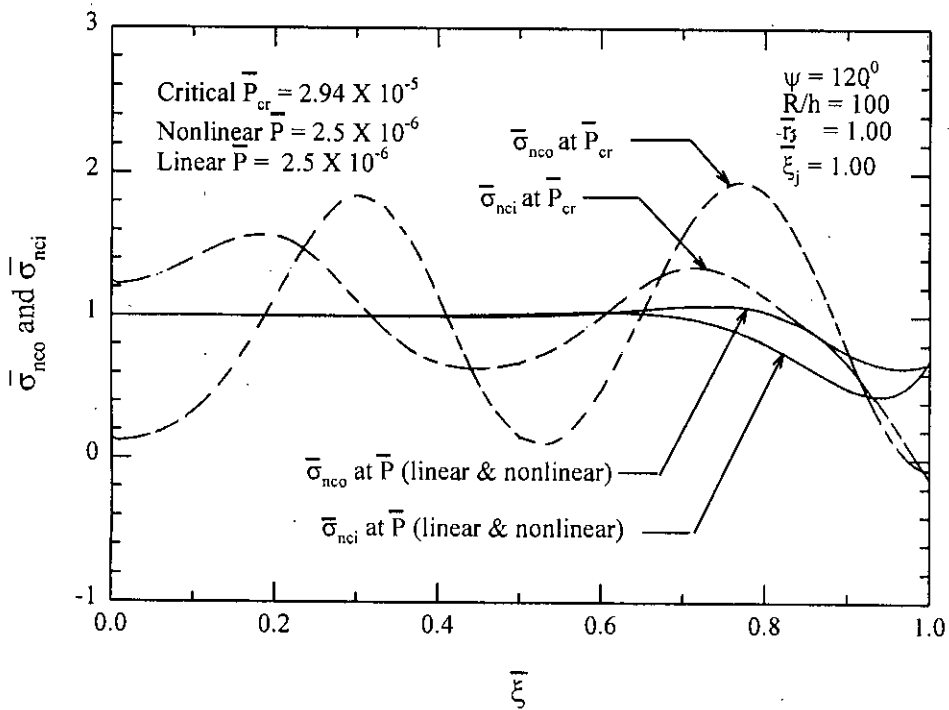


Fig. 5.27c: Circumferential stresses at the inner and outer fiber of cap-cone composite end-closer.

difference between the inner and outer fibre stresses in these figures is a measure of the deviation of the shells from their membrane state. Additionally, the wavy nature in the distribution of stresses arises out of the effect of junctions in the composite shells. The waviness reduces for point away from the junction. From figures 5.26 and 5.27 , the following observations are made:

- (1) The greater is the value of \bar{r}_j , the longer is the region over which the effect of the junction, that is, the wavy nature of stress distribution, propagates.
- (2) There is no difference between the linear and non-linear results in the region far off from junctions.
- (3) The difference between the inner and the outer fibre stresses is the greatest near the vessel end junction at about $\bar{\xi} = 0.8$ and decreases towards the tip of the shell meridional except for shells of $\bar{r}_j = 1.00$. For shells of $\bar{r}_j = 1.0$, the distribution of stresses are severe throughout the meridian.
- (4) The effect of junction of cap-cone shell on the magnitude of stresses is not too severe as observed from the magnitude of stresses here in comparison to their corresponding magnitude in a spherical cap end-closure.
- (5) The most noticeable fact from figures 5.26 and 5.27 is that the sensitivity of stress to the loading, as seen from the increasing difference between the linear and non-linear results, increases rapidly as the critical loading is approached.
- (6) In contrast to the shells with $\bar{r}_j=1.00$ the other shells, that is, the cap-cone shells are found to be always highly stressed around the base irrespective of tip ratio, \bar{r}_j . Thus it is clear that the cap-cone shells will fail at the base either due to instability or due to yielding whereas spherical caps have the scope to fail either at the tip or at the base.

5.1.1.2 Cup-cylinder and dome-cylinder composite shells

Hulls of submarines are generally constructed from combination of cylinders, cones, and domes, as shown in Fig.1.1. The ends of conventional submarine hulls are convex domes and are often the zone of danger under external pressure loading. This is because the pressure sustaining capacity of these shells is limited by the buckling strength of the dome end instead of the yielding strength of the dome material. Ross in one of his papers on the design of dome ends [128] introduced a new idea of using inverted spherical domes, shown in Fig.5.28, as ends of submarine hulls. He argued that as the inverted dome end, concave to external pressure, will be in tension, the possibility of dome buckling will thus be virtually eliminated. In the absence of the possibility of failure due to instability, the pressure sustaining capacity of the hull will be enormously increased as now it will fail due to yielding. In his paper [128] Ross analysed the stresses in the cup-cylinder composite shell shown in Fig.5.29 by finite-element method and made conclusions in support of his new idea.

To investigate the suitability and the superiority of the cup-cylinder composite shells over the conventional dome-cylinder ones under uniform external pressure, as proposed by Ross [128], four shells of each group were studied. The geometry of the cup-cylinder and dome-cylinder shells are shown in Figs.5.30 and 5.31, respectively. Particulars of the cup-cylinder and dome-cylinder composite shells, studied in this present work, are given in Table 5.2.

As the maximum membrane stress for a thin-walled sphere is half the maximum membrane stress for a thin-walled cylinder of the same radius, it was decided to make the radius of the cup-end or dome-end twice the radius of the cylinder. With such a combination the inverted spherical cap of the cup-end composite shell extends 0.27 times the radius of the cylinder into the cylindrical space, reducing the total internal space of the submarine. The lost space may be compensated by lengthening the pressure hull. As the space available inside the spherical dome is only a fraction of the volume provided by the cylindrical segment of the pressure hull, the loss of buoyancy is not significant. Submarine hulls are strengthened by bulkheads at reasonably close intervals. As the end-closures are the vulnerable zones for instability, it is wise to use bulkheads near the cup-cylinder junction. In the present case, use of bulkhead very near the junction may help increase the critical pressure. In the case of the cup-cylinder shell, setting of

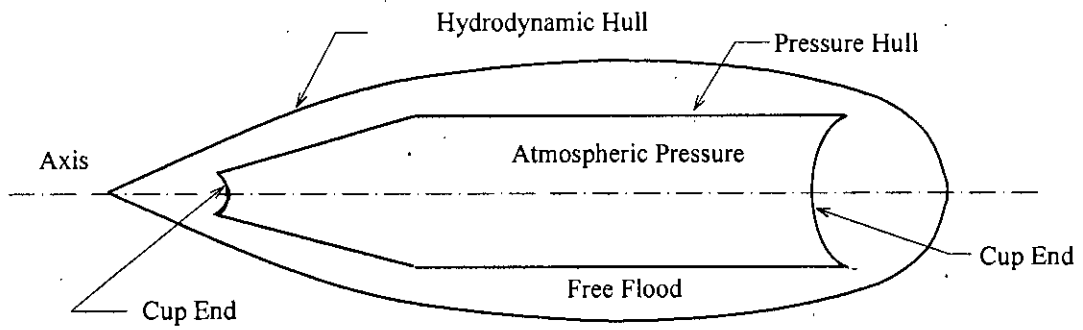


Fig. 5.28: Submarine pressure hull with inverted dome-end (cup-end)

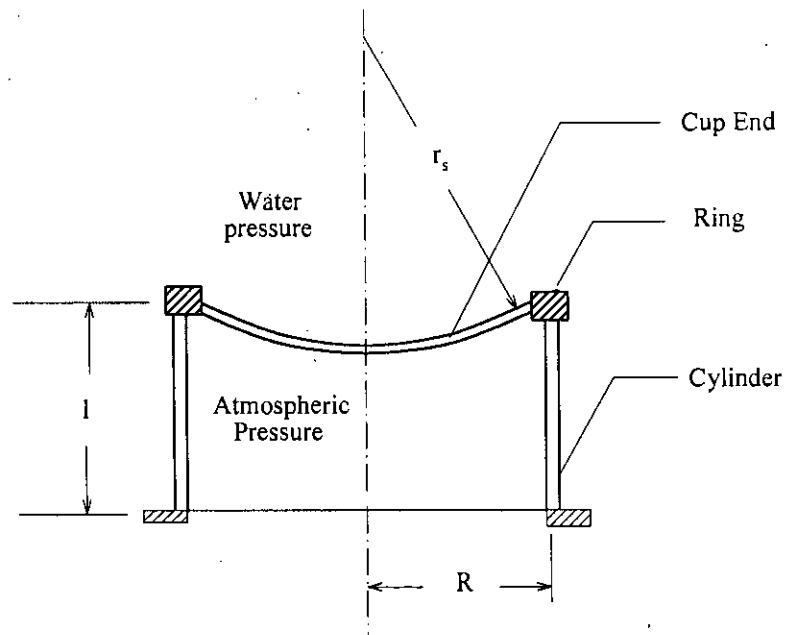


Fig. 5.29: Cup-cylinder composite shell under uniform external pressure.

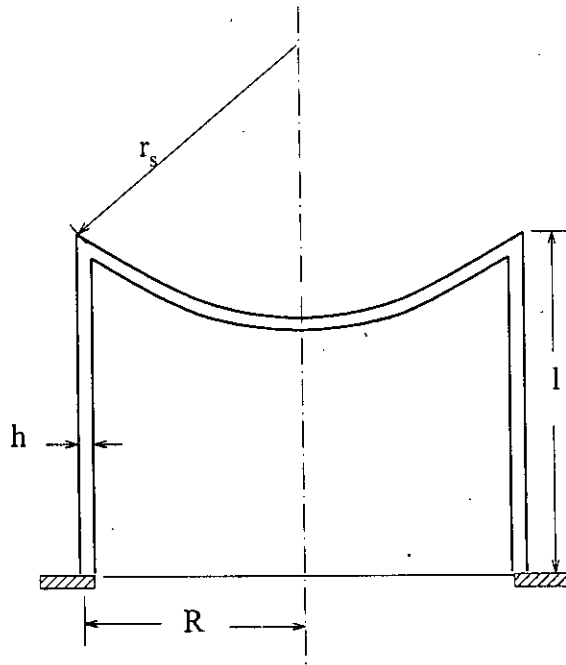


Fig. 5.30: Geometry of a cup-cylinder composite shell.

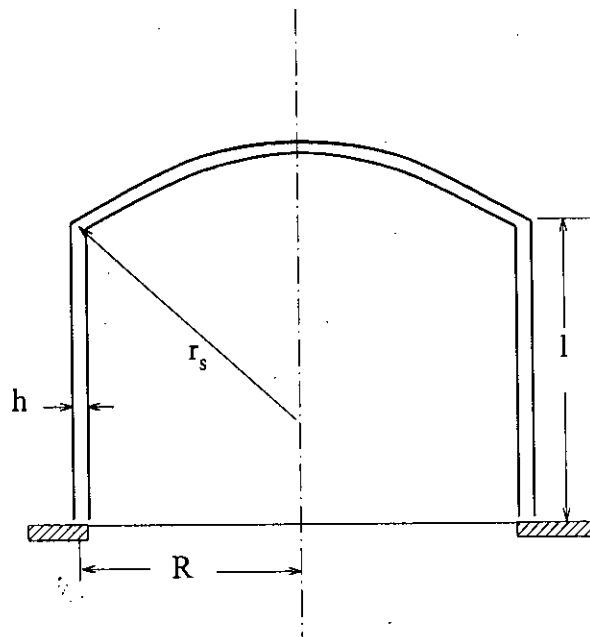


Fig. 5.31: Geometry of a dome-cylinder composite shell.

an internal bulkhead at cylinder length to radius ratio, $l/R = 0.3$, that is, near the tip of the inverted cup, may make the whole space between the cup and the bulkhead useless; thus $l/R = 0.4$ may be assumed to be more reasonable.

In the present analysis, the boundary conditions at the centre of the spherical cup or the spherical dome become

$$\bar{u} = 0, \quad \beta = 0, \text{ and } \bar{V} = 0$$

and those at a point in the cylinder far from the cup-cylinder or dome-cylinder junction become

$$\bar{H} = 0, \quad \beta = 0, \text{ and } \bar{w} = 0$$

but, in order to keep the analysis parallel to that of Ross, the boundary conditions in the cylindrical portion are taken as

$$\bar{u} = 0, \quad \beta = 0, \text{ and } \bar{w} = 0$$

Results of the investigation for the meridional mode of buckling of the cup-cylinder and dome-cylinder shells are presented in Table 5.3.

Instability pressures for the cylindrical portion of the shell, considering simple supports at the ends and subjected to combined action of uniform lateral and axial pressure, calculated from the Windenburg [190] formula,

$$\frac{P_{cr}}{E} = \frac{2.6 \left(\frac{t}{d}\right)^{5/2}}{\frac{1}{d} - 0.45 \left(\frac{t}{d}\right)^{1/2}},$$

are given in column 3 of Table 5.3.

The Windenburg equation is the modified version of the Von Mises [182] equation,

$$\frac{P_{cr}}{E} = \frac{t/a}{[n^2 + 0.5(\pi a/l)^2]} \times \left\{ \frac{1}{[n^2(l/\pi a)^2 + 1]^2} + \frac{t^2}{12a^2(1-\nu^2)} [n^2 + (\pi a/l)^2]^2 \right\}$$

The Windenburg equation is an approximation that minimises the circumferential wave number 'n'. Therefore the wave number n is considered here in the Windenburg formula even though it does not appear in the equation.

Table 5.2: Particulars of Cup-Cylinder and Dome-Cylinder shells. C and D in shell numbers stand for Cup-Cylinder and Dome-Cylinder Composite shells respectively.

Shell No.	R/h	L/R	r_s/R	Type of junction
1C,1D	100	0.40	2.0	No ring
2C,2D	100	0.40	2.0	With ring
3C,3D	250	0.40	2.0	No ring
4C,4D	250	0.40	2.0	With ring

Table 5.3: Critical loads of different shells. (1C), (1D) etc. indicate shell numbers.

$P_{cr}/E \times 10^6$			
Present Analysis		Windenburg Equation for Cylinder	Von Mises Equation for Cylinder
Cup-Cylinder	Dome-Cylinder		
86.6 (1C)	17.35 (1D)	27.3	27.3 (12)
103.3 (2C)	17.5 (2D)		
8.56 (3C)	2.63 (3D)	2.59	2.59 (16)
9.46 (4C)	2.98 (4D)		

Critical loads of composite shells in Table 5.3 show that the cup-cylinder composite shells are superior to the dome-cylinder shells of the same physical parameters and that the critical load for the former is a few times greater than that for the latter. Results for the dome-cylinder and pure cylinder given in columns 2, 3 and 4 of Table 5.3 show that the instability load for the dome-cylinder is dependent on the radius to thickness ratio. Considering thicker shells, dome-cylinders are found to buckle axisymmetrically at loads much lower than that for the asymmetric instability of a pure cylinder. The load-displacement curves for such a dome-cylinder shown in Fig.5.32(b) show that buckling takes place both in the cylinder and the dome portion of the end-closure. From this discussion it is seen that the dome-cylinder combination may even reduce the instability load of the attached cylinder. In the case of the cup-cylinder shells, only the cylindrical portion of the shell buckles. Fig.5.32(a) shows load versus radial deflection of the cylinder of the cup-cylinder shell (1C). In Figs.5.33(a) and 5.33(b), the buckled modes of shells (1C) and (1D) are shown.

In Figs.5.34(a) and 5.34(b), the circumferential stresses in the shells (1C) and (2C) of Table 5.2, corresponding to the critical load of shell (1C) are plotted against the meridional distance, and in Fig.5.35 the circumferential stresses in the cup end of the cup-cylinder shell with clamped boundary (shown in the inset of Fig.5.35) and at a pressure equal to the critical load of (1C) are plotted. From Table 5.2 it is seen that the critical load of shell (1C) is lower than that of shell (2C). Figures 5.34(a) and 5.34(b) show that, at the junction of cup and cylinder, stresses are maximum and compressive at both the inner and outer surfaces. The maximum stresses in Figs.5.34(a) and 5.34(b) are around 40 and 25 times greater than that developed in the simple cup of Fig.5.35. These high compressive stresses around the junction may lead to local circumferential instability and either one of the two shell components may buckle asymmetrically before the initiation of axisymmetric buckling.

5.1.1.3 Theoretical analysis of the experimental models of composite shells

The geometry of the fabricated shells deviated slightly from the assumed geometry and, from the measured data, it was found that the CS100 shells, described in chapter-4, can be considered as

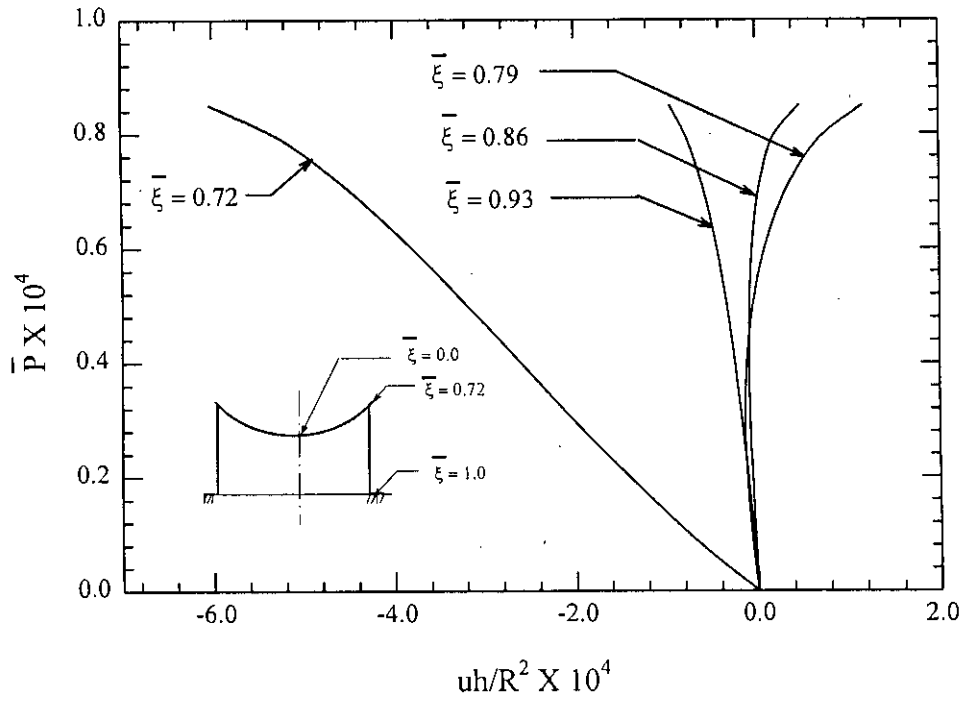


Fig. 5.32a: Fundamental configuration path of different points on the surface of cup-cylinder composite shell.

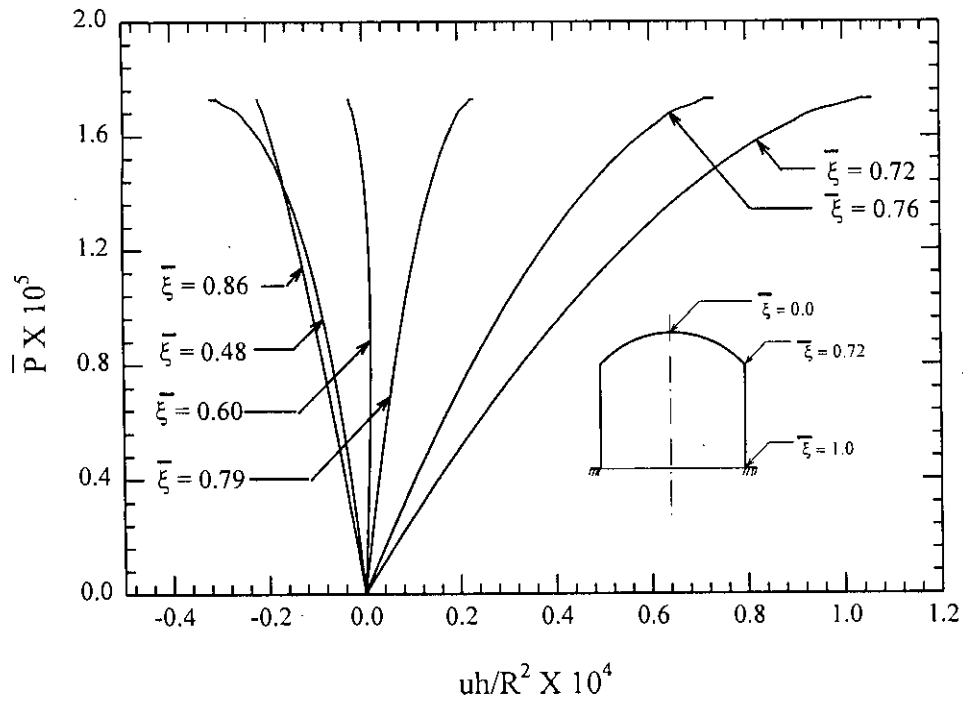


Fig. 5.32b: Fundamental configuration path of different points on the surface of dome-cylinder composite shell.

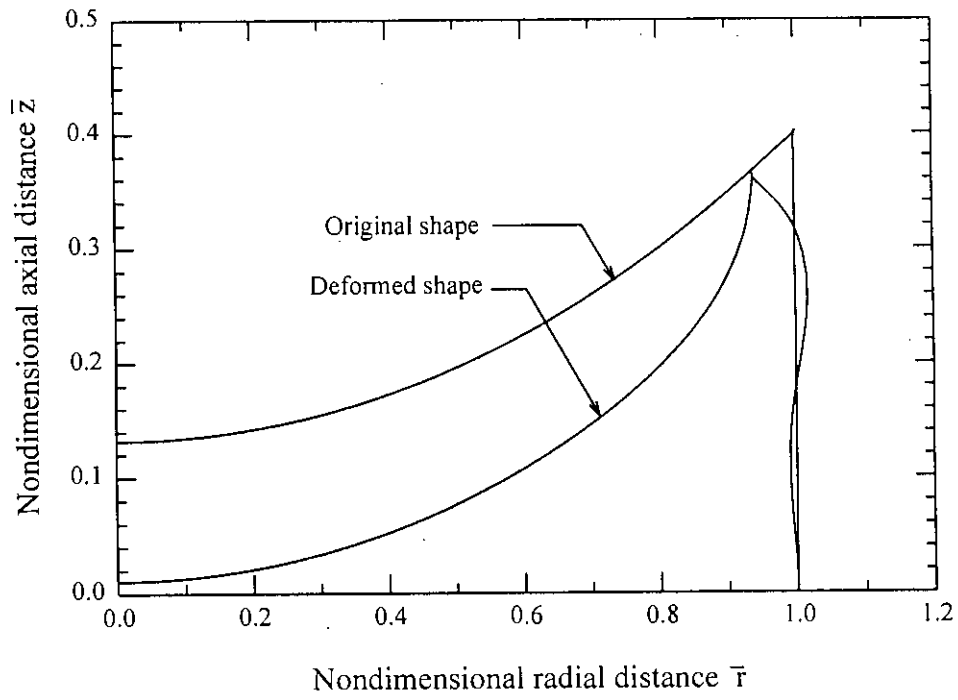


Fig. 5.33a: Undeformed and deformed shape of cup-cylinder composite shell.

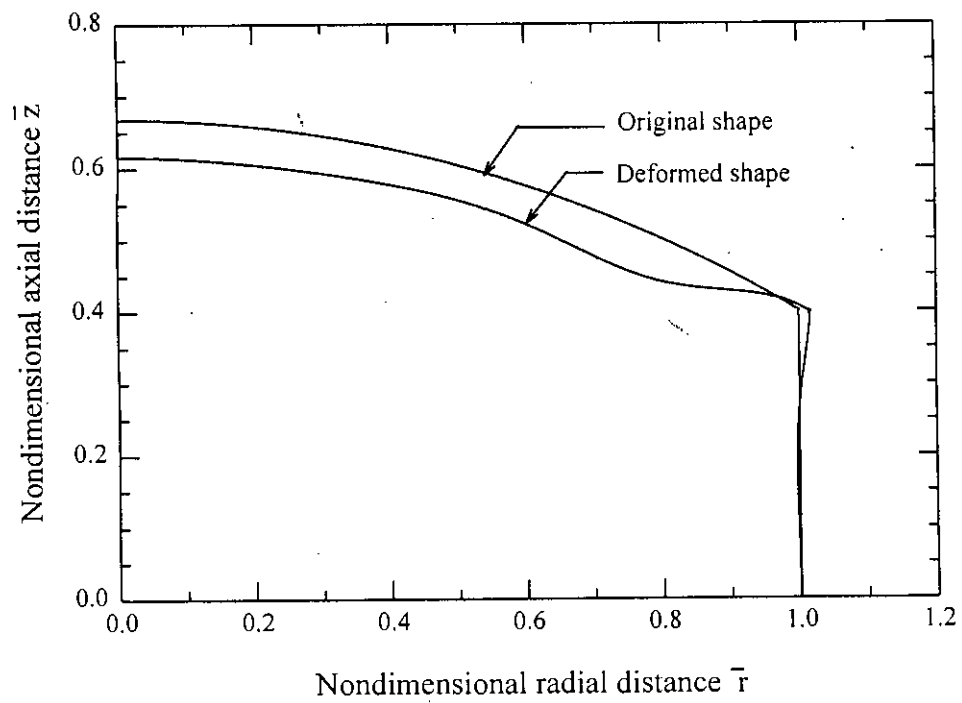


Fig. 5.33b: Undeformed and deformed shape of dome-cylinder composite shell.

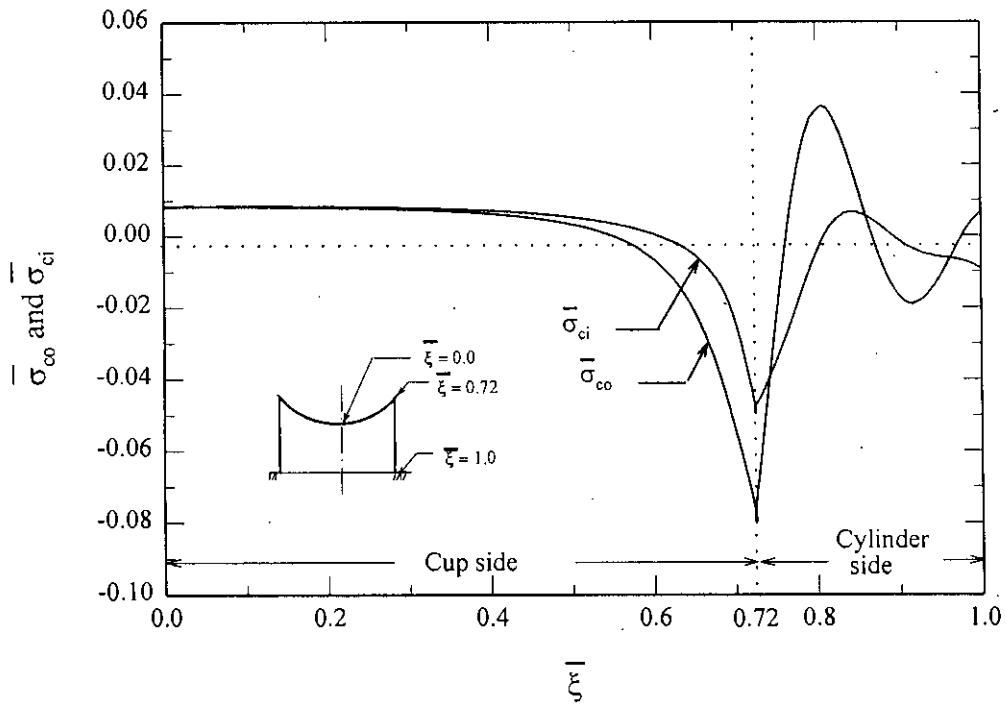


Fig. 5.34a: Circumferential stresses at critical pressure in cup-cylinder composite shell (1C).

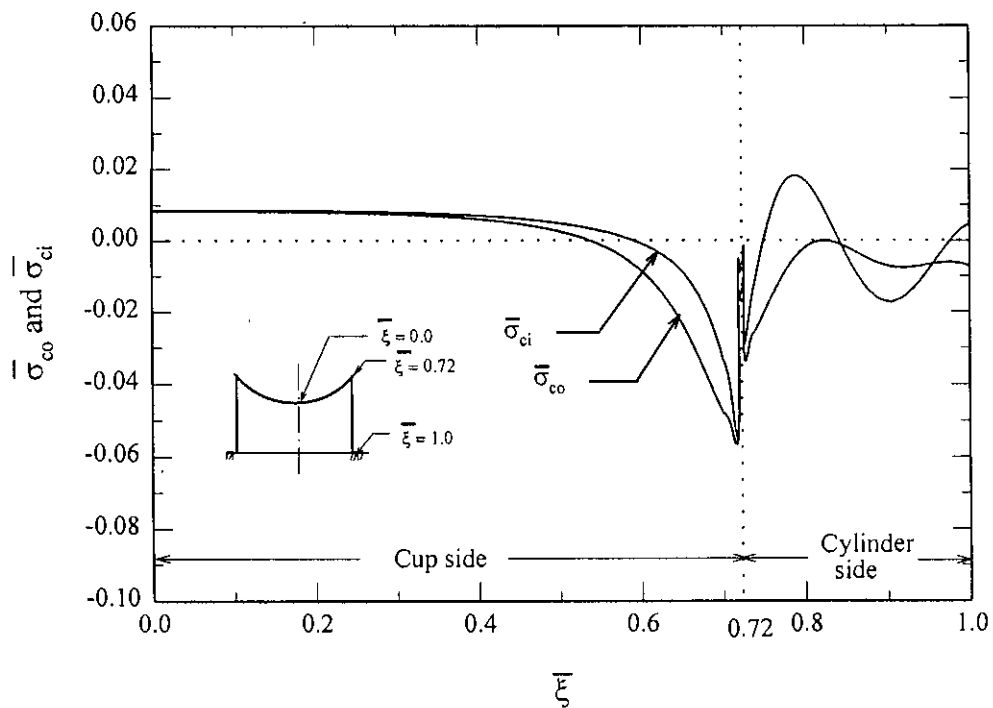


Fig. 5.34b: Circumferential stresses at critical pressure in cup-cylinder composite shell (2C).

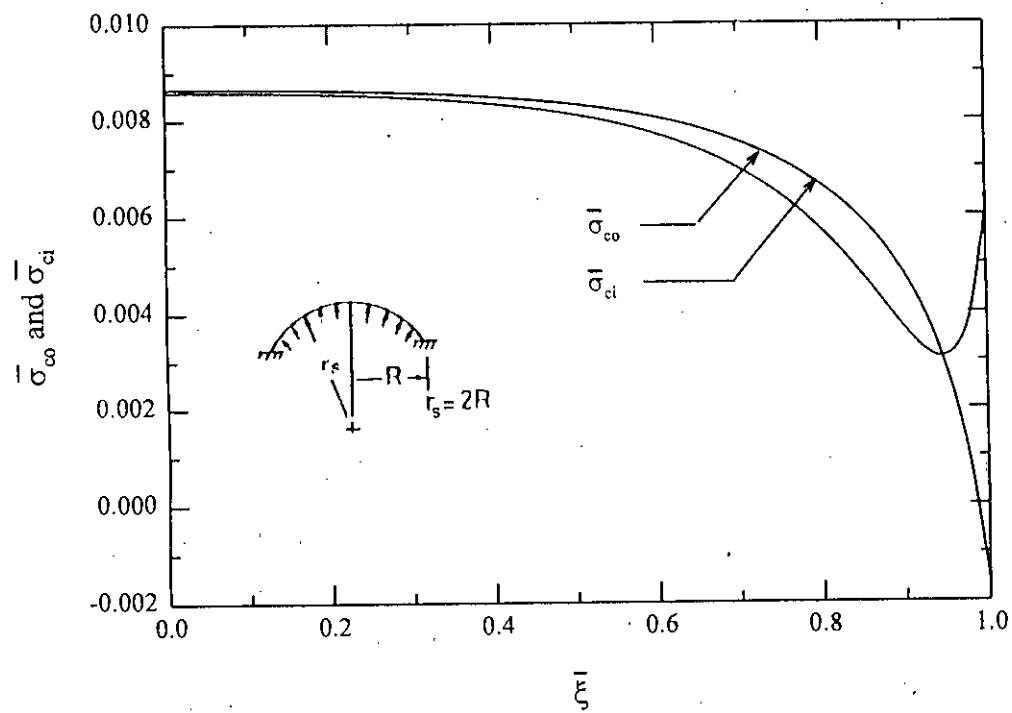


Fig. 5.35: Circumferential stresses in a spherical cap under an internal pressure of $P/E = 0.86 \times 10^{-4}$

composite of two axisymmetric segments of two different radii of curvature. The geometric parameters described in Fig.4.5(a) of the measured CS100 shells, and thickness variations along the meridian of these shells are presented in Table 4.1 .

Axisymmetric buckling loads for the different CS100 shells are presented in column 3 and 4 of Table 5.4. In column 3 the results are the axisymmetric buckling loads of imperfect experimental models, generated from measured geometric data and in column 4 the results are the buckling loads for perfect spherical caps with thickness equal to the minimum thickness of the corresponding imperfect models.

The theoretical results obtained for the CS100 models without considering their geometric imperfection are found to be higher than the results obtained with geometric imperfections. The geometric imperfection, in the form of depression of the crown of the shell, when measured in terms of height variation of the shell, is quite negligible but the results of analysis show that slight deviation of height at the crown of these shells drastically changes the buckling load. Thus it may be concluded from the above observations that the spherical-caps are very much sensitive to geometric imperfections.

During the experiment, the CS100 models were found to buckle axisymmetrically at the tip. For the comparison of experimental deformation pattern with the analytical deformation pattern, axisymmetric prebuckling shape of these shells were calculated. The computational deformation pattern for these shells are shown in Figs.5.36-5.40. The computational patterns are the prebuckling shapes of the shells, and the magnitude of the displacements are very small. Only exaggerated patterns are shown here for better perception of the geometry at the inception of buckling.

The axisymmetric buckling loads of experimental models CS30, CS60 and CS80 are presented in column 6 of Table 5.5. Comparison of axisymmetric buckling results of CS100 models from Table 5.4 with other cap-cone composite models from Table 5.5 show that cap-cone models of higher slant height buckles at higher loads.

Table 5.4: Experimental and analytical buckling loads of spherical cap end-closure CS100.

E for copper is 97.86 Gpa

Model No.	Experimental Critical Load P/E	Axisymmetric Critical Load with Experimental Geometry P/E	Axisymmetric Critical Load for Perfect Geometry with Lowest Thickness P/E
1	2.934×10^{-7}	7.25×10^{-7}	10.15×10^{-7}
2	3.211×10^{-7}	6.04×10^{-7}	8.456×10^{-7}
3	5.299×10^{-7}	8.11×10^{-7}	11.354×10^{-7}
4	5.212×10^{-7}	15.5×10^{-7}	21.7×10^{-7}
5	5.524×10^{-7}	8.99×10^{-7}	12.586×10^{-7}

Table 5.5: Experimental and analytical buckling loads of spherical tip conical end-closures.

E for copper is 97.86 Gpa

End-closure type	Model No.	Experimental Critical Load P/E	Asymmetric Critical Load for Cone P/E		Axisymmetric Critical Load for Experimental Geometry P/E
			Ends Hinged	Ends Fixed	
CS30	1	$1.666 \times 10^{-7}(7)$	$1.94 \times 10^{-7}(8)$	$1.94 \times 10^{-7}(8)$	26.2×10^{-7}
	2	$1.577 \times 10^{-7}(7)$	$1.91 \times 10^{-7}(8)$	$1.91 \times 10^{-7}(8)$	26.2×10^{-7}
	3	$1.666 \times 10^{-7}(6)$	$2.03 \times 10^{-7}(8)$	$2.04 \times 10^{-7}(8)$	26.3×10^{-7}
CS60	1	$2.036 \times 10^{-7}(8)$	$5.085 \times 10^{-7}(11)$	$5.195 \times 10^{-7}(11)$	18.7×10^{-7}
	2	$3.711 \times 10^{-7}(9)$	$5.082 \times 10^{-7}(14)$	$5.199 \times 10^{-7}(14)$	27.0×10^{-7}
	3	$3.711 \times 10^{-7}(9)$	$5.928 \times 10^{-7}(14)$	$6.071 \times 10^{-7}(14)$	31.6×10^{-7}
	4	$3.728 \times 10^{-7}(8)$	$5.461 \times 10^{-7}(14)$	$5.88 \times 10^{-7}(14)$	20.0×10^{-7}
CS80	1	$5.457 \times 10^{-7}(13)$	$6.784 \times 10^{-7}(25)$	$7.340 \times 10^{-7}(26)$	15.9×10^{-7}
	2	$3.970 \times 10^{-7}(13)$	$4.142 \times 10^{-7}(27)$	$4.445 \times 10^{-7}(27)$	10.5×10^{-7}
	3	$4.800 \times 10^{-7}(13)$	$5.513 \times 10^{-7}(26)$	$5.937 \times 10^{-7}(26)$	13.0×10^{-7}

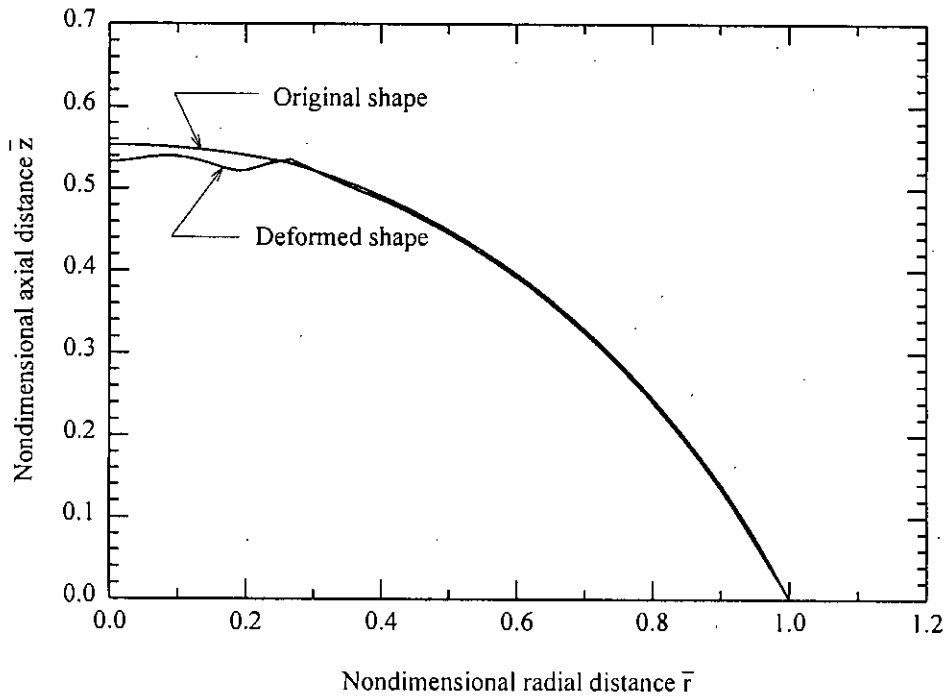


Fig 5.36: Undeformed and deformed shape of CS100.1 shell model.

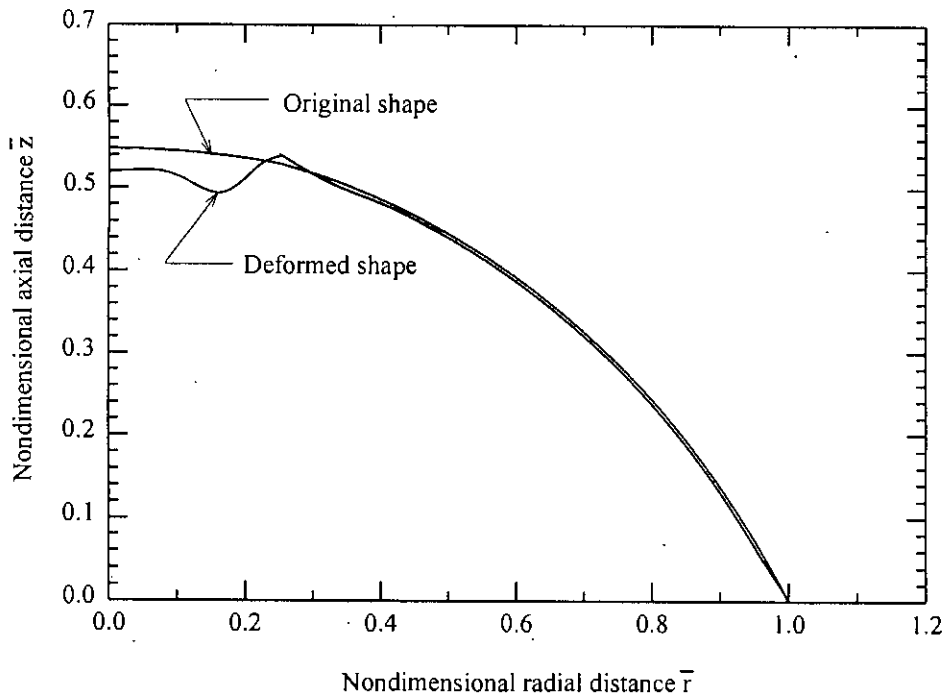


Fig 5.37: Undeformed and deformed shape of CS100.2 shell model.

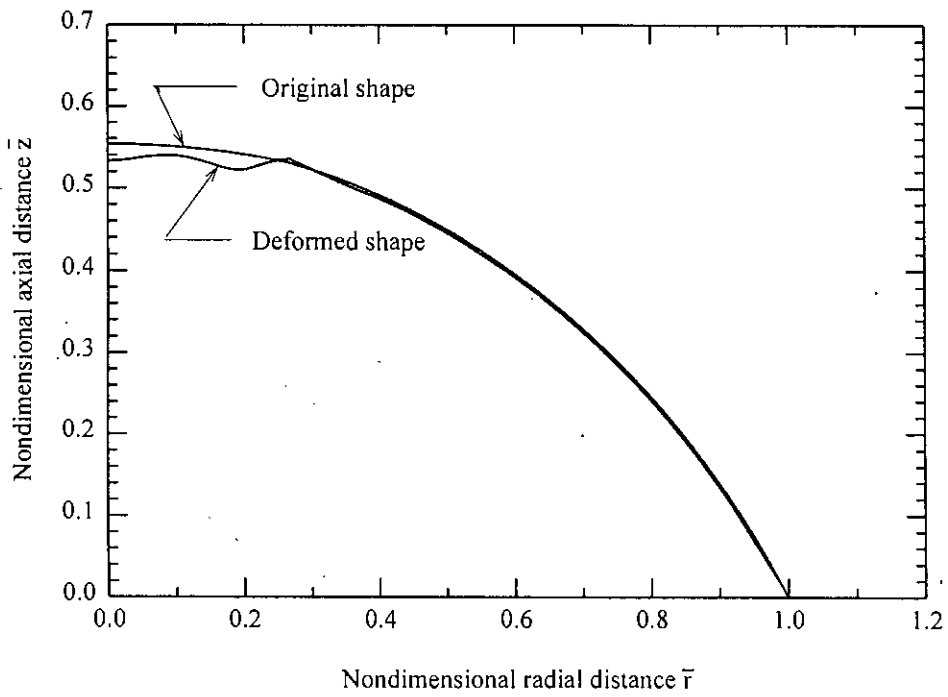


Fig 5.38: Undeformed and deformed shape of CS100.3 shell model.

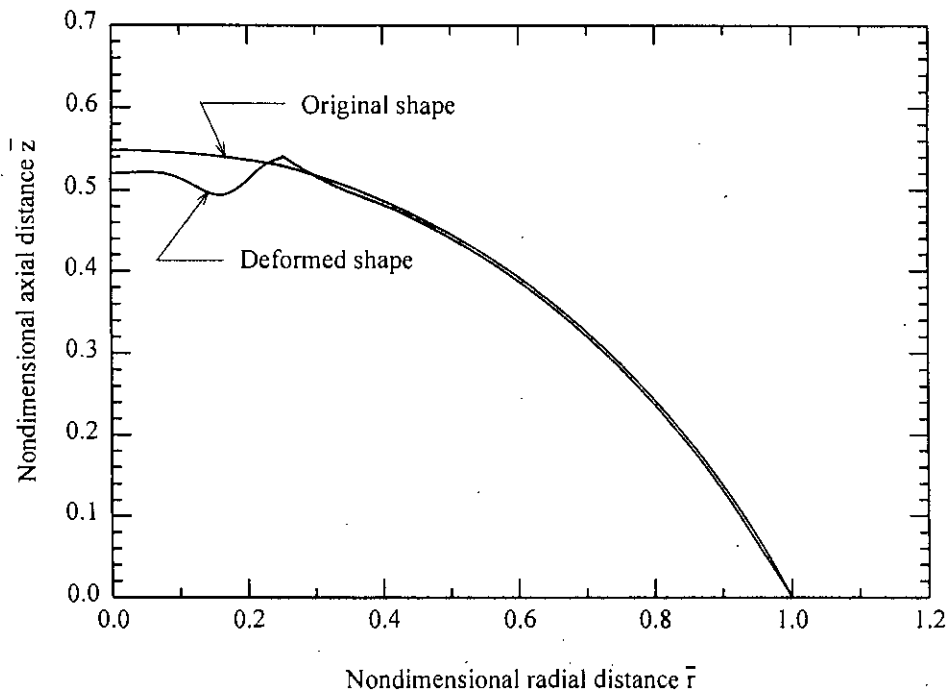


Fig 5.39: Undeformed and deformed shape of CS100.4 shell model.

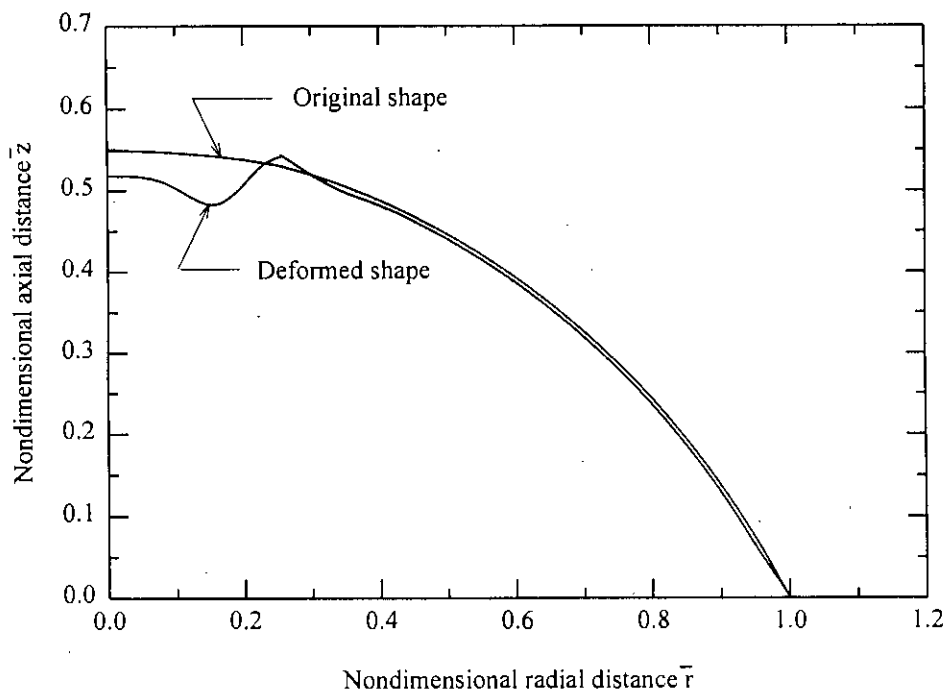


Fig. 5.40: Undeformed and deformed shape of CS100.5 shell model.

The meridional stresses in the imperfect experimental models, CS100, at their theoretical critical loads are shown in Figs.5.41(a) to 5.45(a) corresponding to their model numbers 1,2,3,4 and 5, respectively as presented in Table 4.1, and the circumferential stresses in them are shown respectively in Figs.5.41(b) to 5.45(b). Earlier comments about the nature of distribution and magnitude of stresses in cap-cone end-closure also hold true here. But here the junction near the crown of the end-closures as created by the imperfection, is causing far larger perturbation in the membrane state of the end-closures than the junction at the base. In between these two junctions, the membrane state of stress prevails. The junction in the crown due to imperfection has caused high compression in the crown which has ultimately enhanced the instability of the crown. The effect of geometrical imperfection on the development of stresses explain to a large extent the difference in the theoretical and experimental critical pressure of spherical shells.

Non-linear axisymmetric stress analysis of the cap-cone models CS30, CS60 and CS80 at the analytical asymmetric critical load of the conical frusta are presented in Figs.5.46 to 5.50. Comparison of stresses in the cap-cone end-closures and the corresponding conical frustum show that both the axial and circumferential stresses in the composite shells are smoother than those in the conical frustum with fixed edges.

5.1.2 Asymmetric Buckling Analysis of Experimental Models

Buckling tests were performed on four different sets of shells, described earlier. Photograph of the electrodeposited models are shown in Fig.5.51. It has already been described in chapter-4 that the stainless steel base was fabricated by removing the spherical tip of the die of the composite cap-cone shell of the highest \bar{r}_j ($\bar{r}_j = r_j/R$), so the shells with the highest \bar{r}_j , when attached to this plate, practically became a simple spherical cap with $\bar{r}_j=1.00$, where the conical portion of these shells worked as the base fixing element. For the other three sets, the same portion of the conical segment from the bottom of the shell base worked as base fixing element. Thus practically R is the radius at the junction of the shell and the stainless steel base-plate and r_j is the radius at the junction of the spherical tip and the conical frustum of the end-closure.

While performing experiment on the cap-cone models, it was observed that buckling occurs within the individual shell elements and not in regions across the junctions. Buckling occurred in

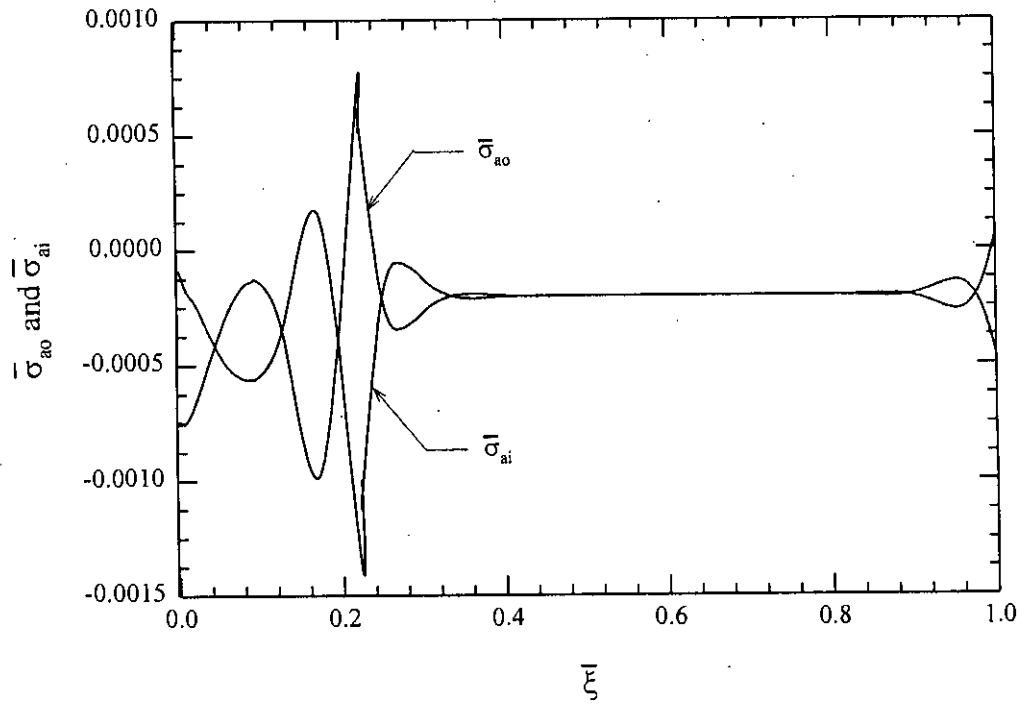


Fig. 5.41a: Meridional stresses at inner and outer fibre of shell model CS100.1 at buckling load.

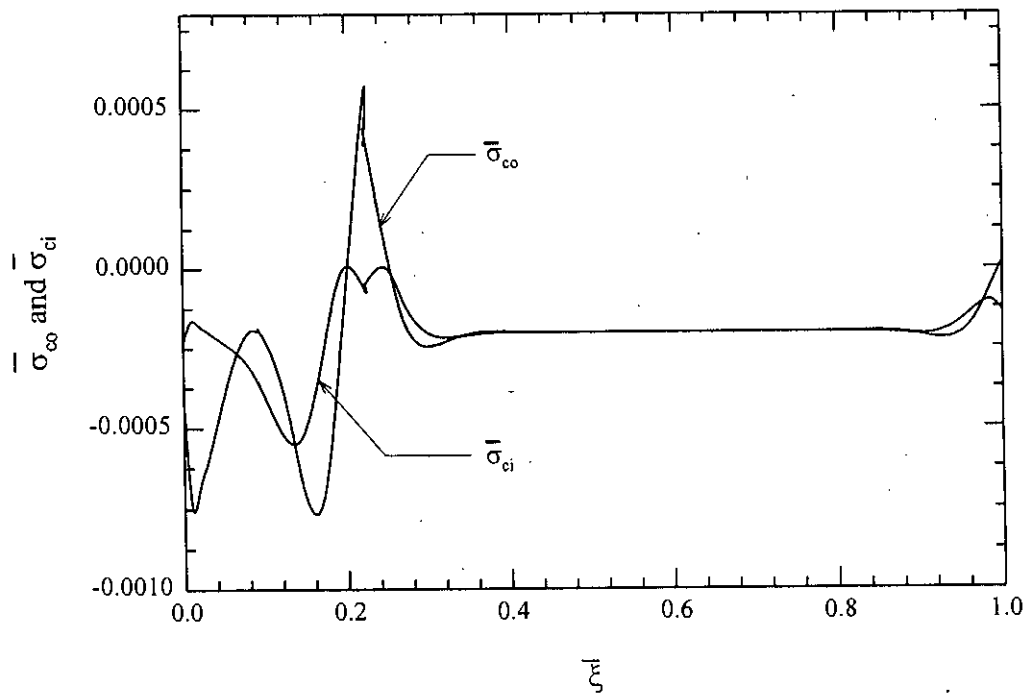


Fig. 5.41b: Circumferential stresses at inner and outer fibre of shell model CS100.1 at buckling load.

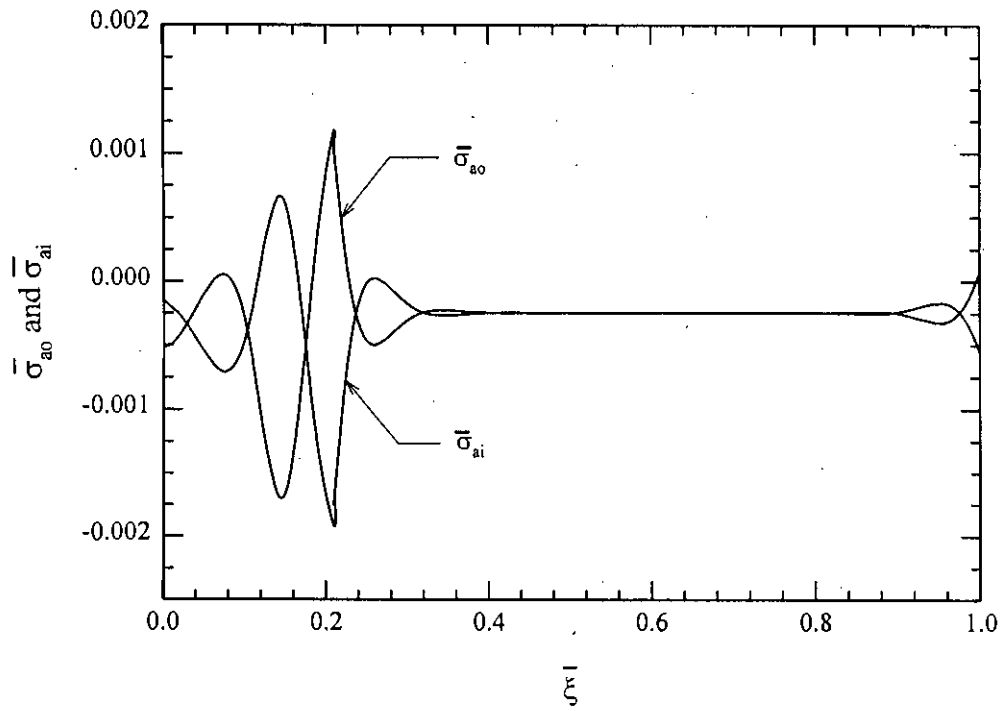


Fig. 5.42a: Meridional stresses at inner and outer fibre of shell model CS100.2 at buckling load.

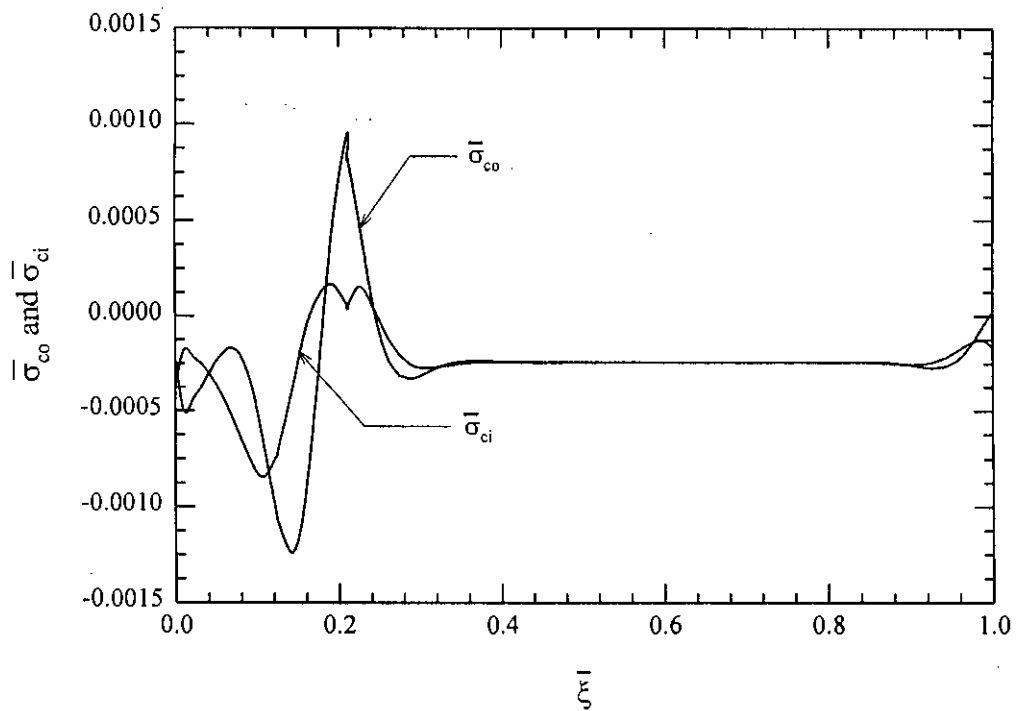


Fig. 5.42b: Circumferential stresses at inner and outer fibre of shell model CS100.2 at buckling load.

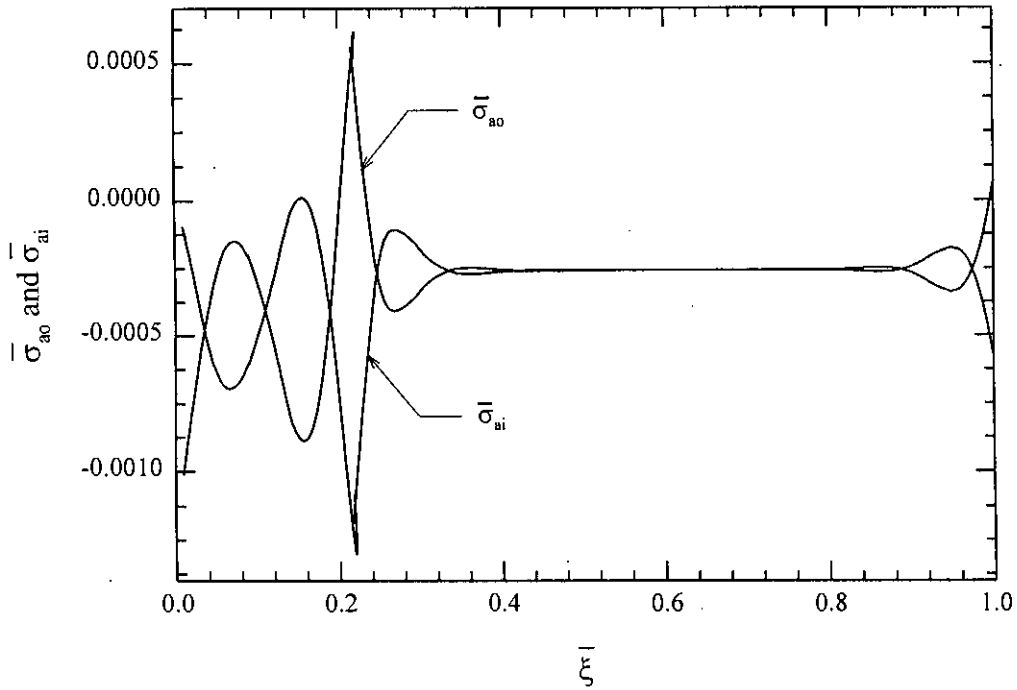


Fig. 5.43a: Meridional stresses at inner and outer fibre of shell model CS100.3 at buckling load.

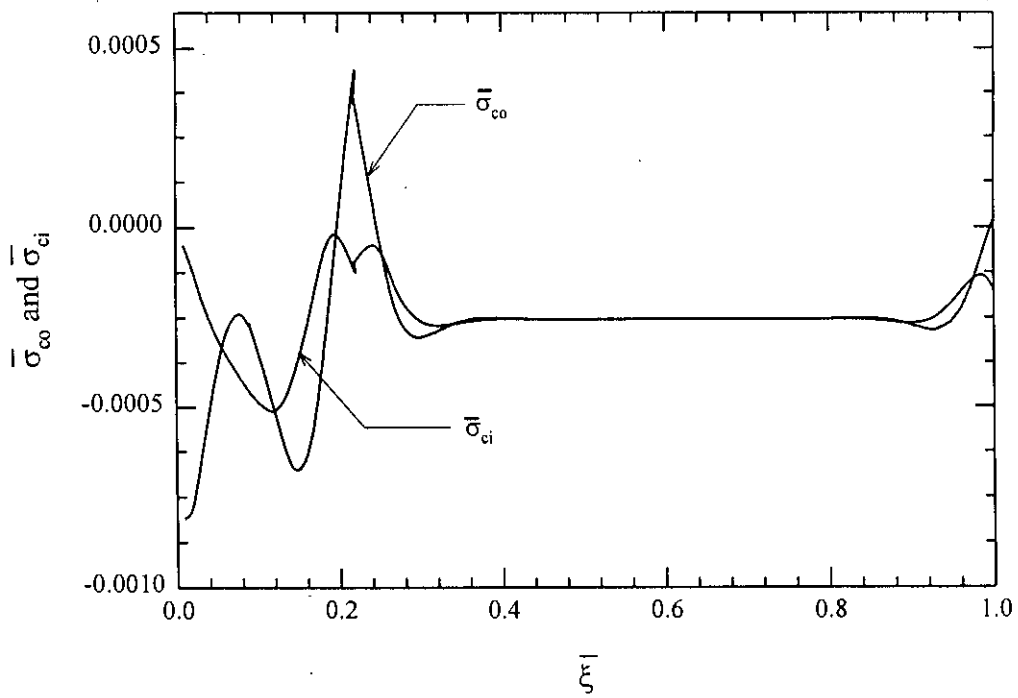


Fig. 5.43b: Circumferential stresses at inner and outer fibre of shell model CS100.3 at buckling load.

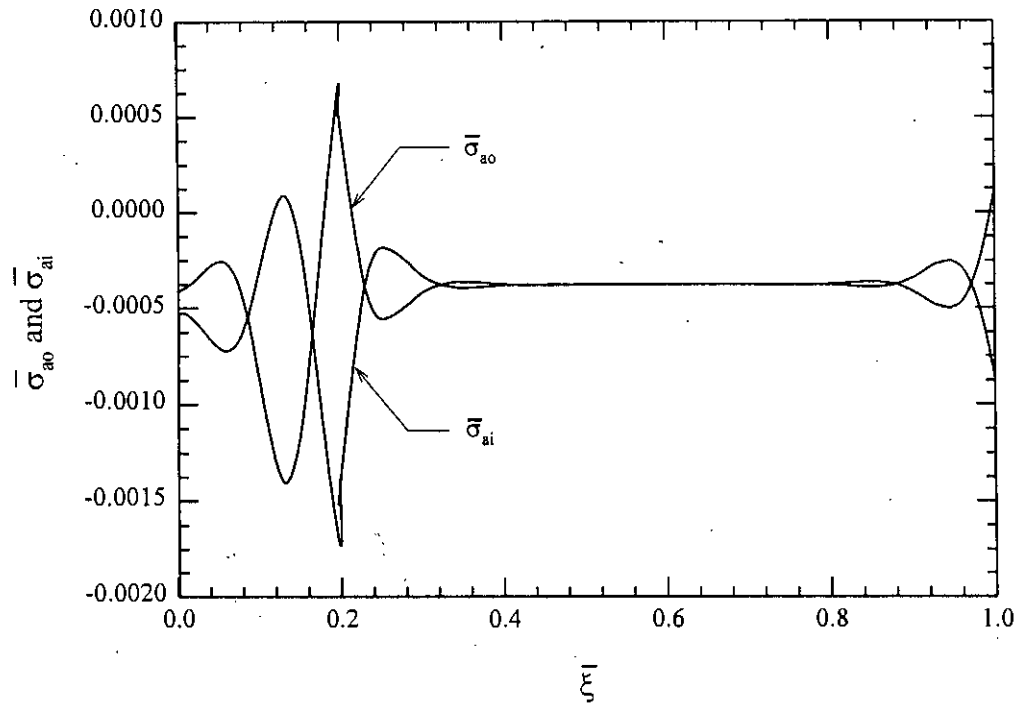


Fig. 5.44a: Meridional stresses at inner and outer fibre of shell model CS100.4 at buckling load.

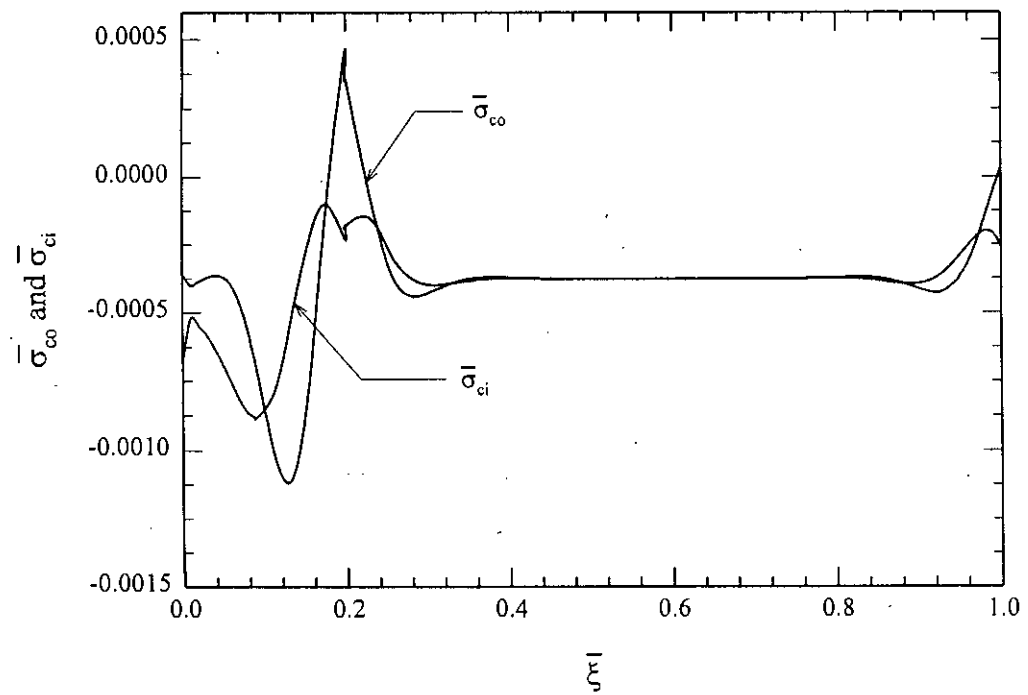


Fig. 5.44b: Circumferential stresses at inner and outer fibre of shell model CS100.4 at buckling load.

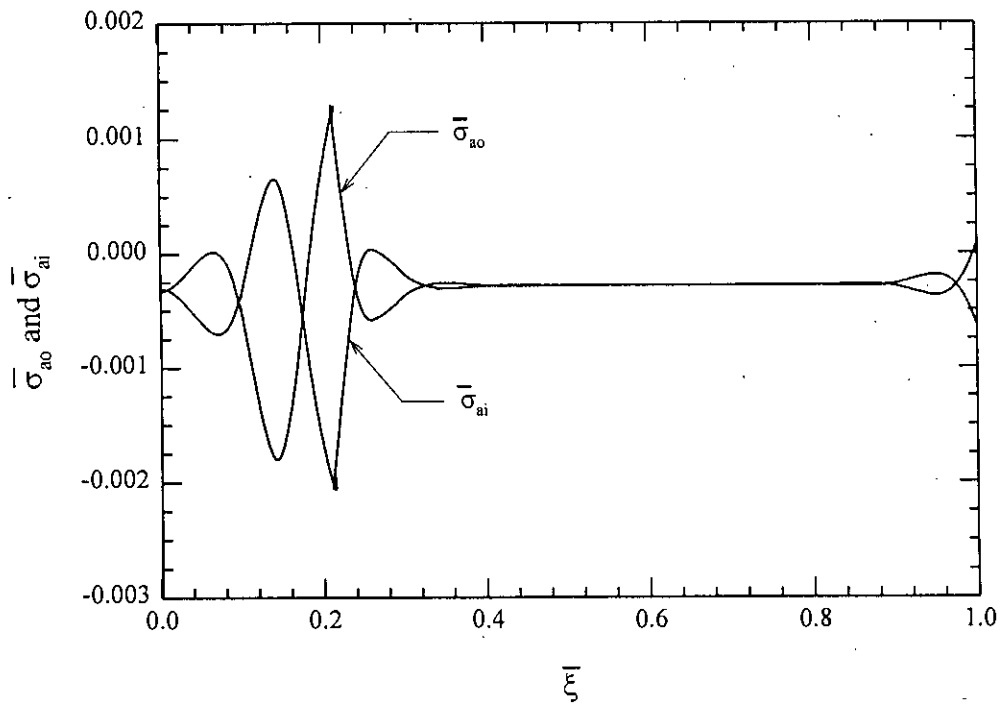


Fig. 5.45a: Meridional stresses at inner and outer fibre of shell model CS100.5 at buckling load.

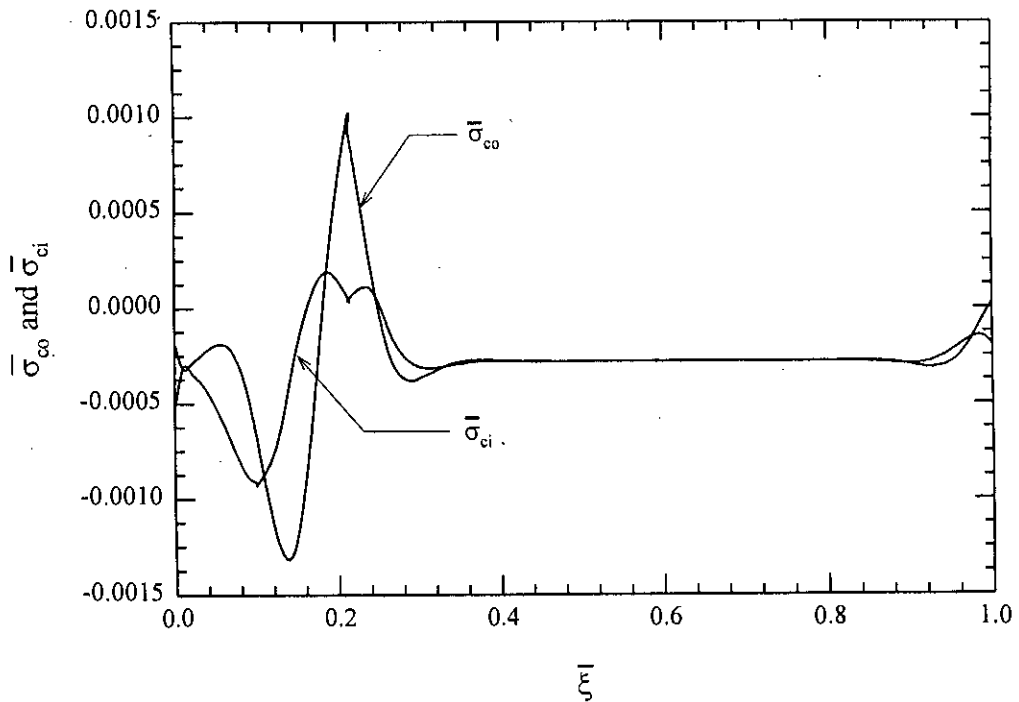


Fig. 5.45b: Circumferential stresses at inner and outer fibre of shell model CS100.5 at buckling load.

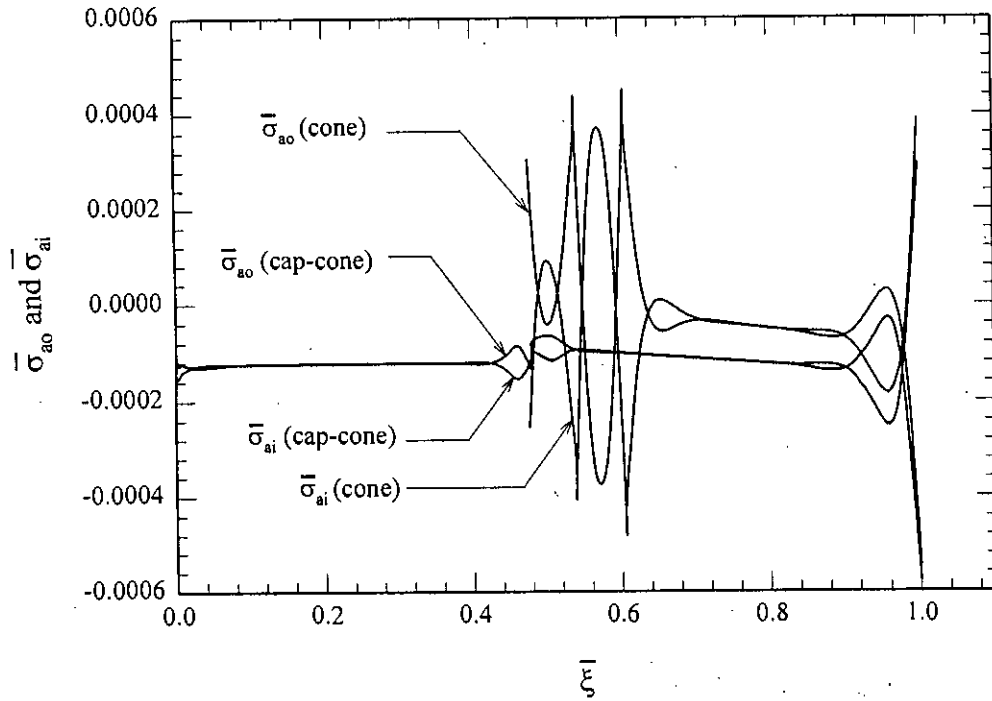


Fig.5.46a: Meridional stresses at inner and outer fibre of CS60.1 (cap-cone) shell and its conical frustum (cone) at asymmetric buckling load. Boundary condition for the conical frustum is fixed at both ends.

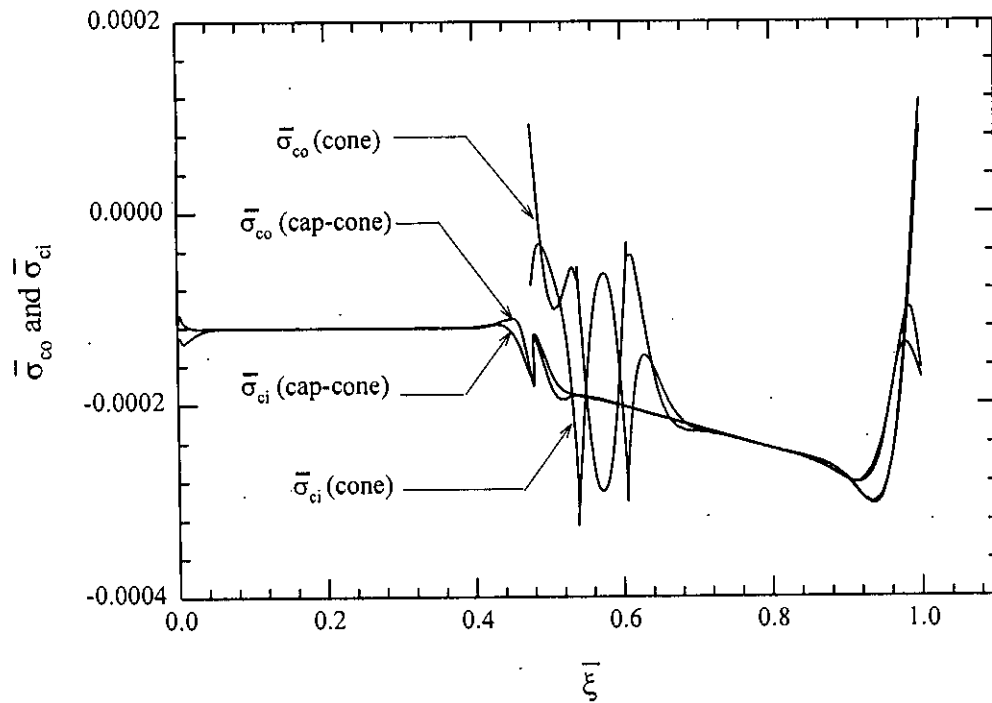


Fig. 5.46b: Circumferential stresses at inner and outer fibre of CS60.1 (cap-cone) shell and its conical frustum (cone) at asymmetric buckling load. Boundary condition for the conical frustum is fixed at both ends.

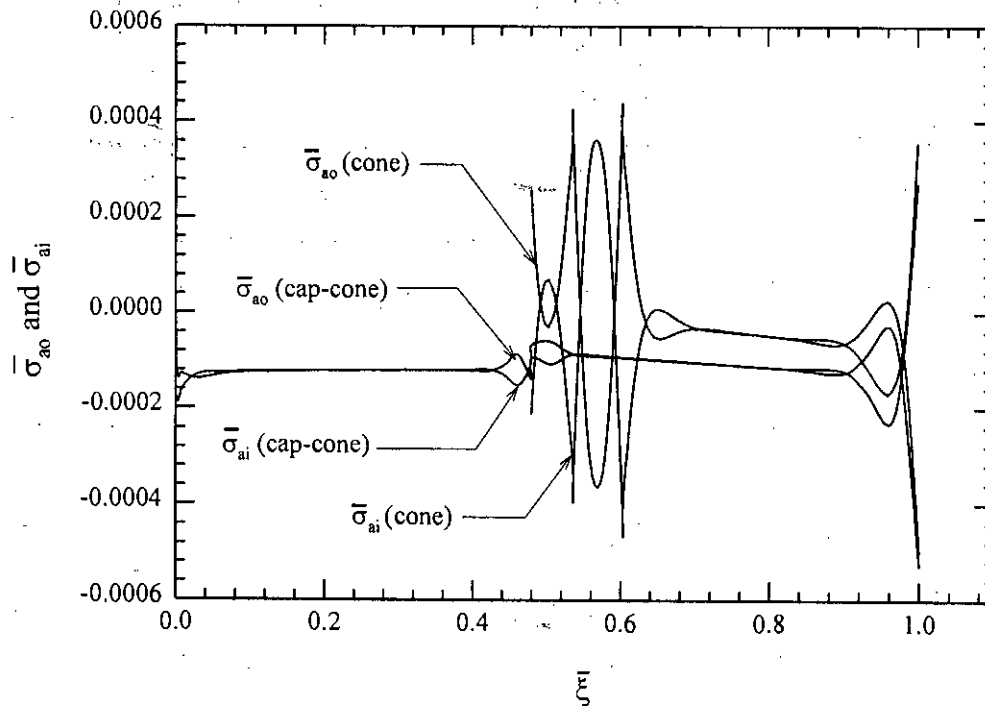


Fig.5.47a: Meridional stresses at inner and outer fibre of CS60.2 (cap-cone) shell and its conical frustum (cone) at asymmetric buckling load. Boundary condition for the conical frustum is fixed at both ends.

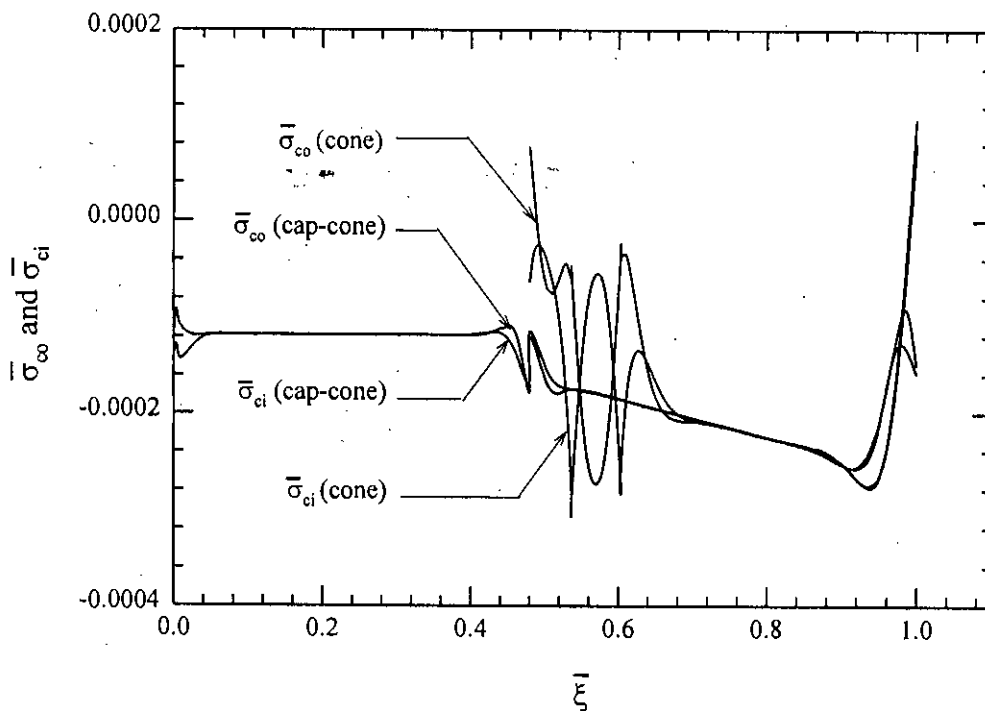


Fig. 5.47b: Circumferential stresses at inner and outer fibre of CS60.2 (cap-cone) shell and its conical frustum (cone) at asymmetric buckling load. Boundary condition for the conical frustum is fixed at both ends.

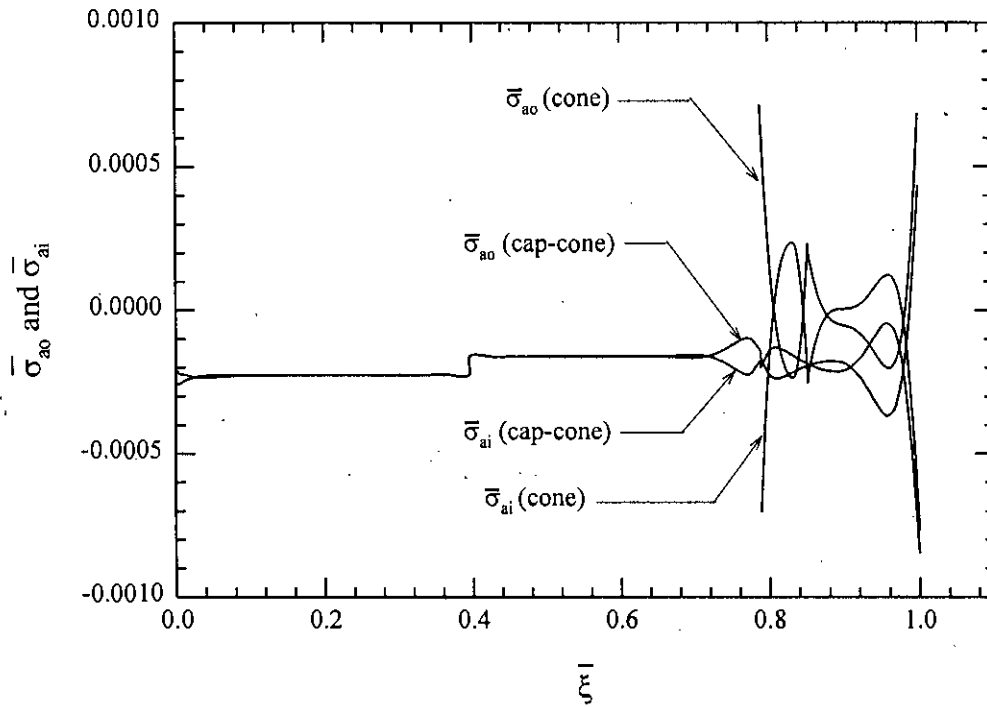


Fig. 5.48a: Meridional stresses at inner and outer fibre of CS80.1 (cap-cone) shell and its conical frustum (cone) at asymmetric buckling load. Boundary condition for the conical frustum is fixed at both ends.

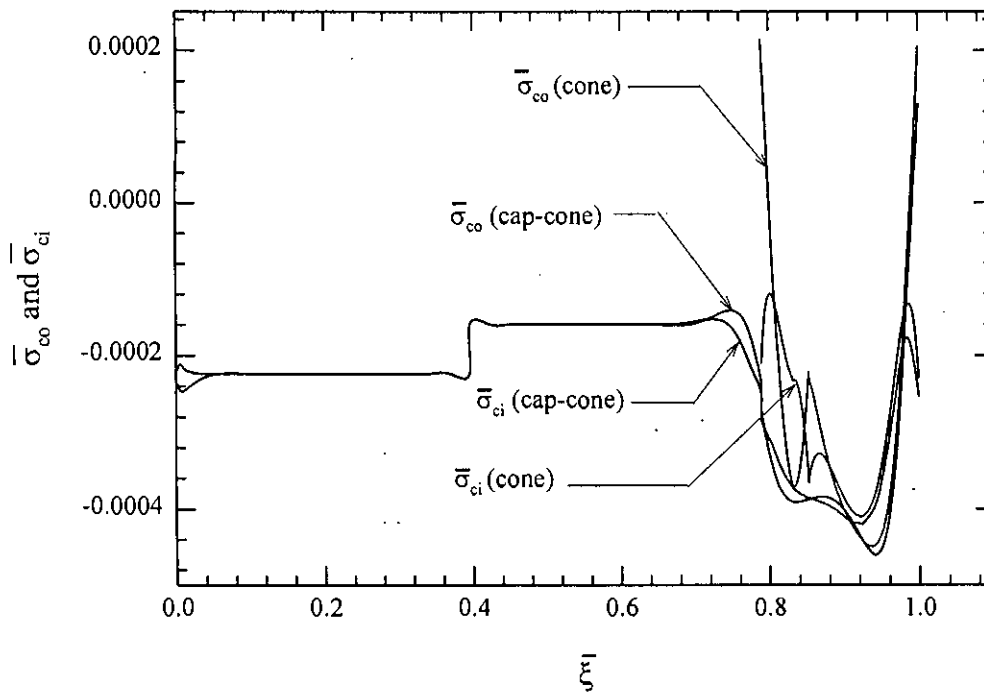


Fig. 5.48b: Circumferential stresses at inner and outer fibre of CS80.1 (cap-cone) shell and its conical frustum (cone) at asymmetric buckling load. Boundary condition for the conical frustum is fixed at both ends.

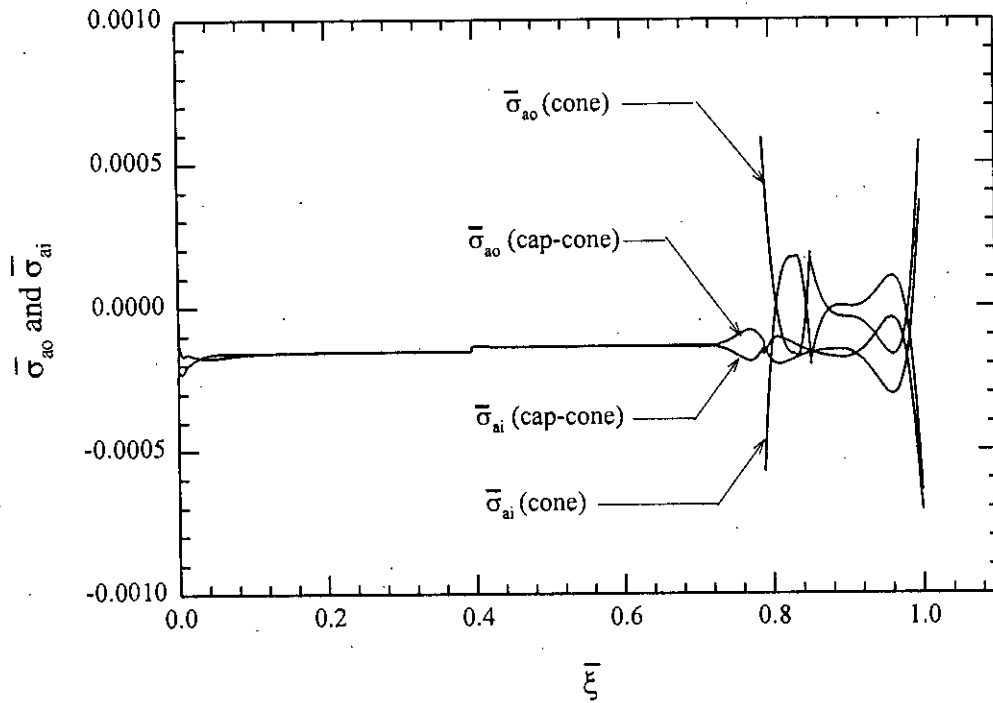


Fig. 5.49a: Meridional stresses at inner and outer fibre of CS80.2 (cap-cone) shell and its conical frustum (cone) at asymmetric buckling load. Boundary condition for the conical frustum is fixed at both ends.

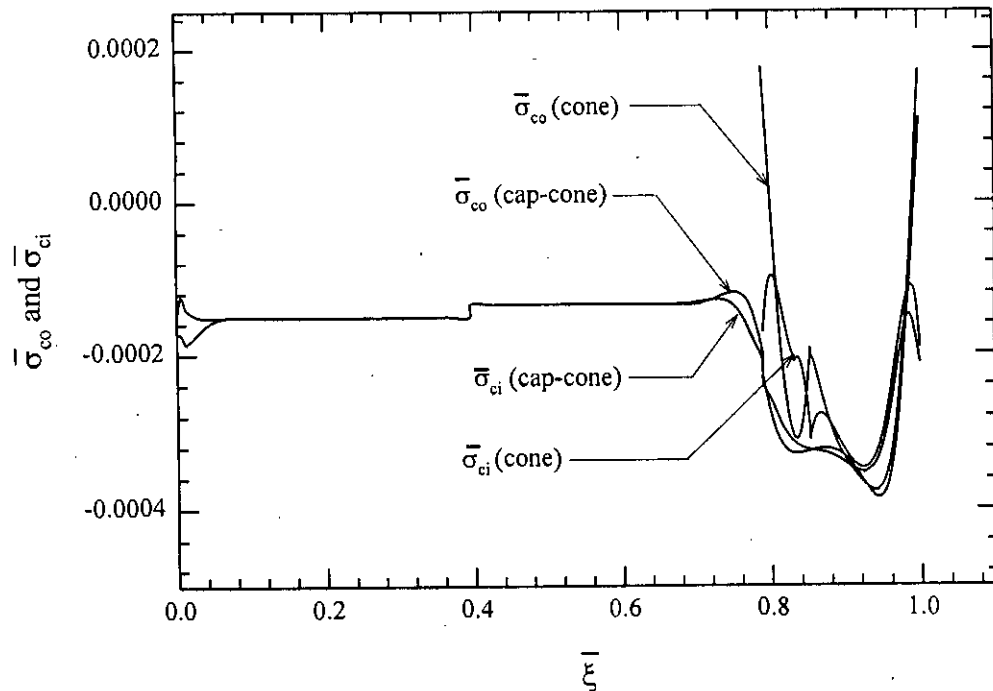


Fig. 5.49b: Circumferential stresses at inner and outer fibre of CS80.2 (cap-cone) shell and its conical frustum (cone) at asymmetric buckling load. Boundary condition for the conical frustum is fixed at both ends.

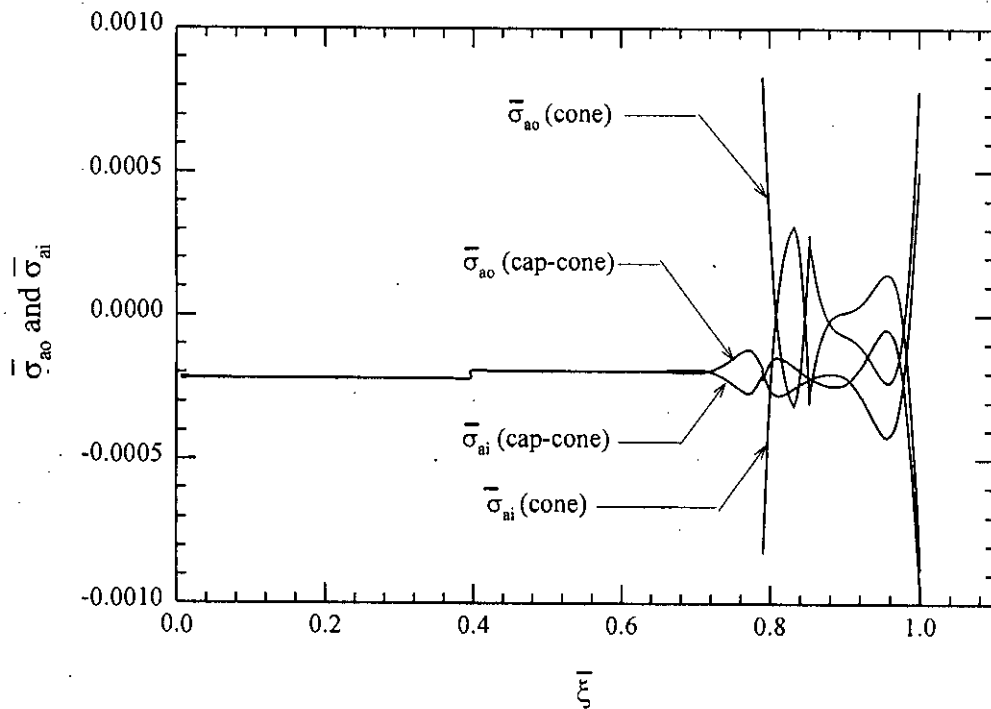


Fig. 5.50a: Meridional stresses at inner and outer fibre of CS80.3 (cap-cone) shell and its conical frustum (cone) at asymmetric buckling load. Boundary condition for the conical frustum is fixed at both ends.

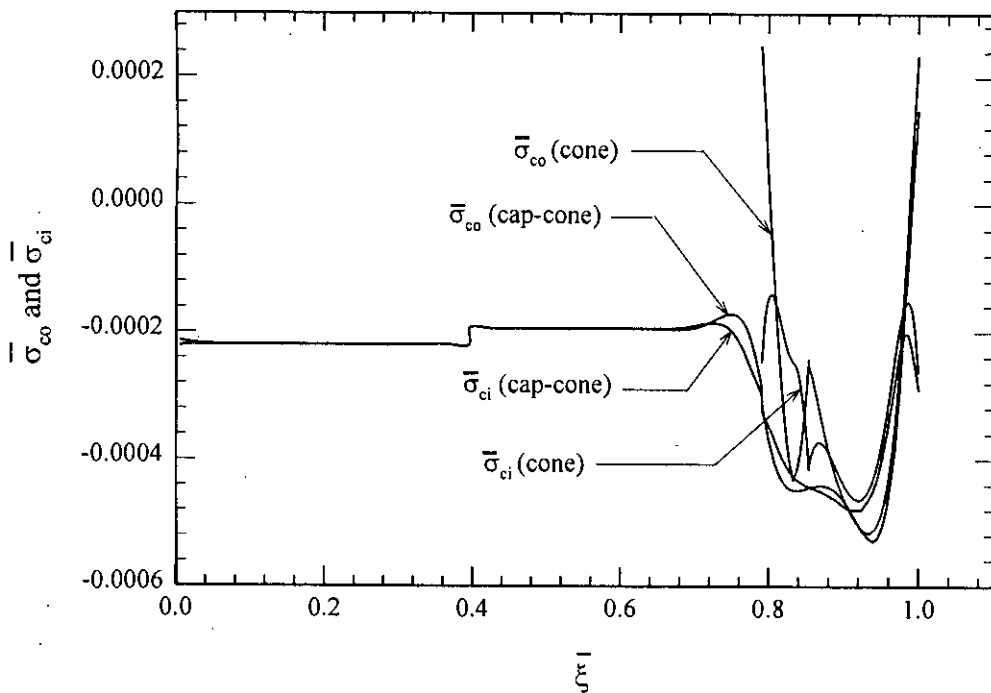


Fig. 5.50b: Circumferential stresses at inner and outer fibre of CS80.3 (cap-cone) shell and its conical frustum (cone) at asymmetric buckling load. Boundary condition for the conical frustum is fixed at both ends.

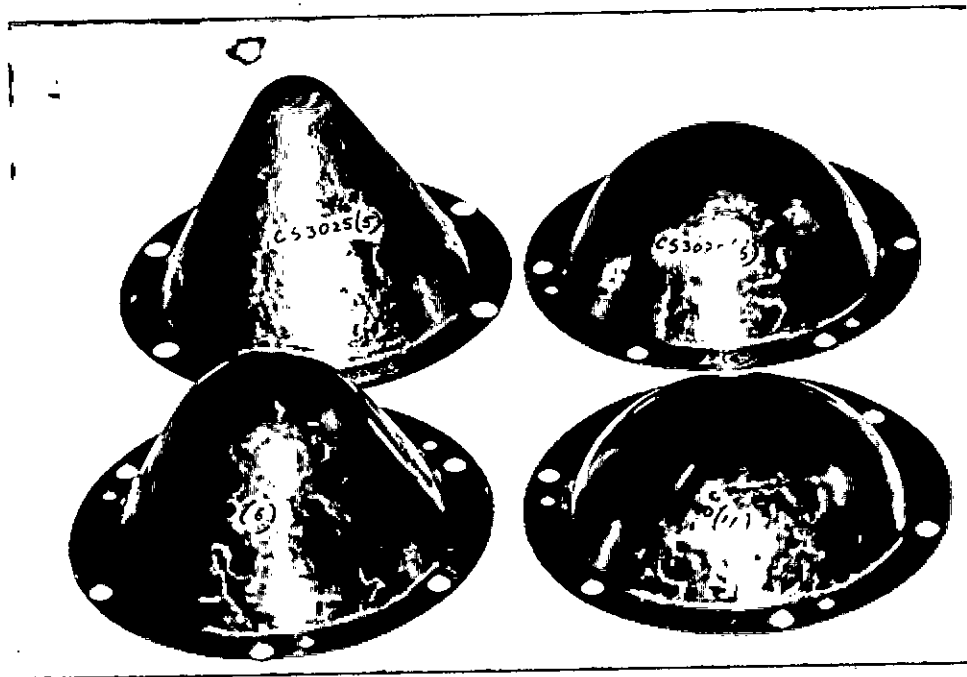


Fig.5.51: Test models of electrodeposited shells.

the conical frustums asymmetrically with different number of circumferential lobes depending on the value of \bar{r}_j . To make comparison between the experimental and theoretical buckling loads of these models, eigenvalue solution of the stability equations described in chapter-3, was obtained. The asymmetric buckling load for the conical frusta of the CS30, CS60 and CS80 models with both edges fixed ($u = v = w = \beta = 0$) and both edges hinged ($u = v = w = M_\xi = 0$) were computed using the geometric data of these shells presented in Table 4.2. The computed asymmetric buckling loads are given in column 4 and 5 of Table 5.5. The results show that, for cones of longer slant height, the buckling loads are independent of edge conditions, and for smaller slant height, they are around 5% to 10% higher than those for hinged edges. It is also found that asymmetric buckling loads of shorter cones are higher than that of the longer ones.

5.2 RESULTS OF EXPERIMENTAL INVESTIGATION

Experimental results of the four sets of cap-cone composite shells, whose theoretical results are presented above, are discussed here.

5.2.1 CS100 Models

The CS100 models are simple spherical caps of 120° angle. The geometry of the fabricated models deviated slightly from the assumed geometry. From the measured data, it was found to be a combination of two axisymmetric shells of revolution of two circular arcs of two different radii of curvature. Experimental buckling loads for different models of this group are presented in column 2 of Table 5.4.

The experimental load versus changes in volume of these shells are given in Fig.5.52. The experimental load-volume curves are almost linear in their initial stages and the change in volume is very small upto a certain load level where from the change in volume increases with a high rate up to the critical point where it suddenly turns either downward or becomes flat. As the wall of the pressure chamber was transparent, during the experiment, at every load step, the shape of the shell was also visually monitored. No visible deformation was found to appear before the critical load, when, all on a sudden, large deformation took place at the tip of each shell of this group. The deformation pattern as photographed after the experiment is shown in

Fig.5.53. Though the shells were slightly imperfect (geometric) at the tip, the deformation were not limited in the imperfect zone, rather it extended far beyond the imperfect zone.

5.2.2 CS30 Models

Submarines and many other pressure-sustaining systems often use a hemispherical or spherical cap as the end-closure of cylindrical shells. Spherical caps, when combined with cylindrical shells, develop sharp geometric discontinuity which in turn develop high discontinuity stress and makes the junction vulnerable. Moreover spherical cap of same thickness but of higher radius of curvature are generally very weak in stability in comparison to a spherical cap of smaller radius of curvature. A conical frustum of smaller slant height are found to be stronger against external loading than that of a frustum of longer slant height. Considering these facts, it is expected that a conical frustum with a spherical tip would prove to be a superior end-closure for pressure vessels. With this in mind a group of cap-cone combinations were studied analytically and discussed earlier in this chapter. Theoretical study of axisymmetric buckling load for such combinations show that cap-cone composite end-closures are superior to spherical end-closure under uniform external pressure (Ref.78). To ascertain the validity of this study, three sets of cap-cone combinations were fabricated and tested under uniform external pressure. CS30 is one of these combinations. Geometric data and thickness of these shells are presented in Table 4.2. Results of the experiment are discussed below.

Experimental results of the CS30 shells are presented in column 3 of Table 5.5. All the CS30 shells are found to buckle asymmetrically with about 6 or 7 number of circumferential lobes around the circumference. The lobes are found to form only in the conical portion of the shells. The load versus volume change curves for these shells, presented in Fig.5.54, shows that, initially, when load is gradually increasing, the change in volume is negligible upto a certain load level and then suddenly become almost flat within a few steps of load with a very high rate of change in volume with respect to load. The circumferential lobes were found to form within a few steps of the flat portion of the load versus volume curves. After the initiation of the lobes, further attempt of increasing the load, made the lobes more prominent with large increase in volume for a very small increase in the load. At this stage an attempt of load release made the lobes disappear. This indicates that the buckling phenomena of these shells are elastic even in

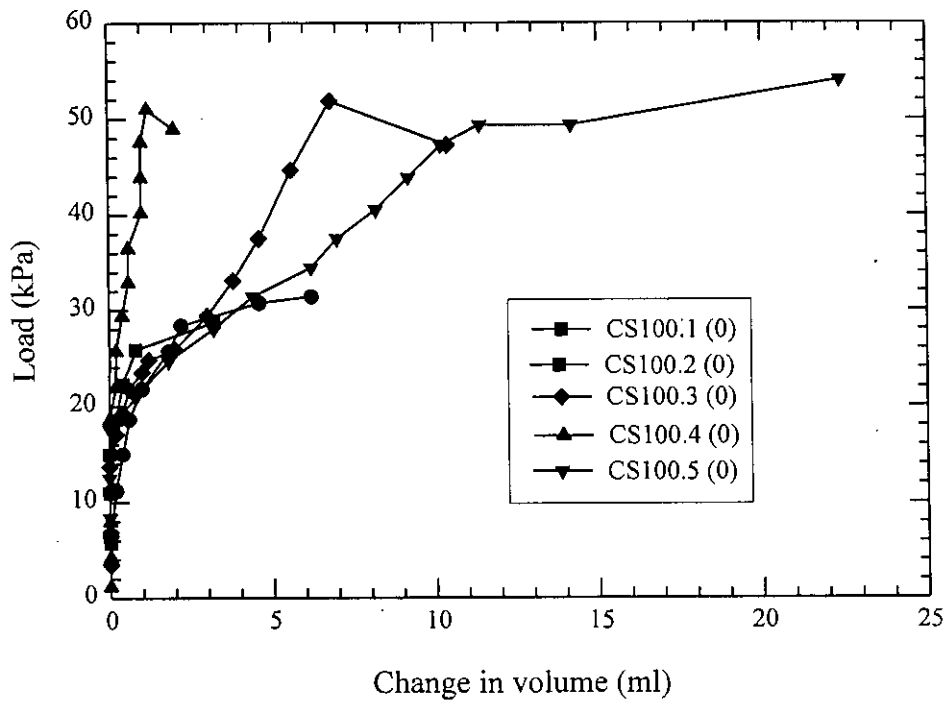


Fig. 5.52: Interior volume change of test models with increasing pressure.

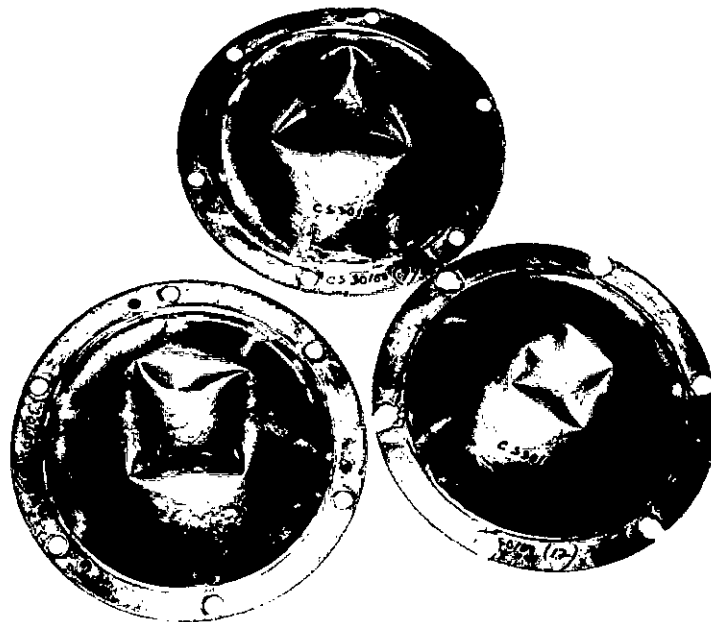


Fig. 5.53: Deformed shape of CS100 shells after experiment.

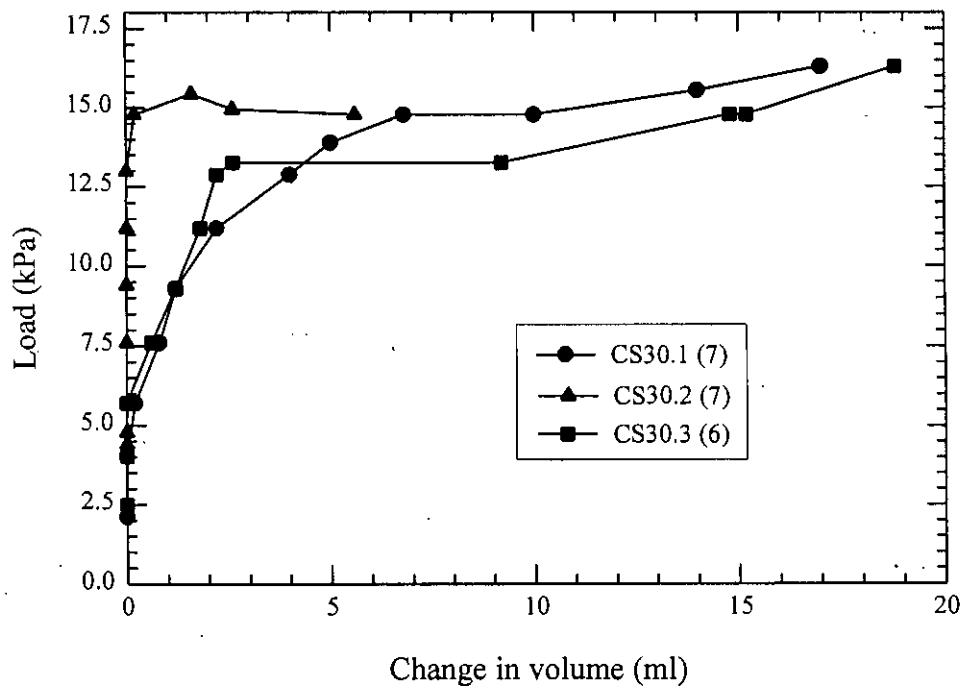


Fig. 5.54: Interior volume change of test models with increasing pressure.

the post buckling region. To develop permanent deformation pattern in these shells, load was increased until the shells collapsed suddenly. In this last attempt, the load remained almost unchanged and the deformation pattern got distorted.

5.2.3 CS60 Models

The CS60 models were the experimental shells with \bar{r}_j about 0.60. Geometric data and thickness of these shells are given in Table 4.2. Experimental buckling loads of these cap-cone shells are given in Table 5.5. As seen in this table, all the shells of these group buckle asymmetrically with about 8 or 9 circumferential lobes. Similar to the CS30 shells, lobes formed only in the conical portion of these models. The load versus volume change curves for these models shown in Fig.5.55, are straight lines at the beginning of loading and gradually become non-linear at higher loads. Near the critical load the change of volume is very high with respect to the increase of load. Circumferential lobes are found to form near the critical load. When load was released most of the circumferential lobes disappeared, keeping about two or three lobes permanent. An attempt was made to increase load above its critical value, but that did not succeed, rather the volume change increased further making the circumferential lobes more prominent with the valleys of the lobes deflected further inward and finally it collapsed leaving two or three lobes permanent and the remaining lobes distorted. The photograph of the collapsed shape of the shells are shown in Fig.5.56.

5.2.4 CS80 Models

In these group of composite cap-cone models, the conical portion is very small. Here the tip ratio \bar{r}_j , of the models are about 0.80. Thickness and geometric data of these models are given in Table 4.2. Experimental results of these shells, presented in Table 5.5, show that all of the shells buckled asymmetrically with 13 circumferential lobes. During the experiment, near the critical load, the lobes were found to form around the circumference of the conical frustum of the models. When load was released from a state at which all the circumferential lobes were visible, all the lobes disappeared. An attempt to increase load further above that at which the lobes were all visible was made and it was found that all the shells of these group suddenly collapsed with one large lobe at one side extending from the base up to the tip of the shells

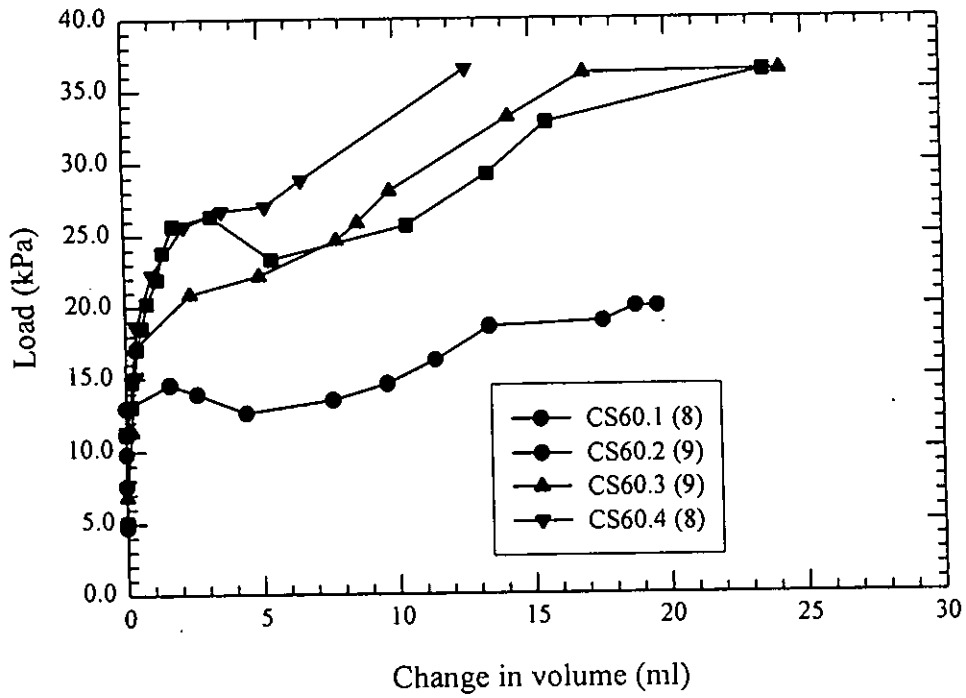


Fig. 5.55: Interior volume change of test models with increasing pressure.

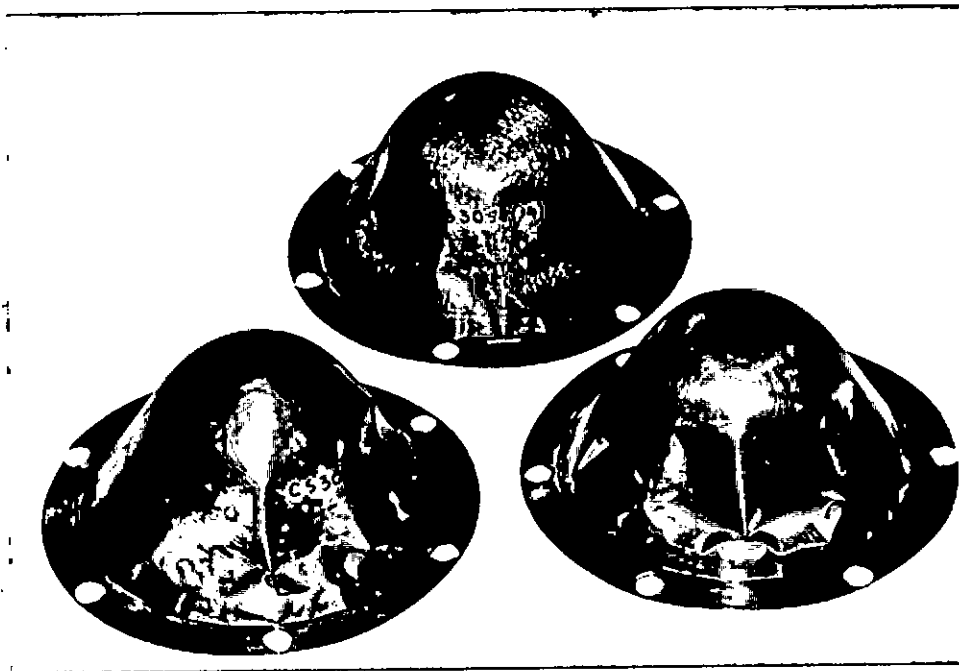


Fig. 5.56: Deformed shape of CS60 shells after experiment.

keeping the remaining surface of the shells slightly distorted with no appreciable change in load. The load versus volume change curves for these models are shown in Fig.5.57 and the photograph of the collapsed shape of these models are shown in Fig.5.58. This exceptional phenomenon may be due to the reason that these shells are stressed throughout with stresses that corresponds to the buckling state of both portions of the shells.

Comparison of the load versus volume change curves of these shells shown in Fig.5.57 with those of the CS100 shells shown in Fig. 5.52 show that these two sets of curves are similar in nature though the buckling pattern is quite different.

5.3 COMPARISON OF THEORETICAL AND EXPERIMENTAL RESULTS

The buckling loads found both from the theoretical analysis and the experiment on the experimental models are presented in Fig.5.59 against \bar{r}_j for all the four sets of shells. The analytical results for the cap-cone composite shells are the asymmetric buckling loads of the attached cones. In the case of the pure spherical caps the analytical results are the axisymmetric buckling loads of the experimental models. From column 6 of Table 5.5 it is seen that the axisymmetric analytical results of the experimental models CS30, CS60 and CS80 are always much higher than the experimental results, and these are shown in Fig.5.59.

The buckling loads of CS100, presented in Table 5.4, show that the experimental results are always lower than the corresponding theoretical results of the experimental models. The theoretical results obtained for these shells without geometric imperfection are found even higher than the results obtained with geometric imperfections. Comparison of load versus axial and radial displacement curves for these experimental models, presented in Figs.5.60-5.64 and 5.65-5.69, respectively, with the load versus volumetric change curves presented in Fig.5.52 show that, the load versus change in volume curves are more or less similar to the load versus tip displacement curves.

The theoretical deformation pattern of these shells are shown earlier in Figs.5.36-5.40. The theoretical patterns are the prebuckling shapes of the shells where the magnitude of the displacements are very small. On the other hand, the photographs of the deformed shells shown

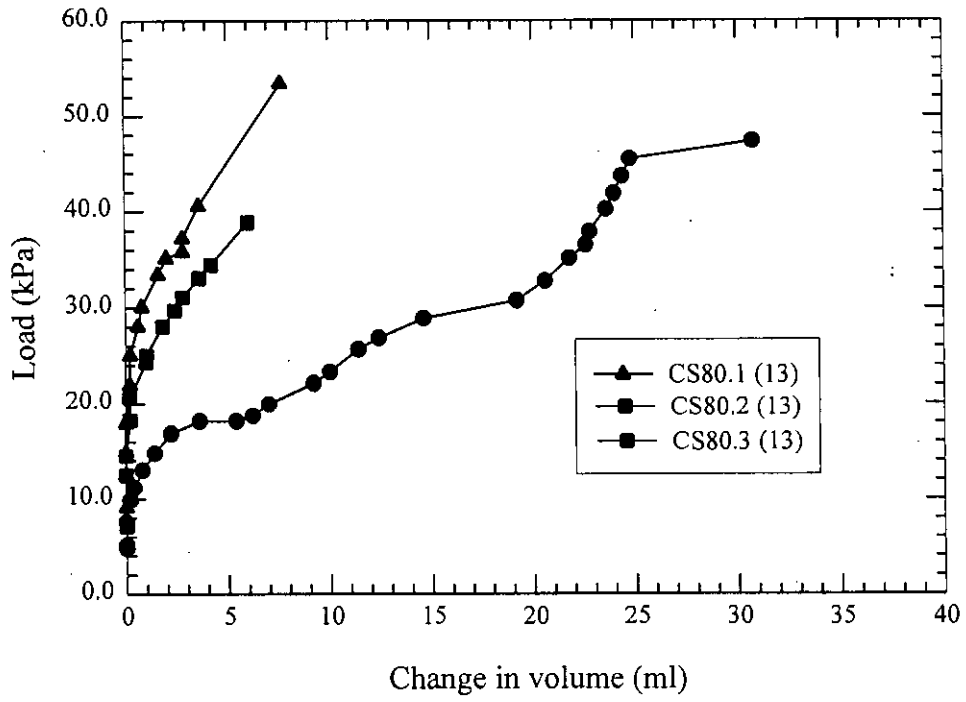


Fig. 5.57: Interior volume change of test models with increasing pressure.



Fig. 5.58: Deformed shape of CS80 shells after experiment.

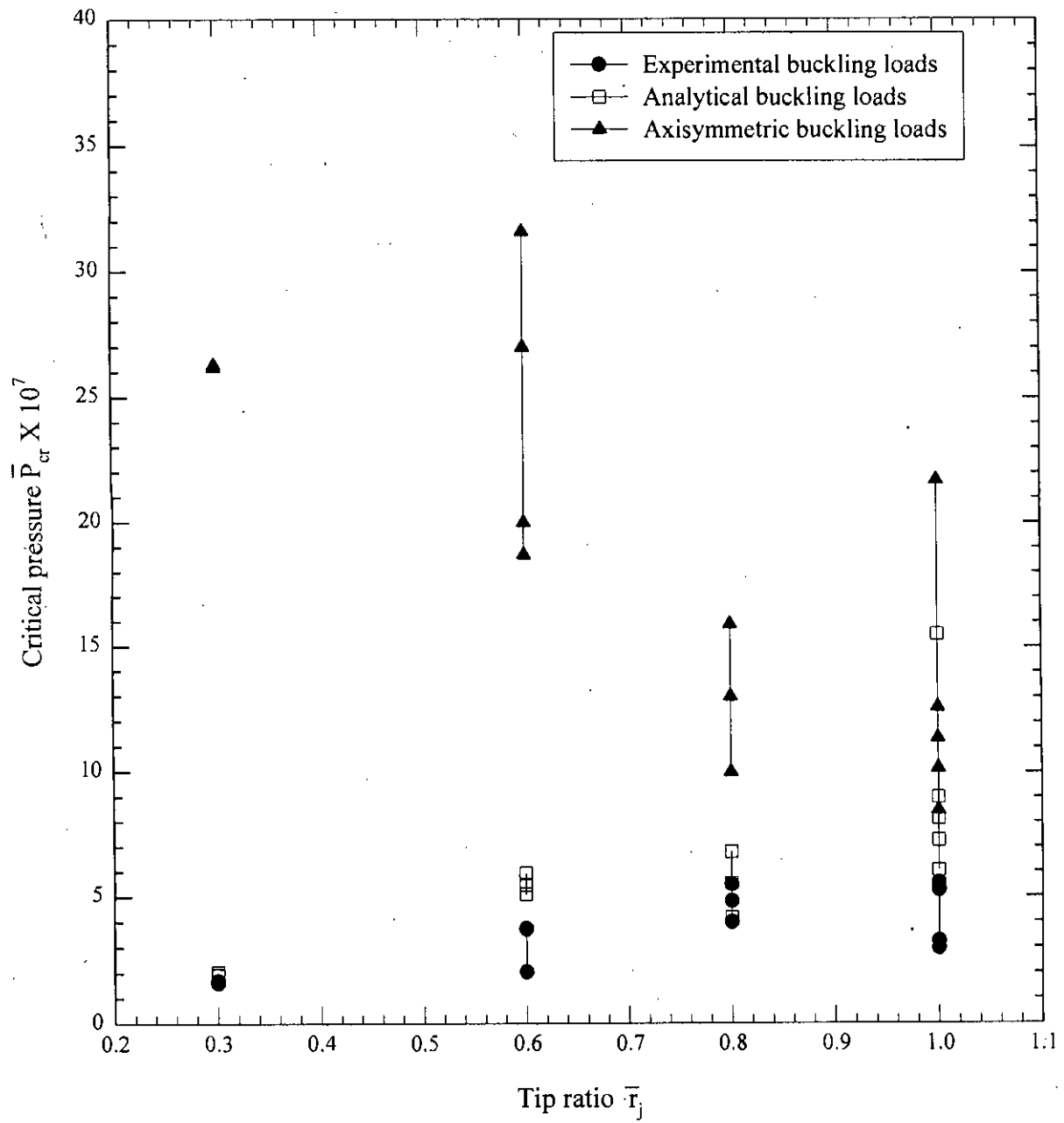


Fig. 5.59: Comparison of analytical and experimental buckling loads.

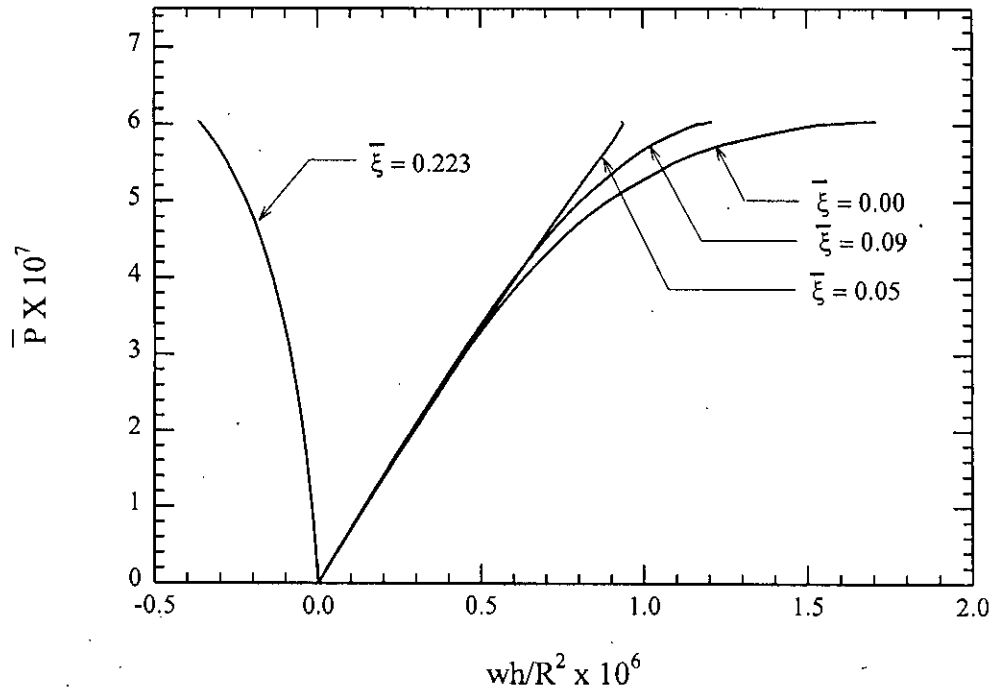


Fig. 5.60: Fundamental configuration path of points on CS100.1 shell model.

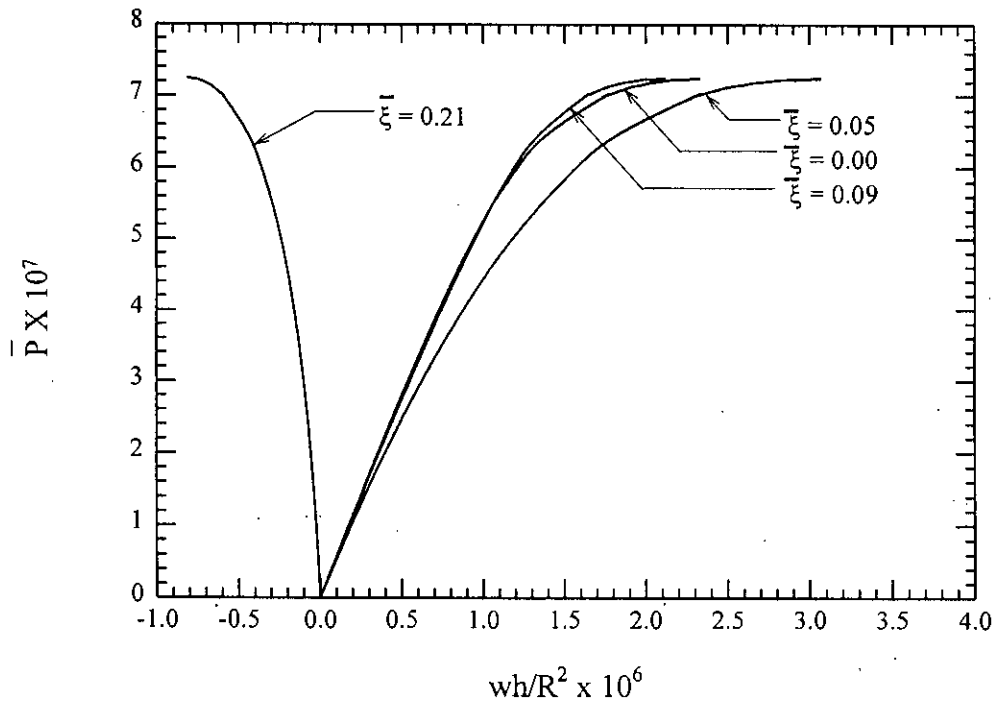


Fig. 5.61: Fundamental configuration path of points on CS100.2 shell model.

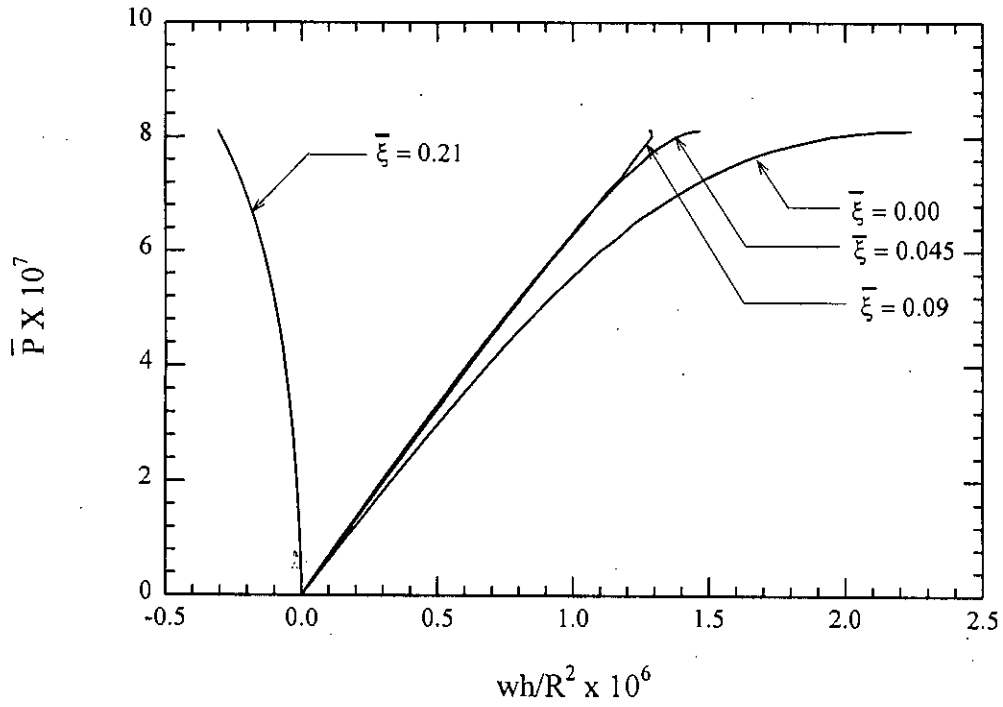


Fig. 5.62: Fundamental configuration path of points on CS100.3 shell model.

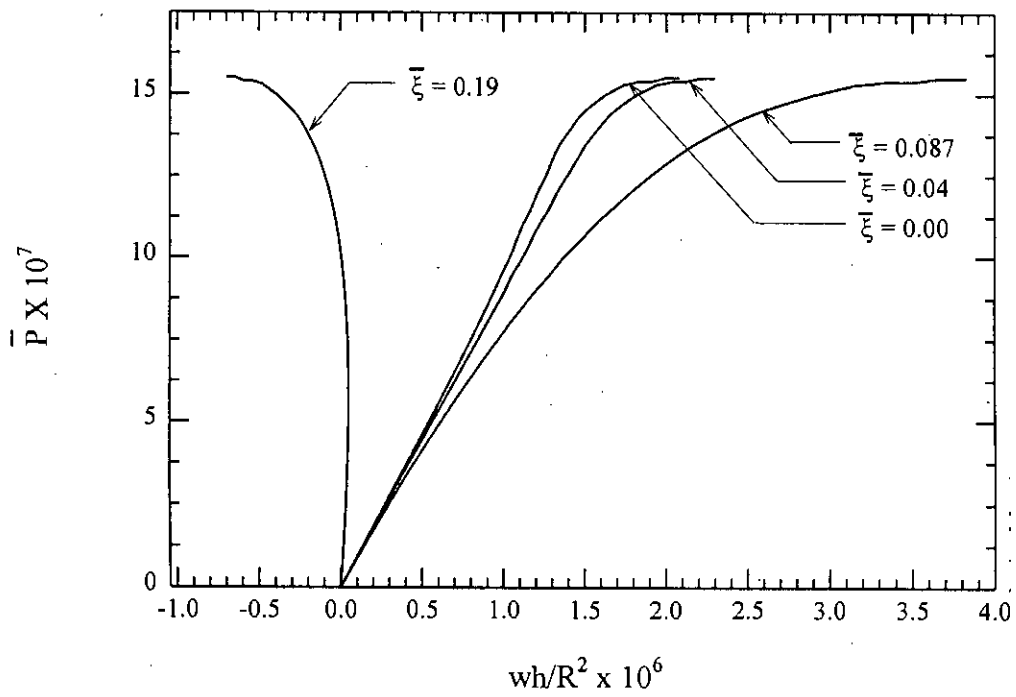


Fig. 5.63: Fundamental configuration path of points on CS100.4 shell model.

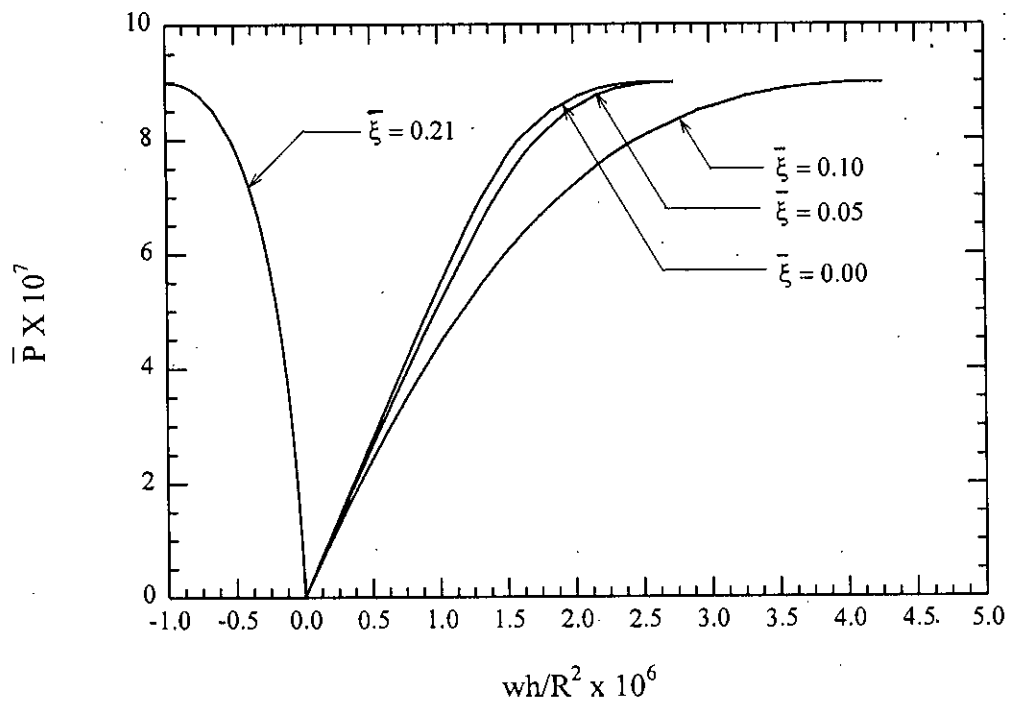


Fig. 5.64: Fundamental configuration path of points on CS100.5 shell model.

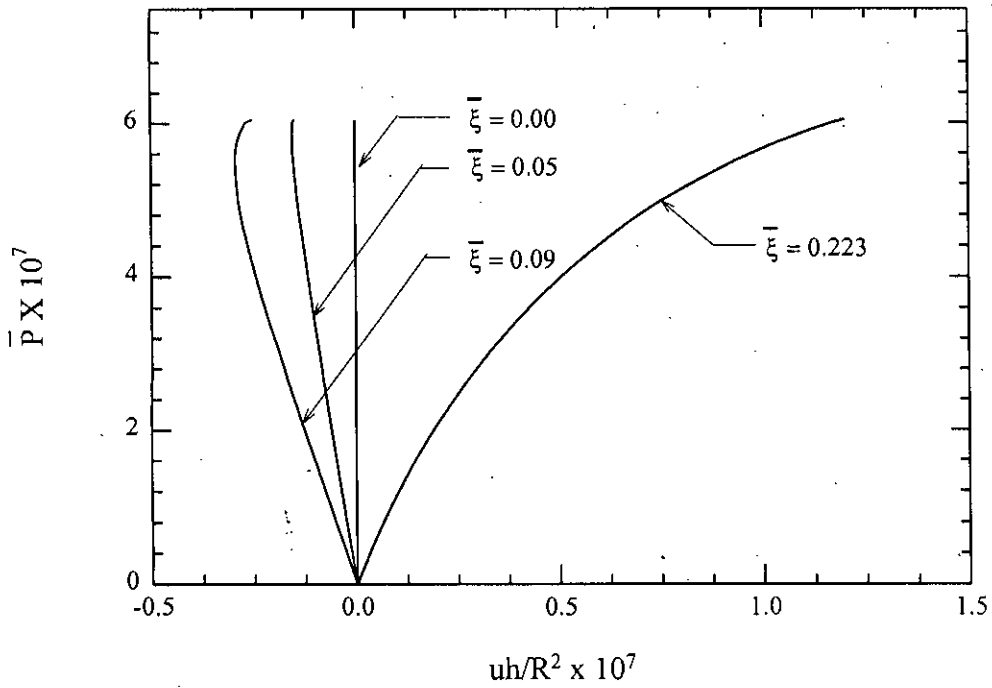


Fig. 5.65: Load versus radial displacement behaviour of CS100.1 shell model.

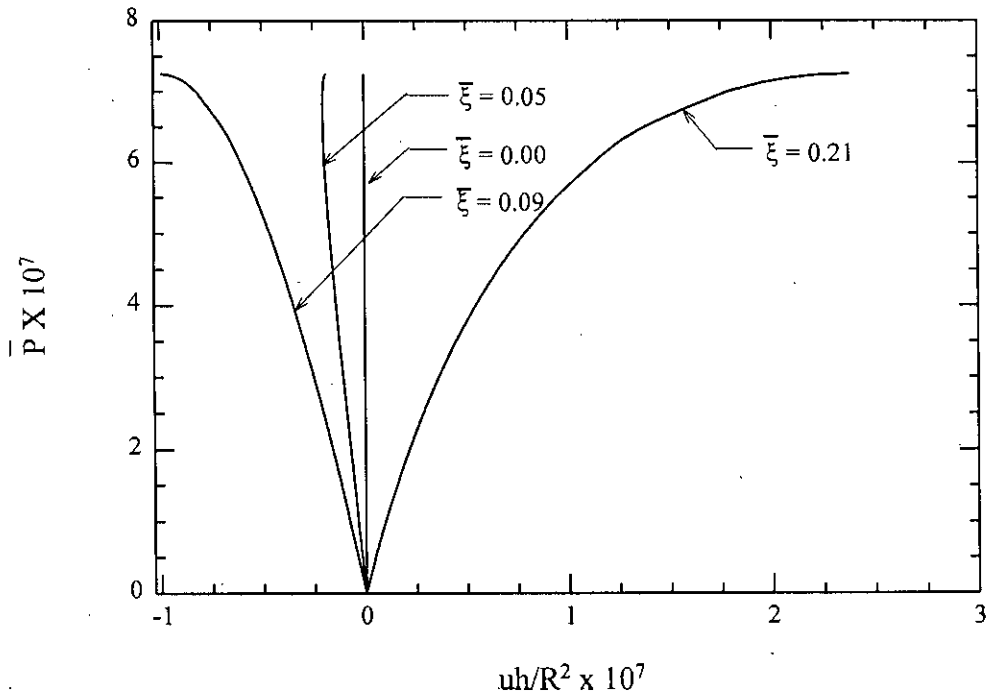


Fig. 5.66: Load versus radial displacement behaviour of CS100.2 shell model.

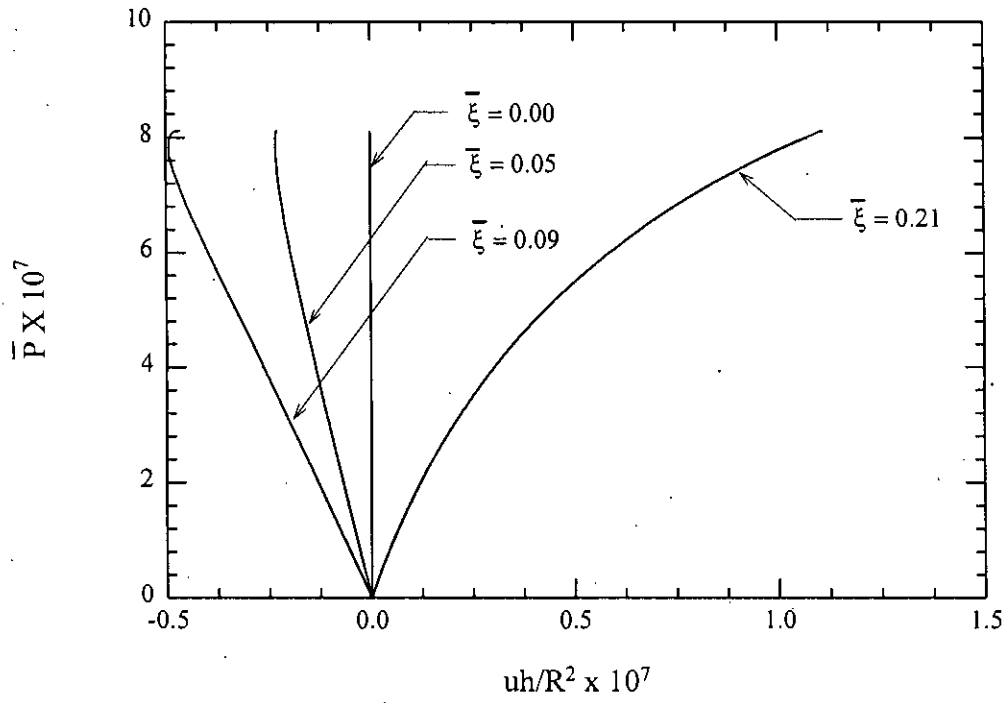


Fig. 5.67: Load versus radial displacement behaviour of CS100.3 shell model.

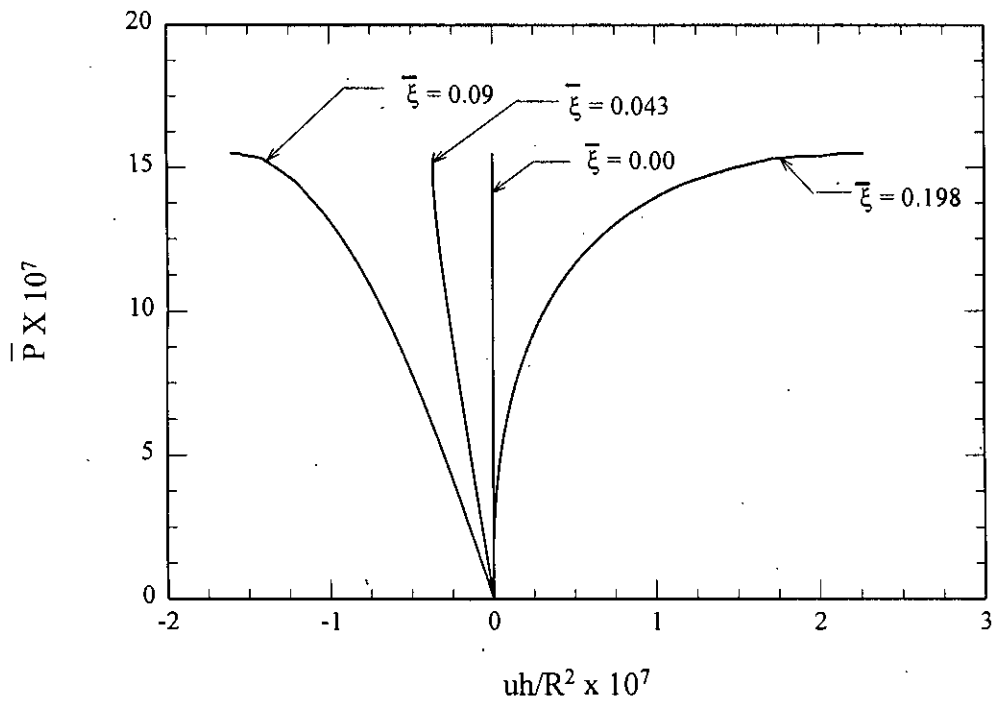


Fig. 5.68: Load versus radial displacement behaviour of CS100.4 shell model.

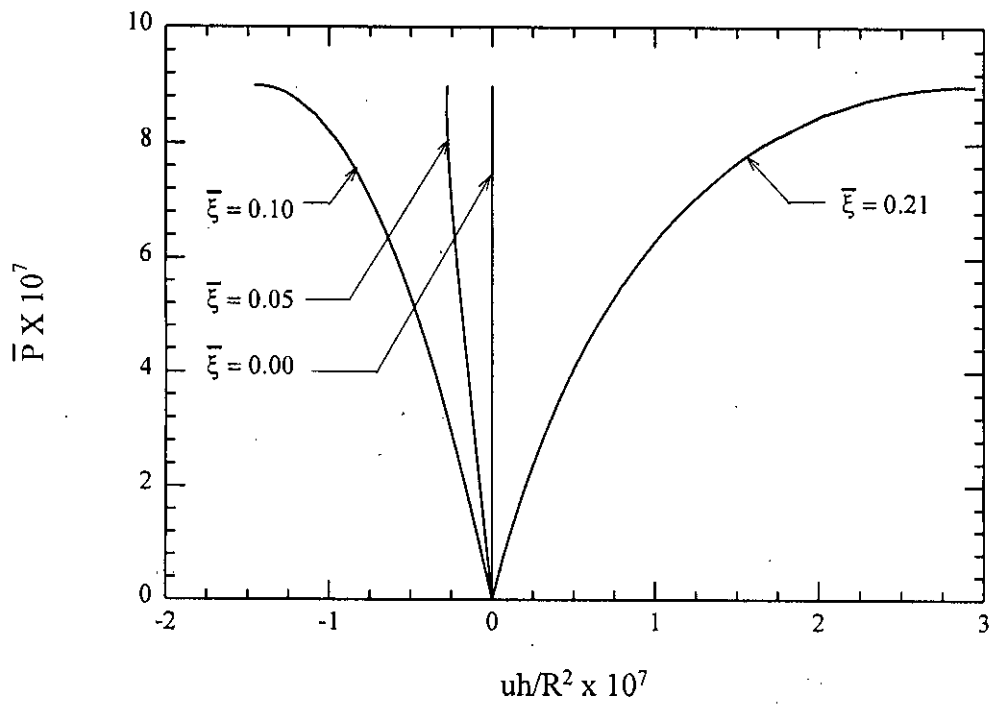


Fig. 5.69: Load versus radial displacement behaviour of CS100.5 shell model. .

in Fig.5.53 are the post-buckling patterns. In the case of the CS100 shells the prebuckling theoretical deformed shapes and post-buckling experimental shapes are in good agreement.

Comparison of the experimental and the theoretical results of other cap-cone shells, presented in Table 5.5, show that, the analytical axisymmetric buckling results for the cap-cone shells are always higher than the experimental results, and the theoretical results of asymmetric buckling of the attached cones are close to the experimental results. Fig.5.59 also shows that, with the increase of \bar{r}_j , both the theoretical (asymmetric) and the experimental buckling loads increase. For the longer (CS30) and shorter (CS80) cap-cone composite shells the experimental and analytical asymmetric results are in very good agreement. For the cap-cone shell models of intermediate height (CS60) and for pure spherical cap models (CS100), the difference between the experimental and analytical results are relatively higher than the other two cap-cone shells (CS30, CS80). Though analytical axisymmetric results of the spherical-cap models are higher than all other cap-cone models, the experimental results of spherical cap models are found either equal to or less than the experimental results of CS80 models.

Comparison of the experimental results of the CS30 models with the theoretical results of the asymmetric mode of buckling of the attached conical frustum show that experimental results are about fifteen percent lower than the asymmetric results of the relevant conical frustum. Circumferential lobe numbers for both the experimental and analytical results are given with the buckling loads in parenthesis. Analytical axisymmetric buckling loads for all these shells given in column 6 of Table 5.5 show that axisymmetric buckling results of the CS30 shells are about fifteen times higher than the experimental results.

Asymmetric analysis of the conical frustum of the CS60 cap-cone models was also done with two edge conditions. Experimental and analytical results of these shells, given in Table 5.5; show that the experimental results are lower than the asymmetric analytical results of the relevant cone by some factors ranging from 1.5 to 2. The number of circumferential lobes from the analysis are found to be almost twice of that found from experiment. This discrepancy may be due to the reason that observed lobes in the experiment are in the post buckling state whereas the numbers found from analysis are corresponding to the state when

buckling just starts with an infinitesimal displacement which may be apprehended with a very high speed camera along with proper magnification facilities.

Comparison of the computed axisymmetric buckling loads of the CS60 models corresponding to geometric and thickness data presented in column 6 of Table 5.5 with their experimental buckling loads show that theoretical axisymmetric buckling loads are around 8 to 10 times the experimental loads.

Comparison of the experimental results of the CS80 models and analytical asymmetric buckling results of relevant conical frustum, presented in Table 5.5, show that, the analytical buckling loads are very close to the experimental results. Theoretical axisymmetric buckling results of these shells with geometric imperfection, given in column 6 of Table 5.5, are about twice the experimental results.

Whatever may be the fabrication technique, the tips of the spherical caps are always found to be imperfect, both in terms of the geometry and the thickness. The geometric imperfections that mostly occur at the tip is flat-spot type, that is the tip is generally a cap of higher radius of curvature. The present analysis shows that this type of imperfection is very much sensitive to buckling load, and even the analytical solution of this type of imperfect shells gives buckling load 1.25 to 1.5 times lower than that obtained with perfect geometry. The scatter of analytical and experimental results of spherical caps (CS100), shown in Fig.5.59, are quite wide. Inclusion of both the geometric and the thickness imperfection in the analysis improved the predictability of the buckling load. With very small deviation in geometry of the spherical-cap models, the loads (Table 5.4 shell no 4 and 5) are found widely scattered, which reveals that, not only the tip geometric imperfection, but even the geometric variation at any point on the meridian of spherical-cap models are also sensitive to external pressure loading.

The analytical and experimental results of the CS80 models show that, these are quite insensitive to both geometric and thickness imperfections. None of the CS80 shells initiated buckling at the tip, the zone of all sorts of imperfections. Further, their experimental buckling loads were found to be the highest among all other composite end-closures studied in this

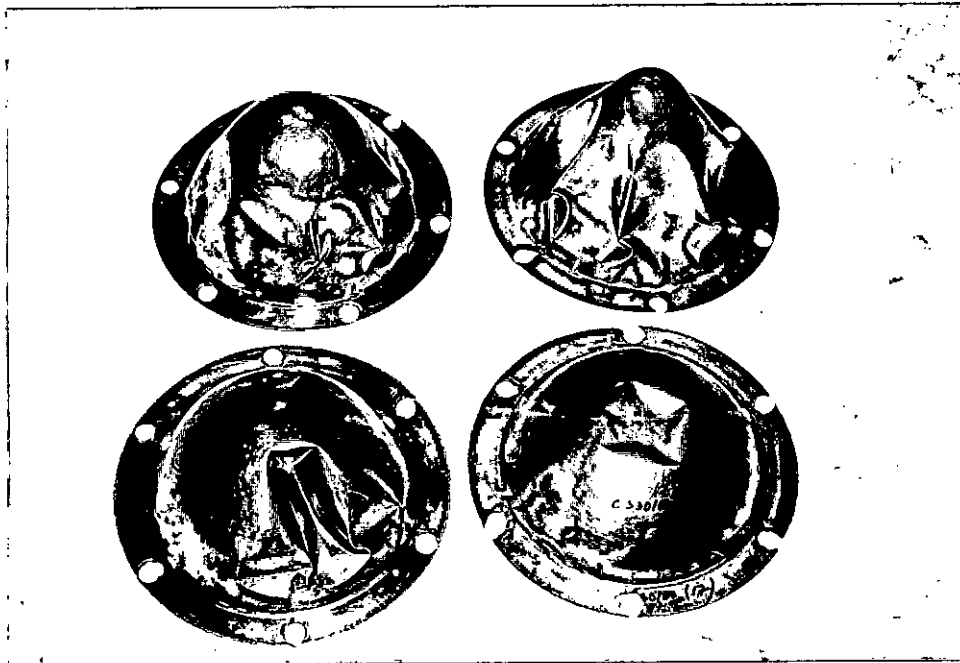
work. Thus it may be inferred that a spherical cap with a slight tangential conical extension may serve as a better end-closure under uniform external pressure.

The stresses in the experimental cap-cone models at their analytical asymmetric critical load and the corresponding stresses of the conical frusta, presented in Figs.5.46-5.50, show that, both the axial and the circumferential stresses in them are smoother than those of the conical frustum with edges fixed. The axial stresses in the conical frustum with fixed edges are lower than that in the composite models, which might be the cause of higher buckling loads of the conical frustum with fixed edges.

Photograph of the collapse modes of the four different cap-cone model shells are shown in Fig.5.70. Comparison of these collapse modes shows that the deformation of the CS80 shells extends from the base upto the tip of these models, whereas in case of the other cap-cone shells (CS30, CS60 and CS100) either the shells deform at the tip (CS100) or along the conical portion of the shells (CS30 and CS60). From these deformation pattern it may be concluded that the CS80 shells are efficiently stressed throughout the meridian, which makes these shells strong against external load.

(a) CS60

(b) CS30



(c) CS80

(d) CS100

Fig.5.70: Deformed shape of experimental models.

CHAPTER 6

CONCLUSIONS AND RECOMMENDATIONS

6.1 CONCLUSIONS

The objectives of this research work ultimately lead to the searching of an axisymmetric shell, suitable as an end-closure for pressure vessels under uniform external pressure. In line with these objectives, the following conclusions have been drawn from the investigation carried out in this thesis.

1. The buckling of spherical-cap end-closures are highly sensitive to imperfections in geometry as well as in thickness.
2. Spherical-cap end-closures buckle axisymmetrically.
3. The tip of the spherical-cap end-closure buckles inward under external pressure.
4. Cap-cone composite end-closures buckle asymmetrically.
5. The asymmetric buckling of cap-cone end-closure takes place in its conical frustum.
6. Buckling loads of cap-cone composite end-closures can be predicted with an asymmetric analysis of the relevant conical frustum with both edges clamped.
7. Imperfection sensitivity of cap-cone end-closures is much less in comparison to that of spherical-cap end-closures.
8. Imperfection sensitivity of cap-cone composite end-closures of \bar{r}_j around 0.8 is negligible and fails at about 2.5 times the loads of the other cap-cone end-closures investigated here. Thus a cap-cone end-closure of \bar{r}_j about 0.8 may be recommended as the most suitable end-closure of pressure vessel under uniform external pressure. As these end-closures are less imperfection sensitive, lower safety factor can thus be used in their design.

9. The present technique of experimental determination of critical load from the tracing of fundamental path in terms of volume change is found to be highly reliable and very sharply defined. Earlier techniques of detection of critical load from the measurement of geometrical displacement not only required very precise instrumentations but also lead to controversial conclusions as discussed in Ref. 177.
10. Axisymmetric buckling of the cup-cylinder end-closures as proposed by Ross [128] and the conventional dome-cylinder end-closures under external pressure show that cup-cylinder end-closures are superior to dome-cylinder end-closures as pressure hulls of submarines.
11. In case of cup-cylinder composite end-closure, within the limited ranges of parameters studied here, axisymmetric buckling takes place only in the cylinder portion, and the buckling load is around 4 times higher than that of the dome-cylinder end-closures of the same physical parameters.
12. Both the dome and the cylinder of a dome-cylinder end-closure buckle almost simultaneously. Sometimes the cylinder portion of a dome-cylinder shell is found to buckle axisymmetrically even at loads lower than the axisymmetric buckling pressure of a cylinder.

6.2 RECOMMENDATIONS FOR FUTURE WORK

In the light of experiences gained during this research work, the author feels that the following further investigations will enrich and enhance the comprehensibility of the field of the present work.

1. The present experimental work on only one apical angle of the cap-cone composite end-closures should be extended to include other apical angles in both the analytical and experimental studies.
2. In case of cap-cone end-closure, maximum stress develops at the vessel and end-closure junction due to sharp geometric discontinuity. This may be eliminated by adding a suitable toroidal knuckle at this junction, which may further improve the

buckling load capability of the cap-cone composite end-closures. Thus, the effect of using toroidal knuckle at vessel and end-closure junction should be studied.

3. Axial loading in shell structures is a very common phenomenon. Rockets and underwater vessels are under high axial compression while accelerating. Thus instability of composite shells under axial compression and axial tension along with external pressure may be undertaken for stability analysis.
4. Circumferential stresses at the junction of the cup-cylinder composite end-closures are compressive both at the inner and outer surfaces, which may lead to asymmetric buckling prior to meridional buckling. Thus, asymmetric analysis should be undertaken for ultimate conclusion on the suitability of cup-cylinder pressure hulls.
5. In composite shells with sharp geometric discontinuity at the junction of different segments, compressive stress develops at the junctions even under the action of internal pressure. So buckling analysis of composite shells under internal pressure should be undertaken to add to the comprehensibility of the stability problems of composite end-closure of vessels.
6. Buckling analysis of imperfect composite shells may also be undertaken for understanding imperfection sensitivity of these shells. It is a fact that shells are generally very imperfection sensitive with respect to stability and all the shells in use are imperfect.
7. In pharmaceutical and petrochemical industries composite shells are used in high temperature environment. Thermal stressing may lead these shells to buckling failure near the junctions of geometrically dissimilar segments. Buckling analysis of composite shells under thermal stressing is also an area of exploration.

REFERENCES

1. Abu-Farsakh, G.A.F.R. and Lusher, J.K., "Buckling of Glass Reinforced Plastic Cylindrical Shells Under Combined Axial Compression and External Pressure," *AIAA Journal*, Vol. 23, No. 12, Dec. 1985, pp. 1946-1951.
2. Ahmed, K. Noor, "Survey of Computer Programs for Solution of Nonlinear Structural and Solid Mechanics Problems," *Comp. & Struct.*, 13, 1981, pp. 425-465.
3. Ahmed, K. Noor, "Hybrid Analytical Technique for Nonlinear Analysis of Structures," *AIAA Journal*, 23, 1985.
4. Akkas, N. and Bauld, N. R. Jr., "Axisymmetric Dynamic Buckling of Clamped Shallow Spherical and Conical Shells Under Step Load," *AIAA Journal*, 8, 1970. pp. 2276-2277
5. Akkas, N. and Bauld, N. R. Jr., "Static and Dynamic Buckling Behavior of Clamped Shallow Conical Shells," *Int. J. Mech. Sc.*, 8, 689-706, (1971).
6. Alfutov, N. A., "Stability of a Cylindrical Shell Reinforced with Transverse Stiffening Rings and Subject to Uniform External Pressure," *Inzb. Sbornik Akad. Nauk SSSR* 23, 36-46, 1956.
7. Ali, G.M.Z., "Stability and Stress Analysis of Conical Reducers", M. Sc. Engineering Thesis, Bangladesh University of Engineering and Technology, 1991.
8. Almroth, B.O., Burns, A.B. and Pittner, E.V., "Design Criteria for Axially Loaded Cylindrical Shells," *J. Spacecraft and Rockets*, Vol. 7, No. 6, pp. 714-720, 1970.
9. Almroth, B. O., Brogan, F. A. and Stanley, G. M., "Structural Analysis of General Shells," Vol. 11: *User Instruction for STAGS*. Lockheed Missiles & Space Co., Report LMSC-D633873 (1979).
10. Arbocz, J., "The Effect of Initial Imperfections on Shell Stability" in *Thin Shell Structures, Theory, Experiment and Design*, Y.C. Fung and E.E. Sechler, eds., Prentice-Hall, Englewood Cliffs, N.Y., 1974, pp.205-245.
11. Archer, R. R., "Stability Limits for a Clamped Spherical Shell Segment Under Uniform Pressure," *Quarterly of Applied Mathematics*, 15, (1958).
12. Aylward, R.W., Galletly, G.D. and Moffat, D.G., "Buckling Under External Pressure of Cylinders with Toriconical or Pierced Torispherical Ends: A Comparison of Experiment with Theory" *J. of Mech. Eng. Sci.* © IMechE, Vol. 17, No. 1, 1975, pp. 11-18.

13. Baker, E.H., "Experimental Investigation of Sandwich Cylinders and Cones Subjected to Axial Compression," *AIAA Journal*, Vol. 6, No. 9, pp. 1767-1770, Sept. 1968.
14. Ball, R.E., "A geometrically Nonlinear Analysis of Arbitrarily Loaded Shells of Revolution," *NASA CR-909*, January (1968).
15. Bermus, I.M. and Srubshchik, L.S., "Non-axisymmetric Buckling of Shallow Spherical Shells," *PMM USSR*, Vol. 54, No. 3, pp. 375-388, 1990.
16. Brebbia, C. and Connor, J.J., "Geometrical Nonlinear Finite Element Analysis," *Proc. J. Eng. Mech. Div.*, ASCE 95 (EM2), 463-483, (1969).
17. Broadland, G.W. and Cohen, H., "Large-Strain axisymmetric Deformation of Cylindrical Shells," *Journal of Applied Mechanics*, 54, 287-291, (1987).
18. Brodland, G.W. and Cohen, H., "Deflection and Snapping of Ring Loaded Spherical Caps", *ASME Journal of Appl. Mech.*, Vol. 56, Series E, pp. 127-132, March 1989.
19. Brogan, F. and Almroth, B., "Buckling of Cylinders with Cutouts," *AIAA Journal*, Vol. 8, No. 2, pp. 236-240, Feb. 1970.
20. Brush, D.O. and Almroth, B.O., "*Buckling of Bars, Plates and Shells*," McGraw-Hill Book Company, New York, 1975.
21. BS 5500: 1984 Specification for Unfired Fusion Welded Pressure Vessels, 1984 (British Standards Institution, London).
22. Budiansky, B. and Hutchinson, J.W., "A Survey of Some Buckling Problems," *AIAA Journal*, Vol. 4, No. 9, pp. 1505-1510, Sept. 1966.
23. Bushnell, D., "Nonlinear Axisymmetric Behavior of Shells of Revolution," *AIAA Journal*, Vol. 5, No. 3, pp. 432-439, March 1967.
24. Bushnell, D., "Symmetric and Nonsymmetric Buckling of Finitely Deformed Eccentrically Stiffened Shells of Revolution," *AIAA Journal*, Vol. 5, No. 8, pp. 1455-1462, Aug. 1967.
25. Bushnell, D., "Bifurcation Phenomena in Spherical Shells Under Concentrated and Ring-Loads," *AIAA Journal*, Vol. 5, No. 11, pp. 2034-2040, Nov. 1967
26. Bushnell, D., "Buckling of Spherical Shell Ring-Supported at the Edge," *AIAA Journal*, Vol. 5, No. 11, pp. 2041-2046, Nov. 1967.
27. Bushnell, D. and Smith, S., "Stress and Buckling of Nonuniformly Heated Cylindrical and Conical Shells," *AIAA Journal*, Vol. 9, No. 12, pp. 2314-2321, Dec. 1971.
28. Bushnell, D., "*Computerized Buckling Analysis of Shells*," Martinus Nijhoff Publishers, Dordrecht, Netherlands, 1985.

29. Bushnell, D., "BOSOR5, Program for Buckling of Elastic-Plastic Complex Shells of Revolution Including Large Deflection and Creep," *Comput. Struct.* **6** (1976) 221.
30. Bushnell, D., BOSOR4, Program for Stress, Buckling and Vibration of Complex Shells of Revolution, *Structural Mechanics Software Series (Edited by N. Perrone and W. Pilkey)*, pp. 11-143. University Press of Virginia (1977).
31. Bushnell, D. and Galletly, G. D., "Stress and Buckling of Internally Pressurized Elastic-Plastic Torispherical Vessel Heads: Comparison of Tests and Theory," *J. Press. Vessel Technol.* **99** (1977) 39.
32. Bushnell, D., Nonsymmetric Buckling of Internally Pressurized Ellipsoidal and Torispherical Elastic-Plastic Pressure Vessel Heads, *J. Press. Vessel Technol.* **99** (1977) 54.
33. Bushnell, D., Elastic-Plastic Buckling of Internally Pressurized Torispherical Vessel Heads, *Nuclear Engg. Des.* **48** (1978) 405.
34. Bushnell, D., Elastic-Plastic Buckling of Internally Pressurized Ellipsoidal Pressure Vessel Heads, *Welding Research Council Bulletin 267*, United Engineering Centre, New York (1981).
35. Bushnell, D., Plastic Buckling of Various Shells, *J. Press. Vessel Technol.* **104** (1982) 51.
36. Chan, H.C. and Chung, W.C., "Geometrically Nonlinear Analysis of Shallow Shells Using High Order Finite Elements", *computers and Structures*, Vol. 31, No. 3, pp. 329-338, 1989.
37. Chien, W.Z., The Intrinsic Theory of Thin Plate and Shells; Part-I General Theory. *Q. Appl. Math.*, **1**, 297-327, (1944).
38. Chien, W.Z., The Intrinsic Theory of Thin Plate and Shells; Part-III Application to Thin Shells. *Q. Appl. Math.*, **2**, 120-135, (1944).
39. Cunnigham, W.J., Introduction to Nonlinear Analysis. McGraw-Hill Book Company Inc., 1958.
40. Danielson, D.A., "Buckling and Initial Post-Buckling Behavior of Spherical Shells Under Pressure", *AIAA Journal*, Vol. 7, No. 5, pp. 936-944, May 1969.
41. Donnel, L. H., A New Theory for The Buckling of Thin cylinders Under Axial Compression and Bending. *Trans. ASME* **56**, 795-806, (1934).
42. Dumir, P. C. and Khatri, K. N., Axisymmetric Static and Dynamic Buckling of Orthotropic Shallow Conical Caps, *AIAA Journal*, Vol. **23** (1985) pp. 1762-1767.

43. Dumir, P. C. and Khatri, K. N., Axisymmetric Static and Dynamic Buckling of Orthotropic Truncated Shallow Conical Caps, *Comp. & Struct.*, **22** (1986) pp. 335-342.
44. Dutta, P., "*Stability and stress analysis of toroidal pipe-reducers*" M.Sc. Eng. Thesis, BUET, 1996.
45. Dym, C.L. and Hoff, N.J., Perturbation solution for the Buckling Problems of Axially Compressed Thin Cylindrical Shells of Infinite Length", *ASME Journal of applied Mechanics*, vol. 35, No. 4, pp. 754-762, Dec. 1988.
46. Ericksen, J. L., and Truesdell, C., Exact Theory of Stress and Strain in Rods and Shells. *Archive for Rational Mech. and Anal.*, 1, 295-323, (1959).
47. Esslinger, M., Hochgeschwindigkeitsaufnahmen von beulvorgang dünnwandiger, axialbelasteter Zylinder, *Stahlbau*, Vol. 39, pp. 73-76, March 1970.
48. Euler, L., *Methods Inveniendi Lineas Curvas Maximi Minimive Proprietate Gaudents* (Appendix, De Curvis Elastics), Marcum Michaellem Bousquet, Lausanne and Geneva, (1744).
49. Famili, J., Archer, R.R., Finite Asymmetric Deformation of Shallow Spherical Shells. *AIAA Journal*, 3, 506-570, (1965).
50. Faulkner, D., "Structural Developments in Underwater Operations", *Progress in ship Buildings*, pp. 69-83, 1988.
51. Feinstein, G., Chen, N.Y. and Kemper, J., Buckling of Clamped Oval Cylindrical Shells Under Axial Loads", *AIAA Journal*, Vol. 9, No. 9, pp. 1733-1738, Sept. 1971.
52. Fitch, J.R. and Budiansky, B., "Buckling and Post-Buckling Behavior of Spherical Caps Under Axisymmetric Load", *AIAA Journal*, Vol. 8, No. 4, pp. 686-692, April 1970.
53. Flugge, W., "Die Stabilität der Kreiszyllinderschale, *Ing. Arch.* Vol. 3, pp. 463-506, 1932.
54. Galletly, G.D., Kyner, W.T., Moller, C.E., Numerical Methods and Bending of Elliptical Shells. *Journal of the Society of Industrial and Applied Mathematics*, 9, 489-513, (1961).
55. Galletly, G.D., Aylward, R.W. and Bushnell, D., "An Experimental and Theoretical Investigation of Elastic and Elastic-Plastic Asymmetric Buckling of Cylinder-Cone Combinations Subjected to Uniform External Pressure", *Ingenieur- Archiv* 43, pp. 345-358, 1974.

56. Galletly, G.D. and Blachut, J., "Elastic buckling of internally pressurized cylinder-bulkhead combinations" Proc Instn Engrs © IMechE Vol. 201 No. C4, pp. 259-262, 1987.
57. Galletly, G.D., "Buckling of Shallow Dished Ends Under External Pressure- A Caveat", Proc. Instn. Mech. Engrs., Vol. 201, No. C5, pp. 373-378, 1987.
58. Galletly, G.D. and Blachut, J., "Buckling Design of Imperfect Welded Hemispherical Shells Subjected to External Pressure", Proc. Inst. Mech. Engrs. Vol. 205, Part C: Journal of Mechanical Engineering Science, pp. 175-187, 1991.
59. Goncalves, P.B. and Croll, J.G.A., "Axisymmetric Buckling of Pressure Loaded Spherical Caps", ASCE Journal of Structural Engineering, Vol. 118, No. 4, pp. 970-985, April 1992.
60. Grigoliuk, E.I., On the Instability with Large Deflections of a Closed Laminated Conical Shell Subject to Uniform Normal Surface Pressure. Inzb, Sbornik, Akad. Nauk SSSR 22, 111-119, (1955).
61. Haque, Md. Monzurul, Axisymmetric Buckling of Ellipsoidal Shells Under External Pressure. M.Sc. Engg. Thesis, Bangladesh University of Engineering and Technology, Dhaka, Bangladesh, (1984).
62. Hoff, N.J., "The Perplexing Behavior of Thin Cylindrical Shells in Axial Compression, Israel J. Technol., Vol. 4, pp. 1-28, 1966.
63. Hoff, N.J., "Thin Shells in Aerospace Structures", Astronautics and Aeronautics, Vol. 5, No. 2, pp. 26-45, Feb. 1967.
64. Holston, A., Jr., Approximate Analytical Solution of the Finite Difference Equations for a Shallow Spherical Shell. Journal of Applied Mechanics. 34, 65-72, (1967).
65. Huang, N.C., Unsymmetrical Buckling of Thin Shallow Spherical Shells, *J. Appl. Mech.*, Series E, No. 3, (1964).
66. Hubner, W., Deformation and Spannungen bei Tellerfedern. Konstruktion, 34, 387-392, (1982).
67. Hubner, W. and Emerling, F.A., Axisymmetrische grobe Deformation einer Elastischen Kegelschale. Zeitschrift Fuer Angewandte Mathematik und Mechanik, 62, 408-411, (1982).
68. Hutchinson, J.W., "Imperfection Sensitivity of Externally Pressurized Spherical Shells", *J. appl. Mech.*, Vol. 34, pp. 49-55, 1967
69. Hyman, B.I. and Healey, J.J., "Buckling of Prolate Spherical Shells Under Hydrostatic Pressure", *AIAA Journal*, Vol. 5, No. 8, pp. 1469- 1477, Aug. 1967.

70. Jerath, S. and Ghosh, A.K., "Buckling of Cylindrical Shells Under the Action of Nonuniform External Pressure", *Computers and Structures*, Vol. 25, No. 4, pp. 607-614, 1987.
71. Kalnins, A., Analysis of Shells of Revolution Subject to Symmetrical and Nonsymmetrical Loads. *Journal of Applied Mechanics*, 31, 467-478, (1954).
72. Kalnins, A., and Lestingi, J.E., On Nonlinear Analysis of Elastic Shells of Revolution. *J. Appl. Mech.*, 34, 59-64,(1967).
73. Kalnins, A. and Biricikoglu, V., "On the Stability Analysis of Imperfect Spherical Shells", *ASME Journal of Appl. Mech.*, Vol. 37, No. 3, pp. 629-634, Sept. 1970.
74. Kaplan, A., Fung, Y.C., A Nonlinear Theory for Bending and Buckling of Thin Elastic Shallow Spherical Shells. NACA TN 3212, (1954).
75. Kaplan, A., "Buckling of Spherical Shells", from *Thin Shell Structures, Theory, Experiment and Design*, Y.C. Fung and E.E. Eecler (eds.), Prentice-Hall, Inc., Englewood Cliffs, N.J., pp. 248-288, 1974.
76. Kempiski, M.H., Taber, L.A. and Wing-Chen Su, Large Elastic Deformation Results. *Journal of Applied Mechanics*, 55, 629-632, (1988).
77. Kendrick, S., The Buckling Under External Pressure of Circular Cylindrical Shells with Evenly Spaced, Equal Strength, Circular Ring Frames. Part III, Naval Construction Research Establishment, Great Britain, Rep. N. 244, (1953).
78. Khan, M.R. and Uddin, Md.W., "The stability of conical end caps with spherical tips as end closures for pressure vessels" *Int. J. Pres. Ves. & Piping*, 64, pp. 11-16, 1995.
79. Khan, M.R., and Uddin, M.W., Instability of Cup-Cylinder Compound Shell Under Uniform External Pressure, *Journal of Ship Research*. 39, No. 2 pp.160-165 (1995)
80. Khat, N.S., "Buckling and Post-Buckling Behavior of Composite Cylindrical Shells Under Axial Compression", *AIAA Journal*, Vol. 8, No. 2, pp. 229-235, Feb. 1970.
81. Kloppel, K. and Jungbluth, O., "Der Stahlbau", Vol. 22, p. 121, 1953.
82. Kwok, S.K., An Improved CFD Method for Arbitrary Mesh Systems. *Comp. & Struct.*, 18, 719-731, (1984).
83. Kwok, S.K., Numerical Computations of Tensor Quantities on a Curved Surface by the CFD Method. *Comp. & Struct.*, 18, 1087-1097 (1984).
84. Kwok, S.K., Linear and Nonlinear Analysis of General Thin Shells Using a Curvilinear Finite Difference Energy Approach. Ph.D. Thesis, Univ. of Western Australia, Medlands, Australia (1984).

85. Kwok, S.K., Geometrically Nonlinear Analysis of General Thin Shells Using a Curvilinear Finite Difference Energy Approach. *Comp. & Struct.*, 20, 683-697, (1985).
86. Kyriakides, S., "Propagating Buckles in Long Confined Cylindrical Shells", *Int. J. of Solid Structures*, Vol. 22, No. 12, pp. 1579-1597, 1986.
87. Lackman, L. and Penzien, J., "Buckling of Circular Cones Under Axial Compression", *ASME Journal of Applied Mechanics*, Vol. 27, No. 3, pp. 458-460, Sept. 1960.
88. Lagrange, J.L., *Mecanique Analytique*, Courcier, Paris, (1788).
89. Leonard, R.W., *Nonlinear First Approximation Thin Shells and Membrane Theory*. Thesis, Virginia Polytechnic Institute, June, (1961).
90. Levy, R. and Spillers, W.R., "Optimal Design for Axisymmetric Cylindrical Shell Buckling", *ASCE Journal of Engineering Mechanics*, Vol. 115, No. 8, pp. 1683-1690, Aug. 1989.
91. Liapunov, A., *Probleme General de la Stabilite du Mouvement*, Kharkov, 1982. French Translation in *Ann. Fac. Sci. Univ. Toulouse*, 9, 1907; Reproduced in *Ann. Math. Studies*, 17, Princeton Univ. Press, Princeton, N.J., (1949).
92. Lohmann, W., *Beitrag Zur Integration der Reissner-Meissnerschen Schalengleichung fur Behalter unter Konstantem Innerdruck*. *Ingenieur Archiv*, 6, 338-346, (1935).
93. Loo, T.C. and Evan-Iwanonski, R.M., "Interaction of Critical Pressures and Critical Concentrated Loads Acting on Shallow Spherical Shells", *ASME Journal of Appl. Mech.*, Vol. 33, No. 3, Series E, pp. 612-616, Sept. 1966.
94. Lundquist, E.E., *Strength Tests of Thin-Walled Duraluminium Cylinders in Compression* NACA Rep. 473, 1933.
95. MacCaldev, P.B. and Matthiesen, R.B., "Combination Torsion and Axial Compression Tests of Conical Shells", *AIAA Journal*, Vol. 5, No. 2, pp. 305-309, Feb. 1967.
96. Maewal, A. and Nachbar, W., "Stable Post-Buckling Equilibria of Axially compressed, Elastic Circular Cylindrical Shells: A Finite Element Analysis and Comparison with Experiments", *ASME Journal of Applied Mechanics*, vol. 44, No. 3, pp. 475-481, Sept. 1977.
97. Mamalis, A.G., Manolakos, D.E., Viegelaahn, G.L., Vaxevanidis, N.M. and Johnson, W., "On the inextensional axial collapse of thin PVC conical shells" *Int. J. Mech. Sci.*, Vol. 28, No. 5, pp. 323-335, 1986.
98. Mansfield, E.H., *The Bending and Stretching of Plates*. The Macmillan Company, New York, 1964.

99. March, H.W. and Kuenzi, E.W., Buckling of Cylinders of Sandwich Construction in Axial Compression. For Prod. Lab., U.S. Dept. Agric., Bull. No. 1830, 1952, AMR 6, Rev. 811, (1953).
100. Marguerre, K., Zur Theorie der Gekrummten Platte Grosser Formanderung. Proc. of Fifth International Congress of Appl. Mech., wiley and Sons, 1938, pp. 93-101.
101. McCoy, J.C., An Experimental Investigation of the General Instability of Ring stiffened, Unpressurized, Thin Walled Cylinders under Axial compression. California Institute of Technology, Ph.D. Thesis., (1958).
102. Milne, W.E., Numerical Solutions of Differential Equations. Jhon Willey and Sons Inc., p. 49, (1962).
103. Mitroperskii, Yu.A., Problem of the Asymptotic Theory of Nonstationary Vibration. Israel Program for Scientific Translations, Jerusalem, (1965).
104. Mondkar, D. P. and Pawell, G. H., ANSR, A General Purpose Computer Program for Analysis of Nonlinear Structural Response, *4th SMiRT Conf., Paper M1/4*, San Francisco (1977).
105. Mushtari, Kh.M., Some Generalization of the Theory of Thin Shells with Application to the Stability of Elastic Equilibrium (in Russian). *Izvestiia fiz.-mat ob-va pri kazan unte*, 11, p.71-150, (1938).
106. Mushtari, Kh.M. and Galimov, K.Z., Nonlinear Theory of Thin Elastic Shells. Israel Program for Scientific Translation, (1961).
107. Nash, W.A., Cooley, I.D., Large Deflection of a Clamped Elliptical Plate Subjected to Uniform Pressure. *Journal of Applied Mechanics*, vol. 26, Series E, No. 2, June, (1959).
108. Nayfeh, A.H., Introduction to Perturbation Techniques. John Willey and Sons, New York, 1981.
109. New, J.C. and Spring, S.M., "A Nondestructive Differential-Pressure Test for Thin Shells" *J. Appl. Mech.* Vol. 75, March 1953, pp. 48-52.
110. Novozhilov, V.V., Theory of Thin Shells. P. Noordhoff Ltd., 1959.
111. Pansford, H.T., The Effect of Stiffeners on the Buckling of Cylinders With Moderate Wall Thickness. California Institute of Technology, Ph.D. Thesis, (1953).
112. Pedersen, P.T. and Jensen, J.J., "Buckling of Spherical Cargo Tanks for Liquid Natural Gas", *The Royal Institution of Naval Architects*, Vol. 5, 1975.
113. Pegg. N.G., An Investigation of Dynamic Pulse Buckling of Thick Rings, *Trans. ASME*, September, Vol.59/615 (1992)

114. Penning, F.A., "Experimental Buckling Modes of Clamped Shallow Shells Under Concentrated Load", ASME Journal of Applied Mechanics, Vol. 33, No. 2, pp. 297-304, June 1966.
115. Peter F. Jordan, Stiffness of Thin Pressurized Shells of Revolution. AIAA Journal, 3, (1965).
116. Pipes, L.A., Solution of Nonlinear Differential Equations by the Reversion Method. J. Appl. Physic., 24, 180-186, (1953).
117. Poincare, H., Sur l'Equilibre d'Une Masse Fluide An'Imme d'Un Mouvement de Rotation, Acta Math., 7, 259 (1885).
118. Radkowski, P.P., Buckling of Thin Single and Multi-layer Conical and Cylindrical Shells with Rotationally Symmetric Stresses. AVCO Report RAD-TR-2-57-32, (1957).
119. Rahman, N.M. Anisur, Axisymmetric Buckling of Imperfect Ellipsoidal Shells Under External Pressure. M.Sc. Engg. Thesis, Bangladesh University of Engineering and Technology, Dhaka, Bangladesh, (1986).
120. Rahman, M.A., "*Stability and stress analysis of parabolic pipe-reducers*" M.Sc. Eng. Thesis, BUET, 1994.
121. Rajaiah, K. and Kumar, R.R., "Stress Around Circular, Square and Optimized Holes in Circular Cylindrical Shells Under Torsion", Int. Journal of Solids and Structures, Vol. 21, No. 2, pp. 177-185, 1985.
122. Raville, M.E., Buckling of Sandwich Cylinders of Finite Length Under Uniform External Lateral Pressure. For Prod. Lab., U.S. Dept. Agric., Bull. No. 1844-B 1955; AMR 9 (1956) Rev. 719.
123. Reddy, J.N. and K. Chandrashekhara, Nonlinear Analysis of Laminated Shells Including Transverse Shear. AIAA Journal, 23, (1985).
124. Reiss, E.L., Greenberg, H.J., Kelley, H.B., Nonlinear Deflections of Shallow Spherical Shells Under External Pressure. J. Aero. Sci., Series 24, 1951, pp. 533-543.
125. Reiss, Edward L., Axially Symmetric Buckling of Shallow Spherical Shells Under External Pressure. Journal of Applied Mechanics, 25, 556-560, (1958).
126. Reissner, E., On the Theory of Thin Elastic Shells, H. Reissner Anniversary Volume, J. W. Edwards, Ann Arbor, Michigan. 231 (1949).
127. Reissner, E., On Axisymmetric Deformations of Thin Shells of Revolution. Proc. Symposia Appl. Math., Vol. 3, McGraw-Hill, pp. 27-52, 1950.

128. Ross, C.T.F., Design of Dome Ends to Withstand Uniform External Pressure. *Journal of Ship Research*, 31, No. 2, 139 (1987)
129. Ross, C.T.F., A Novel Submarine Pressure Hull Design. *Journal of Ship Research*, 31, No. 3, 186 (1987)
130. Ross, C.T.F. and Palmer, A., "General Instability of Swedge-Stiffened Circular Cylinders Under Uniform External Pressure" *Journal of Ship Research*, Vol.37, No. 1, March 1993, pp. 77-85.
131. Rossettos, J.N., Sanders, J.L., Jr., Torodial Shells Under Internal Pressure in Transitive Range. *AIAA Journal*, 3, 1901-1909 (1965).
132. Rotter, J.M., "Load Collapse of Axially Compressed Pressurized Thin Steel Cylinders", *ASCE Journal of Structural Engineering*, Vol. 116, No. 7, pp. 1955-1970, July 1990.
133. Rotter, J.M. and Zhaug, Q., "Elastic Buckling of Imperfect Cylinders Containing Granular Solids", *ASCE journal of Struct. Engg.*, Vol. 116, No. 8, pp. 2253-2271, Aug. 1990
134. Salerno, V.L., Levine, B., General Stability of Reinforced Shells Under Hydrostatic Pressure. *Polytech. Inst. Brooklyn, PIBAL Rep. No. 189*, 1951.
135. Samuelson, L.A., "Creep Buckling of a Circular Shell", *AIAA Journal*, Vol. 7, No. 1, pp. 42-49, Jan. 1969.
136. Sanders, J.L., Jr., Nonlinear Theories for Thin Shells. *Q. Appl. Math.*, 21, 21-36, (1963).
137. Schmidt, R. and Reddy, J.N., A Refined Small Strain and Moderate Rotation Theory of Elastic Anisotropic Shells. *Journal of Applied Mechanics*, 55, 611-617, (1988).
138. Schneider, M.H.Jr., Snell, R.F., Tracy, J.J. and Power, D.R., "Buckling and Vibration of Externally Pressurized Conical Shells with Continuous and Discontinuous Rings" *AAIA Journal*, Vol. 29, No. 9, September 1991, pp. 1515-1522.
139. Schnel, Von W., Zur Stabilität Dünnwandiger Langsgedruelter Kreiszyklinderschalen bei Zusatzlichen Innerdruck. *Symposium on the Theory of Thin Elastic Shells*, I.U.T.A.M., Delft, 1959.
140. Schroeder, F.J. and Kusterer, E.T., "An Experimental Determination of the Stability of Conical Shells" *J. of Appl. Mech.*, *Trans. of the ASME*, March 1963, pp. 144-146.
141. Seah, L. K. and Rhodes, J., Simplified Buckling Analysis of Plates with Compound Edge Stiffeners, *ASCE Journal of Engineering Mechanics*, Vol. 119 No. 1, p-19 (1993)

142. Seide, P., "Axisymmetric Buckling of Circular Cones Under Axial Compression", *ASME Journal of Applied Mechanics*, Vol. 23, No. 4, pp. 625-628, Dec. 1956.
143. Seide, P., "On the Buckling of Truncated Conical Shells in Torsion", *ASME Journal of Appl. Mech.*, Vol. 29, No. 2, Series E, pp. 321-328, June 1962.
144. Sepetoski, W.K., Pearson, C.E., Dingwell, I.W., and Adkins, A.W., A Digital computer Program for the General Axially symmetric Thin Shell Problem. *Journal of Applied Mechanics*, 29, 655-661, (1962).
145. Shen-Hui and Williams, F.W. , Postbuckling Analysis of Stiffened Laminated Box Columns., *ASCE Journal of Engineering Mechanics*, Vol 119 No. 1, p-39 (1993)
146. Simitzes, G.T., Shaw, D. and Sheinman, I., "Stability of Imperfect Laminated Cylinders: A comparison Between Theory and Experiment", *AIAA Journal*, Vol. 23, No. 7, pp. 1086-1092, July 1985.
147. Singer, J. and Bendavid, D., "Buckling of Electroformed Conical Shells Under Hydrostatic Pressure", *AIAA Journal*, Vol. 6, No. 12, pp. 2332-2338, Dec. 1968.
148. Singer, J., Arbocz, J. and babcock Jr. C.D., "Buckling of Imperfect Stiffened Cylindrical Shells Under Axial Compression", *AIAA Journal*, Vol. 9, No. 1, pp. 68-75, jan. 1971.
149. Singer, J., "Buckling Experiments on Shells- A Review of Recent Developments", *Solid Mech. Archives*, Vol. 7, No. 3, pp. 213-313, 1982.
150. Soong, T.C., "Buckling of Cylindrical Shells with Eccentric Spiral Type Stiffness", *AIAA Journal*, Vol. 7, No. 1, pp. 65-72, Jan. 1969.
151. Soong, T.C., "Buckling of Cylindrical Shells with Intermittently Attached Stiffness", *AIAA Journal*, Vol. 8, No. 5, pp. 928-936, May 1970.
152. Soper, W.G., Large Deflection of Stiffened Plates. *Journal of Applied Mechanics*, 25, 444-448, (1958).
153. Steele, Charles R. and Kim, Yoon Young , Modified Mixed Variational Principle and The State-Vector Equation for Elastic Bodies and Shells of Revolution. *Trans. ASME*, Vol.59/587 (1992).
154. Stein, M., "Some Recent Advances in the Investigation of Shell Buckling", *AIAA Journal*, Vol. 6, No. 12, pp. 2339-2345, Dec. 1968.
155. Stricklin, J.A., Haisler, W.E., and Von Reisseman, W.A., Geometrically Nonlinear Structural Analysis by Direct Stiffness Method. *J. Structural Div., ASCE*, 97, 2299-2314, (1971).

156. Svriski, I.V., Methods of the Type of Bubnov-Galerkin and Successive Approximations. Nakua, Moscow, 1968 (in Russian).
157. Synge, J.L., and Chien, W.Z., The Intrinsic Theory of Thin Shells and Plates. Th. Von Karman Anniverssry Volume, Cal. Inst. of Tech., 1941, p. 103.
158. Tabler, L.A., Large Elastic Deformation of Shear Deformable Shells of Revolution: Theory and Analysis. Trans. of ASME, 54, 578-584, (1987).
159. TAKEZONO, Shigeo, TAO, Katsumi and Tani, Kiyoyuki, Elasto/Visco Plastic Deformation of Multi Layered Moderately Thick Shells of Revolution, *JSME International Journal Series I*, Vol 34, 1 (1991).
160. Tani, J. and Yamaki, W., "Buckling of Truncated Conical Shells Under Axial Compression", *AIAA Journal*, Vol. 8, No. 3, pp. 568-571, March 1970.
161. Tani, J., "Influence of Deformations Prior to Instability on the Dynamic Instability of Conical Shells Under Periodic Axial Load", *ASME Journal of Applied Mechanics*, Vol. 43, No. 1, pp. 87-91, March 1976.
162. Tani, J., "Buckling of Truncated Conical Shells Under Combined Axial Load, Pressure and Heating", *ASME Journal of Applied Mechanics*, Vol. 52, No. 2, pp. 402-408, June 1985.
163. Teng, J.G. and Rotter, J.M., Elastic-Plastic Large Deflection Analysis of Axisymmetric Shells. *Comp. & Struct.*, 31, 211-233, (1989).
164. Teng, J.G. and Rotter, J.M., "Collapse behavior and Strength of Steel Silo Transition Junctions, Part I: Collapse Mechanics", *ASCE Journal of Structural Engineering*, Vol. 117, No. 12, pp. 3587-3604, Dec. 1991.
165. Tennyson, R.C., "Buckling Modes of Circular Cylindrical Shells under Axial Compression" *AAIA Journal*, Vol. 7, No. 8, August 1969, pp. 1481-1487.
166. Thompson, J. M. T. and Hunt, G. W., A General theory of Elastic Stability, *Jhon Wiley and Sons*, London, U.K. (1973).
167. Thruston, G.A., "A Numerical Solution of the Nonlinear Equations for Axisymmetric Bending of Shallow Spherical Shells", *ASME Journal of Appl. Mech.*, Vol. 28, No. 4, Series E, pp. 557-562, Dec. 1961.
168. Thurston, G. A., Newton's Method Applied to Problems in Nonlinear Mechanics. *Journal of Applied Mechanics*, June 1965, pp. 383-388.
169. Thurston, G.A. and Penning, F.A., "Effect of Axisymmetric Imperfections on the Buckling of Spherical Caps Under Uniform Pressure", *AIAA Journal*, Vol. 4, No. 2, pp. 319-327, Feb. 1966.

170. Timoshenko, S.P. and Gere, J.M., "Theory of Elastic Stability", 2d. ed., McGraw-Hill, New York, 1961.
171. Uddin, Md. W., Large Deflection Analysis of Composite Shells of Revolution, Ph. D. Thesis, *Carleton University*, Canada (1969).
172. Uddin, Md. W., A Computer Program for Nonlinear Analysis of Pressure Vessels, *Int. J. Press. Ves. & Piping* **22** (1986) 271-309.
173. Uddin, Md. W., Large Deformation Analysis of Ellipsoidal Head Pressure Vessels. *Comp. & Struct.*, **23**, 487-495, (1986).
174. Uddin, Md. W., Large Deformation Analysis of Plate-end Pressure Vessels., *Int. J. Pres. Ves. & Piping*, **29**, 47-65, (1987).
175. Uddin, Md. W., Buckling of General Spherical Shells Under External Pressure. *Int. J. Mech. Sci.*, **29**, 469-481, (1987).
176. Uddin, Md. W. and Haque, Md. M., Instability of Semi-ellipsoidal Shells, *Int. J. Pres. Ves. & Piping*, **58**, pp. 47-65, (1994).
177. Uddin, Md. W. and Haque, Md. M., Comments on the Paper 'Instability of Semi-ellipsoidal Shells', Letter to the Editor, *Int. J. Pres. Ves. and Piping*, **64**, pp. 83-84, (1995).
178. Updike, D.P. and Kalnins, A., "Axisymmetric Behavior of a Elastic Spherical Shell Compressed Between Rigid Plates", *ASME Journal of Appl. Mech.*, Vol. 37, No. 3, pp. 635-640, Sept. 1970.
179. Van Dyke, M., *Perturbation Methods in Fluid Mechanics*. Parabolic Press, Stanford, Calif, 1975.
180. Von Karman, T., *Festigkeit Lehre in Maschinenbau*. Math. Niss., Vol. IV/4, Teubner, Leipzig, pp. 311-385, (1910).
181. Von Karman, T. and Kerr, A.D., Instability of Spherical Shells Subjected to External Pressure. *topics in Applied Mechanics*, Memorial Volume to the Late Professor E. Schwerin, pp. 1-22, (1965).
182. von Mises, R., *Stodola-Festschrift.*, Zurich, 1929, 418.
183. Wang, G.T. and De Sant, D.F., Buckling of Sandwich Cylinders Under Axial Compression, Bending and Combined Loads. NYU Report to Office of Naval Research, Contr. No. N6-onr-279, 1953.
184. Wang, L.R.L., "Boundary Disturbance and Pressure Rate on the Buckling of Spherical Caps", *AIAA Journal*, Vol 6, No. 11, pp. 2192-2193, Nov. 1968.

185. Wang, J.T.S. and Lin, Y.J., "Stability of Discretely Stringer Stiffened Cylindrical Shells", AIAA Journal, Vol. 11, No. 1, pp. 810-814, June 1973.
186. Weingarten, V.I., "Elastic Stability of Thin-Walled Cylindrical and Conical Shells under Combined External Pressure and Axial Compression" AIAA Journal, Vol. 3, No. 5, May 1965, pp. 913-920.
187. Wempner, G., A General Theory of Shells and the Complementary Potentials. Journal of Applied Mechanics, 53, 881-885, (1986).
188. Wilson, P.E., Boresi, A.P., Large Deflection of a Clamped Circular Plate Including Effects of Transverse Shear. Journal of Applied Mechanics, 31, 540-541, (1964).
189. Wilson, P.E., Spier, E.E., Numerical Analysis of Large Axisymmetric Deformations of Thin Spherical Shells. AIAA Journal, 3, 1716-1725 (1965).
190. Windenburg, D.F. and Trilling, C., "Collapse by instability of thin cylindrical shells under external pressure" Trans. ASME, 11, 1934, pp.819-825.
191. Wood, J.D., The Flexure of a Uniformly Pressurized Circular Cylindrical Shell. *Journal of Applied Mechanics*, 25, 453-458 (1958).
192. Wu, M.T. and Cheng, S., "Nonlinear Asymmetric Buckling of Truncated Spherical Shells", ASME Journal of Applied Mechanics, Vol. 37, No. 3, pp. 651-660, Sept. 1970.
193. Yao, J.C. and Tenkins, W.C., "Buckling of Elliptic Cylinders under Normal Pressure", AIAA Journal, Vol. 8, No. 1, pp. 22-27, Jan. 1970.
194. Zienkiewicz, O.Z., The Finite Element Method. McGRAW-HILL Book Company (U.K) Limited, 1977.

PROGRAMMING FEATURES

A.1 GENERAL FEATURES

The computer program used in the present investigation is adopted from that of Uddin [160] with necessary modifications to suit the requirements of solving stability problems of composite shells of revolution under uniform external pressure. The program is based on Reissner's non-linear theory of axisymmetric deformation of shells of revolution [120]. The multisegment method of solution, developed by Kalnins and Lestingi [69], takes care of solving the governing equations and the integration in it is carried out by a predictor-corrector method. The predictor and corrector are given, respectively, by formulas (19.16) and (19.17) of Ref. [97]. To secure the six starting values necessary for the application of this pair of predictor and corrector, the six-point formulas, (19.10-19.14), of Ref. [97] are being used. It should be noted here that all these formulas contain an error of the order of H^7 where H is the distance between two consecutive computational points and, thus, they are highly sophisticated.

In solving the governing equations, the shell meridian is divided into suitable number of segments depending upon the length of the meridian and the thickness ratio, R/h , of the shell. The program first prints out the nondimensional values of the fundamental variables (u , β , w , V , H , M_ξ) based on linear theory which is followed by the print-out of non-linear results at the same value of the loading parameter. From here on, the program will produce non-linear results for increasing loading steps.

The program also prints out the detail results in terms of radial displacement \bar{u} , axial displacement \bar{w} , circumferential moment \bar{M}_θ , meridional moment \bar{M}_ξ , circumferential stress resultant \bar{N}_θ , meridional stress resultant \bar{N}_ξ , circumferential stress at the inner surface $\sigma_{ci}/(PR/h)$, circumferential stress at the outer surface $\sigma_{co}/(PR/h)$, meridional stress at the inner surface $\sigma_{ai}/(PR/h)$, and meridional stress at the outer surface $\sigma_{ao}/(PR/h)$, in that order, columnwise.

A.2 TREATMENT OF BOUNDARY CONDITIONS

Equations (3.153a), written in terms of normalised fundamental variables and in accordance with the statement of Eqns. (3.12c), appear as

$$\begin{bmatrix} 1 & 0 & 0 & 0 & 0 & 0 & u \\ 0 & 1 & 0 & 0 & 0 & 0 & \beta \\ 0 & 0 & 1 & 0 & 0 & 0 & w \\ 0 & 0 & 0 & 1 & 0 & 0 & V \\ 0 & 0 & 0 & 0 & 1 & 0 & H \\ 0 & 0 & 0 & 0 & 0 & 1 & M_\xi \end{bmatrix} = \begin{bmatrix} u \\ \beta \\ w \\ V \\ H \\ M_\xi \end{bmatrix} \quad (\text{A-1})$$

In the matrix Eqns. (A-1), the elements of the column matrix on the left hand side remain in the same order, whereas, those on the right hand side should be arranged in such a manner that the three prescribed elements at the boundary become the first three elements of this column matrix. According to Eqns. (3.12c), if u is specified at the boundary, the first and the 5th rows of the unit-matrix of (A-1) remain the same, while specification of H at the boundary will require the interchange of these two rows which will interchange u and H in the column matrix on the right hand side. Similarly, if β is specified at the boundary, the second and the last rows remain as they are, and interchanged when M_ξ is specified. Lastly, the third and the fourth rows of the unit-matrix are kept the same or interchanged depending on whether w or V is specified at the boundary. The same operation is carried out for both the boundary points. The transformed unit matrices of (A-1) are then designated by T_1 at the starting boundary and by T_{M+1} at the finishing boundary.

A.3 ON THE USE OF THE PROGRAM

In order to use the program for obtaining solutions of different problems the knowledge of the definitions of input and output variables is essential. Therefore these variables with their definitions are given in the table at the end of Appendix A.

In part A of the program the necessary information required for the solution of a problem is read in. The first READ statement here is for 'CLS', is the nondimensional distance of the top boundary of a shell from its axis. For shells closed at the tip, 'CLS' is zero. The subsequent READ statements are for the initial value of the loading parameter 'EM', the value of incremental step of the loading parameter 'EM1', the number of segments 'M' into which the shell meridian is divided for solution, Poisson ratio of the shell material 'AN', the number of loading steps 'SOB1', radius to thickness ratio 'T', type of shell 'IZ', type of shell segments in case of composite shells 'IG(I)', and the representative values for different shell segments 'CIND(I)'. The value of IZ from 1 to 5 represents different types of shells. IZ=1 stands for cylindrical shell, IZ=2 for spherical shell, IZ=3 for conical shell, IZ=4 for ellipsoidal shell and IZ=5 for composite shell. For composite shell 'IG(I)' and 'CIND(I)' are read from the input data file for each segment of the composite shell. If the value of IG is 1 at any node then the shell element from that node to the next node is a line element and if it is 2 then it is a circular arc element. CIND at any node against IG value of 1 is the nondimensional distance of the line element and against the IG value of 2 is the nondimensional radius of curvature (r_s/R) of the circular arc element. The 'READ' statement for the variable APHH(I) reads angular position of a shell segment with reference to the axis of the shell. The variable X(J,1) reads arbitrary given values of the independent variable for shells other than the composite shells. For composite shells X(J,1) is calculated by the program itself from given data. The initial values of the six fundamental variables are read by the variable X(J,I), (I=2,7), for nodal points J, (J = 1, M+1). The boundary values for any three of the six fundamental variables at the starting boundary are accepted by the variable XX(I,1), where XX(1,1) stands for u or H, XX(2,1) for β or M and XX(3,1) for w or V. In the present analysis for clamped boundary the prescribed boundary conditions are:

$$\begin{aligned} \text{XX}(1,1) &= u = 0.0 \\ \text{XX}(2,1) &= \beta = 0.0 \\ \text{XX}(3,1) &= w = 0.0 \end{aligned}$$

and for hinged boundary, these become

$$\begin{aligned} \text{XX (1,1)} &= u = 0.0 \\ \text{XX (2,1)} &= M = 0.0 \\ \text{XX (3,1)} &= w = 0.0 \end{aligned}$$

The 'READ' statement next to the above statement reads in the three prescribed boundary conditions at the final boundary. For the present analysis, for a shell open at the tip with clamped boundary these three boundary conditions are:

$$\begin{aligned} \text{XY (1,1)} &= u = 0.0 \\ \text{XY (2,1)} &= \beta = 0.0 \\ \text{XY (3,1)} &= w = 0.0 \end{aligned}$$

and for a shell open at the tip with hinged boundary, these are

$$\begin{aligned} \text{XY (1,1)} &= u = 0.0 \\ \text{XY (2,1)} &= M = 0.0 \\ \text{XY (3,1)} &= w = 0.0 \end{aligned}$$

In case of closed boundary at the tip, the final boundary XY(I,1) become

$$\begin{aligned} \text{XY (1,1)} &= u = 0.0 \\ \text{XY (2,1)} &= \beta = 0.0 \\ \text{XY (3,1)} &= V = 0.0 \end{aligned}$$

The values of the boundary condition indicators at the starting are read in by the variables 'IS1', 'IS2', 'IS3'. The appropriate values of the indicators 'IS1', 'IS2', and 'IS3' are given in the following table:

Specified quantity	Indicator and its value
u	IS1 = 0
β	IS2 = 0
w	IS3 = 0
V	IS3 = 1
H	IS1 = 1
M_{ξ}	IS2 = 1

The values of the boundary condition indicators at the final boundary are read in by the variables 'IF1', 'IF2', 'IF3'. Their appropriate value are given in the above table where the quantities 'IS1', 'IS2', and 'IS3' should be replaced by 'IF1', 'IF2', and 'IF3', respectively. The variable 'MX(I)' reads segment type of a composite shell similar to 'IG(I)', and 'MXN(I)' reads the location of junction of dissimilar segment in a composite shell. As for example if there are junctions at node 3 and node 5 then $MXN(3)=3$ and $MXN(5)=5$ and the rest MXN are zero.

The variables 'NNN1' and 'NNN2' read the range of values of circumferential lobes for the determination of the stability determinant in case of asymmetric buckling. Asymmetric analysis of shells need specification of four fundamental variables at each boundary of a shell and these are read in by the variables 'ITP' and 'IBT' at the final boundary and starting boundary, respectively. $ITP=IBT=1.0$ stands for clamped boundary and $ITP=IBT=2.0$ for hinged boundary.

In the initialisation block of part A of the program, certain quantities are initialised and certain fixed parameters of the shell are calculated. Part B of the program deals with the problem of adjusting the given boundary conditions to the solutions of the matrix equations. Part C of the program concerns with the calculation of normalised constants involving shell parameters, material constants, and loading. Under part D of the program the output of the results is handled. The remaining portion of the program deals with the integration of different systems of differential equations and the solution of matrix equations.

A.4 OUTPUT OF THE PROGRAM

The first output is the given initial nodal values of the independent variable ξ and the six fundamental variables u , β , w , V , H and M_ξ , in their written order, columnwise, and in tabular form. The first output is accompanied the various input parameters and indices. The second output gives the value of number of pass, residue, that is, the sum of the differences of the absolute values of the fundamental variables at the nodal points of the two recent consecutive passes, and the current value of the normalised load.

The first output is then repeated for solution based on linear theory. The next output presents the details of the solution based on the linear theory. Here the following quantities are printed out in tabular form and in the order of ξ , u , w , M_θ , M_ξ , N_θ , N_ξ , $\sigma_{ci}/(PR/h)$, $\sigma_{co}/(PR/h)$, $\sigma_{ai}/(PR/h)$, $\sigma_{ao}/(PR/h)$ columnwise. For each segment, these quantities are printed out at six equidistant points. This can be changed to twenty-one or eleven points by simply changing the increment of the loop parameter of part D of the program that handles the output of results. With the results of first linear output, the linear solution is repeated once again to get better solution. After the print-out of the second linear solution, there will be repetition of the second and first out-put (now based on non-linear theory) for a number of times until the solution converges. When convergence is attained the details of the non-linear solution will be printed out. The solution at the nodal points are printed out twice, first, based on the initial value integration and second, based on the solution of matrix equations, to check the accuracy of the results. From this point onward the non-linear solutions will be repeatedly printed out for increasing loadings.

The output files 'AX', 'RD' and 'SHAPE' are opened additionally for the convenience of plotting the load-deflection curves and the deformed shell meridian. The first column of the output file 'AX' prints out the absolute value of the loading parameter, (P/E) , while the rest of the columns print out the axial displacements, (wh/R^2) , for the nodal points. Similarly, the output file, 'RD', prints out the radial displacements, (uh/R^2) . In the output file, 'SHAPE', the first and the third columns print out the points along the shell axis while the second and the fourth columns print out the corresponding points along the shell meridian, before and after deformation, for the increasing values of the loading parameter.

A.5 TABLE OF INPUT-OUTPUT VARIABLES OF THE PROGRAM

Variable	Definition
CLS	Meridian length of a shell at the open tip
EM	P/E, Normalised load
EM1	Increasing step of EM
SOB1	Number of desired loading step
M	Number of segments
APHH(I)	Meridional angle at the nodal point I
RC	Constant, $\bar{R} = \xi_c/R$
AN	Poisson's ratio, ν
TK	R/h, thickness ratio
IG(I)	Segment type in a composite shell
CIND(I)	Segment length or radius of curvature of segments
X(1,I)	$\bar{\xi}$ at the nodal point I
X(2,I)	\bar{u} at the nodal point I
X(3,I)	$\bar{\beta}$ at the nodal point I
X(4,I)	\bar{w} at the nodal point I
X(5,I)	\bar{V} at the nodal point I
X(6,I)	\bar{H} at the nodal point I
X(7,I)	\bar{M}_ξ at the nodal point I
XX(1,I)	value of \bar{u} or \bar{H} at the starting boundary
XX(2,I)	value of $\bar{\beta}$ or \bar{M}_ξ at the starting boundary
XX(3,I)	value of \bar{w} or \bar{V} at the starting boundary
XY(1,I)	value of \bar{u} or \bar{H} at the finishing boundary
XY(2,I)	value of $\bar{\beta}$ or \bar{M}_ξ at the finishing boundary
XY(3,I)	value of \bar{w} or \bar{V} at the finishing boundary

IS1,IS2,IS3	indicators of boundary conditions at the starting boundary
IF1,IF2,IF3	indicators of boundary conditions at the finishing boundary
IBT	indicator of boundary condition at the starting boundary for asymmetric analysis
ITP	indicator of boundary condition at the final boundary for asymmetric analysis
NP	Number of Pass; NP = 1 indicates linear solution
T22(N)*	$\bar{N}_\xi = N_\xi / (PR)$
T7(N)	$\bar{N}_\theta = N_\theta / (PR)$
T9(N)	$\bar{M}_\theta = M_\theta / (PRh)$
Y(1,N)	$\bar{\xi} = \xi / \xi_e$
Y(2,N)	$\bar{u} = uEh / (PR^2)$
Y(3,N)	$\bar{\beta} = \beta$
Y(4,N)	$\bar{w} = wEh / (PR^2)$
Y(5,N)	$\bar{V} = V / (PR)$
Y(6,N)	$\bar{H} = H / (PR)$
Y(7,N)	$\bar{M}_\xi = M_\xi / (PRh)$
ST1	$\bar{\sigma}_{ci} = \sigma_{ci} / E$, normalised circumferential stress at the inner surface of the shell
ST2	$\bar{\sigma}_{co} = \sigma_{co} / E$, normalised circumferential stress at the outer surface of the shell
ST3	$\bar{\sigma}_{ai} = \sigma_{ai} / E$, normalised axial stress at the inner surface
ST4	$\bar{\sigma}_{ao} = \sigma_{ao} / E$, normalised axial stress at the outer surface

* N denotes points in a segment at which the variables are evaluated.

APPENDIX - B

PROGRAM FOR SHELL ANALYSIS

```

* -----
C  IMPLICIT REAL*8 (A-H,O-Z)
   REAL*8 ZXX(31),ZZXX(21),ZZNN(21),YYN(21),PPH(21),ROO(21)
   REAL*8 X(31,7),Y(7,21),Z(7,6),Y1(7,21),Y2(31,3),Y3(31,3),F(7,21)
   REAL*8 FK(21)
   REAL*8 H(30),IG(30),APHH(31),TK(30),X7(31,7),AK(4),T22(21),Z2(3,1)
   REAL*8 AY(3,1),BY(3,1),APH(30)
   REAL*8 TS1(3,3),TS2(3,3),TS3(3,3),TS4(3,3),TF1(3,3),TF2(3,3)
   REAL*8 TF3(3,3),TF4(3,3),A14(3,1),A15(3,1),A16(3,1),A17(3,1)
   REAL*8 A18(3,3),C(31,3,3),A(31,3),E(31,3,3),B(31,3),X1(3,1)
   REAL*8 X2(3,1),C1(21),C2(21),T7(21),T9(21),T10(21),R(21),PH(21)
   REAL*8 RO(21),Z1(3,1),A1(3,3),A2(3,3),A3(3,3),A4(3,3),A6(3,3)
   REAL*8 A7(3,3),A8(3,3),A9(3,1),A10(3,1),A11(3,1),A12(3,1)
   REAL*8 XX(3,1),XY(3,1),U(6,6),XYX4(31),XYX2(31)
   REAL*8 PB2,RC,AKL,EL,FL,DR,TO,TL,ZZ,FF,P3,DP,PHI,ALP,T3,T,T21,TM
   REAL*8 CIND(30),S(30)
   REAL*8 SUMM(30),FF1,FF2,FF3,FF4,FF5,FF6,FF7,FF8,FF9
   REAL*8 Y11(21),Y33(21),HS(30),DXD1(30)
   REAL*8 EM,EM1,DXD,XNN
   REAL*8 P11(4,4),P22(4,4),P33(4,4),P44(4,4),P55(4,4),
+   XA1(4,4),XB1(4,4),XC1(4,4),XD1(4,4)
   REAL*8 XA(4,4),XB(4,4),XC(4,4),SS1
   REAL*8 AB1(4,4),AC1(4,4),AD1(4,4)
   REAL*8 BB1(4,4),BC1(4,4),BD1(4,4)
   REAL*8 CB1(4,4),CC1(4,4),CD1(4,4)
   REAL*8 DB1(4,4),DC1(4,4),DD1(4,4)
   REAL*8 EB1(4,4),EC1(4,4),ED1(4,4)
   DIMENSION MX(30),MXN(30)
   CHARACTER INP * 9,OUTP * 9,OUTP2 * 9,OUTP3 * 9,OUTP4 * 9
   PRINT '(1X,A,$)', 'ENTER NAME OF THE INPUT DATA FILE: '
   READ*,INP
   PRINT '(1X,A,$)', 'ENTER NAME OF THE OUTPUT FILE: '
   READ*,OUTP
   PRINT '(1X,A,$)', 'ENTER NAME OF THE 2ND. OUTPUT FILE: '
   READ*,OUTP2
   PRINT '(1X,A,$)', 'ENTER NAME OF THE 3RD. OUTPUT FILE: '
   READ*,OUTP3
   PRINT '(1X,A,$)', 'ENTER NAME OF THE 4TH. OUTPUT FILE: '
   READ*,OUTP4
   OPEN(1,FILE=INP, STATUS='OLD')
   OPEN(3,FILE=OUTP, STATUS='NEW',RECL=1400)
   OPEN(4,FILE=OUTP2, STATUS='NEW',RECL=1400)
   OPEN(5,FILE=OUTP3, STATUS='NEW',RECL=1400)
   OPEN(7,FILE=OUTP4, STATUS='NEW',RECL=1400)

```

NP=0
IN=1
SOB2=0.
SS=1.
N2=6
N3=3
PB2=1.5707963268

C-----
C===== PART A. (READING IN INFORMATION)=====
C-----

```
READ(I,*)CLS
IF(CLS.EQ.0.0)THEN
  WRITE(3,2200)
  ELSE
  WRITE(3,2201)
  ENDIF
  READ(1,110)EM1,SOB1
  WRITE(3,110)EM1,SOB1
25  READ(1,59)M,IZ
  WRITE(3,59)M,IZ
  IF(IZ-5)515,516,516
516  READ(1,590)(IG(I),I=1,M)
  WRITE(3,590)(IG(I),I=1,M)
  READ(1,110)(CIND(I),I=1,M)
  WRITE(3,110)(CIND(I),I=1,M)
590  FORMAT(30F3.1)
  READ(1,110)(APHH(I),I=1,M+1)
  WRITE(3,110)(APHH(I),I=1,M+1)
2100 FORMAT(31F5.2)
2200 FORMAT('THE TOP IS CLOSE ')
2201 FORMAT('===== OPEN TOP =====')
  SUM=0.0
  DO 100 I=1,M
  IF (IG(I).EQ. 1) THEN
  S(I)=CIND(I)
  ELSE
  S(I)=DABS(CIND(I))*DABS(APHH(I+1)-APHH(I))*PB2/90.0
  ENDIF
  SUM=SUM+S(I)
  SUMM(I)=SUM
100  CONTINUE
  RC=SUMM(M)+CLS
  X(1,1)=1.00
  DO 500 I=1,M
  X(I+1,1)=(SUMM(M)-SUMM(I)+CLS)/RC
500  CONTINUE
  DO 2203 I=1,M
  APH(I)=APHH(I)*PB2/90.0
```

```

2203 CONTINUE
* READ(1,110)RC
  WRITE(3,110)RC
515  READ(1,110)AN,EM,PHI,ALP,ER,XL
  WRITE(3,110)AN,EM,PHI,ALP,ER,XL
  READ(1,1100)(TK(I),I=1,M)
  WRITE(3,1100)(TK(I),I=1,M)
1100 FORMAT(30F7.2)
  MO=M+1
  IF(IZ.LE.4)THEN
    READ(1,41)((X(J,I),I=1,7),J=1,MO)
  ELSE
    DO 1301 I=1,MO
      DO 1301 J=2,7
        X(I,J)=0.0
1301 CONTINUE
  ENDIF
  WRITE(3,41)((X(J,I),I=1,7),J=1,MO)
  READ(1,41)(XX(I,1),I=1,3)
  WRITE(3,41)(XX(I,1),I=1,3)
  READ(1,41)(XY(I,1),I=1,3)
  WRITE(3,41)(XY(I,1),I=1,3)
  READ(1,59)IS1,IS2,IS3
  WRITE(3,59)IS1,IS2,IS3
  READ(1,59)IF1,IF2,IF3
  WRITE(3,59)IF1,IF2,IF3
  READ(1,59)(MX(I),I=1,M)
  WRITE(3,59)(MX(I),I=1,M)
  READ(1,59)(MXN(I),I=1,M)
  WRITE(3,59)(MXN(I),I=1,M)
  READ(1,59) NNN1,NNN2
  WRITE(3,59) NNN1,NNN2
  READ(1,59) ITP,IBT
  WRITE(3,59) ITP,IBT
  READ(1,1100) SINX
  WRITE(3,1100) SINX
  NNN=NNN1

```

```

C =====
C PART B.(TREATMENT OF BOUNDARY CONDITION)
C =====

```

```

DO 21 I=1,N3
DO 21 J=1,N3
TS1(I,J)=0.0
TS2(I,J)=0.0
TS3(I,J)=0.0
TS4(I,J)=0.0
TF4(I,J)=0.0
TF3(I,J)=0.0

```

```

      TF2(I,J)=0.0
21  TF1(I,J)=0.0
      IF (IS1 .EQ. 00) THEN
23  TS1(1,1)=1.0
      TS4(2,2)=1.0
      ELSE
24  TS2(1,2)=1.0
      TS3(2,1)=1.0
      ENDIF
      IF ( IS2 .EQ. 00) THEN
28  TS1(2,2)=1.0
      TS4(3,3)=1.0
      ELSE
29  TS2(2,3)=1.0
      TS3(3,2)=1.0
      ENDIF
      IF (IS3 .EQ. 00) THEN
33  TS1(3,3)=1.0
      TS4(1,1)=1.0
      ELSE
34  TS2(3,1)=1.0
      TS3(1,3)=1.0
      ENDIF
      IF (IF1 .EQ. 00) THEN
36  TF2(1,2)=1.0
      TF3(2,1)=1.0
      ELSE
37  TF1(1,1)=1.0
      TF4(2,2)=1.0
      ENDIF
      IF (IF2 .EQ. 00) THEN
39  TF2(2,3)=1.0
      TF3(3,2)=1.0
      ELSE
40  TF1(2,2)=1.0
      TF4(3,3)=1.0
      ENDIF
      IF (IF3 .EQ. 00) THEN
84  TF2(3,1)=1.0
      TF3(1,3)=1.0
      ELSE
87  TF1(3,3)=1.0
      TF4(1,1)=1.0
      ENDIF
      DO 31 J=1,M
      HS(J)=DABS(X(J+1,1)-X(J,1))*RC
31  H(J)=(X(J+1,1)-X(J,1))*05

```

C =====
C PART C.(CALCULATION OF RC.,FOR PRESSURE VESSELS ONLY)
C =====

```
      GO TO (401,402,403,404,405),IZ
401  RC=PHI/DSIN(PHI)
      GO TO 405
402  RC=1.0
      GO TO 405
403  RC=(1.-XL)/DSIN(ALP)+(PB2-ALP)*XL/DCOS(ALP)
      GO TO 405
404  I=1
      AL=1.
      BL=2.
      AKL=1.-ER**2.
      EL=1.
      CL=1.
406  EL=EL*(AL/BL)**2.
      FL=EL*AKL**I/AL
      CL=CL-FL
      AL=AL+2.
      BL=BL+2.
      I=I+1
      IF(DABS(FL)-.1E-08)407,407,406
407  RC=PB2*CL
405  CONTINUE
      IF(1Z-5)521,522,522
521  DP=PB2
      GO TO 523
522  DP=APH(1)
523  DR=1./RC
      ZZXX(1)=0.0
26   CONTINUE
      DO 175 IS=1,4
      DO 175 IT=1,4
      P11(IS,IT)=0.0
      P22(IS,IT)=0.0
      P33(IS,IT)=0.0
      P44(IS,IT)=0.0
      P55(IS,IT)=0.0
      XA(IS,IT)=0.0
      XB(IS,IT)=0.0
      XC(IS,IT)=0.0
      XA1(IS,IT)=0.0
      XB1(IS,IT)=0.0
      XC1(IS,IT)=0.0
      AB1(IS,IT)=0.0
      AC1(IS,IT)=0.0
```

```

AD1(IS,IT)=0.0
BB1(IS,IT)=0.0
BC1(IS,IT)=0.0
BD1(IS,IT)=0.0
CB1(IS,IT)=0.0
CC1(IS,IT)=0.0
CD1(IS,IT)=0.0
DB1(IS,IT)=0.0
DC1(IS,IT)=0.0
DD1(IS,IT)=0.0
EB1(IS,IT)=0.0
EC1(IS,IT)=0.0
ED1(IS,IT)=0.0
175  CONTINUE
      DO 1 J1=1,M
C=====
C  PART D. (CALCULATION OF CONSTANTS)
C=====
      IF (CIND(J1) .NE. 0.0) THEN
        CDS=CIND(J1)/DABS(CIND(J1))
      ELSE
        CDS=1.0
      ENDIF
      TZ=1.+AN
      T1=RC*(1.-AN*AN)
      T=TK(J1)
      T21=EM*T
      TO=1./(12.*T1*EM*T*T)
      TL=RC/T/EM
      TM=EM*T*T
      PR=EM*T
      N=1
      DO 32 I=1,7
32     Y(I,N)=X(J1,I)
      DO 300 I=1,21
        IF(I-21)312,313,313
312     Y(1,I+1)=Y(1,I)+H(J1)
313     IF(Y(1,I)-1.)306,308,305
308     IF(I-5)306,306,305
305     PH(I)=PB2
        RO(I)=1./RC
        ROO(I)=RO(I)*RC
        GO TO 300
306     GO TO (301,302,303,304,509),IZ
301     PH(I)=Y(1,I)*PHI
        RO(I)=DSIN(PH(I))/PHI
        ROO(I)=RO(I)*RC
        GO TO 300

```

```

302  PH(I)=0.
      RO(I)=Y(1,I)
      ROO(I)=RO(I)*RC
      GO TO 300
303  IF(Y(1,I)-X(M,1))307,309,309
309  PH(I)=PB2-ALP
      RO(I)=XL/RC+(Y(1,I)-X(M,1))*DSIN(ALP)
      ROO(I)=RO(I)*RC
      GO TO 300
307  PH(I)=Y(1,I)*RC/XL*DCOS(ALP)
      RO(I)=XL*DSIN(PH(I))/RC/DCOS(ALP)
      ROO(I)=RO(I)*RC
      GO TO 300
304  PH(I)=DP
      RO(I)=DR
      ROO(I)=RO(I)*RC
      ZZ=PH(I)
      DO 310 J=1,4
      FF=RC/ER**2.*(ER**2.+AKL*DSIN(ZZ)*DSIN(ZZ))**1.5
      AK(J)=H(J1)*FF
      GO TO (311,311,314,310),J
311  V=.5
      GO TO 316
314  V=1.
316  ZZ=PH(I)+V*AK(J)
310  CONTINUE
      DP=PH(I)+(AK(1)+AK(4)+2.*(AK(3)+AK(2)))/6.
      DR=DSIN(DP)/RC/(ER**2.+AKL*DSIN(DP)*DSIN(DP))**.5
      GO TO 300
509  IJK=IG(J1)
      GO TO (510,511,304),IJK
510  PH(I)=APH(J1)
      RO(I)=DR
      ROO(I)=RO(I)*RC
      DR=RO(I)+H(J1)*DCOS(APH(J1))
      ZXX(I)=-H(J1)*RC*DSIN(PH(I))
      ZZXX(I+1)=ZZXX(I)+ZXX(I)
      GO TO 300
511  RM=FLOAT(I-1)
      IF (CIND(J1) .NE. 0.0 ) THEN
      PPH(I)=APH(J1)+RM*H(J1)/CIND(J1)*RC
      ELSE
      PPH(I)=APH(J1)+RM*H(J1)*RC
      ENDIF
      RO(I)=DR+DABS(CIND(J1))*(DSIN(PPH(I))-DSIN(APH(J1)))/RC
      ROO(I)=RO(I)*RC
      IF (CIND(J1) .NE. 0.0 ) THEN
      XKX=-H(J1)/DABS(CIND(J1))*RC

```



```

ELSE
XKX=-(H(J1)*RC)
ENDIF
IF (CIND(J1) .NE. 0.0 ) THEN
ZXX(I)=-RC*H(J1)/XKX*(DCOS(PPH(I)+H(J1)/CIND(J1)*RC)-DCOS(PPH(I)))
ELSE
ZXX(I)=-RC*H(J1)/XKX*(DCOS(PPH(I)+H(J1)*RC)-DCOS(PPH(I)))
ENDIF
ZZXX(I+1)=ZZXX(I)+ZXX(I)
IF (CDS.EQ.1.0) THEN
PH(I)=PPH(I)
ELSE
PH(I)=PPH(I)-PB2*2.0
ENDIF
300 CONTINUE
DR=RO(21)
IF(IZ-5)512,513,513
512 DP=PH(21)
GO TO 514
513 DP=APH(J1+1)
514 N1=1

```

```

C=====
C INTEGRATION OF FUNDAMENTAL SET STARTS
C=====

```

```

60 NO=0
46 CONTINUE
* IF(NP-1)111,111,112
IF(NP-2)111,111,112
112 IF(Y(1,N)-.1E-06)198,198,199
198 F(2,N)=T1*Y(6,N)/TZ
F(3,N)=Y(7,N)/TO/TZ
TQ=TL+F(2,N)
F(5,N)=TQ*PR/2.
F(4,N)=0.
F(6,N)=0.
F(7,N)=0.
GO TO 200
199 T2=Y(2,N)/RO(N)
T3=PH(N)-Y(3,N)
C1(N)=DCOS(T3)
C2(N)=DSIN(T3)
T4=(DSIN(PH(N))-DSIN(T3))/RO(N)
T5=Y(6,N)*C1(N)+Y(5,N)*C2(N)
T22(N)=T5
T8=T1*T5-AN*T2
T6=(Y(7,N)-AN*TO*T4)/TO
T7(N)=(T2+AN*T8)/T1
T9(N)=TO*(T4+AN*T6)

```

```

T10(N)=TL+T8
R(N)=TL*RO(N)+Y(2,N)
F(2,N)=T10(N)*C1(N)-DCOS(PH(N))*TL
F(3,N)=T6
F(4,N)=T10(N)*C2(N)-DSIN(PH(N))*TL
F(5,N)=-T10(N)*(Y(5,N)*C1(N)/R(N)-PR*C1(N))
F(6,N)=-T10(N)*((Y(6,N)*C1(N)-T7(N))/R(N)+PR*C2(N))
F(7,N)=(T10(N)*C1(N)/R(N))*(T9(N)-Y(7,N))-T10(N)
*(Y(6,N)*C2(N)-Y(5,N)*C1(N))*TM
***** BT,X AND NX0,X *****
IF(IG(J1).EQ.1) THEN
XP=0.0
ELSE
XP=RC/CIND(J1)
ENDIF
FK(N)=(F(6,N)*C1(N)+F(5,N)*C2(N)+(Y(5,N)*C1(N)
+ -Y(6,N)*C2(N))*(XP-F(3,N))/RC
GO TO 200
111 C1(N)=DCOS(PH(N))
C2(N)=DSIN(PH(N))
IF(Y(1,N)-.1E-06)598,598,599
598 F(2,N)=T1*Y(6,N)/TZ
F(3,N)=Y(7,N)/TO/TZ
F(4,N)=0.
F(5,N)=RC/2.
F(6,N)=0.
F(7,N)=0.
GO TO 200
599 T2=Y(2,N)/RO(N)
T4=Y(3,N)*C1(N)/RO(N)
T5=Y(6,N)*C1(N)+Y(5,N)*C2(N)
T22(N)=T5
T8=T1*T5-AN*T2
T6=Y(7,N)/TO-AN*T4
T7(N)=(T2+AN*T8)/T1
T9(N)=(T4+AN*T6)*TO
F(2,N)=T8*C1(N)+Y(3,N)*C2(N)*TL
F(3,N)=T6
F(4,N)=T8*C2(N)-Y(3,N)*C1(N)*TL
F(5,N)=-Y(5,N)/RO(N)-RC)*C1(N)
F(6,N)=-Y(6,N)*C1(N)-T7(N))/RO(N)-RC*C2(N)
TX=-Y(7,N)-T9(N))/RO(N)
F(7,N)=TX*C1(N)-RC*T*(Y(6,N)*C2(N)-Y(5,N)*C1(N))
200 IF(N-2)42,43,43
43 IF(N-6)44,47,45
44 N=N+1
GO TO 46
42 DO 81 J=2,6

```

```

P2=FLOAT(J-1)
P3=P2*H(J1)
Y(1,J)=Y(1,1)+P3
DO 81 I=2,7
81  Y(I,J)=Y(I,1)+P3*F(I,1)
    N=2
    IP=1
    GO TO 46
47  DO 48 I=2,7
    Z(I,2)=Y(I,1)+(H(J1)/1440.)*(493.*F(I,1)+1337.
1*F(I,2)-618.*F(I,3)+302.*F(I,4)-83.*F(I,5)+9.*F(I,6))
    Z(I,3)=Y(I,1)+(H(J1)/90.)*(28.*F(I,1)+129.*F(I,2)
1+14.*F(I,3)+14.*F(I,4)-6.*F(I,5)+F(I,6))
    Z(I,4)=Y(I,1)+(3.*H(J1)/160.)*(17.*F(I,1)+73.*F(I,2)
1+38.*(F(I,3)+F(I,4))-7.*F(I,5)+F(I,6))
    Z(I,5)=Y(I,1)+(4.*H(J1)/90.)*(7.*(F(I,1)+F(I,5))
1+32.*(F(I,2)+F(I,4))+12.*F(I,3))
48  Z(I,6)=Y(I,1)+(5.*H(J1)/288.)*(19.*(F(I,1)+F(I,6))
1+75.*(F(I,2)+F(I,5))+50.*(F(I,4)+F(I,3)))
    R1=0.
    IP=IP+1
    DO 49 I=2,7
    DO 49 J=2,6
    R1=DABS(Y(I,J)-Z(I,J))+R1
49  Y(I,J)=Z(I,J)
    IF(IP-15)141,45,45
141 IF(R1-.1E-07)45,45,50
50  N=2
    GO TO 46
45  IF(NO-1)53,53,55
53  N=N+1
    IF(N-21)61,61,62
61  Y(1,N)=Y(1,N-1)+H(J1)
    DO 51 I=2,7
51  Y(I,N)=Y(I,N-6)+(.3*H(J1))*(11.*(F(I,N-5)+F(I,N-1))
1-14.*(F(I,N-4)+F(I,N-2))+26.*F(I,N-3))
99  NO=2
    IP=1
    GO TO 46
55  R1=0.
    IP=IP+1
    DO 56 I=2,7
    Z(I,1)=Y(I,N-6)+(.3*H(J1))*(F(I,N-6)+5.*F(I,N-5)+F(I,N-4)+6.*
1F(I,N-3)+F(I,N-2)+5.*F(I,N-1)+F(I,N))
    R1=R1+DABS(Y(I,N)-Z(I,1))
56  Y(I,N)=Z(I,1)
    IF(IP-10)142,60,60
142 IF(R1-.1E-07)60,46,46

```

```

*62  IF(NP-1)662,762,912
62   F(NP-2)662,762,912
912  IF(AA-.10)911,911,914
914  IF(NP-10)662,911,911
911  IN=2
      GO TO 764
762  RRR=0.
      DO 763 I=2,7
763  RRR=RRR+DABS(Y(I,21)-X(J1+1,I))
      IF(RRR-.1)764,764,766
766  WRITE(3,767)
767  FORMAT(2X,/, 'SEGMENT IS TOO LONG',/)
764  CONTINUE
C=====
C PART E. OUTPUT OF RESULTS
C=====
*****      WRITE(3,508)
*****      WRITE(3,507)
*****      GOTO 729
      DO 793 N=1,21,4
      ST1=(T7(N)+T9(N)*6.)*T21
      ST2=(T7(N)-T9(N)*6.)*T21
      ST3=(T22(N)+Y(7,N)*6.)*T21
      ST4=(T22(N)-Y(7,N)*6.)*T21
C      ROO(N)=RC*RO(N)
      ZZNN(N)=ZZXX(N)-EM*Y(4,N)*100.0
      YYN(N)=ROO(N)+EM*Y(2,N)*100.0
      WRITE(7,116)ZZXX(N),ROO(N),ZZNN(N),YYN(N)
116  FORMAT (4E13.5)
793  WRITE(3,105)Y(1,N),Y(2,N),Y(4,N),T9(N),Y(7,N),T22(N),T7(N),
      1ST1,ST2,ST3,ST4
***** 729  CONTINUE
      IF(AA .LE. 0.1 .AND. SOB2.GT.1.0) THEN
*      DO 1575 N=1,21
      IF (MX(J1) .EQ.50) GOTO 1590
      DO 1575 N=1,20
      XNN=FLOAT(NNN)
      FF1=ROO(N)
      FF2=Y(3,N)/(EM*TK(J1)/RC)
      FF3=F(3,N)/RC
      FF4=T22(N)
      FF5=T7(N)
      FF6=FK(N)
      FF7=PH(N)
      IF(N.EQ.20) THEN
      FF8=PH(20)
      FF9=FK(20)
      ENDIF

```

```

* -----
1111  FORMAT(4(4D12.4//4(4D12.4//4(4D12.4/))
      IF(N.LT.21) THEN
      ITC=0
      ENDIF
      IF(J1.EQ.1 .AND. N.EQ.1) THEN
1113  FORMAT(' J1 = ',I2,' N = ',I2)
      ITC=IBT
      CALL RAT(FF1,FF2,FF3,FF4,FF5,FF6,FF7,SS1,HS,J1,
+EM,TK,CIND,IG,XNN,XA1,XB1,XC1,MXN,ITC)
      ITC=0
      SS1=0.0
      CALL RAT(FF1,FF2,FF3,FF4,FF5,FF6,FF7,SS1,HS,J1,
+EM,TK,CIND,IG,XNN,XA,XB,XC,MXN,ITC)
      CALL PP2(XA1,XB1,XC1,XA,XB,XC,P11)
      DO 171 JX=1,4
      DO 171 JX1=1,4
      P22(JX,JX1)=P11(JX,JX1)
171   CONTINUE
      ENDIF
      IF(J1.NE.1 .AND. J1.EQ.MX(J1) .AND. N.EQ.1) THEN
      CALL JUNC2(FF1,FF2,FF3,FF4,FF5,FF6,FF7,FF8,FF9,SS1,HS,J1,
+EM,TK,CIND,IG,XNN,MX,MXN,BB1,BC1,BD1,CB1,CC1,CD1,
+DB1,DC1,DD1,EB1,EC1,ED1)
      CALL JUNP(AB1,AC1,AD1,XA1,XB1,XC1,P55,BD1,BC1,BB1,
+CD1,CC1,CB1,DD1,DC1,DB1,ED1,EC1,EB1)
      ENDIF
      IF(J1.NE.1 .AND. J1.NE.MX(J1) .AND. N.EQ.1) THEN
      SS1=1.0
      CALL JUNC1(FF1,FF2,FF3,FF4,FF5,FF6,FF7,SS1,HS,J1,
+EM,TK,CIND,IG,XNN,XA,XB,XC,MXN,ITC)
      CALL PP(XA,XB,XC,P22,P33)
      DO 192 JX=1,4
      DO 192 JX1=1,4
      P22(JX,JX1)=P33(JX,JX1)
192   CONTINUE
      ENDIF
* -----
      IF(N.GE.2 .AND. N.LE.20) THEN
      SS1=0.0
      DO 197 JX=1,4
      DO 197 JX1=1,4
      P55(JX,JX1)=P22(JX,JX1)
197   CONTINUE
      CALL RAT(FF1,FF2,FF3,FF4,FF5,FF6,FF7,SS1,HS,J1,
+EM,TK,CIND,IG,XNN,XA,XB,XC,MXN,ITC)
      IF(N.EQ.20) THEN
      DO 195 JX=1,4

```

```

DO 195 JX1=1,4
AB1(JX,JX1)=XA(JX,JX1)
AC1(JX,JX1)=XB(JX,JX1)
AD1(JX,JX1)=XC(JX,JX1)
195 CONTINUE
ENDIF
IF(J1.EQ.MX(J1) .AND. N.EQ.2) THEN
CALL PP2(XA1,XB1,XC1,XA,XB,XC,P11)
DO 193 JX=1,4
DO 193 JX1=1,4
P22(JX,JX1)=P11(JX,JX1)
193 CONTINUE
ELSE
CALL PP(XA,XB,XC,P22,P33)
DO 191 JX=1,4
DO 191 JX1=1,4
P22(JX,JX1)=P33(JX,JX1)
191 CONTINUE
ENDIF
ENDIF
1112 FORMAT(4(4D12.4/)/)
1575 CONTINUE
ENDIF
*1590 CONTINUE
ZZXX(1)=ZZXX(21)
GO TO 1

```

```

C=====
C INTEGRATION OF DERIVED SET STARTS
C=====

```

```

662 N1=N1+1
N=1
Y1(1,N)=X(J1,1)
DO 63 I=2,7
63 Y1(I,N)=0.
Y1(N1,N)=1.
90 NO=0
76 CONTINUE
* IF(NP-1)113,113,114
IF(NP-2)113,113,114
114 IF(Y1(1,N)-.1E-07)201,201,202
201 F(2,N)=T1*Y1(6,N)/TZ
F(3,N)=Y1(7,N)/TO/TZ
F(5,N)=F(2,N)*PR/2
F(4,N)=0.
F(6,N)=0.
F(7,N)=0.
GO TO 203
202 T2=Y1(2,N)/RO(N)

```

```

T3=Y1(3,N)*C1(N)/RO(N)
T4=Y1(6,N)*C1(N)+Y1(5,N)*C2(N)-Y1(3,N)*(Y(5,N)*C1(N)
1-Y(6,N)*C2(N))
T5=T1*T4-AN*T2
T6=Y1(7,N)/TO-AN*T3
Q1=(T2+AN*T5)/T1
T8=TO*(T3+AN*T6)
F(2,N)=T5*C1(N)+T10(N)*Y1(3,N)*C2(N)
F(4,N)=T5*C2(N)-T10(N)*Y1(3,N)*C1(N)
F(3,N)=T6
TA=(Y(6,N)*C1(N)-T7(N))/R(N)
F(6,N)=-T5*(TA+PR*C2(N))-T10(N)*((Y1(6,N)*C1(N)
1+Y1(3,N)*Y(6,N)*C2(N)-Q1-TA*Y1(2,N))/R(N)-PR*Y1
1(3,N)*C1(N))
F(5,N)=-F(2,N)*(Y(5,N)/R(N)-PR)-T10(N)*C1(N)*(Y1(5,N)
1-Y(5,N)*Y1(2,N)/R(N))/R(N)
TX=(T9(N)-Y(7,N))/R(N)
F(7,N)=F(2,N)*(TX+TM*Y(5,N))+T10(N)*(C1(N)*(TM*Y1(5,N)
1+(-Y1(7,N)+T8-TX*Y1(2,N))/R(N))-TM*C2(N)*Y1(6,N))
1-TM*F(4,N)*Y(6,N)
GO TO 203
113 IF(Y1(1,N)-.1E-07)501,501,502
501 F(2,N)=T1*Y1(6,N)/TZ
F(3,N)=Y1(7,N)/TO/TZ
F(4,N)=0.
F(5,N)=0.
F(6,N)=0.
F(7,N)=0.
GO TO 203
502 T2=Y1(2,N)/RO(N)
T4=Y1(3,N)*C1(N)/RO(N)
T5=Y1(6,N)*C1(N)+Y1(5,N)*C2(N)
T8=T1*T5-AN*T2
T6=Y1(7,N)/TO-AN*T4
T7(N)=(T2+AN*T8)/T1
T9(N)=(T4+AN*T6)*TO
F(2,N)=T8*C1(N)+Y1(3,N)*C2(N)*TL
F(3,N)=T6
F(4,N)=T8*C2(N)-Y1(3,N)*C1(N)*TL
F(5,N)=-Y1(5,N)/RO(N)*C1(N)
F(6,N)=-Y1(6,N)*C1(N)-T7(N))/RO(N)
TX=-Y1(7,N)-T9(N))/RO(N)
F(7,N)=TX*C1(N)-RC*T*(Y1(6,N)*C2(N)-Y1(5,N)*C1(N))
203 IF(N-2)72,73,73
73 IF(N-6)74,77,75
74 N=N+1
GO TO 76
72 DO 82 J=2,6

```

```

P2=FLOAT(J-1)
P3=P2*H(J1)
Y1(1,J)=Y1(1,1)+P3
DO 82 I=2,7
82  Y1(I,J)=Y1(I,1)+P3*F(I,1)
    N=2
    IP=1
    GO TO 76
77  DO 78 I=2,7
    Z(I,2)=Y1(I,1)+(H(J1)/1440.)*(493.*F(I,1)+1337.*F(I,2)
1-618.*F(I,3)+302.*F(I,4)-83.*F(I,5)+9.*F(I,6))
    Z(I,3)=Y1(I,1)+(H(J1)/90.)*(28.*F(I,1)+129.*F(I,2)+14.
1*F(I,3)+14.*F(I,4)-6.*F(I,5)+F(I,6))
    Z(I,4)=Y1(I,1)+(3.*H(J1)/160.)*(17.*F(I,1)+73.*F(I,2)
1+38.*(F(I,3)+F(I,4))-7.*F(I,5)+F(I,6))
    Z(I,5)=Y1(I,1)+(4.*H(J1)/90.)*(7.*(F(I,1)+F(I,5))+32.
1*(F(I,2)+F(I,4))+12.*F(I,3))
78  Z(I,6)=Y1(I,1)+(5.*H(J1)/288.)*(19.*(F(I,1)+F(I,6))
1+75.*(F(I,2)+F(I,5))+50.*(F(I,4)+F(I,3)))
    R1=0.
    IP=IP+1
    DO 79 I=2,7
    DO 79 J=2,6
    R1=DABS(Y1(I,J)-Z(I,J))+R1
79  Y1(I,J)=Z(I,J)
    IF(IP-15)143,75,75
143 IF(R1-.1E-06)75,75,80
80  N=2
    GO TO 76
75  IF(NO-1)83,83,85
83  N=N+1
    IF(N-21)91,91,92
91  Y1(1,N)=Y1(1,N-1)+H(J1)
    DO 95 I=2,7
95  Y1(I,N)=Y1(I,N-6)+(.3*H(J1))*(11.*(F(I,N-5)+F(I,N-1))
1-14.*(F(I,N-4)+F(I,N-2))+26.*F(I,N-3))
101 NO=2
    IP=1
    GO TO 76
85  R1=0.
    IP=IP+1
    DO 86 I=2,7
    Z(I,1)=Y1(I,N-6)+(.3*H(J1))*(F(I,N-6)+5.*F(I,N-5)+F(I,N-4)+6.*
1F(I,N-3)+F(I,N-2)+5.*F(I,N-1)+F(I,N))
    R1=R1+DABS(Y1(I,N)-Z(I,1))
86  Y1(I,N)=Z(I,1)
    IF(IP-10)144,90,90
144 IF(R1-.1E-07)90,76,76

```



```

92   DO 22 J=1,N2
22   U(N1-1,J)=Y1(J+1,21)
      IF(N1-7)662,96,96
104  FORMAT (7E14.6)
59   FORMAT (3I12)
508  FORMAT (/ ,2X,'DISTANCE',3X,' DISPLACEMENTS',9X,'MOMENTS',
19X,'STRESS',' RESULTANTS',5X,'CIRCUM. STRESS',7X,
1'AXIAL STRESS')
507  FORMAT (1X,' FROM APEX',2X,'RADIAL',5X,'AXIAL',3X,
1'CIRCUM.',5X,'AXIAL',3X,'CIRCUM.',5X,'AXIAL',4X,'INNER',5X,
1'OUTER',5X,'INNER',5X,'OUTER',/)
41   FORMAT (7E11.5)
110  FORMAT (31E11.5)
105  FORMAT (21E11.4)
505  FORMAT (//,2X,' NO. OF PASS=' ,I2,' RESIDUE=' ,E11.5,
1' LOAD(P/E)= ' ,E11.5,' EM1=' ,E11.5,/)

```

```

C =====
C SOLUTION OF MATRIX EQUATIONS STARTS
C =====

```

```

96   N1=J1
      DO 4 I=1,N3
          DO 4 J=1,N3
              A1(J,I)=U(I,J)
              A2(J,I)=U(I+3,J)
              A3(J,I)=U(1,J+3)
              A4(J,I)=U(I+3,J+3)
              X1(I,1)=X(N1,I+1)
              X2(I,1)=X(N1,I+4)
              Y3(N1+1,I)=Y(I+1,21)
4     Y2(N1+1,I)=Y(I+4,21)
          DO 20 I=1,N3
              AY(I,1)=Y3(N1+1,I)
20    BY(I,1)=Y2(N1+1,I)
          CALL MATM(A1,X1,A9,N3,N3,1)
          CALL MATM(A2,X2,Z1,N3,N3,1)
          CALL MATS(A9,Z1,N3,1)
          CALL MATSB(Z1,N3,1)
          CALL MATS(AY,Z1,N3,1)
          CALL MATM(A3,X1,A9,N3,N3,1)
          CALL MATM(A4,X2,Z2,N3,N3,1)
          CALL MATS(A9,Z2,N3,1)
          CALL MATSB(Z2,N3,1)
          CALL MATS(BY,Z2,N3,1)
          IF(N1-1)6,6,7
6     CALL MATM(A1,TS1,A6,N3,N3,N3)
          CALL MATM(A1,TS2,A7,N3,N3,N3)
          CALL MATM(A2,TS3,A1,N3,N3,N3)
          CALL MATS(A6,A1,N3,N3)

```

```

CALL MATM(A2,TS4,A6,N3,N3,N3)
CALL MATS(A6,A7,N3,N3)
CALL MATM(A3,TS1,A6,N3,N3,N3)
CALL MATM(A3,TS2,A8,N3,N3,N3)
CALL MATM(A4,TS3,A3,N3,N3,N3)
CALL MATS(A6,A3,N3,N3)
CALL MATM(A4,TS4,A6,N3,N3,N3)
CALL MATS(A6,A8,N3,N3)
DO 2 I=1,N3
DO 2 J=1,N3
A4(I,J)=A8(I,J)
2 A2(I,J)=A7(I,J)
CALL MATI(A2,A6,N3)
CALL MATM(A4,A6,A7,N3,N3,N3)
CALL MATI(A7,A8,N3)
CALL MATM(A1,XX,A9,N3,N3,1)
CALL MATS(Z1,A9,N3,1)
CALL MATSB(A9,N3,1)
CALL MATM(A3,XX,A10,N3,N3,1)
CALL MATS(Z2,A10,N3,1)
CALL MATM(A4,A6,A7,N3,N3,N3)
CALL MATM(A7,A9,A11,N3,N3,1)
CALL MATS(A11,A10,N3,1)
CALL MATSB(A10,N3,1)
GO TO 8
7 IF(N1-M)3,5,5
5 CALL MATM(TF1,A1,A6,N3,N3,N3)
CALL MATM(TF3,A1,A7,N3,N3,N3)
CALL MATM(TF2,A3,A1,N3,N3,N3)
CALL MATS(A6,A1,N3,N3)
CALL MATM(TF4,A3,A6,N3,N3,N3)
CALL MATS(A6,A7,N3,N3)
CALL MATM(TF1,A2,A6,N3,N3,N3)
CALL MATM(TF3,A2,A18,N3,N3,N3)
CALL MATM(TF2,A4,A2,N3,N3,N3)
CALL MATS(A6,A2,N3,N3)
CALL MATM(TF4,A4,A6,N3,N3,N3)
CALL MATS(A6,A18,N3,N3)
CALL MATM(TF1,Z1,A14,N3,N3,1)
CALL MATM(TF3,Z1,A15,N3,N3,1)
CALL MATM(TF2,Z2,Z1,N3,N3,1)
CALL MATS(A14,Z1,N3,1)
CALL MATM(TF4,Z2,A14,N3,N3,1)
CALL MATS(A14,A15,N3,1)
DO 19 I=1,N3
Z2(I,1)=A15(I,1)
DO 19 J=1,N3
A3(I,J)=A7(I,J)

```

```

19  A4(I,J)=A18(I,J)
3   CALL MATM(A1,A8,A7,N3,N3,N3)
    CALL MATS(A2,A7,N3,N3)
    CALL MATI(A7,A6,N3)
    CALL MATM(A1,A8,A7,N3,N3,N3)
    CALL MATM(A7,A10,A9,N3,N3,1)
    CALL MATS(Z1,A9,N3,1)
    CALL MATSB(A9,N3,1)
    CALL MATM(A3,A8,A7,N3,N3,N3)
    CALL MATM(A7,A10,A11,N3,N3,1)
    CALL MATS(A4,A7,N3,N3)
    CALL MATM(A6,A9,A12,N3,N3,1)
    CALL MATM(A7,A12,A10,N3,N3,1)
    CALL MATS(A11,A10,N3,1)
    CALL MATS(Z2,A10,N3,1)
    CALL MATSB(A10,N3,1)
    CALL MATM(A3,A8,A7,N3,N3,N3)
    CALL MATS(A4,A7,N3,N3)
    CALL MATM(A7,A6,A1,N3,N3,N3)
    CALL MATI(A1,A8,N3)
    IF(N1-M)8,9,9
9   CALL MATS(XY,A10,N3,1)
8   DO 5000 I=1,N3
    DO 5000 J=1,N3
    E(N1,I,J)=A6(I,J)
    C(N1,I,J)=A8(I,J)
    A(N1,I)=A9(I,1)
    B(N1,I)=A10(I,1)
5000 CONTINUE
1   CONTINUE
1590 CONTINUE
    IF(AA.LE.0.1 .AND. SOB2.GT.1.0 .AND. NNN.LE.NNN2) THEN
        ITC=ITP
        MCK=J1-1
        CALL RAT(FF1,FF2,FF3,FF4,FF5,FF6,FF7,SS1,HS,MCK,
+EM,TK,CIND,IG,XNN,XA,XB,XC,MXN,ITC)
        CALL XMAT(XA,XB,XC,P55,P22,XD1)
        CALL DET4(XD1,DXD)
        PRINT*,' DETER = ',DXD,' NNN = ',NNN
        DXD1(NNN)=DXD*SINX
        NNN=NNN+1
        GO TO 405
    ENDIF
    DO 1015 IJ1=NNN1,NNN2
    IF(AA.LE.0.1 .AND. SOB2.GT.1 .AND. DXD1(IJ1) .LE. 0.0) THEN
        AA=2.0
        NNN=NNN1
        GO TO 153

```

```

        ENDIF
1015  CONTINUE
        NNN=NNN1
        F(NP-2)117,115,117
117   GO TO(718,108),IN
718   AA=0.
        DO 15 I1=1,M
        N1=M-I1+1
        DO 10 I=1,N3
        DO 10 J=1,N3
        A6(I,J)=E(N1,I,J)
        A8(I,J)=C(N1,I,J)
        A9(I,1)=A(N1,I)
10    A10(I,1)=B(N1,I)
        IF(N1-M)11,12,12
12    CALL MATM(A8,A10,A11,N3,N3,1)
        CALL MATS(A11,A9,N3,1)
        CALL MATM(A6,A9,A12,N3,N3,1)
        CALL MATM(TF1,A11,A14,N3,N3,1)
        CALL MATM(TF2,XY,A15,N3,N3,1)
        CALL MATM(TF3,A11,A16,N3,N3,1)
        CALL MATM(TF4,XY,A17,N3,N3,1)
        DO 89 I=1,N3
        X(MO,I+1)=A15(I,1)+A14(I,1)
89    X(MO,I+4)=A17(I,1)+A16(I,1)
        GO TO 16
11    CALL MATS(A12,A10,N3,1)
        CALL MATM(A8,A10,A11,N3,N3,1)
        CALL MATS(A11,A9,N3,1)
        CALL MATM(A6,A9,A12,N3,N3,1)
        DO 17 I=1,N3
17    X(N1+1,I+1)=A11(I,1)
        IF(N1-1)93,93,16
93    CALL MATM(TS1,XX,A14,N3,N3,1)
        CALL MATM(TS2,A12,A15,N3,N3,1)
        CALL MATM(TS3,XX,A16,N3,N3,1)
        CALL MATM(TS4,A12,A17,N3,N3,1)
        DO 98 I=1,N3
        X(1,I+1)=A15(I,1)+A14(I,1)
98    X(1,I+4)=A17(I,1)+A16(I,1)
        GO TO 18
16    DO 13 I=1,N3
13    X(N1,I+4)=A12(I,1)
18    DO 15 I=1,N3
        AA=DABS(Y3(N1+1,I)-X(N1+1,I+1))+AA
15    AA=DABS(Y2(N1+1,I)-X(N1+1,I+4))+AA
115   NP=NP+1
        RES=AA/SS

```

```

SS=AA
WRITE(3,505)NP,AA,EM,EM1
WRITE(6,*)EM,EM1,AA,SOB2
IF(NP-5)151,152,152
152 IF(RES-1.)151,151,153
153 DO 154 I=2,7
DO 154 J=1,MO
154 X(J,I)=X7(J,I)
EM=EM-EM1
EM1=EM1/2.
NP=3
151 WRITE(3,104)((X(J,I),I=1,7),J=1,MO)
IF(AA .LE. 0.1 .AND. SOB2.GT.1.0) THEN
5505 EEM=DABS(EM)
DO 5508 J=1,MO
XYX4(J)=EM*X(J,4)
XYX2(J)=EM*X(J,2)
5508 CONTINUE
WRITE(4,5507)EEM,(XYX4(J),J=1,MO)
WRITE(5,5507)EEM,(XYX2(J),J=1,MO)
5507 FORMAT(31E12.5)
ENDIF
WRITE(6,*)EM,EM1,AA
GO TO 405
108 DO 155 I=2,7
DO 155 J=1,MO
155 X7(J,I)=X(J,I)
IN=1
NP=3
AA=1.
SOB2=SOB2+1.
EM=EM+EM1
IF(DABS(EM1)-.1E-014) 109,109,1011
1011 IF(SOB2-SOB1)405,405,109
109 WRITE(3,1270)EM,EM1,SOB2
1270 FORMAT(/'EM= ',E14.8,'EM1= ',E14.8,' SOB2= ',F6.0)
STOP
END.

```

```

SUBROUTINE RAT(FF1,FF2,FF3,FF4,FF5,FF6,FF7,SS1,HS,J1,
+EM,TK,CIND,IG,XNN,AB1,AC1,AD1,MXN,ITC)
IMPLICIT REAL*8 (A-H,O-Z)
REAL*8 XK1(12,11),XK2(12,11),XK3(12,11),XK4(12,11)
REAL*8 XK5(12,11),XK6(12,11)
REAL*8 CC1(12),CC2(12),CC3(12),CC4(12),
+ AA1(3),AA2(3),AA3(3),AA4(3)
REAL*8 HS(30),TK(30),EM
REAL*8 AB1(4,4),AC1(4,4),AD1(4,4),CIND(30),IG(30)
DIMENSION MXN(30)
DO 300 I=1,3
AA1(I)=0.0
AA2(I)=0.0
AA3(I)=0.0
AA4(I)=0.0
300 CONTINUE
DO 199 I=1,4
DO 199 J=1,4
AB1(I,J)=0.0
AC1(I,J)=0.0
AD1(I,J)=0.0
199 CONTINUE
DO 200 I=1,12
DO 201 J=1,11
XK1(I,J)=0.0
XK2(I,J)=0.0
XK3(I,J)=0.0
XK4(I,J)=0.0
201 CONTINUE
200 CONTINUE
XNU=0.3
BTX=0.0
BTXX=0.0
XXN0=FF6*EM*(1.0-XNU*XNU)*TK(J1)
PHI=FF7
105 FORMAT(21E10.4)
UY1=-XNN
UY2=-XNN*XNN
VY1=XNN
VY2=-XNN*XNN
VY3=UY2*VY1
WY1=-XNN
WY2=-XNN*XNN
WY3=WY1*WY2
WY4=WY3*XNN
XN0=FF4*EM*(1.0-XNU*XNU)*TK(J1)
YN0=FF5*EM*(1.0-XNU*XNU)*TK(J1)
B=FF1

```

```

BX=DCOS(PHI)
IF(MXN(J1) .EQ. 2) THEN
RI2=1.0/CIND(J1)
ELSE
RI2=DSIN(PHI)/B
ENDIF
BI=RI2/DSIN(PHI)
BBX=RI2/DTAN(PHI)
IF(IG(J1).EQ.1) THEN
RI1=0.0
ELSE
RI1=1.0/CIND(J1)
ENDIF
BXX=-DSIN(PHI)*RI1
BIX=-BBX*BI
RX1=0.0
RIX1=0.0
RI12=RI1-RI2
RI21=RI2-RI1
RIX2=RI12*BBX
BIXX=(2.0*BBX*BBX+RI2)*BI
RIXX1=0.0
RIXX2=RI21*(2.0*BBX*BBX+RI1*RI2)
BBXX=BI*BXX+BX*BIX
IF(ITC.EQ.0) THEN
CALL BODY(XK1,XK2,XK3,XK4,TK,BTX,BTXX,XXN0,PHI,UY1,UY2,
+VY1,VY2,VY3,WY1,WY2,WY3,WY4,XN0,YN0,B,BX,RI2,BI,BBX,
+RI1,BXX,BIX,RX1,RIX1,RI12,RI21,RIX2,BIXX,RIXX1,RIXX2,
+BBXX,XNU,J1)
ELSE
CALL BOUND(XK1,XK2,XK3,XK4,TK,BTX,BTXX,XXN0,PHI,UY1,UY2,
+VY1,VY2,VY3,WY1,WY2,WY3,WY4,XN0,YN0,B,BX,RI2,BI,BBX,
+RI1,BXX,BIX,RX1,RIX1,RI12,RI21,RIX2,BIXX,RIXX1,RIXX2,
+BBXX,XNU,J1,ITC,XK5,XK6)
ENDIF
DO 50 L=1,12
CC1(L)=0.0
CC2(L)=0.0
CC3(L)=0.0
CC4(L)=0.0
DO 60 L1=1,11
IF(ITC.EQ.6) THEN
CC1(L)=CC1(L)+(XK3(L,L1)*DCOS(PHI)+XK1(L,L1)*DSIN(PHI))
CC2(L)=CC2(L)+(XK2(L,L1)*DCOS(PHI)+XK4(L,L1)*DSIN(PHI))
CC3(L)=CC3(L)+XK5(L,L1)
CC4(L)=CC4(L)+XK6(L,L1)
ELSE
CC1(L)=CC1(L)+XK1(L,L1)

```

```

        CC2(L)=CC2(L)+XK2(L,L1)
        CC3(L)=CC3(L)+XK3(L,L1)
        CC4(L)=CC4(L)+XK4(L,L1)
        ENDIF
60      CONTINUE
50      CONTINUE
110     FORMAT (31D11.5)
        DO 70 I=1,4
        IF (I.EQ.1) THEN
        CALL DETCO(CC1,HS,J1,SS1,AA1,AA2,AA3,AA4,0)
        ENDIF
        IF (I.EQ.2) THEN
        CALL DETCO(CC2,HS,J1,SS1,AA1,AA2,AA3,AA4,0)
        ENDIF
        IF (I.EQ.3) THEN
        CALL DETCO(CC3,HS,J1,SS1,AA1,AA2,AA3,AA4,0)
        ENDIF
        IF (I.EQ.4) THEN
        CALL DETCO(CC4,HS,J1,SS1,AA1,AA2,AA3,AA4,0)
        ENDIF
        AB1(I,1)=AA1(1)
        AB1(I,2)=AA2(1)
        AB1(I,3)=AA3(1)
        AB1(I,4)=AA4(1)
        AC1(I,1)=AA1(2)
        AC1(I,2)=AA2(2)
        AC1(I,3)=AA3(2)
        AC1(I,4)=AA4(2)
        AD1(I,1)=AA1(3)
        AD1(I,2)=AA2(3)
        AD1(I,3)=AA3(3)
        AD1(I,4)=AA4(3)
70      CONTINUE
        RETURN
        END

```

```

*=====
SUBROUTINE BODY(XK1,XK2,XK3,XK4,TK,BTX,BTXX,XXN0,PHI,
+UY1,UY2,VY1,VY2,VY3,WY1,WY2,WY3,WY4,XN0,YN0,B,BX,RI2,
+BI,BBX,RI1,BXX,BIX,RX1,RIX1,RI12,RI21,RIX2,BIXX,RIXX1,RIXX2,
+BBXX,XNU,J1)
IMPLICIT REAL*8 (A-H,O-Z)
REAL*8 XK1(12,11),XK2(12,11),XK3(12,11),XK4(12,11),TK(30)
C=1.0
D=1.0/TK(J1)/TK(J1)/12.0

```

```

**-----
**      STABILITY EQN-1
** (dB/dx-B*BTx0/R1)*Nx1

```



```

XK1(5,1)=C*(BX-B*BTX*RI1)
XK1(7,1)=-C*(BX-B*BTX*RI1)*BTX
XK1(2,1)=C*(BX-B*BTX*RI1)*XNU*BI*VY1
XK1(1,1)=C*(BX-B*BTX*RI1)*(BTX*RI1
+      +XNU*BX*BI)
XK1(3,1)=C*(BX-B*BTX*RI1)*(RI1+XNU*RI2)
** B*dNx1/dx
XK1(9,1)=C*B
XK1(11,1)=-C*B*BTX
XK1(6,1)=C*XNU*VY1
XK1(2,2)=C*B*XNU*BIX*VY1
XK1(5,2)=C*B*(BTX*RI1+XNU*BBX)
XK1(7,2)=C*B*(RI1-BTXX+XNU*RI2)
XK1(1,2)=C*B*(BTXX*RI1+BTX*RIX1+XNU*BBXX)
XK1(3,2)=C*B*(RIX1+XNU*RIX2)
** dNxy1/dy
CNX=C*(1.0-XNU)/2.0
XK1(6,2)=CNX*VY1
XK1(1,3)=CNX*BI*UY2
XK1(3,3)=-CNX*BTX*BI*WY2
XK1(2,3)=CNX*(-BBX+BTX*RI2)*VY1
** -dB/dx*Ny1
XK1(5,3)=-C*BX*XNU
XK1(7,3)=+C*BX*XNU*BTX
XK1(2,4)=-C*BX*BI*VY1
XK1(1,4)=-C*BX*(XNU*BTX*RI1+BBX)
XK1(3,4)=-C*BX*(XNU*RI1+RI2)
** B/R1*dMx1/dx
XK1(8,1)=D*B*RI1
** dB/dx*(1/R1)*Mx1
XK1(4,1)=D*BX*RI1
** 1/R1*dMxy1/dy
DN=D*(1.0-XNU)/2.0
XK1(7,4)=-2.0*DN*BI*RI1*WY2
XK1(1,5)=DN*RI1*BI*RI1*UY2
XK1(6,3)=DN*RI1*RI2*VY1
XK1(3,5)=DN*RI1*(-BIX+BBX*BI)*WY2
XK1(2,5)=DN*RI1*(RIX2-BBX*RI2)*VY1
** -dB/dx*(1/R1)*My1
XK1(11,2)=+D*BX*RI1*XNU
XK1(7,5)=+D*BX*RI1*BBX
XK1(3,6)=+D*BX*RI1*BI*BI*WY2
XK1(5,4)=-D*BX*RI1*XNU*RI1
XK1(1,6)=-D*BX*RI1*(BBX*RI1+XNU*RIX1)
XK1(2,6)=-D*BX*RI1*BI*RI2*VY1
** -B/R1*Nx0*BTx1
B5=-B*RI1*XN0
XK1(7,6)=-B5

```

```

XK1(1,7)=RI1*B5
** -----
** STABILITY EQN-2
** dNyl/dy
XK2(5,1)=C*XNU*UY1
XK2(7,1)=-C*XNU*BTX*WY1
XK2(2,1)=C*BI*VY2
XK2(1,1)=C*(BBX+XNU*BTX*RI1)*UY1
XK2(3,1)=C*(RI2+XNU*RI1)*WY1
** B*dNxy1/dx
* CNX=C*(1.0-XNU)/2.0
XK2(10,1)=CNX*B
XK2(5,2)=CNX*UY1
XK2(7,2)=-CNX*BTX*WY1
XK2(1,2)=CNX*B*BIX*UY1
XK2(6,1)=CNX*B*(-BBX+BTX*RI2)
XK2(3,2)=CNX*B*(-BTX*BIX-BTXX*BI)*WY1
XK2(2,2)=CNX*B*(-BBXX+BTX*RIX2+BTXX*RI2)
** 1/R2*dMy1/dy
XK2(11,1)=-D*RI2*XNU*WY1
XK2(7,3)=-D*RI2*BBX*WY1
XK2(3,3)=-D*RI2*BI*BI*WY3
XK2(5,3)=D*RI2*XNU*RI1*UY1
XK2(1,3)=D*RI2*(BBX*RI1+XNU*RIX1)*UY1
XK2(2,3)=D*RI2*BI*RI2*VY2
** B/R2*dMxy1/dx
* DN=D*(1.0-XNU)/2.0
XK2(11,2)=-2.0*DN*RI2*WY1
XK2(5,4)=DN*RI2*RI1*UY1
XK2(10,2)=DN*B*RI2*RI2
XK2(7,4)=DN*B*RI2*(-3.0*BIX+BBX*BI)*WY1
XK2(1,4)=DN*B*RI2*(BI*RIX1+BIX*RI1)*UY1
XK2(6,2)=DN*B*RI2*(2.0*RIX2-BBX*RI2)
XK2(3,4)=DN*B*RI2*(-BIXX+
+BBX*BIX+BBXX*BI)*WY1
XK2(2,4)=DN*B*RI2*(RIX2-
+BBXX*RI2-BBX*RIX2)
** 2/R2*dB/dx*Mxy1
XK2(7,5)=-4.0*DN*B*RI2*BI*WY1
XK2(1,5)=2.0*DN*B*RI2*BI*RI1*UY1
XK2(6,3)=2.0*DN*B*RI2*RI2
XK2(3,5)=2.0*DN*B*RI2*(-BIX+BBX*BI)*WY1
XK2(2,5)=2.0*DN*B*RI2*(RIX2-BBX*RI2)
** (2*dB/dx-B*BTx/R2)*Nxy1
CNX1=CNX*(2.0*B*BTX*RI2)
XK2(6,4)=CNX1
XK2(1,6)=CNX1*BI*UY1
XK2(3,6)=-CNX1*BTX*BI*WY1

```

```

      XK2(2,6)=CNX1*(-BBX+BTX*RI2)
** -B/R2*Ny0*BTy1
      ABR2=-B*RI2*YNO
      XK2(3,7)=-ABR2*BI*WY1
      XK2(2,7)=ABR2*RI2
** -----
**   STABILITY EQN-3
**   B*d^2Mx1/dx^2
      XK3(12,1)=D*B
**   (2*B,x)*dMx1/dx
      XK3(8,1)=2.0*D*BX
**   (B,xx)*Mx1
      XK3(4,1)=D*BXX
**   1/B*d^2My1/dy^2
      XK3(11,1)=-D*BI*XNU*WY2
      XK3(7,1)=-D*BI*BBX*WY2
      XK3(3,1)=-D*BI*BI*BI*WY4
      XK3(5,1)=D*BI*XNU*RI1*UY2
      XK3(1,1)=D*BI*(BBX*RI1+XNU*RIX1)*UY2
      XK3(2,1)=D*BI*BI*RI2*VY3
**   -B,x*dMy1/dx
      XNU2=1.0-XNU*XNU
      XK3(8,2)=-D*BX*XNU
      XK3(7,2)=+D*BX*XNU2*BI*BI*WY2
      XK3(11,2)=+D*BX*XNU2*BBX
      XK3(7,3)=+D*BX*XNU2*BBXX
      XK3(3,2)=+D*BX*XNU2*2.0*BI*BIX*WY2
      XK3(6,1)=-D*BX*XNU2*BI*RI2*VY1
      XK3(2,2)=-D*BX*XNU2*(BI*RIX2+RI2*BIX)*VY1
      XK3(5,2)=-D*BX*XNU2*BBX*RI1
      XK3(1,2)=-D*BX*XNU2*(BBX*RIX1+RI1*BBXX)
**   -B,xx*My1
      AB33=-BXX
      XK3(11,3)=-D*AB33*XNU
      XK3(7,4)=-D*AB33*BBX
      XK3(3,3)=-D*AB33*BI*BI*WY2
      XK3(5,3)=D*AB33*XNU*RI1
      XK3(1,3)=D*AB33*(BBX*RI1+XNU*RIX1)
      XK3(2,3)=D*AB33*BI*RI2*VY1
**   2*d^2Mxy1/dxdy
*   DN=D*(1.0-XNU)/2.0
      XK3(11,4)=-4.0*DN*BI*WY2
      XK3(5,4)=2.0*DN*BI*RI1*UY2
      XK3(10,1)=2.0*DN*RI2*VY1
      XK3(7,5)=2.0*DN*(-3.0*BIX+BBX*BI)*WY2
      XK3(1,4)=2.0*DN*(BI*RIX1+BIX*RI1)*UY2
      XK3(6,2)=2.0*DN*(2.0*RIX2-BBX*RI2)*VY1
      XK3(3,4)=2.0*DN*(-BIXX+

```

```

+ BBX*BIX+BBXX*BI)*WY2
  XK3(2,4)=2.0*DN*(RIX2-
+ BBX*RIX2-BBXX*RI2)*VY1
** 2/B*B,x*dMxy1/dy
*   DN=D*(1.0-XNU)/2.0
  XK3(7,6)=-4.0*DN*BBX*BI*WY2
  XK3(1,5)=2.0*DN*BBX*BI*RI1*UY2
  XK3(6,3)=2.0*DN*BBX*RI2*VY1
  XK3(3,5)=2.0*DN*BBX*(-BIX+BBX*BI)*WY2
  XK3(2,5)=2.0*DN*BBX*(RIX2-BBXX*RI2)*VY1
** -(B/R1+B,x*BTX+B*BTX,x)*Nx1
  AB31=-(B*RI1+Bx*BTX+B*BTXX)
  XK3(5,5)=C*AB31
  XK3(7,7)=-C*AB31*BTX
  XK3(2,6)=C*AB31*XNU*BI*VY1
  XK3(1,6)=C*AB31*(BTX*RI1+XNU*BBX)
  XK3(3,6)=C*AB31*(RI1+XNU*RI2)
** -B/R2*Ny1
  XK3(5,6)=-C*B*RI2*XNU
  XK3(7,8)=+C*B*RI2*XNU*BTX
  XK3(2,7)=-C*RI2*VY1
  XK3(1,7)=-C*B*RI2*(XNU*BTX*RI1+BBX)
  XK3(3,7)=-C*B*RI2*(XNU*RI1+RI2)
** -B*Nx0*dBTx1/dx
  XK3(11,5)=+B*XN0
  XK3(5,7)=-B*XN0*RI1
  XK3(1,8)=-B*XN0*RIX1
** -(B,x*Nx0+B*Nx0,x)*BTx1
  BN3=-(Bx*XN0+B*XXN0)
  XK3(7,9)=-BN3
  XK3(1,9)=BN3*RI1
** -B*BTX*dNx1/dx
  XK3(9,1)=-C*B*BTX
  XK3(11,6)=+C*B*BTX*BTX
  XK3(6,4)=-C*BTX*XNU*VY1
  XK3(2,8)=-C*B*BTX*XNU*BIX*VY1
  XK3(5,8)=-C*B*BTX*(BTX*RI1
+ +XNU*BBX)
  XK3(7,10)=-C*B*BTX*(RI1-BTXX
+ +XNU*RI2)
  XK3(1,10)=-C*B*BTX*(BTX*RIX1+BTXX*RI1
+ +XNU*BBXX)
  XK3(3,8)=-C*B*BTX*(RIX1+XNU*RIX2)
** -Ny0*dBTy1/dy
  XK3(3,9)=+YN0*BI*WY2
  XK3(2,9)=-YN0*RI2*VY1
** -BTX*dNxy1/dy
*   CNX=C*(1.0-XNU)/2.0

```

```

XK3(6,5)=-CNX*BTX*VY1
XK3(1,11)=-CNX*BTX*BI*UY2
XK3(3,10)=+CNX*BTX*BTX*BI*WY2
XK3(2,10)=-CNX*BTX*(-BBX+BTX*RI2)*VY1

```

*-----

```

**  EQN-4
    XK4(11,1)=-D*1.0
    XK4(7,1)=-D*XNU*BBX
    XK4(3,1)=-D*XNU*BI*BI*WY2
    XK4(5,1)=D*RI1
    XK4(1,1)=D*(RIX1+XNU*BBX*RI1)
    XK4(2,1)=D*XNU*BI*RI2*VY1
    XK4(4,1)=-D*1.0
    RETURN
    END

```

=====

```

SUBROUTINE DETCO(CCK,HS,J1,SS1,AA1,AA2,AA3,AA4,IS)
c  IMPLICIT REAL*8 (A-H,O-Z)
    REAL*8 CCK(12),HS(30),CO(3,3),A1(3),A2(3),A3(3),A4(3)
    REAL*8 AA1(3),AA2(3),AA3(3),AA4(3),CO1(3,3)
    REAL*8 SUM1,SUM2,SUM3,SUM4,SS1
    DO 5 I=1,3
    AA1(I)=0.0
    AA2(I)=0.0
    AA3(I)=0.0
    AA4(I)=0.0
5  CONTINUE
    IF(IS.EQ.0) THEN
    CALL DFCAL(HS,J1,SS1,CO)
    ELSE
    CALL DFCAL1(HS,J1,SS1,CO1,IS)
    ENDIF
    A1(1)=CCK(1)
    A1(2)=CCK(5)
    A1(3)=CCK(9)
    A2(1)=CCK(2)
    A2(2)=CCK(6)
    A2(3)=CCK(10)
    A3(1)=CCK(3)
    A3(2)=CCK(7)
    A3(3)=CCK(11)
    A4(1)=CCK(4)
    A4(2)=CCK(8)
    A4(3)=CCK(12)
    DO 10 I=1,3
    SUM1=0.0
    SUM2=0.0
    SUM3=0.0

```

```

SUM4=0.0
IF(IS.EQ.0) THEN
DO 20 J=1,3
SUM1=SUM1+CO(J,I)*A1(J)
SUM2=SUM2+CO(J,I)*A2(J)
SUM3=SUM3+CO(J,I)*A3(J)
SUM4=SUM4+CO(J,I)*A4(J)
20 CONTINUE
ELSE
DO 30 J=1,3
SUM1=SUM1+CO1(J,I)*A1(J)
SUM2=SUM2+CO1(J,I)*A2(J)
SUM3=SUM3+CO1(J,I)*A3(J)
SUM4=SUM4+CO1(J,I)*A4(J)
30 CONTINUE
ENDIF
AA1(I)=SUM1
AA2(I)=SUM2
AA3(I)=SUM3
AA4(I)=SUM4
10 CONTINUE
RETURN
END

```

```

*-----
SUBROUTINE DFCAL(HS,J1,SS1,CO)
IMPLICIT REAL*8 (A-H,O-Z)
REAL*8 H(2),CO(3,3),HS(30),SS1,SS
I=2
IF(SS1.EQ.0.0) THEN
H(1)=HS(J1)/20.0
H(2)=H(1)
ELSE
H(1)=HS(J1-1)/20.0
H(2)=HS(J1)/20.0
ENDIF
SS=H(I)+H(I-1)
DD=H(I-1)/H(I)/SS
EE=H(I)/H(I-1)/SS
FF=(DD-EE)
A=2.0/H(I)/SS
B=-2.0/H(I)/H(I-1)
C=2.0/H(I-1)/SS
CO(1,1)=0.0
CO(1,2)=1.0
CO(1,3)=0.0
CO(2,1)=-DD
CO(2,2)=FF
CO(2,3)=EE

```

```

CO(3,1)=A
CO(3,2)=B
CO(3,3)=C
RETURN
END

```

*=====

```

SUBROUTINE MATS1(A5,B5)
c  IMPLICIT REAL*8 (A-H,O-Z)
    REAL*8 A5(4,4),B5(4,4)
    DO 99 L1=1,4
    DO 99 K1=1,4
99  B5(L1,K1)=A5(L1,K1)+B5(L1,K1)
    RETURN
    END

```

```

SUBROUTINE MATS2 (A5)
c  IMPLICIT REAL*8 (A-H,O-Z)
    REAL*8 A5(4,4)
    DO 98 L1=1,4
    DO 98 K1=1,4
98  A5(L1,K1)=-A5(L1,K1)
    RETURN
    END

```

```

SUBROUTINE MATM1(A5,B5,C5)
c  IMPLICIT REAL*8 (A-H,O-Z)
    REAL*8 A5(4,4),B5(4,4),C5(4,4)
    DO 97 L1=1,4
    DO 97 K1=1,4
    C5(L1,K1)=0.
    DO 97 J1=1,4
97  C5(L1,K1)=C5(L1,K1)+A5(L1,J1)*B5(J1,K1)
    RETURN
    END

```

*===== SUBROUTINE FOR MATRIX INVERSION =====

```

SUBROUTINE MATI1(B,CI,N)
DOUBLE PRECISION B(4,4),A(4,8),CI(4,4)
DOUBLE PRECISION XMAX,TT,C,D,DIV
L=N+N
DO 200 I=1,N
DO 200 J=1,L
A(I,J)=0.0
200 CONTINUE
DO 11 I=1,N
A(I,N+I)=1.0
DO 11 J=1,N
CI(I,J)=0.0
11  A(I,J)=B(I,J)

```

```

DO 10 K=1,N
IF(K.EQ.N) GOTO 35
XMAX=DABS(A(K,K))
IC=K
DO 20 IA=K+1,N
IF(XMAX .LT. DABS(A(IA,K))) THEN
XMAX=DABS(A(IA,K))
IC=IA
END IF
20 CONTINUE
IF( IC .EQ. K) GOTO 35
DO 30 IB=1,L
TT=A(K,IB)
A(K,IB)=A(IC,IB)
A(IC,IB)=TT
30 CONTINUE
35 IF( DABS(A(K,K)) .LE.1E-16) THEN
WRITE(3,99)
99 FORMAT(///10X,'BAD SOLUTION'//)
ENDIF
40 C=A(K,K)
100 DO 70 IE=1,N
IF( IE .NE. K) THEN
D=A(IE,K)
DO 80 IG=1,L
80 A(IE,IG) = A(IE,IG) -A(K,IG)*(D/C)
ENDIF
70 CONTINUE
10 CONTINUE
DO 90 I=1,N
DIV=A(I,I)
DO 90 IX=1,L
A(I,IX)=A(I,IX)/DIV
90 A(I,I)=1.0
DO 22 I=1,N
DO 22 J=1,N
22 CI(I,J)=A(I,J+N)
RETURN
END

```

```

=====
SUBROUTINE PP2(A1,B1,C1,A2,B2,C2,P2)
REAL*8 A1(4,4),B1(4,4),C1(4,4),A2(4,4),B2(4,4),C2(4,4),P2(4,4)
REAL*8 A3(4,4),B3(4,4),C3(4,4),A4(4,4),CI(4,4),C3I(4,4),P22(4,4)
REAL*8 C22(4,4)
N=4
DO 10 I=1,N
DO 13 J=1,N
P2(I,J)=0.0

```



```

A3(I,J)=0.0
B3(I,J)=0.0
A4(I,J)=0.0
CI(I,J)=0.0
C3I(I,J)=0.0
P22(I,J)=0.0
C22(I,J)=C2(I,J)
13 CONTINUE
10 CONTINUE
CALL MATI1(C22,CI,N)
CALL MATM1(C1,CI,A3)
CALL MATM1(A3,B2,C3)
CALL MATM1(A3,A2,A4)
CALL MATS2(C3)
CALL MATS2(A4)
CALL MATS1(B1,C3)
CALL MATI1(C3,C3I,N)
CALL MATS1(A1,A4)
CALL MATM1(C3I,A4,P22)
DO 12 I=1,4
DO 11 J=1,4
P2(I,J)=P22(I,J)
11 CONTINUE
12 CONTINUE
RETURN
END

```

```

*-----
SUBROUTINE PP(A1,B1,C1,P2,P3)
REAL*8 A1(4,4),B1(4,4),C1(4,4),P2(4,4),P3(4,4),A3(4,4),C1(4,4)
+,P33(4,4)
N=4
DO 10 I=1,4
DO 11 J=1,4
A3(I,J)=0.0
CI(I,J)=0.0
P33(I,J)=0.0
P3(I,J)=0.0
11 CONTINUE
10 CONTINUE
CALL MATM1(C1,P2,A3)
CALL MATS2(A3)
CALL MATS1(B1,A3)
CALL MATI1(A3,CI,N)
CALL MATM1(CI,A1,P33)
DO 13 I=1,4
DO 12 J=1,4
P3(I,J)=P33(I,J)
12 CONTINUE

```

```
13 CONTINUE
RETURN
END
```

*-----

```
      SUBROUTINE XMAT(A1,B1,C1,P2,P3,XM)
      REAL*8 A1(4,4),B1(4,4),C1(4,4),P2(4,4),P3(4,4),
+ B2(4,4),XM(4,4),XM1(4,4)
      DO 12 I=1,4
      DO 13 J=1,4
      XM(I,J)=0.0
      XM1(I,J)=0.0
      B2(I,J)=0.0
13 CONTINUE
12 CONTINUE
      CALL MATM1(C1,P2,B2)
      CALL MATS2(B1)
      CALL MATS1(B2,B1)
      CALL MATM1(B1,P3,XM1)
      CALL MATS1(A1,XM1)
      DO 10 I=1,4
      DO 11 J=1,4
      XM(I,J)=XM1(I,J)
11 CONTINUE
10 CONTINUE
RETURN
END
```

*-----

```
      SUBROUTINE XMAT1(B1,C1,P2,XM)
      REAL*8 B1(4,4),C1(4,4),P2(4,4),
+ XM(4,4),XM1(4,4)
      DO 12 I=1,4
      DO 13 J=1,4
      XM(I,J)=0.0
      XM1(I,J)=0.0
13 CONTINUE
12 CONTINUE
      CALL MATM1(C1,P2,XM1)
      CALL MATS2(XM1)
      CALL MATS1(B1,XM1)
      DO 10 I=1,4
      DO 11 J=1,4
      XM(I,J)=XM1(I,J)
11 CONTINUE
10 CONTINUE
RETURN
END
```

```

*-----
SUBROUTINE JUNC1(FF1,FF2,FF3,FF4,FF5,FF6,FF7,SS1,HS,J1,
+EM,TK,CIND,IG,XNN,XA,XB,XC,MXN,ITC)
REAL*8 XA(4,4),XB(4,4),XC(4,4),HS(30),IG(30),CIND(30),TK(30)
REAL*8 FF1,FF2,FF3,FF4,FF5,FF6,FF7,XNN,EM,SS1
DIMENSION MXN(30)
DO 13 I=1,4
DO 14 J=1,4
XA(I,J)=0.0
XB(I,J)=0.0
XC(I,J)=0.0
14 CONTINUE
13 CONTINUE
CALL RAT(FF1,FF2,FF3,FF4,FF5,FF6,FF7,SS1,HS,J1,
+EM,TK,CIND,IG,XNN,XA,XB,XC,MXN,ITC)
RETURN
END

*-----
SUBROUTINE BOUND(XK1,XK2,XK3,XK4,TK,BTX,BTXX,XXN0,
+PHI,UY1,UY2,VY1,VY2,VY3,WY1,WY2,WY3,WY4,XN0,YN0,B,
+BX,RI2,BI,BBX,RI1,BXX,BIX,RX1,RIX1,RI2,RI21,RIX2,BIXX,
+RIXX1,RIXX2,BBXX,XNU,J1,ITC,XK5,XK6)
IMPLICIT REAL*8 (A-H,O-Z)
REAL*8 XK1(12,11),XK2(12,11),XK3(12,11),XK4(12,11),TK(30)
REAL*8 XK5(12,11),XK6(12,11)
C=1.0
D=1.0/TK(J1)/TK(J1)/12.0
IF(ITC.EQ.1) THEN
** CLAMPED EDGE ***** U=V=W=BTEA=0
XK1(1,1)=1.0
XK2(2,1)=1.0
XK3(3,1)=1.0
XK4(7,1)=-1.0
XK4(1,1)=RI1
ELSEIF(ITC.EQ.2) THEN
** SIMPLY SUPPORTED EDGE, NOT FREE END M=U=V=W=0
XK1(1,1)=1.0
XK2(2,1)=1.0
XK3(3,1)=1.0
XK4(4,1)=1.0
ELSEIF(ITC.EQ.3) THEN
** Nx=M=V=W=0
XK1(3,1)=1.0
XK2(2,1)=1.0
XK3(5,1)=1.0
XK3(7,1)=-BTX
XK3(2,1)=XNU*BI*VY1
XK3(1,1)=BTX*RI1+XNU*BBX

```

```

XK3(3,1)=RI1+XNU*RI2
XK4(4,1)=1.0
ELSEIF(ITC.EQ.4) THEN
** FREE EDGE Nx=Vn=Tnt=M=0
XK1(5,1)=1.0
XK1(7,1)=-BTX
XK1(2,1)=XNU*BI*VY1
XK1(1,1)=BTX*RI1+XNU*BBX
XK1(3,1)=RI1+XNU*RI2
** Vn=Qn+...
** dMx1/dx
XK3(8,1)=D
** (1/B*B,x)*Mx1
XK3(4,1)=D*BBX
** 2/B*dMxy1/dy
DN=D*(1.0-XNU)/2.0
XK3(7,1)=-4.0*DN*BI*BI*WY2
XK3(1,1)=2.0*DN*BI*BI*RI1*UY2
XK3(6,1)=2.0*DN*BI*RI2*VY1
XK3(3,1)=2.0*DN*BI*(-BIX+BBX*BI)*WY2
XK3(2,1)=2.0*DN*BI*(RIX2-BBX*RI2)*VY1
** -1/B*B,x*My1
DN1=D*(XNU*XNU-1.0)
XK3(4,2)=-D*BBX*XNU
XK3(3,2)=-DN1*BI*BI*BBX*WY2
XK3(2,2)=+DN1*BI*RI2*BBX*VY1
XK3(7,2)=-DN1*BBX*BBX
XK3(1,2)=+DN1*BBX*BBX*RI1
*-----
** Tnt= Nnt+...
** Nxy1
CNX=C*(1.0-XNU)/2.0
XK2(6,1)=CNX
XK2(1,1)=CNX*BI*UY1
XK2(3,1)=-CNX*BTX*BI*WY1
XK2(2,1)=CNX*(-BBX+BTX*RI2)
** 1/R2*Mxy1
XK2(7,1)=-2.0*DN*RI2*BI*WY1
XK2(1,2)=DN*RI2*BI*RI1*UY1
XK2(6,2)=DN*RI2*RI2
XK2(3,2)=DN*RI2*(-BIX+BBX*BI)*WY1
XK2(2,2)=DN*RI2*(RIX2-BBX*RI2)
XK4(1,1)=1.0
ELSEIF(ITC.EQ.5) THEN
** SIMPLY SUPPORTED EDGE, FREE TO MOVE IN NORMAL DIRECTION
* M=Vn=U=V=0
XK1(1,1)=1.0
** dMx1/dx

```

```

      XK3(8,1)=D
** (1/B*B,x)*Mx1
      XK3(4,1)=D*BBX
** 2/B*dMxy1/dy
      DN=D*(1.0-XNU)/2.0
      XK3(7,1)=-4.0*DN*BI*BI*WY2
      XK3(1,1)=2.0*DN*BI*BI*RI1*UY2
      XK3(6,1)=2.0*DN*BI*RI2*VY1
      XK3(3,1)=2.0*DN*BI*(-BIX+BBX*BI)*WY2
      XK3(2,1)=2.0*DN*BI*(RIX2-BBX*RI2)*VY1
** -1/B*B,x*My1
      DN1=D*(XNU*XNU-1.0)
      XK3(4,2)=-D*BBX*XNU
      XK3(3,2)=-DN1*BI*BI*BBX*WY2
      XK3(2,2)=+DN1*BI*RI2*BBX*VY1
      XK3(7,2)=-DN1*BBX*BBX
      XK3(1,2)=+DN1*BBX*BBX*RI1
*-----
**   EQN-2
**   Nxy1
      CNX=C*(1.0-XNU)/2.0
      XK2(6,1)=CNX
      XK2(1,1)=CNX*BI*UY1
      XK2(3,1)=-CNX*BTX*BI*WY1
      XK2(2,1)=CNX*(-BBX+BTX*RI2)
** 1/R2*Mxy1
      XK2(7,1)=-2.0*DN*RI2*BI*WY1
      XK2(1,2)=DN*RI2*BI*RI1*UY1
      XK2(6,2)=DN*RI2*RI2
      XK2(3,2)=DN*RI2*(-BIX+BBX*BI)*WY1
      XK2(2,2)=DN*RI2*(RIX2-BBX*RI2)
**   EQN-4
      XK4(2,1)=1.0
      ELSEIF(ITC.EQ.6) THEN
* RADIAL DISPL = 0.0 , ETC.....////////
* Nx
      XK1(5,1)=1.0
      XK1(7,1)=-BTX
      XK1(2,1)=XNU*BI*VY1
      XK1(1,1)=BTX*RI1+XNU*BBX
      XK1(3,1)=RI1+XNU*RI2
* Vn
      XK3(8,1)=D
** (1/B*B,x)*Mx1
      XK3(4,1)=D*BBX
** 2/B*dMxy1/dy
      DN=D*(1.0-XNU)/2.0
      XK3(7,1)=-4.0*DN*BI*BI*WY2

```

```

XK3(1,1)=2.0*DN*BI*BI*RI1*UY2
XK3(6,1)=2.0*DN*BI*RI2*VY1
XK3(3,1)=2.0*DN*BI*(-BIX+BBX*BI)*WY2
XK3(2,1)=2.0*DN*BI*(RIX2-BBX*RI2)*VY1
** -1/B*B,x*My1
DN1=D*(XNU*XNU-1.0)
XK3(4,2)=-D*BBX*XNU
XK3(3,2)=-DN1*BI*BI*BBX*WY2
XK3(2,2)=+DN1*BI*RI2*BBX*VY1
XK3(7,2)=-DN1*BBX*BBX
XK3(1,2)=+DN1*BBX*BBX*RI1
XK2(1,1)=1.0
XK4(3,1)=1.0
XK5(2,1)=1.0
XK6(4,1)=1.0
ELSE
ENDIF
RETURN
END
*-----*
SUBROUTINE DET4(A,DD)
* CALCULATES 4TH ORDER DETERMINANT
REAL*8 A(4,4),B1(3),B2(3),B3(3),B4(3)
REAL*8 DT1,DT2,DT3,DT4,AA,AB,AC,AD,DD
DO 5 I=1,3
B1(I)=0.0
B2(I)=0.0
B3(I)=0.0
B4(I)=0.0
5 CONTINUE
AA=A(1,1)
AB=A(1,2)
AC=A(1,3)
AD=A(1,4)
DO 10 I=1,3
B1(I)=A(I+1,1)
B2(I)=A(I+1,2)
B3(I)=A(I+1,3)
B4(I)=A(I+1,4)
10 CONTINUE
CALL DET3(B2,B3,B4,DT1)
CALL DET3(B1,B3,B4,DT2)
CALL DET3(B1,B2,B4,DT3)
CALL DET3(B1,B2,B3,DT4)
DD=(AA*DT1-AB*DT2)+(AC*DT3-AD*DT4)
RETURN
END

```

```

SUBROUTINE DET3(X,Y,Z,DT)
REAL*8 X(3),Y(3),Z(3),DT
DT=(X(1)*(Y(2)*Z(3)-Z(2)*Y(3))
+-Y(1)*(X(2)*Z(3)-Z(2)*X(3)))
++Z(1)*(X(2)*Y(3)-X(3)*Y(2))
RETURN
END

```

C-----

```

SUBROUTINE MATS (A5,B5,L,K)
c IMPLICIT REAL*8 (A-H,O-Z)
REAL*8 A5(3,3),B5(3,3)
DO 99 L1=1,L
DO 99 K1=1,K
99 B5(L1,K1)=A5(L1,K1)+B5(L1,K1)
RETURN
END

```

```

SUBROUTINE MATSB (A5,L,K)
c IMPLICIT REAL*8 (A-H,O-Z)
REAL*8 A5(3,3)
DO 98 L1=1,L
DO 98 K1=1,K
98 A5(L1,K1)=-A5(L1,K1)
RETURN
END

```

```

SUBROUTINE MATM (A5,B5,C5,L,K,K2)
c IMPLICIT REAL*8 (A-H,O-Z)
REAL*8 A5(3,3),B5(3,3),C5(3,3)
DO 97 L1=1,L
DO 97 K1=1,K2
C5(L1,K1)=0.
DO 97 J1=1,K
97 C5(L1,K1)=C5(L1,K1)+A5(L1,J1)*B5(J1,K1)
RETURN
END

```

```

SUBROUTINE MATI (A5,B5,K1)
c IMPLICIT REAL*8 (A-H,O-Z)
REAL*8 A5(3,3),B5(3,3)
P=0.
DO 9 L=1,3
DO 9 K=1,3
GO TO (2,3,4),L
2 I1=L+1
I2=L+2
GO TO 5
3 I1=L+1

```

```

      I2=1
      GO TO 5
4     I1=1
      I2=2
5     GO TO (6,7,8),K
6     J1=K+1
      J2=K+2
      GO TO 9
7     J1=K+1
      J2=1
      GO TO 9
8     J1=1
      J2=2
9     B5(K,L)=A5(I1,J1)*A5(I2,J2)-A5(I2,J1)*A5(I1,J2)
      DO 11 L=1,3
11    P=P+A5(1,L)*B5(L,1)
      DO 12 L=1,3
      DO 12 K=1,3
12    B5(L,K)=B5(L,K)/P
      RETURN
      END

```

C-----

```

      SUBROUTINE JUNC2(FF1,FF2,FF3,FF4,FF5,FF6,FF7,FF8,FF9,
+SS1,HS,J1,EM,TK,CIND,IG,XNN,MX,MXN,BB1,BC1,BD1,CB1,
+CC1,CD1,DB1,DC1,DD1,EB1,EC1,ED1)
      IMPLICIT REAL*8 (A-H,O-Z)
      REAL*8 TK(30),CIND(30),EM,IG(30)
      DIMENSION MX(30),MXN(30)
      REAL*8 BB1(4,4),BC1(4,4),BD1(4,4)
      REAL*8 CB1(4,4),CC1(4,4),CD1(4,4)
      REAL*8 DB1(4,4),DC1(4,4),DD1(4,4)
      REAL*8 EB1(4,4),EC1(4,4),ED1(4,4)
      DO 13 IS=1,4
      IF(IS.EQ.1) THEN
      CALL JUNC21(FF1,FF2,FF3,FF4,FF5,FF6,FF7,FF8,FF9,SS1,HS,J1,
+EM,TK,CIND,IG,XNN,BB1,BC1,BD1,MX,MXN,IS)
      ENDIF
      IF(IS.EQ.2) THEN
      CALL JUNC21(FF1,FF2,FF3,FF4,FF5,FF6,FF7,FF8,FF9,SS1,HS,J1,
+EM,TK,CIND,IG,XNN,CB1,CC1,CD1,MX,MXN,IS)
      ENDIF
      IF(IS.EQ.3) THEN
      CALL JUNC21(FF1,FF2,FF3,FF4,FF5,FF6,FF7,FF8,FF9,SS1,HS,J1,
+EM,TK,CIND,IG,XNN,DB1,DC1,DD1,MX,MXN,IS)
      ENDIF
      IF(IS.EQ.4) THEN
      CALL JUNC21(FF1,FF2,FF3,FF4,FF5,FF6,FF7,FF8,FF9,SS1,HS,J1,
+EM,TK,CIND,IG,XNN,EB1,EC1,ED1,MX,MXN,IS)

```



```

      ENDIF
13   CONTINUE
      RETURN
      END

```

```

*-----
      SUBROUTINE JUNC21(FF1,FF2,FF3,FF4,FF5,FF6,FF7,FF8,FF9,SS1,
+HS,J1,EM,TK,CIND,IG,XNN,AB1,AC1,AD1,MX,MXN,IS)
      IMPLICIT REAL*8 (A-H,O-Z)
      REAL*8 XK1(12,11),XK2(12,11),XK3(12,11),XK4(12,11)
      REAL*8 CC1(12),CC2(12),CC3(12),CC4(12),
+AA1(3),AA2(3),AA3(3),AA4(3)
      REAL*8 HS(30),TK(30),EM
      REAL*8 AB1(4,4),AC1(4,4),AD1(4,4),CIND(30),IG(30)
      DIMENSION MXN(30),MX(30)
      DO 300 I=1,3
      AA1(I)=0.0
      AA2(I)=0.0
      AA3(I)=0.0
      AA4(I)=0.0
300   CONTINUE
      DO 199 I=1,4
      DO 199 J=1,4
      AB1(I,J)=0.0
      AC1(I,J)=0.0
      AD1(I,J)=0.0
199   CONTINUE
      DO 200 I=1,12
      DO 201 J=1,11
      XK1(I,J)=0.0
      XK2(I,J)=0.0
      XK3(I,J)=0.0
      XK4(I,J)=0.0
201   CONTINUE
200   CONTINUE
      XNU=0.3
      IF(IS.EQ.1 .OR. IS.EQ.3) THEN
      PHI=FF8
      FF66=FF9
      ELSE
      PHI=FF7
      FF66=FF6
      ENDIF
      BTX=0.0
      BTXX=0.0
      XXN0=FF66*EM*(1.0-XNU*XNU)*TK(J1)
105  FORMAT(21E10.4)
      UY1=-XNN
      UY2=-XNN*XNN

```

```

VY1=XNN
VY2=-XNN*XNN
VY3=UY2*VY1
WY1=-XNN
WY2=-XNN*XNN
WY3=WY1*WY2
WY4=WY3*XNN
XN0=FF4*EM*(1.0-XNU*XNU)*TK(J1)
YN0=FF5*EM*(1.0-XNU*XNU)*TK(J1)
B=FF1
BX=DCOS(PHI)
IF(IS.EQ.1 .OR. IS.EQ.3) THEN
J11=J1-1
ELSE
J11=J1
ENDIF
IF(MXN(J11) .EQ. 2) THEN
RI2=1.0/CIND(J11)
ELSE
RI2=DSIN(PHI)/B
ENDIF
BI=RI2/DSIN(PHI)
BBX=RI2/DTAN(PHI)
IF(IS.EQ.1 .OR. IS.EQ.3) THEN
J12=J1-1
ELSE
J12=J1
ENDIF
IF(IG(J12).EQ.1.0) THEN
RI1=0.0
ELSE
RI1=1.0/CIND(J12)
ENDIF
BXX=-DSIN(PHI)*RI1
BIX=-BBX*BI
RX1=0.0
RIX1=0.0
RI12=RI1-RI2
RI21=RI2-RI1
RIX2=RI12*BBX
BIXX=(2.0*BBX*BBX+RI2)*BI
RIXX1=0.0
RIXX2=RI21*(2.0*BBX*BBX+RI1*RI2)
BBXX=BI*BXX+BX*BIX
C=1.0
D=1.0/TK(J1)/TK(J1)/12.0
IF(IS.LE.2) THEN
IF(IS.EQ.2) THEN

```

```

XIS1=1.0
XIS2=1.0
XIS3=1.0
XIS4=1.0
ELSE
XIS1=-1.0
XIS2=-1.0
XIS3=-1.0
XIS4=-1.0
ENDIF
**-----
**      EQN-1
**      Nx1

      XK1(5,1)=C
      XK1(7,1)=-C*BTX
      XK1(2,1)=C*XNU*BI*VY1
      XK1(1,1)=C*(BTX*RI1
      ++XNU*BX*BI)
      XK1(3,1)=C*(RI1+XNU*RI2)
**      EQN-3
**      dMx1/dx
      XK3(8,1)=D
**      (1/B*B,x)*Mx1
      XK3(4,1)=D*BBX
**      2/B*dMxy1/dy
      DN=D*(1.0-XNU)/2.0
      XK3(7,1)=-4.0*DN*BI*BI*WY2
      XK3(1,1)=2.0*DN*BI*BI*RI1*UY2
      XK3(6,1)=2.0*DN*BI*RI2*VY1
      XK3(3,1)=2.0*DN*BI*(-BIX+BBX*B1)*WY2
      XK3(2,1)=2.0*DN*BI*(RIX2-BBX*RI2)*VY1
**      -1/B*B,x*Myl
      DN1=D*(XNU*XNU-1.0)
      XK3(4,2)=-D*BBX*XNU
      XK3(3,2)=-DN1*BI*BI*BBX*WY2
      XK3(2,2)=+DN1*BI*RI2*BBX*VY1
      XK3(7,2)=-DN1*BBX*BBX
      XK3(1,2)=+DN1*BBX*BBX*RI1
*-----
**      EQN-2
**      Nxy1
      CNX=C*(1.0-XNU)/2.0
      XK2(6,1)=CNX
      XK2(1,1)=CNX*BI*UY1
      XK2(3,1)=-CNX*BTX*BI*WY1
      XK2(2,1)=CNX*(-BBX+BTX*RI2)
**      1/R2*Mxy1

```

```

XK2(7,1)=-2.0*DN*RI2*BI*WY1
XK2(1,2)=DN*RI2*BI*RI1*UY1
XK2(6,2)=DN*RI2*RI2
XK2(3,2)=DN*RI2*(-BIX+BBX*BI)*WY1
XK2(2,2)=DN*RI2*(RIX2-BBX*RI2)
** EQN-4
XK4(4,1)=1.0
ELSE
IF(IS.EQ.4) THEN
XIS1=1.0
XIS2=1.0
XIS3=1.0
XIS4=1.0
ELSE
XIS1=-1.0
XIS2=-1.0
XIS3=-1.0
XIS4=-1.0
ENDIF
XK1(1,1)=1.0
XK2(2,1)=1.0
XK3(3,1)=1.0
XK4(7,1)=-1.0
XK4(1,1)=RI1
ENDIF
DO 50 L=1,12
CC1(L)=0.0
CC2(L)=0.0
CC3(L)=0.0
CC4(L)=0.0
DO 60 L1=1,11
IF(IS.LE.2) THEN
* IF(IS.EQ.1) THEN
CC1(L)=CC1(L)+(-XK3(L,L1)*DSIN(PHI)+XK1(L,L1)*DCOS(PHI))*XIS1
CC2(L)=CC2(L)+(XK3(L,L1)*DCOS(PHI)+XK1(L,L1)*DSIN(PHI))*XIS2
* ENDIF
* IF(IS.EQ.2) THEN
* CC1(L)=CC1(L)+(XK3(L,L1)*DSIN(PHI)+XK1(L,L1)*DCOS(PHI))*XIS1
* CC2(L)=CC2(L)+(XK3(L,L1)*DCOS(PHI)-XK1(L,L1)*DSIN(PHI))*XIS2
* ENDIF
CC3(L)=CC3(L)+XK2(L,L1)*XIS3
CC4(L)=CC4(L)+XK4(L,L1)*XIS4
ELSE
CC1(L)=CC1(L)+(XK3(L,L1)*DSIN(PHI)+XK1(L,L1)*DCOS(PHI))*XIS1
CC2(L)=CC2(L)+XK2(L,L1)*XIS2
CC3(L)=CC3(L)+(XK3(L,L1)*DCOS(PHI)-XK1(L,L1)*DSIN(PHI))*XIS3
CC4(L)=CC4(L)+XK4(L,L1)*XIS4
ENDIF

```

```

60  CONTINUE
50  CONTINUE
110 FORMAT (31D11.5)
    DO 70 I=1,4
    IF (I.EQ.1) THEN
    CALL DETCO(CC1,HS,J1,SS1,AA1,AA2,AA3,AA4,IS)
    ENDIF
    IF (I.EQ.2) THEN
    CALL DETCO(CC2,HS,J1,SS1,AA1,AA2,AA3,AA4,IS)
    ENDIF
    IF (I.EQ.3) THEN
    CALL DETCO(CC3,HS,J1,SS1,AA1,AA2,AA3,AA4,IS)
    ENDIF
    IF (I.EQ.4) THEN
    CALL DETCO(CC4,HS,J1,SS1,AA1,AA2,AA3,AA4,IS)
    ENDIF
    AB1(I,1)=AA1(1)
    AB1(I,2)=AA2(1)
    AB1(I,3)=AA3(1)
    AB1(I,4)=AA4(1)
    AC1(I,1)=AA1(2)
    AC1(I,2)=AA2(2)
    AC1(I,3)=AA3(2)
    AC1(I,4)=AA4(2)
    AD1(I,1)=AA1(3)
    AD1(I,2)=AA2(3)
    AD1(I,3)=AA3(3)
    AD1(I,4)=AA4(3)
70  CONTINUE
    RETURN
    END

```

```

*-----
    SUBROUTINE DFCAL1(HS,J1,SS1,CO1,IS)
    IMPLICIT REAL*8 (A-H,O-Z)
    REAL*8 H(1),CO(3,3),CO1(3,3),HS(30),SS1,SS
    IF(IS.EQ.1 .OR. IS.EQ.3) THEN
    H(1)=HS(J1-1)/20.0
    DLH=2.0*H(1)
* BACKWARD DIFFERENCE
    CO(1,1)=0.0
    CO(1,2)=0.0
    CO(1,3)=1.0
    CO(2,1)=-1.0/DLH
    CO(2,2)=4.0/DLH
    CO(2,3)=-3.0/DLH
    CO(3,1)=0.0
    CO(3,2)=0.0
    CO(3,3)=0.0

```

```

CO1(1,1)=0.0
CO1(1,2)=0.0
CO1(1,3)=1.0
CO1(2,1)=0.0
CO1(2,2)=1.0/H(1)
CO1(2,3)=-1.0/H(1)
CO1(3,1)=0.0
CO1(3,2)=0.0
CO1(3,3)=0.0
ELSE

```

```

* FORWARD DIFFERENCE

```

```

H(1)=HS(J1)/20.0
DLH1=2.0*H(1)
CO(1,1)=1.0
CO(1,2)=0.0
CO(1,3)=0.0
CO(2,1)=3.0/DLH1
CO(2,2)=-4.0/DLH1
CO(2,3)=1.0/DLH1
CO(3,1)=0.0
CO(3,2)=0.0
CO(3,3)=0.0
CO1(1,1)=1.0
CO1(1,2)=0.0
CO1(1,3)=0.0
CO1(2,1)=1.0/H(1)
CO1(2,2)=-1.0/H(1)
CO1(2,3)=0.0
CO1(3,1)=0.0
CO1(3,2)=0.0
CO1(3,3)=0.0
ENDIF
RETURN
END

```

```

*=====

```

```

SUBROUTINE JUNP(A,B,C,F1,F2,F3,P22,A1,B1,C1,A2,B2,C2,A3,
+B3,C3,A4,B4,C4)
REAL*8 A(4,4),B(4,4),C(4,4),AA(4,4),AB(4,4),AC(4,4)
REAL*8 A1(4,4),B1(4,4),C1(4,4),A2(4,4),B2(4,4),C2(4,4)
REAL*8 A3(4,4),B3(4,4),C3(4,4),A4(4,4),B4(4,4),C4(4,4)
REAL*8 P22(4,4),P33(4,4),D1(4,4),D2(4,4),D3(4,4),D4(4,4)
REAL*8 E1(4,4),E2(4,4),E3(4,4),E4(4,4),F1(4,4),F2(4,4),F3(4,4)
REAL*8 CI(4,4),C5(4,4),C6(4,4),C7(4,4),P44(4,4)
DO 100 JX=1,4
DO 100 JX1=1,4
P44(JX,JX1)=0.0
P33(JX,JX1)=0.0
CI(JX,JX1)=0.0

```

```

C5(JX,JX1)=0.0
C6(JX,JX1)=0.0
C7(JX,JX1)=0.0
D1(JX,JX1)=0.0
D2(JX,JX1)=0.0
F1(JX,JX1)=0.0
F2(JX,JX1)=0.0
F3(JX,JX1)=0.0
E1(JX,JX1)=0.0
E2(JX,JX1)=0.0
100 CONTINUE
CALL MATI1(C,C1,4)
CALL MATM1(C1,B,C5)
CALL MATM1(C1,A,C6)
CALL MATM1(C1,C5,D1)
CALL MATM1(C3,C5,E1)
CALL MATM1(C1,C6,D2)
CALL MATM1(C3,C6,E2)
CALL MATS2(D1)
CALL MATS2(D2)
CALL MATS2(E1)
CALL MATS2(E2)
CALL MATS1(B1,D1)
CALL MATS1(A1,D2)
CALL MATS1(B3,E1)
CALL MATS1(A3,E2)
DO 115 JX=1,4
DO 115 JX1=1,4
P44(JX,JX1)=0.0
P33(JX,JX1)=0.0
C1(JX,JX1)=0.0
C5(JX,JX1)=0.0
C6(JX,JX1)=0.0
D3(JX,JX1)=0.0
D4(JX,JX1)=0.0
E3(JX,JX1)=0.0
E4(JX,JX1)=0.0
115 CONTINUE
CALL MATM1(D1,P22,E3)
CALL MATM1(E1,P22,E4)
CALL MATS2(E3)
CALL MATS2(E4)
CALL MATS1(D2,E3)
CALL MATS1(E2,E4)
CALL MATI1(E3,C1,4)
CALL MATM1(C1,A2,C5)
CALL MATM1(C1,B2,C6)
CALL MATM1(C1,C2,C7)

```

```
CALL MATM1(E4,C5,F1)
CALL MATM1(E4,C6,F2)
CALL MATM1(E4,C7,F3)
CALL MATS2(F1)
CALL MATS2(F2)
CALL MATS2(F3)
CALL MATS1(A4,F1)
CALL MATS1(B4,F2)
CALL MATS1(C4,F3)
RETURN
END
```


VITA AUCTORIS

- 1960 Born at Netrokona, Bangladesh, on January 18.
- 1975 Completed Secondary School Certificate Education from Dhaka Collegiate School, Dhaka, Bangladesh.
- 1977 Completed Higher Secondary Certificate Education from Dhaka College, Dhaka, Bangladesh.
- 1983 Received the Degree of Bachelor of Science in Mechanical Engineering from Engineering College, Rajshahi under Rajshahi University, Rajshahi, Bangladesh.
- 1983 Joined as Senior Officer in the Bangladesh Shilpa Bank, Dhaka, Bangladesh.
- 1984 Joined as Lecturer in the Department of Mechanical Engineering, Bangladesh Institute of Technology, Rajshahi (Erstwhile Engineering College, Rajshahi), Bangladesh.
- 1988 Received the Degree of Master of Science in Engineering (Mechanical) from Bangladesh University of Engineering & Technology, Dhaka, Bangladesh.
- 1988 Joined as Assistant Professor in the Department of Mechanical Engineering, Bangladesh Institute of Technology, Chittagong, Bangladesh.

